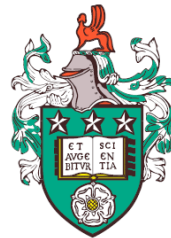


Modelling and Characterization of Soft Materials for Bioinspired Series-elastic Actuators



Rodrigo Daniel Solis Ortega

University of Leeds

Institute of Design, Robotics and Optimization

School of Mechanical Engineering

Submitted in accordance with the requirements for the degree of

Doctor of Philosophy

June, 2020

Intellectual Property Statement

The candidate confirms that the work submitted is his own, except where work which has formed part of jointly authored publications has been included. The contribution of the candidate and the other authors to this work has been explicitly indicated below. The candidate confirms that appropriate credit has been given within the thesis where reference has been made to the work of others.

Section 3.2 of this thesis is based on a jointly-authored conference paper: *Solis-Ortega, R.D., Dehghani-Sanij, A.A. and Martinez-Hernandez, U., 2017, July. Characterization of kinetic and kinematic parameters for wearable robotics. In Annual Conference Towards Autonomous Robotic Systems (pp. 548-556). Springer, Cham..*

Chapter 5 of this thesis is based on a jointly-authored conference paper: *Solis-Ortega, R.D., Dehghani-Sanij, A.A. and Martinez-Hernandez, U., 2018, August. The assessment of viscoelastic models for nonlinear soft materials. In 2018 7th IEEE International Conference on Biomedical Robotics and Biomechatronics (Biorob) (pp. 1274-1279). IEEE..*

The contributions of the candidate to these papers include the literature review, data collection, design and execution of simulation, statistical analysis, and writing. The contributions of the other authors to these papers include guidance, supervision, and revision.

This copy has been supplied on the understanding that it is copyright material and that no quotation from the thesis may be published without proper acknowledgement.

The right of Rodrigo Daniel Solis Ortega to be identified as Author of this work has been asserted by him in accordance with the Copyright, Designs and Patents Act 1988.

© 2020 The University of Leeds and Rodrigo Daniel Solis Ortega.

Acknowledgements

I would like to express my most sincere gratitude to my supervisor Professor Abbas Dehghani-Sanji, and to Dr Uriel Martinez Hernandez for guiding me through the development of this project. I would also like to thank my family for supporting me during the most difficult times, despite of the enormous distance between us. I am very grateful to my wife, who accompanied me during the most challenging stages of this life experience, and for encouraging me when I needed it the most. I would also like to thank all my friends and the many people who directly or indirectly were involved in this personal goal. Lastly, I would like to thank my financial sponsor, the Consejo de Nacional de Ciencia Y Tecnologia (CONACYT).

Abstract

In the field of Soft Robotics, viscoelasticity has been proved beneficial for human assistance applications. The human skeletal muscle system, as well as many soft materials commonly used in soft robotic applications, have viscoelastic properties. Viscoelasticity can be modelled using a set of equations known as the Linear Viscoelastic Models (LVMs). This modelling approach has two main limitations: high mathematical complexity and high computational cost. Here, these limitations are addressed in two ways. Firstly, a piecewise linearization technique is used to reduce the mathematical complexity of LVMs. Secondly, a data-driven modelling approach, based on feedforward artificial neural networks (ANNs), is used to reduce the computational cost. The aim of both modelling approaches is to describe the nonlinear, strain-dependent, and time-dependent stress response of seven thermoplastic elastomers.

The piecewise linearization technique, applied to two different LVMs, yielded the PL-SLS model and the PL-Wiechert model. The PL-Wiechert model was incompatible with the linearization technique, reflected on the poor achieved accuracy. The PL-SLS model was able to account for the nonlinear and strain-dependent stress response of all the materials. However, the PL-SLS model was unable to account for the time-dependent stress response. The research done on the data-driven modelling approach yielded two different ANN models, which in here are differentiated as rate-dependent and rate-independent. The rate-dependent ANN model delivered the best accuracy when accounting for all the viscoelastic properties mentioned above. Due to this, the prediction capability of this ANN model under real-time working conditions was investigated in Simulink using a model of a cable-driven series-viscoelastic actuator. The performance of the ANN model was unsatisfactory under these conditions. The latter is attributed to the large range of strain rates inherent to real-time conditions. These were beyond the ranges included in the training dataset. This limitation might not be present in the rate-independent ANN model. Finally, the developed ANN model was able to address both limitations of traditional modelling tools. Nonetheless, this ANN model requires further tuning and a richer dataset to improve its performance under real-time working condition.

CONTENTS

1	Introduction	1
1.1	Background	2
1.2	Motivation	6
1.3	Aims and Objectives	7
1.3.1	Aims	7
1.3.2	Objectives	7
1.4	Scope of the research	8
1.5	Contributions of the research	8
1.6	Outline of the thesis	9
2	Literature Review	13
2.1	Introduction	14
2.2	Soft Robotics for Human Assistance Applications	14
2.2.1	Soft Actuation Technologies	15
2.2.1.1	Pneumatic Artificial Muscles	15
2.2.1.2	Cable-driven Actuators	22
2.2.1.3	Shape Memory Materials	24
2.2.2	Soft Perception Technologies	28
2.2.3	Control Technologies	32
2.3	Gaps in the Body of Knowledge	35
2.4	Summary	36
3	Biomechanics of the Lower Limb as Design Guidelines for Assistive Devices	40
3.1	Introduction	41
3.2	Characterization of Kinematic and Kinetic Parameters for Activities of Daily Living	41

CONTENTS

6.4.1	Analysis: Impact of the selection of inputs/outputs	130
6.4.2	Analysis: Optimal number of neurons	134
6.5	Summary	140
7	Modelling a bio-inspired series-viscoelastic actuator	141
7.1	Introduction	142
7.2	Matching the Human Tendon Properties	143
7.3	ANN Model Validation in Real-time	145
7.4	Preliminary Design Concept of a Series-viscoelastic Actuator	148
7.5	Summary	151
8	Summary, Conclusions, and Future Work	153
8.1	Summary	154
8.2	Conclusions	158
8.3	Future Work	159
Appendices		161
A	Characterization of the Human Body Lower Limb	163
A.1	Stacked Clustered Bar Charts	164
B	Designed Experimental Protocol to Investigate the Concepts of Variable Recruitment and Co-contraction in Series-viscoelastic Actuators	171
B.1	Aims and Objectives	172
B.1.1	Aim:	172
B.1.2	Objectives:	172
B.2	Methodology	172
B.3	Experiment 1	173
B.4	Experiment 2	173
B.5	Experiment 3	175
B.6	Experiment 4	175
References		177

CONTENTS

LIST OF FIGURES

2.1	Bio-inspired active soft orthosis concept for the treatment of ankle-foot pathologies. From top to bottom: artificial muscles attached to the soft wearable garment, a strain sensor for ankle angle measurements, the tendon-ligament system and pressure sensor for gait cycle detection [1].	17
2.2	Soft orthosis components, (a) pneumatic artificial muscle in its relaxed and contracted state and. (b) complete tendon-ligament system without ligaments and with ligaments. [1].	17
2.3	Different shapes achieved by the prototype. (a) Original shape. (b) All muscles activated, contracting the whole body and amplified image of one muscle. (c) Partial contraction, only the 1st and 2nd top rows are activated. Both (d) and (e) illustrate bending movements, only two adjacent columns are activated. [2].	18
2.4	Virtual anchor concept. The three key anchors (red square) located at the foot, hip and shoulder are interconnected with the soft actuators (orange) and auxiliary connectors (black) in specific points called virtual anchors (red circle) to stabilize the forces created by the actuators. [3].	19
2.5	(a) Flat elastomer pneumatic actuator in its both (1) pressurized and (2) relaxed states. (b) Implementation of the flat actuator in medical leg model assistance, along with the achieved (1) extension, and (2) flexion motion. [4]	20

LIST OF FIGURES

2.6 (a) IPAM developed in its relaxed and pressurized state, the small radial expansion and large axial expansion is appreciated. (b) Cross-sectional view of the jamming effect ongoing inside the actuator, and (c) bending effect caused by heavy load, and correction of the bending using the jamming effect [5].	21
2.7 (a) Developed Bowden cable-based soft exosuit prototype. (b) Initial design concept highlighting the main parts of the soft exosuit. [6].	22
2.8 Soft exosuit implementing the multi-joint actuation concept. There are two anchor points, one at the pelvis (1) and one at the shank (5). The suit is actuated by a bowden cable (2) and positioned at the front of the knee. The contractile element is connected connected to the two anchors by webbing elements (4). Knee module to increase the lever arm (3). Red arrows: reaction forces, and orange arrows: actuation force [7].	24
2.9 Shape memory alloys made of Nitinol. The contraction effect under the increase in temperature is illustrated [8]	25
2.10 Developed soft orthosis for the ankle joint. The developed SMA artificial muscle along the main parts are highlighted. [9].	26
2.11 Flexible actuator around the arm in a wrist exoskeleton prototype. [10].	27
2.12 Schematic illustrating McKibben with embedded SMP functionality [11]. T_g : transition temperature, P_H : high pressure, P_L : low pressure.	28
2.13 Soft strain sensor. The microchannel filled with liquid metal can be appreciated in: a) concept design and b) the prototype. [1].	29
2.14 Soft sensor sleeve: (a) design concept, (b) developed prototype, (c) magnified view of the embedded sensor-actuator concept. (d) Soft strain sensor change in resistance during stretch and relax. [2].	30
2.15 Implementation of soft strain sensors into a Soft sensing suit, (a) hip sensor, (b) knee sensor and (c) ankle sensor position. [12].	31
2.16 Hybrid soft strain sensor, the interface between the liquid metal and the ionic solution can be clearly seen in dark areas. [13].	31
2.17 ‘Smart Braid’ concept. The variation in the actuator length cause a change in the electric circuit inductance. [14].	32
2.18 Control system architecture implemented for the ankle soft orthosis. [1].	34

LIST OF FIGURES

3.1 Dimensional spaces used to understand human motions: a) Sagittal plane, b)Horizontal plane and c)Frontal plane. [15].	42
3.2 Lower limb motions for a) sagital plane, b) horizontal plane and c) frontal plane. Image adapted from [15].	43
3.3 Clustered-stacked bar charts of reviewed gait analyses [16].	47
3.4 Torque range values during several activities. The values for the maximum and minimum torque are mean values from the data of all the different gait analysis experiments enclosed in one main activity. [16–24]	48
3.5 Comparison between subjects' age and the knee range of motion during walking over ground. The areas surrounded by solid lines and dotted lines represent the intersection between three and two areas, respectively. The overlapping squares highlight the great similarity among the range of motion despite subjects' age. The data used to create this chart is presented in Table 3.1 [16].	50
3.6 Hill's model of the skeletal muscle. The contractile element (CE), the parallel element (PE) and the series element (SE) are shown [25] . .	51
3.7 Tendon stress-strain curve. Image adapted from [26].	53
3.8 Tendon curves for the experiments of: (a) stress relaxation and (b) creep. The experiments were executed several times under the same conditions, the curve labelled <i>n</i> illustrates the tendon reaching a steady state where repeatability between experiments is achieved. Image reproduced from [26]	54
3.9 Hysteresis of the human tendon. (a) Deformation chart shows both loading and unloading paths for few cycles and (b) displacement chart shows 200 loading-unloading cycles. The preconditioned state of the tendon is reached for cycles above 50. Images taken from [26, 27] respectively.	55
3.10 Series-viscoelastic actuator proposed by Parietti et al. The end-effector is rigidly mounted on the revolving lever (i), which also supports the laser sensor. A Nylon line (ii) connects the end-effector handle to the high-precision piezoelectric force sensor (iii), which is fixed to a rigid support [28].	58
3.11 Developed soft rotary spring: a)photo and b)cross-section [29]. . . .	59

LIST OF FIGURES

3.12 Benchtop setup for rubber characterization and observer testing. The load side of the rubber is fixed. Load cells in-line with the rubber give rubber force measurements for testing. The choice of electric motors and transmission is illustrated [30]	60
4.1 Typical stress-strain curve of elastomers. There are three main regions: the toe region ($1.0 < \lambda < 1.5$), the elastic region ($1.5 < \lambda < 3.5$), and the yield/failure region ($\lambda > 3.5$) [31].	64
4.2 Hysteresis in stress-strain curve. [31].	67
4.3 Specimen Type C Dumbbell Layout from the ASTM D412 [32]. In this example, the specimen thickness is 3mm, the width is 6mm, and the initial length, l_o , is 33mm.	68
4.4 Undesired data on the tensile strength results. On the top left, the take-up slack phenomenon at the beginning of the experiment is observed. On the right, the different failure points of each specimen from the same material are highlighted.	70
4.5 Abrupt changes observed at the last portion of the stress-strain curve, caused by the different failure points for each specimen. This phenomenon is observed after unifying the data from all individual specimens of a specific strain rate, into a single stress-strain curve.	71
4.6 Stress-strain curves, during different strain rates, for the (a) EPR and (b) FR materials. On the bottom right, the initial section of the curve, where a linear behaviour was observed, is presented.	74
4.7 Stress-strain curves, during different strain rates, for the (a) NatPolR and (b) NR materials. On the bottom right, the initial section of the curve, where a linear behaviour was observed, is presented.	75
4.8 Stress-strain curves, during different strain rates, for the (a) PR and (b) SR materials. On the bottom right, the initial section of the curve, where a linear behaviour was observed, is presented.	76
4.9 Stress-strain curve, during different strain rates, for the NatR. On the bottom right, the initial section of the curve, where a linear behaviour was observed, is presented.	77
4.10 Offset Yield Strength for the FR material	79
4.11 Offset Yield Strength for the NatPolR material	80
4.12 Offset Yield Strength for the NR material	81
4.13 Offset Yield Strength for the PR material	82

LIST OF FIGURES

4.14	Offset Yield Strength for the NatR material	83
4.15	Offset Yield Strength for the SR and EPR (50mm/min) material. . .	84
4.16	Offset Yield Strength for the EPR (500mm/min) material	85
4.17	Stress Relaxation curves for (a) 180 minutes and (b) 15 minutes, of the EPR, FR, NatPolR, NR and SR materials. Different values of ε_o were investigated.	89
4.18	Stress Relaxation curves for (a) 180 minutes and (b) 15 minutes, of the PR, and NatR materials. Different values of ε_o were investigated.	90
5.1	Hooke's Law and linear viscoelastic models: (a) Hooke's Law (b) Kelvin-Voigt, (c) Maxwell, (d) Standard Linear Solid, and (e) Burger. The parameters k and η represent the spring stiffness and the dashpot viscous constant, respectively [33].	96
5.2	Wiechert Model. The components k_1 , η_1 , and the equilibrium spring k_e , together represents the SLS model. The components k_j , and η_j represents the Maxwell Branch. The Wiechert model can contain as many branches as required, this is symbolised by the subscript j . . .	97
5.3	(a) Standard Linearized Solid model with Strain-Dependent Stiffness. (b) Piecewise linearization method applied to the slope of the material load-displacement curve. This is analogous to many parallel springs which contribute to the material response depending on the material strain [33]	99
5.4	SLS model fitted to a typical stress relaxation curve of a viscoelastic material. The parameters k_e , k_1 and η can be obtained by analyzing three points in the curve: $t = 0$, $t = \tau$, and $t = \infty$. The variable τ is the time constant of the exponential decaying curve.	100
5.5	Obtained fit from the Standard Linear Solid (SLS) and Wiechert model on the stress relaxation curve of the Silicone Rubber material. The obtained optimal number of branches of the Wiechert model fit is $j = 8$	102
5.6	Relationship of the desired tolerance between the number of strain segments (blue bars), and the achievable NRMSE of the PL-SLS (solid red) and the PL-Wiechert (solid green) models, for all the soft materials (a-f) [34]	106

LIST OF FIGURES

- 5.7 Comparison between the experimental data from the Tensile Strength test and the stress response of the PL-SLS (dashed red) and the PL-Wiechert (solid green) models for all the soft materials (a-f). The number of strain segments required to meet the slope variation tolerance of 20% for each material are EPR=20, FR=37, NatPolR=88, NR=73, PR=455 and SR=33 [34] 109
- 5.8 Generalization capabilities of the PL-SLS model for the (a) EPR, (b) FR, (c) NR, (d) NatPolR, (e) PR and (f) SR materials. The strain dependent stiffness k^* is extracted from the stress-strain curve of the studied materials using a range of 10 different tolerance values. Subsequently, the obtained k^* is used to predict the stress-strain curves of the strain rates that were not used in the extraction of k^* 112
- 5.9 Generalization capabilities of the PL-SLS model for the NatR material. The chart was divided into two due to the large difference in the achieved NRMSE for the strain rate of (a) 250 mm/min and (b) 50 mm/min. The strain dependent stiffness k^* is fitted to the stress-strain curve of the materials for a 500 mm/min strain rate, using a range of 10 different tolerance values. Subsequently, the obtained k^* is used to predict the stress-strain curve of the mentioned materials for other strain rates. 113
- 5.10 PL-SLS model prediction of a strain rate different to the one used in the fitting process. (a) Worst prediction performance case, for the FR material stress-strain curve with mm/min strain rate. (b) Best prediction performance case, for the SR material stress-strain curve with mm/min strain rate. The chosen tolerances values for (a) and (b), were 50% and 10%, respectively. 114
- 6.1 (a) Feedforward artificial neural network (b) Internal structure of an artificial neuron [35] 120
- 6.2 Generalization error, based on a 10-fold cross-validation, for the (a) EPR, (b) FR, (c) NatPolR, (d) NR, (e) PR, and (f) SR materials. The best input combination is the one with the smallest generalization error, which in most cases if the FFRD4 configuration. 132

LIST OF FIGURES

6.3 Generalization error, based on a 10-fold cross-validation, for the (a) PR, (b) NR, and (c) NatR materials. The best input combination is the one with the smallest generalization error, which in most cases is the FFRD4 configuration.	133
6.4 Impact of the number of neurons on the Generalization error (a), (c), (e), and the R^2 value (b), (d), (f), for the EPR, FR, and NatPolR materials. A total of five training sessions were executed per number of neurons. The best R^2 value is circled.	136
6.5 Impact of the number of neurons on the Generalization error (a), (c), (e), and the R^2 value (b), (d), (f), for the NR, PR, and SR materials. A total of five training sessions were executed per number of neurons. The best R^2 value is circled.	137
6.6 Impact of the number of neurons on the Generalization error (a) and the R^2 value (b), for the NatR material. A total of five training sessions were executed per number of neurons. The best R^2 value is circled.	138
7.1 Simulink implementation of the ANN model. The ANN model takes the strain and strain rate as inputs, and delivers the stress response of the material in MPa as output. The gain blocks ensure that the units are consistent.	146
7.2 ANN model stress response to a sine wave strain input. The solid and dotted blue line are the strain and strain rate, respectively. The ANN model response is affected by both the frequency (a), (b), and the amplitude (c) of the input signal. Also, the ANN model is only stable when the strain rate presented to it is constant, as in (d) . . .	148
7.3 CAD Design of the detachable clamping device (a) Bottom part, (b) Final assembly, the soft material is coloured in black, and the T-shape attachment in blue. Units are in millimeters.	150
A.1 Knee joint characteristics for walking over ground activities. The weight next to the name of some activities dictates the load carried by the subjects during the experiment [16]. Data collected from: (1) [17], (2) [18], (3-8) [19].	164

LIST OF FIGURES

A.2 Ankle joint characteristics for walking over ground activities. The weight next to the name of some activities dictates the load carried by the subjects during the experiment [16]. Data collected from: (1) [17], (2) [18], (3-8) [19].	165
A.3 Hip joint characteristics for step ascending/descending experiments [16]. Data collected from: (1) [20], (2) [21], (3) [36].	165
A.4 Ankle joint characteristics for step ascending/descending experiments [16]. Data collected from: (1) [20], (2) [21], (3) [36].	166
A.5 Hip joint characteristics for ramp ascending/descending experiments [16]. Inclination in brackets. Data collected from [22]	166
A.6 Knee joint characteristics for ramp ascending/descending experiments [16]. Inclination in brackets. Data collected from [22].	167
A.7 Ankle joint characteristics for ramp ascending/descending experiments [16]. Inclination in brackets. Data collected from [22].	167
A.8 Hip joint characteristics for sit to stand/stand to sit experiments [16]. In brackets (h) healthy subjects, and (p) subjects with Parkinson's. Data collected from: (1) [23], (2) [24].	168
A.9 Knee joint characteristics for sit to stand/stand to sit experiments [16]. In brackets (h) healthy subjects, and (p) subjects with Parkinson's. Data collected from: (1) [23], (2) [24].	168
A.10 Ankle joint characteristics for sit to stand/stand to sit experiments [16]. In brackets (h) healthy subjects, and (p) subjects with Parkinson's. Data collected from: (1) [23], (2) [24].	169
B.1 Experimental setup 1. Two electric motors work together to create the co-contraction effect in the joint. The required instrumentation is highlighted in yellow. Two different inputs are provided, and the actuator's performance observed.	173
B.2 Experimental setup 2. Several motors activate in pairs to create co-contraction of the rotating joint. For the sake of clarity in the illustration, the two Bowden cables of each motor are grouped into a single orange cable.	175
B.3 Experimental setup 3. Same as in experiment 1 with the only variation of including a viscoelastic element in series with the rotating link.	176

LIST OF FIGURES

- B.4 Experimental setup 4. Same as in experiment 2 with the only variation of including a viscoelastic element in series with the rotating link. 176

LIST OF TABLES

2.1	Pneumatic artificial muscles main features. Modified from [37]	16
3.1	Colour code used in Figure 3.5 for each combination of age range and knee range of motion [16].	49
4.1	Number of specimens used per type of test	69
4.2	Elastic properties of the selection of soft materials. The materials are: Polyethylene Rubber (PR), Ethylene Polypropylene Rubber (EPR), Natural Rubber with Polyester (NatPolR), Natural Rubber (NatR), Silicone Rubber (SR), Fluorocarbon Rubber (FR), and Nitrile Rubber (NR).	86
4.3	Parameters and number of collected datasets for the stress relaxation tests.	87
4.4	Stress relaxation properties for the selection of soft materials.	88
6.1	Summary of proposed and optimized hyper-parameters.	129
6.2	Proposed ANN architectures. The architectures FFRI1, FFRI2 and FFRI3 are rate-independent, whereas the architecture FFRD4 is rate-dependent.	130
6.3	Proposed parameters for the selection of best inputs	131
6.4	Proposed hyper-parameters for the number of neurons optimization .	135
6.5	Best ANN candidate compared against the PL-SLS model. The generalization error is based on the mean NRMSE value. In the case of the PL-SLS the latter is based on the mean NRMSE value from the available strain rates in Figures 5.8 and 5.9	138

LIST OF TABLES

7.1	Viscoelastic properties of the patellar tendon and the quadriceps ligament ([27, 38, 39]), compared against the viscoelastic properties of the studied soft materials (Tables 4.2 and 4.4).	143
7.2	Matching factors required for the soft materials to achieve the human tendon E_{small} value. The width proposed for the material strips is 66 mm. (REVIEW THIS)	145
7.3	Simulation parameters	150
B.1	Torque requirements for each individual motor in relation to the number of participating motors in the task. The actuator's peak torque $T_p = 18\text{Nm}$ is based on the 50% of the knee joint peak torque (29 Nm).	174

Abbreviations

ADL	Activities of Daily Living	NatPolR	Natural Rubber with Polyester
ANN	Artificial Neural Network	NMAD	Normalized Mean Absolute Difference
ASTM	American Society for Testing and Materials	NR	Nitrile Rubber
BR	Bayesian Regularization	NRMSE	Normalized Root Mean Square Error
CE	Contractile Element	PAM	Pneumatic Artificial Muscle
CAM	Computer Assisted Manufacturing	PE	Passive Element
EPR	Ethylene Polypropylene rubber	PL	Piecewise Linearization
FEA	Finite Element Analysis	PHRI	Physical Human-Robot Interaction
FFNN	Feedforwad Artificial Neural Network	PR	Polyethylene Rubber
FFRD	Feedforwad Rate-dependent	RMSE	Root Mean Square Error
FR	Fluorocarbon Rubber	SE	Series Element
FFRI	Feedforwad Rate-independent	SDS	Strain-dependent Stiffness
HMS	Human Musculoskeletal System	SEA	Series-elastic Actuator
IMU	Inertial Measurement Unit	SLS	Standard Linear Solid
IPAM	Inverse Pneumatic Artificial Muscle	SMA	Shape Memory Alloy
KKP	Kinetic and Kinematic Parameters	SMP	Shape Memory Polymer
LDA	Large Deformation Actuators	SSE	Sum of Square Errors
LM	Levenberg-Marquardt	SR	Silicon rubber
LVM	Linear Viscoelastic Model	SVA	Series-viscoelastic Actuator
MAD	Mean Absolute Difference	TSSE	Total Sum of Square Errors
MSE	Mean Square Error	TPE	Thermoplastic Elastomer
NLS	Non-linear Spring	TPU	Thermoplastic Polyurethane
NatR	Natural Rubber		

Common Symbols

A_o	Cross-sectional Area
ΔL	Elongation
ΔL_o	Initial Elongation
E	Elastic Modulus
E_{large}	Elastic Modulus at Large Strains
E_{small}	Elastic Modulus at Small Strains
ε	Strain
ε_o	Initial Strain
ε_{offset}	Strain Offset
ε_u	Ultimate Strain
ε_{ue}	Engineering Ultimate Strain
ε_y	Yield Strain
η	Damper Constant
F	Force
k	Spring constant
k_e	Equilibrium Spring constant
k^*	Strain-dependent Spring
l_o	Initial Length
λ	Extension Ratio
$S.R.$	Stress Relaxation
σ	Stress
σ_{end}	Final Stress
σ_o	Initial Stress
σ_u	Ultimate Stress
σ_{ue}	Engineering Ultimate Stress
σ_y	Yield Stress
R^2	Coefficient of Determination

CHAPTER 1

Introduction

1. INTRODUCTION

1.1 Background

The field of Soft Robotics deals with the implementation of soft and deformable materials in traditional robotic applications. The interest in this field has increased in the past decade. The latter is due to the outstanding developments in terms of manufacturing of soft materials, such as elastomers, and the development of new soft materials which can be stimulated, i.e. deformed, by heat, light, and magnetism.

The coordination action called RoboSoft, supported by the IEEE Robotics and Automation Society (RAS) and the European Commission, has played a very important role in spreading the awareness of the wide number of soft robotic applications. The RoboSoft committee formally defines the field of Soft Robotics as “Soft robot/devices that can actively interact with the environment and can undergo ‘large’ deformations relying on inherent or structural compliance” [40]. The categorization of when a robotic application fall into the field of Soft Robotics depends on the material’s Young Modulus, a mechanical property which relates the material’s deformation with the amount of stress applied to it; which must be between the range of 10^2 – 10^6 Pascals (Pa). The Young’s modulus is usually a measure of a solid material stiffness; a high value refers to a stiff material in the same way as a low value refers to an elastic or soft material. In the context of Soft Robotics, the term compliance is commonly used instead of stiffness since it refers to the adaptability of the material under certain circumstances.

Early applications in Soft Robotics were inspired in nature, by observing that most biological organisms are not rigid, e.g. the human skeleton only contributes with 11% of an adult’s weight, on contrast, the skeletal muscle in our body only contributes with 42% of the weight [41]. This inspiration gave birth to several soft bio-inspired robots, as well as the interest in studying the embodied intelligence of biological organisms. The latter refers to the ability of biological organisms to adapt to different situations by exploring their body morphology and properties. This is one of the main differences between soft and rigid robots. The embodied intelligence of soft robots releases the controller from the task of accurately controlling the position of the robot and of constantly monitoring the working environment; allowing the controller to focus on the execution of commands. This is only possible with the implementation of soft and deformable materials able to automatically adapt to perturbations from the environment, such as uneven terrains and obstacles. Bio-inspired soft robots are now being developed for a broad range of applications, such as locomotion, manipulation, and even replicating biological processes such

as digestion. The research done in the field of Soft Robotics has an interesting multidisciplinary potential. For example, the locomotion of caterpillars and snake could be study by building a soft robot which replicates this motion. The knowledge extracted from this could be useful for the development of actuated bendable soft cylinders which ultimately could replace the current rigid tools being used in laparoscopic surgery [42].

The mechanical behaviour of soft materials is very difficult to model using traditional mathematical models due to their non-linear, time-dependent and strain-rate-dependent stress response. This great challenge motivated the research in Soft Robotics to develop bio-inspired soft bodies, arms and legs able to perform the task at hand using minimal control. This caused a shift in the traditional design approach for rigid robots from “rigidity by design, safety by sensors and control” to the design approach used in soft robots, “safety by design, performance by control”. The added feature of safety, inherent in most soft robots, allowed the development of Physical Human-Robot Interaction (PHRI) applications [43]. Many other challenges faced by this emerging field are: actuation of soft materials, development and implementation of soft sensors into soft robots, control systems able to deal with the nonlinear behaviour of soft materials, and modelling tools able to accurately predict the mechanical behaviour of soft materials in real-time [40, 44]. Most of these limitations come from the simple fact that soft robots cannot be considered as a chain of rigid links able to rotate or slide as common robots are, but soft robots are deformable and continuous which means that all the foundation in which Robotics is based on, is not easily transferable to the Soft Robotics field.

The design and development of soft robots is very challenging, but the potential benefits are many such as: soft robots have the potential of being very dexterous due to the ability of modifying their shape depending on the environment; soft robots can manipulate objects of different shapes, sizes; and most importantly soft robots are safe to interact with humans in the event of an unplanned collision [45]. These benefits highlight the potential of soft robotic applications for PHRI such as, orthoses, surgical tools, and wearable devices. This research aims to contribute to the technological advance of Soft Robotics for human assistance applications.

For a long time, humans have pursued the idea of increasing their strength, stamina and speed through different means. Nowadays, this is a reality due to the technological advances on wearable robotic devices, commonly known as robotic exoskeletons. This wearable device was motivated by military applications where

1. INTRODUCTION

a soldier is required to carry a heavy load in its back for a long period of time, ultimately causing him injuries or early fatigue. The robotic exoskeleton is able to carry a payload and transmit the payload weight to the ground, ideally relieving the wearer from feeling the payload, which allows the wearer to walk greater distances without premature fatigue. The rigid nature of these devices and the big actuators implemented to achieve forces able to enhance humans, impose many limitations, such as, restriction of body movements, interference on subject natural biomechanics and high inertia which impedes the device to follow the subject intentions smoothly, creating a drag feeling [46].

In the field of Soft Robotics, research is being done to develop a soft version of a robotic exoskeleton, formally called soft exosuit, in an attempt to solve the previously mentioned limitations. Soft exosuits are wearable robotic systems meant to be worn in the same way as clothes, by attaching both the actuation and perception systems into a wearable structure, made of textiles, strapped to the human body which will ultimately assist the wearer's motions. Despite the many benefits of this technology, in comparison to the robotic exoskeleton, current developments of soft exosuits are not able to deliver enough mechanical power to be called an enhancement device. Currently, soft exosuits are considered an assistive device. This limitation is inherent from the idea of having a soft wearable device. The accurate delivery of assistive forces generated by the actuators attached to a wearable textile, or directly to the user's body, is very challenging. In a rigid exoskeleton the reaction forces produced by the actuators are sustained by the exoskeleton mechanical frame, but this is not the case in soft exosuits, where the reaction forces must be dissipated through the worn textile attached to the human body, which generates uncomfortable frictions between the user skin and the textile. Nevertheless, the human body naturally possesses areas able to sustain high amounts of forces, these areas are currently being exploited into soft exosuit designs to prevent discomfort, skin injury, and to increase the efficiency of transmitted forces. The latter principle is implemented in [3] where a lower limb soft exosuit using pneumatic muscles is developed. The other, most common approach is to fix a wearable soft material to the skin, as in [1, 47] where pneumatic artificial muscles (PAM) were attached to a soft cloth and disposed in such a way that they can mimic the biological musculo-skeletal behaviour of a human foot. Among the available soft exosuit developments, few of them implements a closed loop control system, due to the high complexity of dealing with the non-linearity of soft materials.

The progress in the field of Soft Robotics has been very quick and very diverse. Most of the research is focused on studying the benefits of using a specific new soft material in a robotic application, leaving the control system on the background. This is mostly due to the complexity of developing a modelling tool to accurately predict the mechanical behaviour of soft materials. As previously mentioned, this is one of the main challenges in Soft Robotics applications and the main focus of this research.

In the literature, most of the works are based on one of two approaches, either a model-driven approach or a data-driven approach. On one hand, the model-driven approach, as suggested, is based on using mathematical models to predict the mechanical behaviour of soft materials. Due to the time-dependent properties, or viscoelasticity, exhibited in most soft materials, model-driven approaches use a set of equations for model viscoelasticity known as the Linear Viscoelastic Models (LVM). These models describe a material using two basic mechanical components, a spring and a dashpot, arranged in different configurations. Inside this group, there are two models which can be expanded as required. In theory, this means these two models could be able to describe the most complex soft material as long as they are expanded as required. In practice, expanding a mathematical model is translated into solving more equations at a given time, and this is translated into demanding more computational power. Therefore, the model-driven approach has a well-known trade-off between achievable accuracy and required computational power, making the deployment of control systems based on this approach prohibitive.

On the other hand, the data-driven approach is based on machine learning tools, specifically Artificial Neural Networks (ANNs). The implementation of these tools for the prediction of the mechanical behaviour of viscoelastic materials has been researched for more than a decade, showing very good performance. ANNs are very good at identifying patterns inside complex data. The training process is known to take plenty of time, depending on the complexity and amount of data. However, once the ANN is trained, they are able to receive an input and produce an output almost immediately. This is the main advantage of ANNs in comparison to model-driven approaches, which have to perform intensive calculations every time new data is presented as input.

As the field of machine learning advances, better tools are becoming available, which leaves room for performing optimizations on previous works and on assessing new machine learning algorithms. At the time of starting this research and at the

1. INTRODUCTION

best of my knowledge, there was no documented work assessing the performance of ANNs as an alternative to model-driven approach when being deployed as part of a control system for a robotic application. In other words, the real-time prediction performance of neural network has not been assessed. Therefore, this research aims to fill this gap in the body of knowledge.

1.2 Motivation

The global percentage of elderly population is constantly rising. The World Health Organization has estimated that the global percentage of people aged 65 or older will triple by 2050, with respect to 2010 [48]. Moreover, the amount of elderly people living alone is also increasing. Solely in the United Kingdom, there are 1 million people aged over 65 living on their own [49]. Although, the social triggers of the mentioned phenomenons are out of the scope of this research, they represent a strong motivation to push forward the research on Soft Robotics applications for human assistance. Currently, there are viable concepts of assistive exosuits targeted to increase the quality of life of elderly people during activities of daily living, such as walking over ground, ascending stairs, and using a chair. However, the concept of an assistive exosuit is relatively new, the first documented prototype is dated from 2013 [3]. The idea behind an exosuit is to translate the proven concept of a robotic exoskeleton, which is a heavy and bulky wearable device aimed to enhance the strength of humans, into a soft, light weight and compliance version aimed to provide assistance to the elderly or disabled people.

One of the main challenges in this field of research is the modelling of the mechanical behaviour of soft materials. The accuracy of current modelling approaches is restricted by the computational cost required. This prevent them to be deployed in most micro-controllers, due to the limited computational power available in this devices. Commercially ready exosuits might be possible in a decade time, meanwhile there is plenty of research to be done to translate well developed technologies used in Robotics into the field of Soft Robotics. Summarizing, this research can improve the quality of life of the elderly and disabled population by developing a novel modelling approach which will enable current soft actuation technologies to be more reliable when being implemented in soft exosuits.

1.3 Aims and Objectives

1.3.1 Aims

The aims of this research are:

- To investigate the concept of implementing viscoelasticity, a property found in the human skeletal muscle system, in soft robotic applications for the assistance of the human lower limb.
- To develop a reliable modelling tool to be implemented in a bio-inspired soft actuator for the prediction of the stress response of soft materials in real-time.

1.3.2 Objectives

In accordance to the research aims, the following objectives are identified:

- Survey the literature to identify: the terminology related to the biomechanics of the human lower limb, and the current soft robotic developments on the field of human assistance.
- Investigate the biomechanics of the human lower limb during activities of daily living.
- Characterize the viscoelastic properties of suitable soft materials.
- Identify the soft materials with the most similar mechanical properties to the human tendon.
- Address the limitations of the modelling tools currently being used for the prediction of the viscoelastic behaviour of soft materials, by optimizing a current modelling tool or by developing a new modelling tool.
- Develop a better modelling approach, or optimize current ones, to allow the accurate prediction of the viscoelastic stress response of soft materials.
- Assess the modelling tool prediction accuracy in a real-time environment.
- Design a bio-inspired soft actuation for human-assistance applications.

1. INTRODUCTION

1.4 Scope of the research

This research is focused on developing a reliable modelling tool, able to be implemented in a control system, for the prediction of the mechanical behaviour of soft materials. Therefore, the following is included in the scope of the research.

The biomechanics from the lower limb of the human body during several activities of daily living are characterized. The potential benefits of using a viscoelastic material instead of the traditional metallic spring in series-elastic actuators, is investigated. For this reason, the following soft materials are studied: ethylene polypropylene rubber (EPR [50]), fluorocarbon rubber (FR [51]), nitrile rubber (NR [52]), natural rubber with polyester (NatPolR [53]), polyethylene rubber (PR [54]), silicone rubber (SR [55]), and natural rubber (NatR [56]). A recent and accurate model-drive approach, based on a piecewise linearization of the Linear Viscoelastic Models (LVMs) is studied. Furthermore, a systematic analysis on the performance of a popular data-driven approach, Artificial Neural Networks (ANNs) is executed. The analysis includes the effect of the number of neurons, output activation function, training algorithm, and combination of inputs/outputs presented to the network. Moreover, a comparison analysis on the performance of these approaches when being implemented as part of a bio-inspired series-elastic actuator model, in a control system, is performed. The control system requirements are designed to meet the knee joint torque-speed characteristics during level ground walking. Finally, the most suitable modelling approach for this application is identified.

1.5 Contributions of the research

The research contributes to the field of Soft Robotics for human assistance by investigating the performance of Artificial Neural Networks, as an alternative to the Linear Viscoelastic Models, for the modelling of viscoelasticity in soft materials. Some parts of this thesis are published in peer-reviewed conference papers. The contributions are summarized as follows:

- Assessment of relationship between the accuracy and the mathematical complexity, of the Piecewise Linearized Standard Linear Solid model (PL-SLS).
- (REPHRASE THIS-COME BACK TO THIS WHEN ADDRESSING EXAMINERS CORRECTIONS: "which is to provide insight on the accuracy versus

complexity trade-off of applying the PL method to the Wiechert model") Development of a model-driven modelling approach, based on the piecewise linearization method, applied to one of the most complete LVMs, the Wiechert model.

- Development of a data-driven modelling approach, based on ANNs, for the prediction of the mechanical behaviour of soft materials.
- (This might need to be removed) Concept design of a bio-inspired series-elastic actuator, which uses the data-driven modelling approach to predict the mechanical behaviour of the soft elastic element in the actuator.

1.6 Outline of the thesis

This thesis is divided and organized in six chapters, as follows:

- **Chapter 1:** This chapter presents the research background, motivation of the researcher, aims and objectives. Moreover, the specific contributions of this research to the respective field of knowledge, and the scope of the thesis are also presented in here.
- **Chapter 2:** The second chapter describes the state of the art on Soft Robotics applied to human assistance. The latter is organized in three main sections: soft actuation technologies, soft perception systems and soft robotic controllers. However, the main focus of this chapter is directed to innovative soft actuation technologies by describing their advantages and limitations. The design approach of mimicking the human musculoskeletal functionality is also described in here. Finally, this literature review highlighted the research opportunities of implementing a soft material as the elastic element of traditional series-elastic actuators, replacing the commonly used metallic spring. To do this, a reliable modelling tool, able to predict the mechanical behaviour of soft materials, must be developed.
- **Chapter 3:** In this chapter, the terminology related to human biomechanics is presented. Also, the mechanical properties of the human muscle-tendon component is discussed. Polymer materials were identified as potential candidate to imitate the mechanical properties of the human tendon. Moreover, the characterization of the kinetic and kinematic parameters of the human lower

1. INTRODUCTION

limb during activities of daily living (ADLs), is performed. A total of four main ADLs are investigated from clinical trials: ground level walking, going up/down steps, going up/down a ramp and sitting down/standing up from a chair. The compiled data is processed to obtain a graphical representation and facilitate the comparison and analysis of the parameters variations from subject to subject and activity to activity. The work done in this chapter was substantial enough to produce a conference paper [16].

- **Chapter 4:** In this chapter, the characterization of a selection of seven composite materials is presented. The mechanical tests of tensile strength and stress relaxation are performed to characterize the viscoelastic properties of the materials. The processing of the data and extraction of the material parameters are described in detail.
- **Chapter 5:** (REPHRASE) This chapter describes the investigation performed on one of the most recently developed modelling tool focused on soft materials. In here, two models were developed based on the one available in the literature. These are the PL-Wiechert and the PL-SLS models. The performance of these models is assessed for the description of the nonlinear, time-dependent, and strain-dependent stress response of viscoelastic materials. The work done in this chapter was substantial enough to produce a conference paper [34].
- **Chapter 6:** In this chapter, the development of a data-driven modelling tool, based on artificial neural networks (ANNs), is presented. The research about implementing ANNs in the field of composite materials is very scarce. Nonetheless, ANNs have been proven useful for many function approximation applications. Two hyper-parameters of the developed ANN were optimized: the number of neurons in the hidden layers, and the selection of inputs. The ANN model was able to achieve a better accuracy than the PL-SLS model and also to generalize better, i.e. to account for the velocity-dependent stress response of the materials.
- **Chapter 7:** This chapter presents the design concept of a bio-inspired soft actuator. The work on this chapter is focused on design due to time limitations. Nonetheless, the concept design takes the bio-inspiration from the concept of mimicking the human skeletal muscle functionality. Therefore, a

comparison analysis between the mechanical properties of the human tendon and the studied soft materials is performed. Also, the ANN model is evaluated in real-time to observe its prediction capabilities when being deployed as part of a control system. In here, the design of a clamping mechanism is presented, which is aimed to be the interface between the actuator and a load in a series-viscoelastic actuator. Finally, the experimental protocol documented as part of this design process is presented in here, which is focused on investigating concepts such as co-contraction and variable recruitment, commonly functionalities of the human muscle-tendon component.

- **Chapter 8:** The final chapter is reserved for the summary, conclusions, and future work.

CHAPTER 2

Literature Review

2. LITERATURE REVIEW

2.1 Introduction

This chapter presents the performed literature review about soft robotic applications implemented in human assistance, such as soft exosuits and soft orthoses. The chapter is organized to present three main aspects of current soft robotic applications, which are the soft actuation system, the soft perception system, and the control system. In addition to this, the design process involved in developing soft wearable suits, as part of each soft robotic application, is described. Following the latter, the identified gaps in the body of knowledge are presented. Lastly, the relevant findings of the performed literature review are summarized at the end of this chapter.

2.2 Soft Robotics for Human Assistance Applications

The adoption of soft robotics in human assistance applications started with the replacement of rigid and bulky actuators, commonly used in traditional robotic exoskeletons, with soft and flexible actuators such as Pneumatic Artificial Muscles (PAMs) and cable-driven actuators. The latter gave birth to hybrid systems as found in [57], where a combination of both the previously mentioned technologies were implemented to overcome the limitation of having high inertia in robotic exoskeletons. The latter work also describes the first attempt of imitating the functionality of the human musculoskeletal system by using cable-driven actuators to transmit the forces created by the PAMs, which resembles the functionality of human muscle-tendon component.

During the following years of this transition many rigid devices were implementing soft actuators motivated by the same principle as mentioned earlier. However, in the early stages of soft robotics there was a lack of soft materials able to be implemented as actuators which encouraged researchers to focus mainly on pneumatic actuators [37]. As soft robotics gained popularity, researchers in material sciences started to develop new soft materials able to function as actuators. Nonetheless, there still plenty of research to be done to make these new materials safe to be used in soft robotic applications for human assistance. Due to this, current developments in soft exosuits and soft orthoses are built around two well established technologies: pneumatic artificial muscles (PAMs) and cable-driven actuators, commonly based

on electric motors, using Bowden cables as the pulling element. In a lesser quantity, technologies such as shape memory alloys (SMAs) and shape memory polymers (SMPs) have been implemented in soft orthoses with unsuccessful results mainly due to their large recovery time which make them unsuitable for human assistance applications. The extent of how these technologies have been implemented in soft robotic applications is presented in the next subsection.

2.2.1 Soft Actuation Technologies

2.2.1.1 Pneumatic Artificial Muscles

The usage of compressed air or gases into engineering applications is called Pneumatics, if an incompressible fluid is used, it is called Hydraulics; when applied in Soft Robotics, the idea is to expand or contract a soft material mainly to produce forces but it can also be used to produce different types of locomotion in particular soft robots. As previously mentioned, soft pneumatic actuators were extensively researched in different applications for Soft Robotics. in fact, the usage of soft polymers, such as silicone and elastomers, in combination with PAMs enabled different applications such as legged locomotion [58], pneumatic fingers for grasping objects with sensing capabilities [59], soft skin with embedded sensors [60, 61] and even implantable cardiac stimulators [62]. In the field of human assistance, soft pneumatic actuators can be categorized in four main groups: textile muscles, braided fluid muscles (McKibben type), large deformation actuators (LDA) bellows and LDA worm. Only the former three are suitable for some kind of human assistance, however, according to Belforte et al. [37], the most suitable for biomedical application in rehabilitation are the McKibben muscles due to the advantages described in Table 2.1.

Early works on assistance to human lower limbs using soft robotics [1, 63] describe a soft orthosis for the foot intended to treat gait pathologies, particularly the drop-foot condition. One important aspect of this device is its design, inspired in the musculoskeletal human system, i.e. the actuation system was designed to comply a muscle-tendon-ligament functionality mimicking the natural behaviour of the human body (Figure 2.1). The soft orthosis is powered by Mckibben-type pneumatic actuators. They are attached to a soft support structure consisting of an adapted neoprene knee sleeve and a five toed leather shoe. A total of three off-the-shelf pneumatic muscles assisted the dorsiflexion, eversion and inversion movements of the ankle joint by generating tension forces in artificial tendons, made of a flexible

2. LITERATURE REVIEW

Table 2.1: Pneumatic artificial muscles main features. Modified from [37]

Muscles Type	Advantages	Limits	Applications
Textile muscles	Easily connected to textiles: they can be used with flat end fittings	Operating pressure range: 1 bar; not negligible hysteresis; contractions of 10%–15%	Biomedical applications in rehabilitation
Braided fluid muscles (McKibben type)	Operating pressure range: up to 4 bar; Higher strength; Negligible hysteresis; Behavior independent of the applied load; Contractions of 25%; Easily connected to textiles: they can be used with flat end fittings		Biomedical applications in rehabilitation
Large deformation actuators: Bellows	Lightweight; Compact; Easy to handle; Large elongations	Possible misalignments in elongation phase	Movement of upper limbs
Large deformation actuators: Worm	Lightweight; Compact; Easy to handle; Large elongations	Low forces	Mini robot

but non-extensible metal cable, positioned close to the foot tendons (Figure 2.2(a)). The tendons were located inside a low friction material tube to prevent generated force losses; two of them were anchored to a single point in the foot brace while the other one was anchored in four different points in order to distribute the pulling force, again, mimicking the human body behaviour. The artificial ligaments provided with the same functionality as the biological ones, which is to restrict the movement of the tendons in all the directions other than the one of actuation (Figure 2.2(b)). The pneumatic actuators were strategically anchored in two points, at the bottom of the knee sleeve providing nonrestrictive motion of the knee, and at the foot brace.

Another soft orthosis using pneumatic actuation is presented in [2] which extends the concept of embedded sensor and create an embedded sensor-actuator module, which is referred to as a muscle-sensor unit. In order to obtain some degree of compliance with human's lower limb, the device has a cylindrical shape and it is made of a flexible silicone elastomer (EcoFlex 0300). The muscle-sensor units are

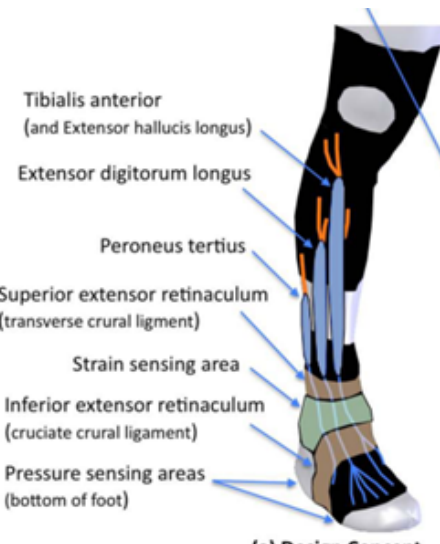


Figure 2.1: Bio-inspired active soft orthosis concept for the treatment of ankle-foot pathologies. From top to bottom: artificial muscles attached to the soft wearable garment, a strain sensor for ankle angle measurements, the tendon-ligament system and pressure sensor for gait cycle detection [1].

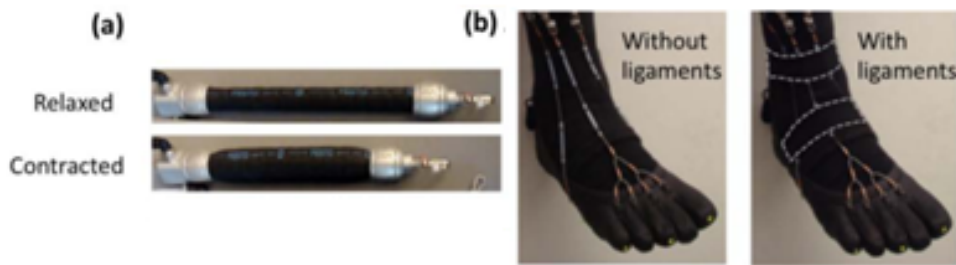


Figure 2.2: Soft orthosis components, (a) pneumatic artificial muscle in its relaxed and contracted state and. (b) complete tendon-ligament system without ligaments and with ligaments. [1].

embedded into the latter shape to form a distributed array of four columns and four rows (16 actuators), allowing the device to have plenty of different motions and delivered torques depending on the number of activated actuators at a given time (Figure 2.3). During the casting process, each column of actuators is tied to each other with Kevlar fibres so they can pull each other when contracting. The fibres are anchored to both caps of the cylinder to allow the desired movement to be achieved. When the pneumatic muscle is activated, its radius increases and its length decreases,

2. LITERATURE REVIEW

creating a compression force. This design provides some degree of modularity due to the many embedded actuators which can be activated independently. Nevertheless, it has little compliance with the human's lower limb which ultimately complicates the conversion of generated forces into useful torques for assisting the joint of interest.

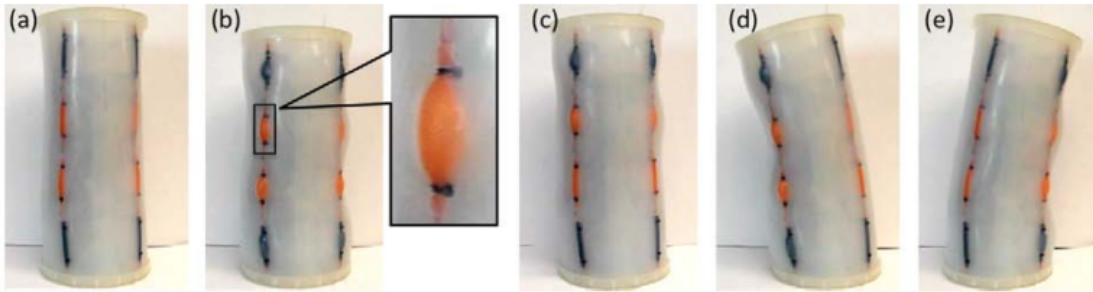


Figure 2.3: Different shapes achieved by the prototype. (a) Original shape. (b) All muscles activated, contracting the whole body and amplified image of one muscle. (c) Partial contraction, only the 1st and 2nd top rows are activated. Both (d) and (e) illustrate bending movements, only two adjacent columns are activated. [2].

On the other hand, a novel implementation called virtual anchor technique, which used pneumatic artificial muscles, can be seen in [3]. Addressing the challenge of force transmission using soft materials attached or strapped to the skin, which for high forces (such as those required in normal walking) will be intolerable for the user, the key anchor points of the human body are defined as the ones exhibiting large bony landmarks. These regions are able to withstand high forces and minimize the slippage or chaffing of soft materials positioning on them. Furthermore, the virtual anchor technique was also motivated by the changes in length of some parts of the skin surface during joint motion in where some parts exhibit more changes than others. Therefore, the soft exosuit was developed by interconnecting PAMs and nylon straps, replicating the extensible and non-extensible paths of the skin, respectively, in the specific points where the changes in the skin length take place, also called virtual anchor points which in combination with the key anchor points allow a good transmission of forces without causing discomfort to the user. In Figure 2.4 the described concept can be appreciated, the orange lines represent the pneumatic actuators interconnected with the key anchors and the virtual anchors. The latter constrain the actuator's movements other than the desired, as well as redirect the actuator's reaction forces to the body areas able to sustain them. Finally, this design was able to reduce the metabolic cost caused by wearing the complete

device of about 10 kg, by almost 100%. Considering that no control system, other than a timed activation sequence, and no perception system was implemented, this technique opens the door for further improvements to achieve a better degree of assistance.

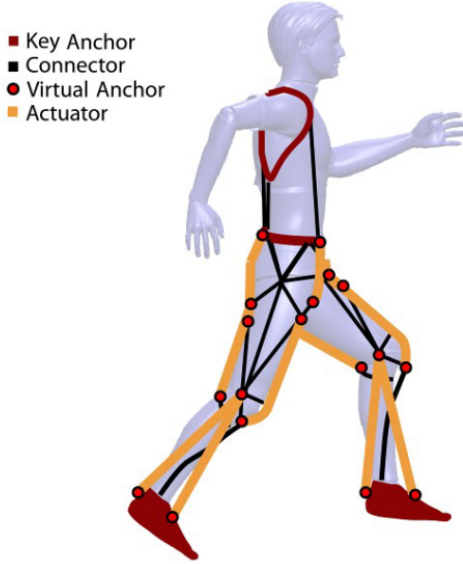


Figure 2.4: Virtual anchor concept. The three key anchors (red square) located at the foot, hip and shoulder are interconnected with the soft actuators (orange) and auxiliary connectors (black) in specific points called virtual anchors (red circle) to stabilize the forces created by the actuators. [3].

Putting aside the McKibben-type actuators as the most common choice for pneumatic muscles, elastomers such as high-flexible silicone can be used to build PAM as shown in [4]. This PAM consists of interconnected flat chambers made of silicone rubber which inflate when pressurized air is injected (Figure 2.5), the innovative concept in this work is the zero-volume air chamber which provides a higher degree of compliance and compactness (traditional PAMs retain air inside them even when they are not actuated). Kevlar fibres are embedded inside this soft actuator to constrain the expansion direction and create a contraction movement when pressurized. The flatness of this actuators simplifies the casting process. Furthermore, the chamber based design make it possible to join each chamber together not only in series, which increases the contraction length, but in parallel as well to increase the contraction force. In order to test the actuator performance, a soft exosuit similar to the previously described was developed using nylon straps and hooks to connect the soft actuator to the points of interest. The developed soft orthosis, intended

2. LITERATURE REVIEW

for infant-toddler rehabilitation, was able to deliver a 38 N contraction force and 18 mm contraction length by implementing a muscle with an array of four elastomer actuators inter-connected in series. In addition, a total excursion for the knee joint of 132° was achieved, considering both flexion and extension motions (Figure 2.5). Moreover, in a most recent development by [64], it can be found the implementation of elastomers for ankle assistance, in this case the pulling force of the PAM is generated when the actuator deflates and a pushing force is generated when it inflates, an inverted behaviour in comparison to previously mentioned applications. This soft orthosis consists of a regular sock which is attached to both ends of the PAM, that is enclosed into textile to restrict its longitudinal and radial expansion mainly. Despite the simplicity and assistance capabilities of the device, it cannot be worn with shoes, restricting the assistance to indoor activities

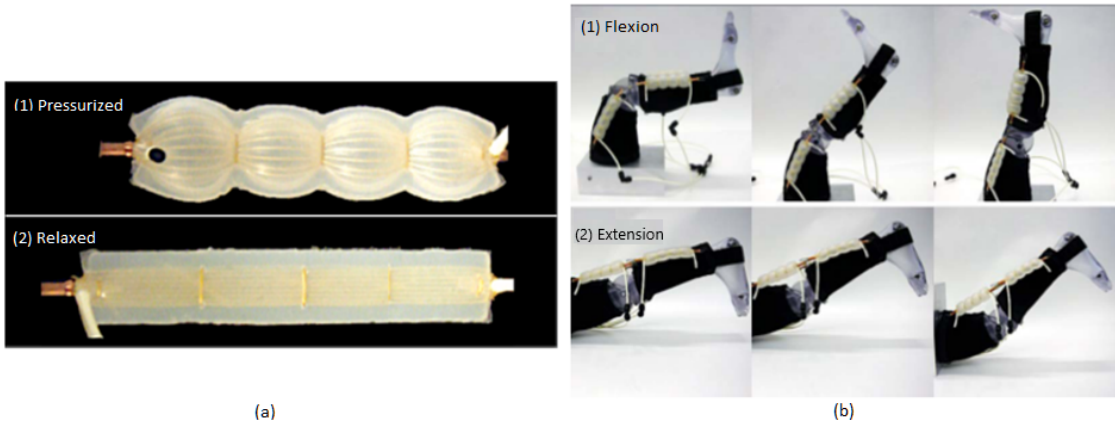


Figure 2.5: (a) Flat elastomer pneumatic actuator in its both (1) pressurized and (2) relaxed states. (b) Implementation of the flat actuator in medical leg model assistance, along with the achieved (1) extension, and (2) flexion motion. [4]

This concept, of expanding instead of contracting the PAM when pressurizing, is called Inverse PAM (IPAM). This soft actuator is called ‘Hydro Muscle’, and is directly compared with McKibben muscles since it overcomes the main limitations of the latter. The main difference between this actuator and the previously mentioned is the shift from pneumatic technology to hydraulics, in fact, it is reported that the pressure found in homes tap water is enough to actuate it [5]. Therefore, the cylindrical shape ‘Hydro Muscle’ is capable of elongating axially, increasing its stiffness radially, when pressurized; and of the exact opposite behaviour when de-pressurized (Figure 2.6). The actuator functionality is due to two structural layers of different materials. The inner layer is a tube made of an elastic material (latex

showed better performance than the commonly used silicon) and the outer layer is made of a soft but inelastic material, such as polyester, which restricts the inner layer radial expansion and allows its axial expansion. Despite the simplicity of the design, this new concept of actuator is free of energy losses in radial expansion. Also, the energy losses inherent when using compressed air as the power source are not present in this design (in comparison to PAMs).

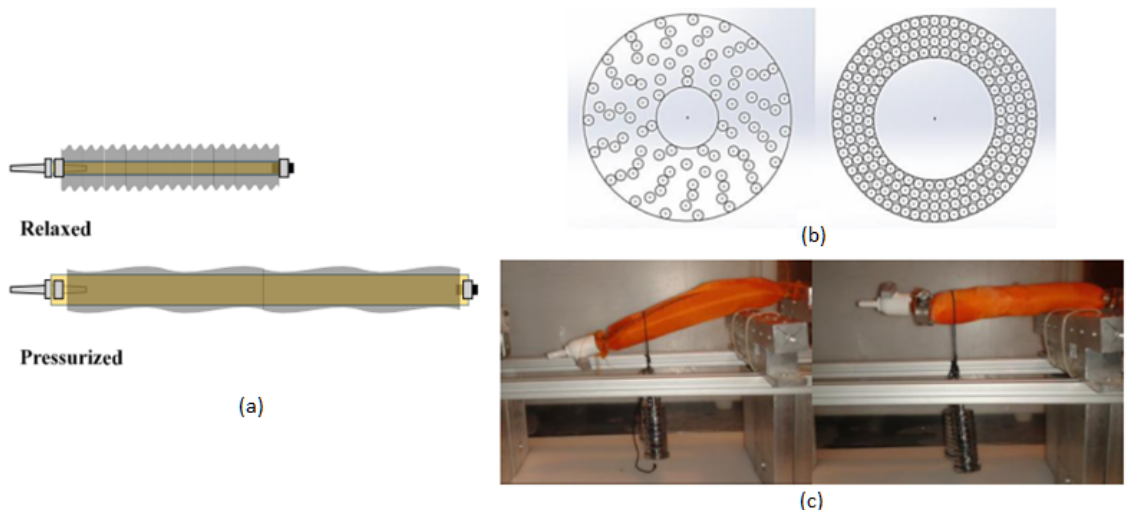


Figure 2.6: (a) IPAM developed in its relaxed and pressurized state, the small radial expansion and large axial expansion is appreciated. (b) Cross-sectional view of the jamming effect ongoing inside the actuator, and (c) bending effect caused by heavy load, and correction of the bending using the jamming effect [5].

The experiments performed in the paper showed that this innovative soft actuator is 33% more efficient in comparison to a McKibben muscle using hydraulics. Furthermore, this actuator can be easily manufactured with off-the-shelf components. On the other hand, the convenience of using both pneumatic and hydraulic muscles for performing pulling instead of pushing tasks, is to prevent the bending effect caused when the actuator is fixed in one of its ends and has a heavy load attached to the other end. The latter effect is amplified for pushing tasks being one of the main drawbacks of the proposed actuator concept. The solution to this is to use the principle of jamming by filling the gap between the inner and outer layer with granular media which will jam when the actuator is pressurized (Figure 2.6). Another IPAM which implements a very similar concept as the one illustrated in (Figure 2.6) can be found in [65]. This IPAM managed to achieve a strain of 300% of its length, which is three times more the achieved strain of the IPAM illustrated

2. LITERATURE REVIEW

in (Figure 2.6). This improvement is achieved due to the complete restriction on the stretchable material in the inner layer to only expand along its axis and not radially. The main benefits of recent IPAMs in comparison with traditional PAMs are reported as follows: high strain and nearly linear control (since no radial deformation is present). Finally, the ability to achieve high strains make IPAMs suitable for joints like the elbow.

2.2.1.2 Cable-driven Actuators

Another actuation technology implemented in soft orthoses are cable-driven actuators, based on electric motors, in combination with Bowden cables. Following the same principle as pneumatic muscles, this technology relies on generating tensions along a cable which, with a right positioning along the human lower limb, can transmit torques to the human body. The work in [6] presents the design and implementation of a battery operated soft exosuit built with Bowden cables (Figure 2.7).

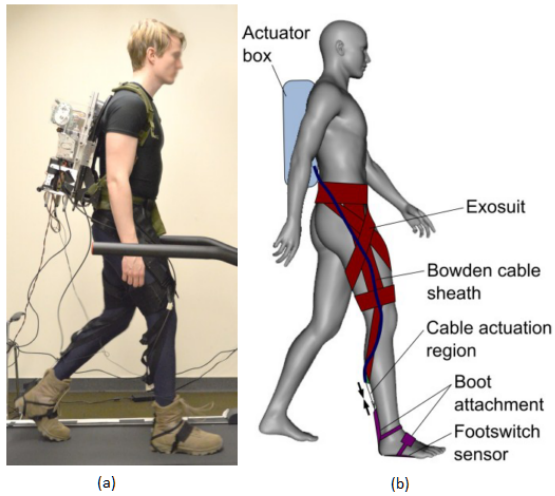


Figure 2.7: (a) Developed Bowden cable-based soft exosuit prototype. (b) Initial design concept highlighting the main parts of the soft exosuit. [6].

The exosuit is based on the leg's muscles functionality during normal walking, with the objective of assisting the forward propulsion stage of the gait. The soft exosuit structure made of fabrics is attached to the waist and above the knee, from the former the Bowden cable follows a path of webbing straps into the lower limb, ending at the ankle. In order to minimize the chaffing and displacement on the webbing strap structure caused by the tension on the cables while actuated, the

strap along the waist of the user terminates at the hip which is a natural bony part of the human body. In other words, there is almost no muscle and fat tissue between the skin and the bone, which improves the transmission of forces without causing discomfort to the user. This soft exosuit delivers 18% and 30% of the torques required for normal walking on the knee and hip, respectively. However, despite the innovative design, the main limitation of this exosuit structure is the large displacement experienced on its structure, of 13 cm, when the cables are under tension. This displacement caused the cable-driven actuators to have a very low efficiency since almost 45% of the generated mechanical power is lost in the form of friction forces in the soft exosuit structure. Nonetheless, the proposed multi-joint concept allows the actuation of two joints using a single actuator.

Following the multi-joint actuation concept, another soft exosuit is designed in [7] with the objective of not only providing assistance but also to enable impaired users. This concept, illustrated in (Figure 2.8), exploits the benefits of using a single cable-driven actuator to control more than one joint, i.e. multi-joint actuation. The difference in this case is the deep analysis performed regarding the compatibility of the joints, taking into account synergy of torque and equal polarity of torque, as well. In order to assist the desired movements of sit-to-stand, walking and stairs ascend, the knee and the hip joints were selected as the most suitable combination. Despite the limited scope of this work, being focused only on the concept design, the authors expect the selected joint combination to support the movements of sit-to-stand and stairs ascend.

The next follow up on the concept of multi-joint actuation is documented in [66] where a testing platform for soft exosuits was developed. The aim of this platform is to study the performance of the multi-joint actuation concept when being implemented in different soft exosuits. The off-board platform integrates several cable-driven actuators and the sensors required to evaluate their performance. In addition, this platform can deploy sensors to be attached to the exosuit and compare relevant metrics such as mechanical power efficiency. This platform, which can be re-configurable to meet different applications, has been used to evaluate the advantages of implementing single joint and multi-joint actuation [67], highlighting the benefits of the latter. Furthermore, the study performed with the aid of this platform provided designing parameters for the development of an exosuit, in other words, the multi-joint platform assists the designing phase, ultimately reducing designing times.

2. LITERATURE REVIEW

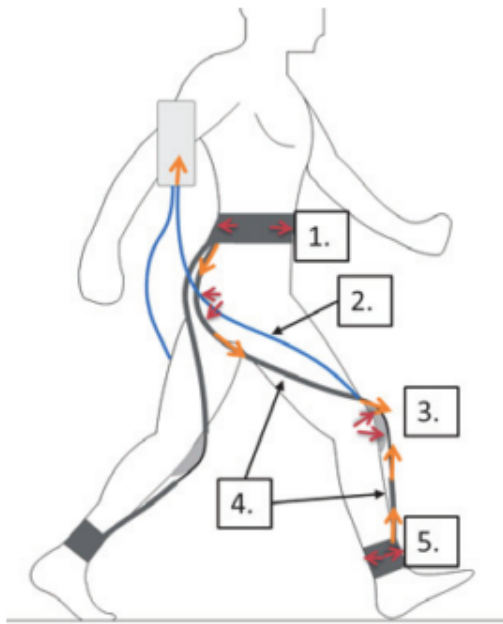


Figure 2.8: Soft exosuit implementing the multi-joint actuation concept. There are two anchor points, one at the pelvis (1) and one at the shank (5). The suit is actuated by a bowden cable (2) and positioned at the front of the knee. The contractile element is connected to the two anchors by webbing elements (4). Knee module to increase the lever arm (3). Red arrows: reaction forces, and orange arrows: actuation force [7].

2.2.1.3 Shape Memory Materials

The main two groups of shape memory materials implemented in soft robotics are: shape memory alloys (SMA) and shape memory polymers (SMP). Both technologies function under the same principle: they are able to switch into a different shape when a stimulus such as heat is in contact with them. Nevertheless, there are some differences to be mentioned. The SMA have two main phases, one for high temperature (austenite) and one for low temperature (martensite), when they suffer deformation while being in the martensite phase they can recover from the deformation by exposing them to heat, therefore SMA convert the energy from heat into mechanical energy to return to their original shape [8]. This property is usually exploited to cause contraction changes in the material (Figure 2.9). Therefore, SMA are commonly used in combination with cable-driven actuators.

The implementation of SMAs into robotic applications have three main challenges to be addressed: response speed, high power consumption and low opera-

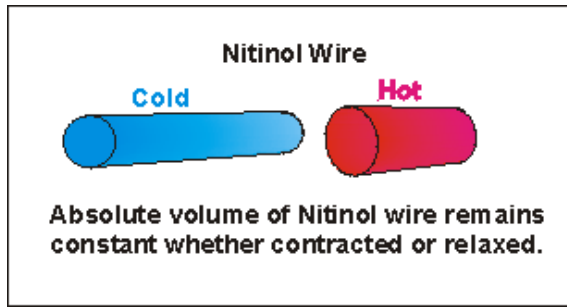


Figure 2.9: Shape memory alloys made of Nitinol. The contraction effect under the increase in temperature is illustrated [8]

tional bandwidth. The functionality of SMAs is based on the property found in metals in which heat is generated when an electric current flows through it, this is also known as the Joule effect. Depending on the metals used in the alloy, the amount of heat required for the SMA to recover from deformation is high enough to melt plastics, this excess of energy is what makes SMAs inefficient [68, 69]. Furthermore, SMAs have a very low response time due to the large amount of time required to cool them down, limiting their operation frequency. This limitation is only present when air convection is used as the cooling process. Due to this, SMAs have been found to be unsuitable for most orthoses in which an operating frequency of roughly 6 Hz is required. However, plenty of authors have successfully developed the latter devices, in both rigid [70] and soft variations [71], capable of assisting human motions proving to be suitable for applications such as clinical rehabilitation where slow and repetitive cycles are required [72, 73]. Two comprehensive reviews documented in [74, 75] report other applications where SMAs are being used, being some of these applications for rehabilitation such as: re-positioning, muscle toning, functional exercise and assistive robotics. Moreover, the review done by W. Coral in [75] also describes many works focused on addressing the SMAs limitations.

The very interesting work done by J. Zhang in [9] describes a SMA-based artificial muscle. This configuration facilitates the addition of a cooling system, due to the cylindrical hollow shape of the artificial muscle. Therefore, a mini pump is used to create a flow of air inside the artificial muscle which is able to reduce the cooling time by 10 times. The performance of this artificial muscle is further improved by taking into account the hysteresis behaviour typically found in SMAs when shifting between the low and high temperature phases. Furthermore, there is again evidence of trying to replicate the muscle-tendon functionality, in this case by adding a spring in series with the artificial muscle which aids the SMA recovery phase and simulate

2. LITERATURE REVIEW

a more realistic condition to the one at which the human muscles are subjected. The author is the first one able to model this behaviour and develop an adequate controller, which can be implemented in other scenarios involving SMAs. Finally, this artificial muscle is implemented into an active foot orthosis (Figure 2.10) which achieves large contractile forces by using in parallel more than one SMA wire to form each of the pulling tendons. The main drawbacks were having low efficiency and low operational bandwidth.

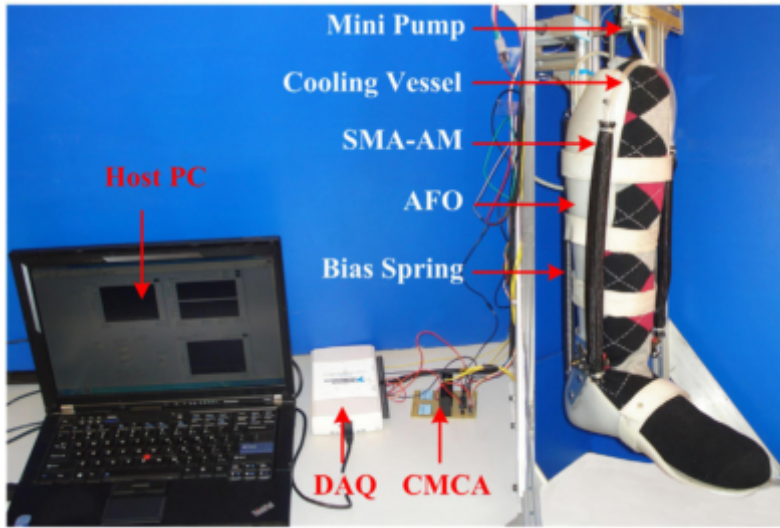


Figure 2.10: Developed soft orthosis for the ankle joint. The developed SMA artificial muscle along the main parts are highlighted. [9].

Current SMAs are also limited by the amount of contraction they can achieve, which is commonly 3% of its original length. The latter is also known as the operating bandwidth. Recent solutions to the latter limitation are based on deploying the SMAs in several loops, exploiting the same concept of using pulleys with cables, essentially increasing the usable length of the SMA wire without increasing the size of the final actuator. However, relying on pulleys in a soft actuator greatly reduce compliance, increase the actuator weight, and may cause twisting between the individual turns of the SMA wire. Therefore, a new approach described in [10], make use of the outer sheath of Bowden cables to contain the SMA wires inside. This concept allows the SMA to be directed in many ways to the point of interest, allowing the actuator to have different shapes that can be compliant with the user's body, e.g. the SMA can be wrapped around the user's arm in a solenoid-like shape which also increases the SMAs wire length (Figure 2.11). Furthermore, pulleys are also implemented to allow the SMAs to have a maximum number of three turns

contained inside the Bowden sheath. Two main drawbacks were discovered during an experimental testing: SMAs wires were twisting between each other which caused high friction losses and prevented the SMA to recover its initial length completely; the other drawback was the Bowden sheath material which was found to have low force transmission efficiency. In order to solve the latter, the Bowden cable sheath made of nylon was replaced by flexible tubes of Polytetrafluoroethylene (PTFE) and every SMA wire turn was individually encased in a narrow-gauge sheath. The final experiments showed that the developed actuator is able to contract 9% of its length which is three times the theoretical contraction length of an SMA wire.



Figure 2.11: Flexible actuator around the arm in a wrist exoskeleton prototype. [10].

Shape memory polymers (SMPs) are a little bit more complex than SMA. They have two main phases: a glassy state (high stiffness) and a rubbery state (low stiffness). Furthermore, when they are in their rubbery state, they can be deformed by applying small forces and preserve the deformation by cooling the SMP. In this state, the SMP can be considered rigid and it has to be heated to the point of the transition temperature to return to its original shape, hence having shape memory. This property of preserving a deformation is analyzed by K. Takashima et al. [11] in an attempt to boost the McKibben artificial muscle performance. McKibben actuators are unable to maintain their contraction shape unless precise and continuous control is implemented which cause premature wear on controlling elements as well as increase energy consumption. Therefore, a SMP is embedded into the McKibben braid which, by controlling the SMP temperature, allows the artificial muscle to hold its contracted position as illustrated in Figure 2.12. It is worth mentioning that SMP can be stimulating in different ways to obtain the change of shape, such as infrared

2. LITERATURE REVIEW

light, electric field, magnetic field and even manipulating the material water content. In this work, the SMP made use of a heating source as well as compressor which drastically limited the developed actuator portability, but as previously mentioned, different stimulus sources can be used for different SMP.

The benefits of SMPs, in comparison to SMAs, can be summarized as: light weight, low cost, rigidity in low temperature and flexibility in high temperature, higher strains (around 400% in comparison with 7% for SMAs), and they can be easily molded into 3D shapes. Furthermore, the main positive aspects of the improved McKibben are: allows rigidity fixing, the parameter to control stiffness can be used to control actuation, and controllability of the actuator surface by individually stimulating certain segments of the SMP.

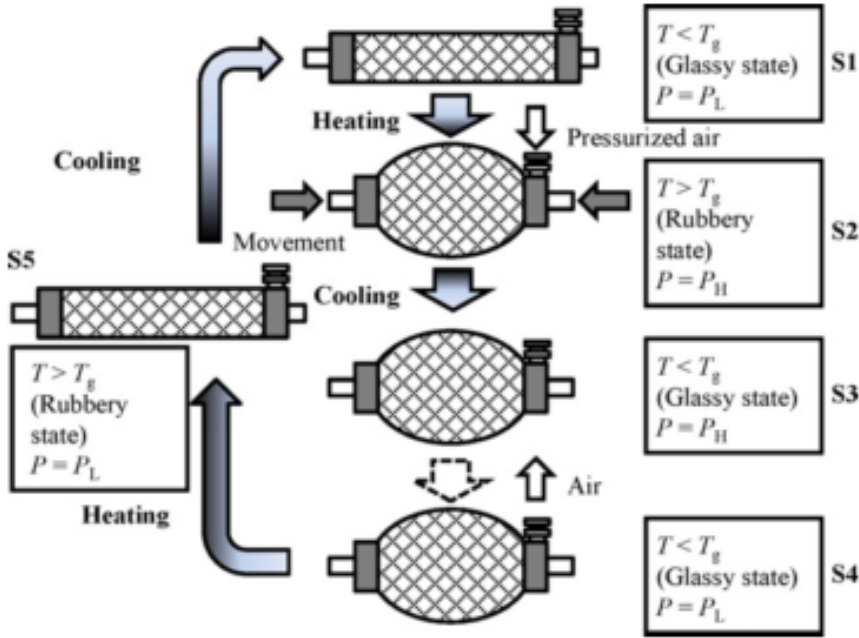


Figure 2.12: Schematic illustrating McKibben with embedded SMP functionality [11]. T_g : transition temperature, P_H : high pressure, P_L : low pressure.

2.2.2 Soft Perception Technologies

Currently, the most common soft perception technologies are based on liquid metal alloys embedded into soft materials such as elastomers. These strain soft sensors are widely used in soft orthoses, such as the one in [1]. The materials used in this case were Eutectic Gallium Indium (eGaIn), as the liquid metal alloy, and silicon

2.2 Soft Robotics for Human Assistance Applications

rubber as the flexible layer, which creates a highly deformable sensor (Figure 2.13). The sensor was implemented to measure changes in the ankle joint proportional to the skin strain which it was attached to, by measuring the changes in resistance caused by the variations in the path length and cross-sectional area of the channel containing the liquid metal. Nevertheless, the developed soft orthoses implemented two other non-soft sensors: an inertial measurement unit (IMU) as an angle position detection and a pressure sensor attached to the shoe insole to detect foot strikes, hence the gait cycle. The developed strain sensor delivered good performance and contributed in the development of a feedback controller for this soft orthosis.

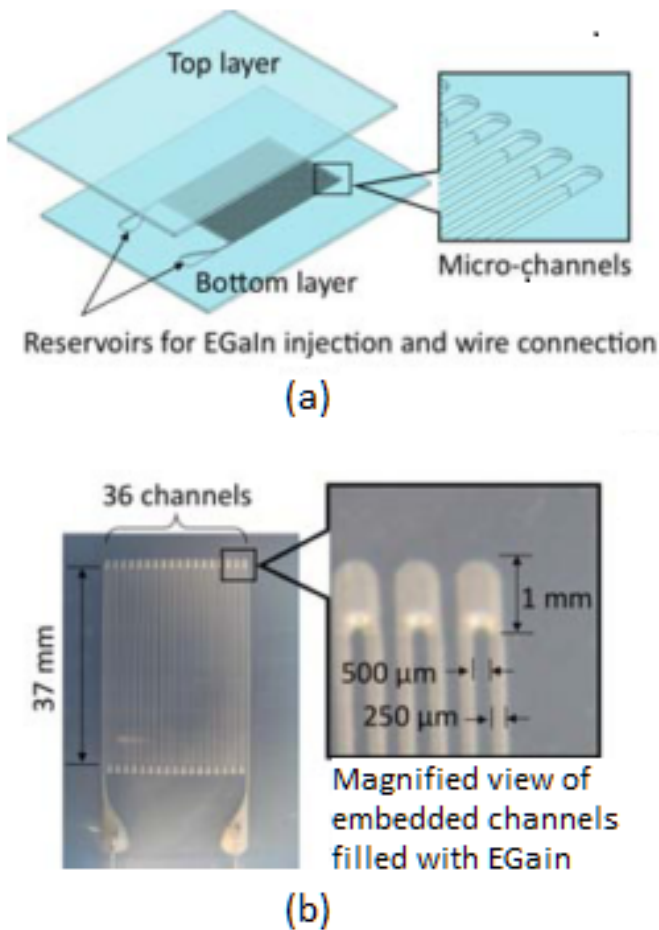


Figure 2.13: Soft strain sensor. The microchannel filled with liquid metal can be appreciated in: a) concept design and b) the prototype. [1].

Liquid metal alloys are also implemented in [2], as previously described, in the form of embedded muscle-sensor units (Figure 2.14). The soft strain sensor was able to estimate the contraction length of a pneumatic muscle by measuring its radial expansion. In order to preserve softness, thin flexible copper wires were embedded

2. LITERATURE REVIEW

into the cylindrical soft orthosis to obtain the sensor readings.

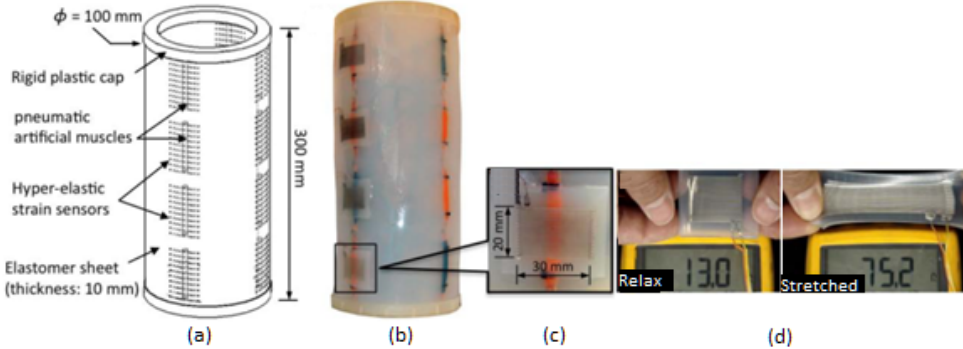


Figure 2.14: Soft sensor sleeve: (a) design concept, (b) developed prototype, (c) magnified view of the embedded sensor-actuator concept. (d) Soft strain sensor change in resistance during stretch and relax. [2].

Taking the application of soft strain sensors with eGaIn a step further, a wearable soft suit capable of sensing the joint angles of the hip, knee and ankle joints, is presented in [12]. With the sensors properly positioned along the lower limb, by measuring the strain caused by the joint rotation, the joint angle can be known. The sensors were able to track motions with a mean absolute error of 8° , being the most precise tracking achieved on the hip joint and the less precise on the ankle joint. In the mentioned work, only sagittal plane motions were measured, however, due to the great success and linearity of the sensors, they are planned to be implemented to measure motions in the frontal plane as well. The complete suit characterization can be found in [76], and is illustrated in Figure 2.15.

On the other hand, a potentially improved version of these soft strain sensors is presented in [13] where the highly stretchable elastomer is filled with two different conductive liquids, a traditional liquid metal and an ionic solution, instead of one. Interconnecting the strain soft sensor with the external application has been a big challenge, since the strain caused by the connection, usually soft wires, affects the sensor accuracy by increasing the total electrical resistance and by generating additional strain. Nevertheless, the ionic solution is intended to decouple the signal routing part from the sensing part in order to solve the latter challenge, creating a noise-free interface with the external application (Figure 2.16).

One direct implementation of the embedded microchannel with conductive fluid sensors, can be seen in a recent improvement to the McKibben type PAM (Figure 2.17). McKibben actuators were widely adopted in soft robotics applications and there is plenty of information in the literature about their implementations,

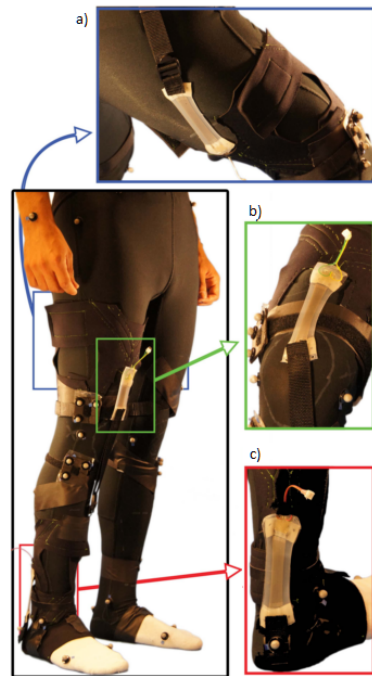


Figure 2.15: Implementation of soft strain sensors into a Soft sensing suit, (a) hip sensor, (b) knee sensor and (c) ankle sensor position. [12].

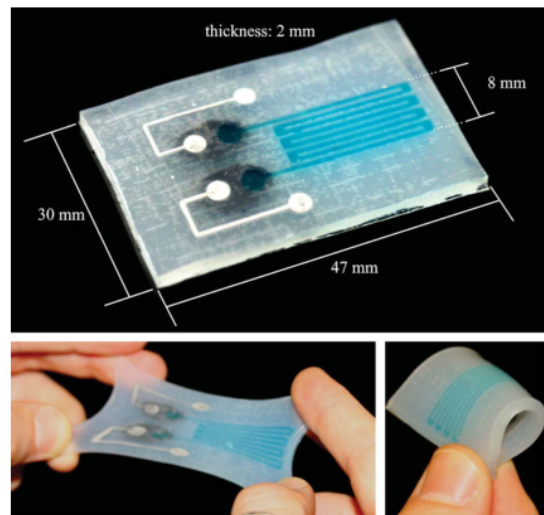


Figure 2.16: Hybrid soft strain sensor, the interface between the liquid metal and the ionic solution can be clearly seen in dark areas. [13].

2. LITERATURE REVIEW

modelling, etc. However, accurately sensing the deformation and force of these actuators still remains challenging. This has been addressed in many ways such as: cylindrical dielectric elastomers with carbon grease disposed on their surface to function as electrodes [77]; and also by attaching soft elastomer sheaths to the actuator, which are capable of sensing deformation due to their microchannels filled with conductive fluid [78]. The implementation of carbon grease electrodes and conductive microchannels allows the measuring of the actuator deformation. The conductive elements, mentioned before, change their electrical resistance when they are deformed. Furthermore, the concept of attaching these sensors to the actuator was refined in [14, 79], where the sensing elements surrounding the actuator are now disposed in a helical shape. From the electric circuit created, it is possible to measure both the output force and length deformation of the actuator by correlating them with the circuit resistance and inductance respectively. This work proposed the implementation of conductive wires to build the reinforced braid of a McKibben actuator allowing the actuator to ‘sense’, from there the given name of ‘Smart Braid’, creating a solenoid-like circuit from which the inductance can be measured using a couple of mathematical approximations such as: the Neumann approximation and the long solenoid approximation, being the former one the most accurate and general; but at the same time the most expensive in terms of computation. The author exerts that this new sensing concept can be applied to multitude of scenarios in soft robotics, which includes soft orthosis.

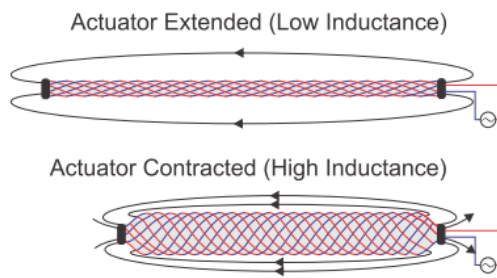


Figure 2.17: ‘Smart Braid’ concept. The variation in the actuator length cause a change in the electric circuit inductance. [14].

2.2.3 Control Technologies

One of the successfully implemented control systems is documented in [1], which forms part of the previously mentioned concept illustrated in Figure 2.13. The

control system is comprised of several micro-controllers for parallel processing, and is divided into four main stages: sensing, signal processing, control and actuation (Figure 2.18). The soft orthosis makes use of three different sensor technologies which requires different sampling and signal processing algorithms for each one, the IMU being the most complex one. Thereafter, another micro-controller with access to all the sensors, decides when to activate the solenoid valves that control the pneumatic muscles by generating pulse width modulated (PWM) signals. The latter describes a basic proportional control system. No mathematical model was deducted to describe the non-linear behaviour of the pneumatic muscles, instead, simpler controller approaches as feed forward and feedback controller were being implemented, with the latter being able to achieve a response time of 500 ms when a perturbation was present on the system, such as letting a weight hang from the device toe. The feedback controller made use of a soft strain sensor (Figure 2.13) to correct the ankle angle. Finally, although the controller performance is good it is still not enough to provide active gait assistance nor to predict user intentions. Another drawback, minor in this case, is that the system requires calibration every time a new user wears it. Nevertheless, the developed soft orthosis is suitable for rehabilitation because it can achieve a dorsiflexion of 12° and 20° when foot was at resting position, and when foot was forced to a plantarflexion position, respectively; in addition, the perception system could provide the clinician with meaningful data about the patient progress. The previous work was continued in [47] where a new controller was designed by considering the interaction between the soft exosuit and the human body as a black box, i.e. instead of trying to model the non-linear behaviour of the whole system some experiments were performed to obtain a system input/output relationship and after that implement classic control techniques to model a linear time-invariant controller. The results were promising since the original complex system was able to perform accurately using simple techniques. Finally, the implementation of electromyography sensors was discussed to add the involuntary muscle contractions of the user into the system as a disturbance and improve the accuracy during different scenarios.

In some cases, the design and development complexity of a controller for soft devices restrain the research extend to focus only on the implementation and study of soft actuation and perception systems. This is the case for the work documented in [2], the cylindrical soft sleeve with embedded muscle-sensor units; where the developed controller is well designed but with no close-loop architecture nor complex

2. LITERATURE REVIEW

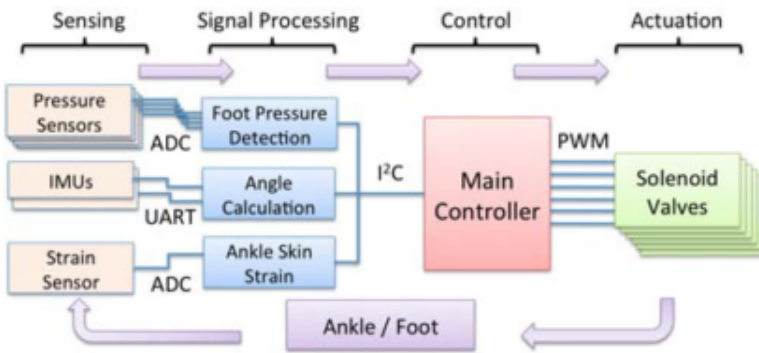


Figure 2.18: Control system architecture implemented for the ankle soft orthosis. [1].

mathematical model to predict the soft material behaviour. In the latter work, the control system consist of several micro-controller units, each of those communicated with their surrounding neighbours (Figure 2.14). Each of the 16 nodes embedded into the cylindrical soft sleeve has a microcontroller unit with independent functionalities, such as recollecting and distributing the data. On top of this, there is a scheduling routine embedded in each unit which allows the synchronization between the otherwise independent microcontroller units, simulating a network of microcontrollers. Every unit has four tasks to execute at a given time and a given order: sensing, communicate, process data and actuate. The actuation parameters are generated using a mathematical approximation of the soft material behaviour which assumes no other deformation around the soft sleeve is caused by the compression of the pneumatic actuators. This assumption neglects the fact that when one side of the cylinder is under compression, the opposite side is under tension, i.e. the length on this side does not remain constant. The authors highlighted the necessity for a better approximation method when analyzing the experimental results. For a desired bending angle of 15°, an actual bending angle of 11.5° was achieved. In simulation, feeding the soft sensors data into the mathematical approximation, a bending of 13° was estimated, which translates into an accuracy of 76%.

The fact that few soft exosuit developments fully implement a control system does not imply that no research is being performed in the field. The implementation of current soft actuators into functional devices, as well as the proof of concept of emerging soft actuators are usually followed by an extensive study about modelling their behaviour to translate that information into a control system. On the field of PAMs, many interesting new approaches are being researched, such as implementing

fuzzy logic techniques to improve their performance [80–83]. The next step in the research cycle of all the soft actuation technologies is to implement the tested models into functional devices, which then will allow new concepts to be developed, hence new modelling research to be performed.

2.3 Gaps in the Body of Knowledge

The available literature suggests a growing interest in the research and development of soft actuation technologies, soft perception systems, and control systems to pair with the latter two. Also, and following the bioinspiration driving the field of Soft Robotics, many works are attempting to imitate the capabilities of the human musculoskeletal system by developing soft actuators capable of behaving like the human muscle-tendon component. This is more evident when looking at the available works on Pneumatic Artificial Muscles (PAMs) described in Section 2.2.1.1, where an actuator is used as the contractile force generator element (muscle), and a flexible interface (tendon) is used to transmit that force to the desired location. Similarly, established technologies such as electric motors, which are able to deliver forces in both directions of rotation, are being used in combination with Bowden cables to create pulling forces, as mentioned in Section 2.2.1.2. This type of setup is known as a redundant system because more than one actuator is required to control both directions of rotation of a joint. Moreover, the research and development of new soft materials, such as the SMA and SMP, is also focused on creating materials able to contract when stimulated. There is still plenty of work to be done in this matter, which is why this is identified as one gap in the body of knowledge.

The vast majority of available literature is focused on testing a new soft actuation concept in an open-loop environment, i.e. with no control system implemented. This is caused by the fact that modelling the mechanical behaviour of a soft material is very complex. Even the control system of the most documented work in the literature, the ankle-foot orthosis, does not implement a modelling technique to monitor the behaviour of the PAMs, instead it is focused on extracting as many information as possible from the environment and use this to decide when and how to activate the PAM [1]. The scarce literature about the control systems of soft robotic applications, as evidenced in Section 2.2.3, is identified as another gap in the body of knowledge.

Therefore, two main gaps are considered in the body of knowledge which are

2. LITERATURE REVIEW

addressed by this research. On the one hand, there is still many work to do in understanding the functionality of the human musculoskeletal system, and in developing a soft actuation technology which mimics the functionality of the muscle-tendon component. On the other hand, there is a lack of reliable modelling tools to predict the complex mechanical behaviour of soft materials being used in soft actuation technologies.

2.4 Summary

According to the literature, the most commonly implemented soft actuation technologies in soft robotic applications for human assistance are: Pneumatic/hydraulic artificial muscles, cable-driven actuators based on electric motors, and shape memory alloys/polymers. In cable-driven actuators, the amount of generated assistance is proportional to the electric motor mechanical output power. This means, large forces can be generated to even enhance the user capabilities, yet again, the transmission of these forces via the human body prevents this enhancement. A common problem is the relative displacement of the soft structure worn by the user when tensile forces are generated by the pulling action of Bowden cables. Nevertheless, one advantage of this technology in soft exosuits is the ‘remote’ actuation capability, which means that the electrical motors can be placed distal to the joint to be assisted, concentrating the weight of the heavy parts of the soft exosuit in convenient locations of the human body, e.g. as a backpack. Another advantage of this technology is the flexibility of the Bowden cables which allows them to be deployed in many different trajectories along the human body, facilitating the use of the body parts capable of sustaining high forces.

In contrast, the other two soft technologies are commonly placed proximal to the joint to be assisted, which might allow a better distribution of the soft orthosis weight. Recent works have tackled the main limitations of PAMs, SMA and SMP. Particularly, big improvements have been achieved for PAMs and SMA. For the case of PAMs, the traditional and extensively implemented McKibben type muscle have been improved in terms of performance by the development of the Inverse PAM (IPAM). This latter technology surpasses the McKibben type muscle in assistance capabilities, efficiency and controllability. Furthermore, the concept of the IPAM can also be implemented using hydraulics which again comes with several advantages, a crucial one, the amount of generated force. The main disadvantage of both

pneumatic and hydraulic actuators is the need for a compressor unit, which greatly decreases the soft orthosis autonomy and portability. Nevertheless, the recently developed ‘Hydro Muscle’, which uses pressurized water from a home tap, greatly increases the appealing of this technology. In a similar way, the greater efficiency of IPAMs allows portable tanks with pressurized air to be used.

The situation is quite similar for SMAs, many of the limitations from this technology, such as low strain, slow speed response and complex controllability have been addressed and improved. However, this technology is still in its early stages and their main drawbacks are high energy consumption and large amounts of generated heat, which makes them unsafe for human assistance applications. In the field of soft sensors, one of the main advantages of the soft strain sensors is that they can be custom-built to fit any application. When characterizing these sensors, two parameters are always mentioned: the electrical resistance and the gauge factor, the latter relates the strain with the change in resistance. Despite their original purpose of measuring strain changes, they can be used for angle measurements. On the controller side, the amount of research being performed in modelling the complex behaviour of soft actuators is slowly but constantly increasing. Nevertheless, the complexity of tackling the latter is evidenced in the scarce literature available.

In summary, this literature review highlighted a very specific and bioinspired trend in soft robotic applications for human assistance, which is mimicking the human musculoskeletal system, specifically the muscle-tendon component. This approach is very compatible with soft technologies that are commonly placed proximal to the assisted joint (PAMs, SMAs, IPAMs, etc.), and many soft artificial muscles have already been developed. These works, however, have mainly focused on the contractile element of the muscle-tendon component, leaving plenty of room to research about the viscoelastic element, the tendon. The most straightforward way to study the potential benefits of mimicking the human tendon behaviour is to incorporate soft materials to current soft actuation technologies as part of the mechanism to transmit generated forces. Essentially, creating a soft artificial tendon. Nevertheless, the success of maturing the previous concept into a soft robotic application greatly depends on having a reliable modelling tool which predicts the mechanical behaviour of soft materials. Finally, as mentioned in Section 2.3, this research aims to address two main gaps in the body of knowledge. On the one hand, the lack of literature about the implementation of soft materials as part of the force transmitting mechanism, which could allow for a better mimicking of the human

2. LITERATURE REVIEW

musculoskeletal system. On the other hand, the lack of a modelling tool able to predict the mechanical behaviour of soft materials.

CHAPTER 3

Biomechanics of the Lower Limb as Design
Guidelines for Assistive Devices

3.1 Introduction

Previously, the bioinspired trend of mimicking the human skeletal muscle system, specifically the muscle-tendon component, in soft robotic applications for human assistance was identified. The available literature is mainly focused on the muscle component. In line with the aims of this research, this chapter is focused on understanding the biomechanics of the human body, specifically of the lower limb due to its great contribution on the Activities of Daily Living (ADLs). Therefore this chapter is divided as follows. Section one focuses on understanding the terminology involved in the biomechanics of the human lower limb. In section two, many clinical trials, also known as gait analysis, are reviewed to characterize the parameters of torque, angle, and power of the human lower limb during ADLs. Section three describes the muscle-tendon component from a mechanical perspective. Section four introduces many recent works and approaches which attempt to translate the functionality of the muscle-tendon component into soft robotic applications. Section five describes how recent works are addressing the lack of modelling tools for soft materials, considering two main modelling approaches: model-driven and data-driven. Finally, the last section presents a summary of the relevant findings of this chapter.

3.2 Characterization of Kinematic and Kinetic Parameters for Activities of Daily Living

The biomechanics of the human lower limb are self-contained between three planes of action, which are the sagittal plane, the frontal plane and the transverse (horizontal) plane [15]. In combination with these planes there are three axes used to identify specific motions: frontal horizontal axis, vertical axis and sagittal horizontal axis. The positioning of each of them is illustrated in Figure 3.1. The sagittal plane divides the body vertically into left and right parts, the frontal plane divides the body vertically into front (posterior) and back (anterior) parts and the transverse plane divides the body horizontally into upper (superior) and lower (inferior) parts. This coordinate system allows the many motions of each joint in the human body to be clearly identified.

3. BIOMECHANICS OF THE LOWER LIMB AS DESIGN GUIDELINES FOR ASSISTIVE DEVICES

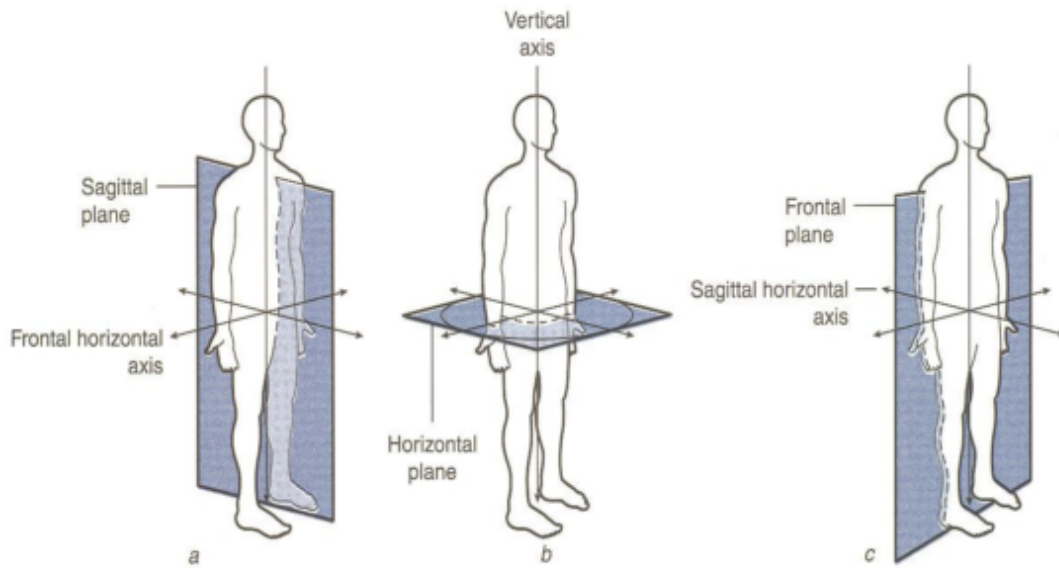


Figure 3.1: Dimensional spaces used to understand human motions: a) Sagittal plane, b) Horizontal plane and c) Frontal plane. [15].

The motions of each joint are named according to the plane and axis where they happen. This allows the easy recognition of the human body motions (Figure 3.2). The biomechanics of the lower limb are categorized in five groups, each containing two individual motions, as follows:

- Flexion and extension describe the bending motion which decreases, or increases the angle between two parts of the body, respectively.
- Abduction and adduction describe the motion away from, or towards the body midline, respectively.
- Eversion and inversion of the foot describe the motion away from, or towards the body midline, respectively.
- External rotation and internal rotation describe the motion away from, or towards the body midline, respectively.
- Horizontal abduction and adduction describe the motion away from, or towards the body midline, respectively.

3.2 Characterization of Kinematic and Kinetic Parameters for Activities of Daily Living

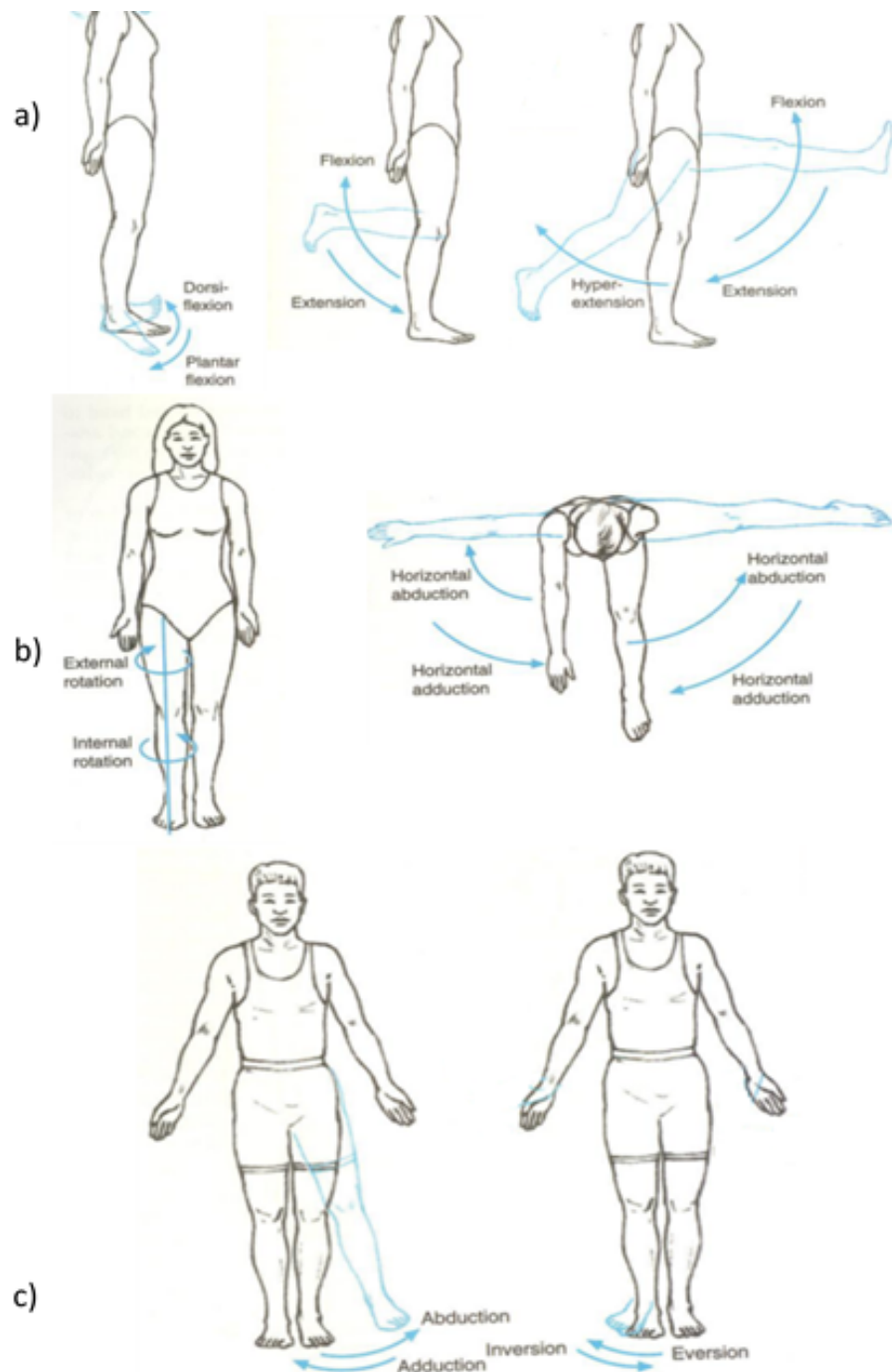


Figure 3.2: Lower limb motions for a) sagittal plane, b) horizontal plane and c) frontal plane. Image adapted from [15].

3. BIOMECHANICS OF THE LOWER LIMB AS DESIGN GUIDELINES FOR ASSISTIVE DEVICES

The biomechanics of the lower limb also involves a set of kinetic and kinematic parameters of each joint. The kinematic parameters describe the human body motion in terms of the joint angle, velocity, and acceleration. The kinetic parameters describe the forces causing this motion, e.g. joint torque and power. Motion capture is the most commonly used method to extract these parameters. However, other technologies such as soft strain sensors [76], electrogoniometers [85], and inertial measurement units (IMU) have also been used. The process of characterizing these parameters is very important for the development of any wearable robotic device. This allows the intended device to be tailored for a specific application, it being assisting an elder adult or enabling a disabled subject to move. Alternatively, the kinetic and kinematic parameters can be also used to measure the effectiveness and compatibility of an already available assistive device. Measuring the effectiveness of an assistive device in this way is more convenient than calculating the metabolic cost reduction, which involves specialized equipment [84].

The kinetic and kinematic parameters can be obtained from gait studies. These studies differ between one another in many aspects, in addition to the technology of choice, such as subjects' gender, age, weight, etc., as well as the setup of the experiments. Therefore, the following subsection describes the process of extracting and digesting the kinetic and kinematic parameters from gait studies. As previously mentioned, these parameters are useful design guidelines for wearable robotic devices. The gait studies compiled in the following section cover the main activities of daily living (ADLs), which are: walking, ascending/descending stairs, ascending/descending ramps and chair sitting down/standing up. In the context of studying the human lower limb, the joints of interest are the hip, knee and ankle joints.

3.2.1 Gait Analysis Data

In clinical studies focused on analyzing the human gait, parameters regarding the subjects involved and the experiment performed are commonly provided. Regarding the subjects characteristics, information about their age, subject age, weight, height, gender and health condition are included. Similarly, contextual information about the experiment performed such as: loading conditions, plane geometry, and activity of choice is provided. Subjects characteristics are always presented in mean values with the respect to the whole group participating. In a similar way, measured and calculated data, such as torque and power, is presented in mean normalized values.

3.2 Characterization of Kinematic and Kinetic Parameters for Activities of Daily Living

The gait cycle is usually normalized using the subjects height, whereas the joint torques are normalized using the subjects weight. The latter is clearly expressed in the units of the reported values, being Nm/kg for the joint torque, and W/kg for the joint mechanical power. Nonetheless, some studies do not follow the same guidelines when reporting the obtained results, or when normalizing the calculated values, preventing the reported information to be compared against other clinical studies [18].

The diversity on the subjects characteristics difficult the comparison process against similar clinical studies. Due to this, some clinical studies focuses on studying a common characteristic among all participants, such as age or health condition. This is the case for the performed in [17], where the study group is segmented in two age groups. One group included subjects from 22 to 72 years old, meanwhile, the subjects from the other group have ages ranged from 6 to 17 years old. With this segmentation approach, the clinical study can present the results with respect to age range. In some cases where the difference between age groups is very small, the clinical study condense the reported data into a single dataset [18].

The technology of choice to extract the kinematic parameters of the human gait, such as the joint angle, is motion capture. Similarly, the human body kinetics parameters are extracted by measuring the ground reaction forces using force plates. The latter is required to calculate the joint torque and joint power. Therefore, the three most common parameters found in gait analysis studies are the angle, torque, and power of the joint of interest. The gait cycle of the studied activity is usually presented in a chart accompanied with tables to clearly indicates the maximum, minimum and mean values of the gait cycle. The difference between the maximum and minimum values of the kinematic and kinetic parameters of a gait cycle are very important for the characterization process. Commonly, these values are provided in the studies in the form of tables and charts [19, 86], in other cases the complete experiment dataset is included [87]. The extraction of the parameter of interest is straightforward when the data is presented in a form of a table. Alternatively, when data is provided in the form of charts, the process of extracting it must be done by visual inspection, which inherently add some degree of error to the extracted value [20–24]. Likewise, it can be the case for some studies to focus on specific features of the gait cycle, such as maximum and minimum values of each parameter; or not provide one or more of the parameters of interest (angle, torque or power). Due to all these different scenarios, the process of curating and compiling the data found

3. BIOMECHANICS OF THE LOWER LIMB AS DESIGN GUIDELINES FOR ASSISTIVE DEVICES

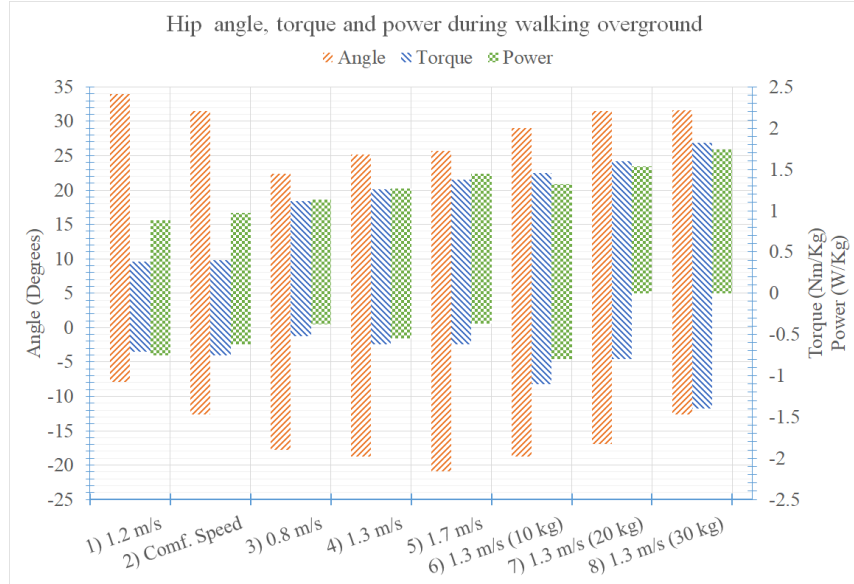
in clinical studies is very lengthily. The latter motivated the process described in the following section in which the data of several clinical studies is compiled and visually presented to serve as design guidelines for the development of soft robotic applications for human assistance.

Add introductory paragraph to this section.

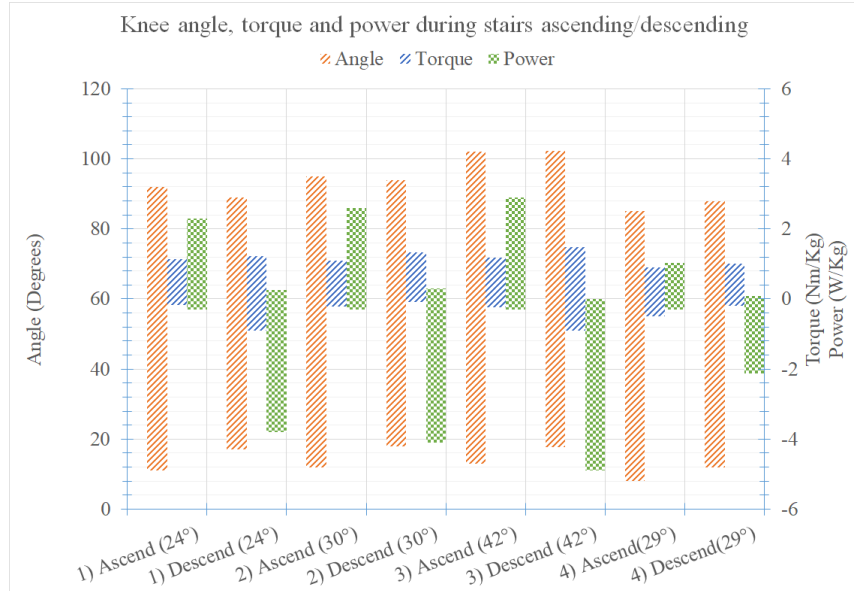
The variations of the data from one experiment to another can be reduced by focusing on the range obtained from the difference between the maximum and minimum values of each parameter. This is illustrated in Figure 3.3a, despite the variations between the maximum and minimum values from one experiment to another, the actual range of each parameter is similar among all the experiments. The mean range of motion for the hip joint angle throughout different walking over-ground experiments was found to be 44.63° (Figure 3.3a). Also, the greatest variation between the mean range value and the range value of each experiment is 18% of the mean value. The previous calculation can be used to decide design parameters of wearable robotic devices, such as which range of motion should be covered by the device depending on which sector of the population is intended to be assisted. Alternatively, the device can be tailored to cover as much of the population as possible by choosing the maximum and minimum values of the range of motion, out of all the experiments.

Different design guidelines can be extracted when visually analyzing other parameters together. For example, in Figure 3.3b , the parameters of the knee joint are now compared against many experiments of stairs ascending/descending. Now, the main feature is not the range of motion of the knee, but the characteristics of the torque values. They appeared mirrored, in other words, the torque values required for descending stairs are of similar magnitudes but opposite in direction. Also, the amount required for ascending stairs is generally twice as much as the amount required for descending stairs. The latter illustrates an optimization opportunity. When designing a wearable robotic device for human assistance, the actuator is chosen to satisfy a certain torque range of a particular activity. Without the characterization of the parameters performed, the actuator is most likely to be oversized to comply with the most demanding part of the activity. However, a different approach could be proposed: agonist-antagonist actuators; a technique implemented in several wearable robotic devices which at the same time complies with the actual

3.2 Characterization of Kinematic and Kinetic Parameters for Activities of Daily Living



(a) Hip joint characteristics for walking over ground activities. The weight next to the name of some activities dictates the load carried by the subjects during the experiment [16]. Data collected from: (1) [17], (2) [18], (3-8) [19].



(b) Knee joint characteristics for several stairs ascending/descending experiments. The number enclosed in brackets represents the stairs slope. Data collected from: (1) [21], (2-4) [36].

Figure 3.3: Clustered-stacked bar charts of reviewed gait analyses [16].

3. BIOMECHANICS OF THE LOWER LIMB AS DESIGN GUIDELINES FOR ASSISTIVE DEVICES

functionality of the human skeletal muscle system.

Another useful way of extracting design guidelines from the gait analyses is to plot the range of a specific parameter against different ADLs. To the best of the author's knowledge, this approach has only been documented once in [88], where the range of motion of the knee joint is compiled into a chart for 11 different ADLs. This concept, illustrated in Figure 3.4, can provide insight of two important design parameters. On the one hand, the actuators meant for this application must be able to deliver torques in both directions of rotation, i.e. clockwise and anti-clockwise. On the other hand, the selected actuation technology must meet the torque requirements of the activity of interest, illustrated in Figure 3.4. Figure 3.4 was constructed using the mean range of the hip joint torque during different activities [17–24].

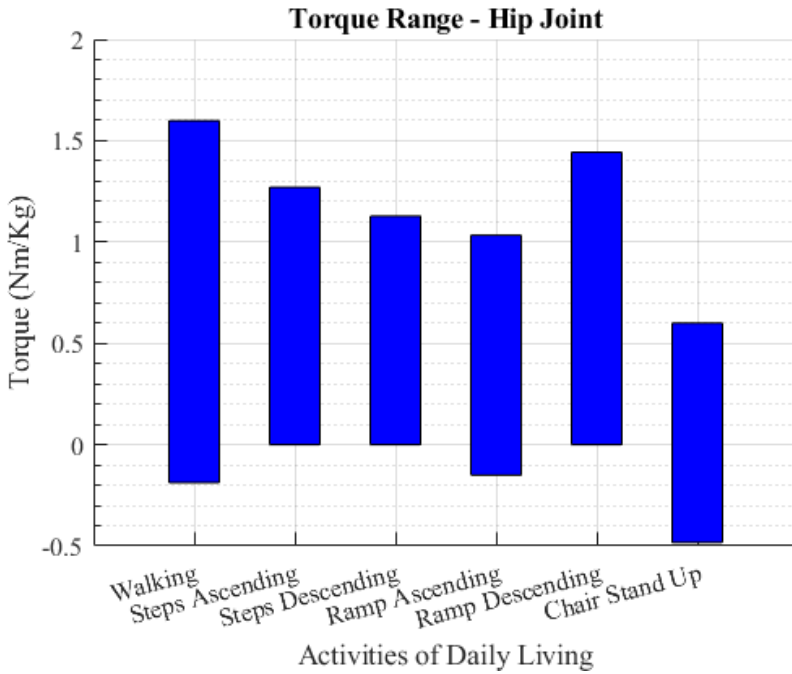


Figure 3.4: Torque range values during several activities. The values for the maximum and minimum torque are mean values from the data of all the different gait analysis experiments enclosed in one main activity. [16–24]

Another alternative of visual representation of the data can be done by grouping the range of a specific parameter and comparing it with any of the subjects' physical characteristics, e.g. the age range. This is illustrated in Figure 3.5, where the dependency of the subjects' age with the knee range of motion is evidenced. The colour code used in Figure 3.5, the age ranges and knee ranges of motion are presented in Table 3.1. The chart shown in Figure 3.5 concentrates the data from three

3.2 Characterization of Kinematic and Kinetic Parameters for Activities of Daily Living

different gait analyses, in which six age groups are contained. The approach used in Figure 3.5 is to overlap areas of different colours, each area represents the range of motion of the knee for a specific age range. The area in which several areas intersect can be appreciated due to the enabled transparency property. Nevertheless, the areas where three and two areas are intersected are manually highlighted by a surrounding solid line and dotted line respectively, to improve their visualization. This simple intersection of areas can provide information regarding the required range of motion to be delivered by the wearable robotic device, depending the sector of the population focused on. For example, if a wearable robotic device was aiming to assist the population sector aged from 50 to 70 years old, then a range of motion of the knee joint from 5° to 63° would be enough to cover the mentioned population. The range of motion is taken from the triple intersection of areas illustrated in Figure 3.5, which can provide a certain degree of confidence since three different clinical studies were compared. This approach can be used to compare other characteristics, e.g. subject's weight against torque. Summarizing, the areas overlapping approach can provide guidelines to avoid oversizing of the wearable robotic device to be developed by analysing the intersection of different areas which ultimately provides a degree of confidence when deciding design parameters.

Table 3.1: Colour code used in Figure 3.5 for each combination of age range and knee range of motion [16].

Colour Code	Knee Range of Motion ($^\circ$)	Age Range (Years)	Clinical Study
Red	2.2 - 67.4	49 - 90	[88]
Green	5 - 66.5	6 - 17	[17]
Blue	4.5 - 63.5	22 - 72	[17]
Yellow	0 - 69	18 - 30	[18]
Magenta	0 - 69	50 - 70	[18]
Cyan	8 - 63.6	23 - 27	[19]

In this section the process of characterizing the human lower limb kinematics and kinetics parameters during some ADLs was described. The relevant information provided in gait analysis experiments, and the challenges faced when extracting it from the clinical trials, were described. Data compiled for the activities of walking, ascending/descending stairs, ascending/descending ramps and chair standing up were presented in the form of clustered stacked bar charts. This type of chart allowed quick and easy detection of similarities between several clinical trials of

3. BIOMECHANICS OF THE LOWER LIMB AS DESIGN GUIDELINES FOR ASSISTIVE DEVICES

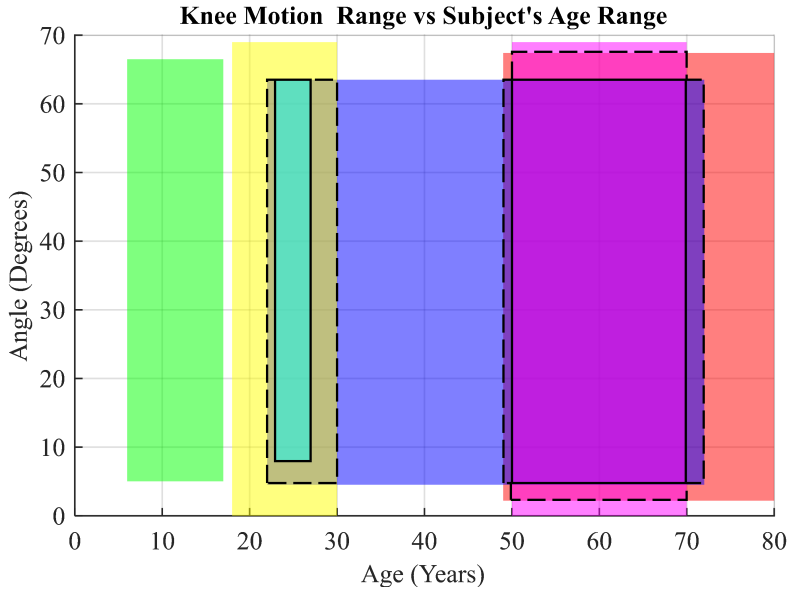


Figure 3.5: Comparison between subjects' age and the knee range of motion during walking over ground. The areas surrounded by solid lines and dotted lines represent the intersection between three and two areas, respectively. The overlapping squares highlight the great similarity among the range of motion despite subjects' age. The data used to create this chart is presented in Table 3.1 [16].

the same activity. In contrast, the spotted differences, as the ones for the knee torque values during ascending/descending stairs, are indicators for optimization opportunities where instead of using a single actuator to satisfy the torque range, an agonist-antagonist system could be more suitable.

The reliability of the data can also be observed using the type chart of overlapping areas with subjects' ranges of age against the knee ranges of motion. In other words, the specific ranges in which the data from different experiments overlaps, gives a measure of consistency which can be used to tailor the developed wearable device coverage.

The chart style with ranges of motion versus activities, facilitates the choice of the actuator type and dimension (depending on the activities of interest). The styles used to represent the charts were kept as simple as possible while providing useful information about the KKP. However, more complex plotting methods can be used. Finally, a total of 12 charts were produced in Excel® using the compiled data from the gait analyses. In favour of keeping the length of this section adequate, only two out of the 12 charts were included in here. The remainder charts were moved to Appendix A.

3.3 The Muscle-tendon Component

Having defined the terminology involved in the biomechanics of the human skeletal muscle system, and characterized the kinetic and kinematic parameters of its lower limb, this section focuses on describing the muscle-tendon component from a mechanical point of view.

In the literature, the mechanical model commonly used to describe the mechanical behaviour of the muscle-tendon component is the Hill's model [25]. This model is considered to be the most representative of all the available models [89]. Hill's model describes the skeletal muscle as a three elements system, which contains a contractile element, a passive element, and a series element. The contractile element (CE) represents the muscle fibres in charge of generating the contractile forces, the parallel (passive) element (PE) is formed by the tissue surrounding the muscle which prevents it from overstretching, and the series element (SE) represents the human tendon, as illustrated in Figure 3.6.

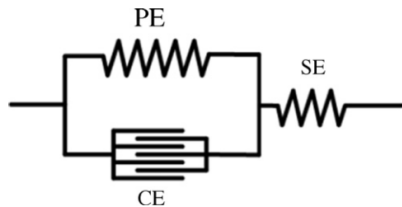


Figure 3.6: Hill's model of the skeletal muscle. The contractile element (CE), the parallel element (PE) and the series element (SE) are shown [25]

Hill's model makes the important assumption of considering the SE to be purely elastic, i.e. the deformation of the element is entirely dependent on the force applied to it. Nevertheless, the non-linear viscoelastic properties of the human tendon are acknowledged in his work. The latter simplification is a common practice among studies of the skeletal muscle system because the muscle and tendon are studied as a whole (muscle-tendon component) [90]. Evidence of the actual benefits of this simplification is found in the literature for the field of robotics exoskeletons. The complex muscle-tendon model developed in [91], considered the viscoelastic properties of the human tendon to estimate forces and joint torques in real time. The model achieved high accuracy at the cost of high computational load. In an attempt to reduce the computational load, the assumption of an infinitely stiff tendon was made which proved to be reliable as well [92].

3. BIOMECHANICS OF THE LOWER LIMB AS DESIGN GUIDELINES FOR ASSISTIVE DEVICES

In a similar way, developments in the field of soft robotics which are inspired in the skeletal muscle system functionality are also based in Hill's model, as highlighted in Section 2.2.1. Commonly, springs [1] or Bowden cables [9] are implemented as the SE of the muscle-tendon model. Nevertheless, the fact is that the human tendon has viscoelastic properties [26]. At the time of starting this research, the documented works in the literature were mainly focused on developing and testing soft materials to be used as the contractile element in soft artificial muscles. The latter, previously identified as a research opportunity, indicates that the viscoelastic properties of soft materials have not been studied with the aim of developing a soft artificial tendon, which in combination with current soft artificial muscles could deliver better performance in soft robotic applications for human assistance.

The first step towards the investigation on the potential benefits of adding viscoelasticity, in the form of a soft SE, to soft actuators is described as follows. As a starting point, the mechanical properties of the human tendon must be investigated. Due to the large contribution of the knee joint in the ADLs, the present investigation is focused in this joint of the human lower limb. Subsequently, the selection and characterization of many soft materials with mechanical properties similar to the human tendon, is proposed. The extracted properties from the studied soft materials and from the human tendon are compared against each other. This comparison analysis has the potential of providing evidence on the benefits and disadvantages of implementing a viscoelastic element as the way to transmit tensile forces in soft orthoses and soft exosuits.

Tendons are connective tissues that link muscles with bones. They have a non-linear viscoelastic behaviour, i.e. the proportional relationship between the reaction force experienced by the tendon and the applied deformation is not constant throughout the whole range of possible deformations. This reaction force is also dependent on the history of previous deformations. At rest, the collagen fibres (core components of tendons) are in a relaxed wavy state. When the tendon experiences a tensile force, the collagen fibres are easily stretched and realigned, opposing little resistance to deformation. However, when the collagen fibres are completely stretched they begin to offer more resistance to deformation which is proportional to the applied force. Finally, fibres can be stretched to their limit and failure of the tendon will occur [93]. This non-linear response to the applied deformation is better explained using Figure 3.7 where the characteristic S-shape curve for tendon stress-strain graph is appreciated.

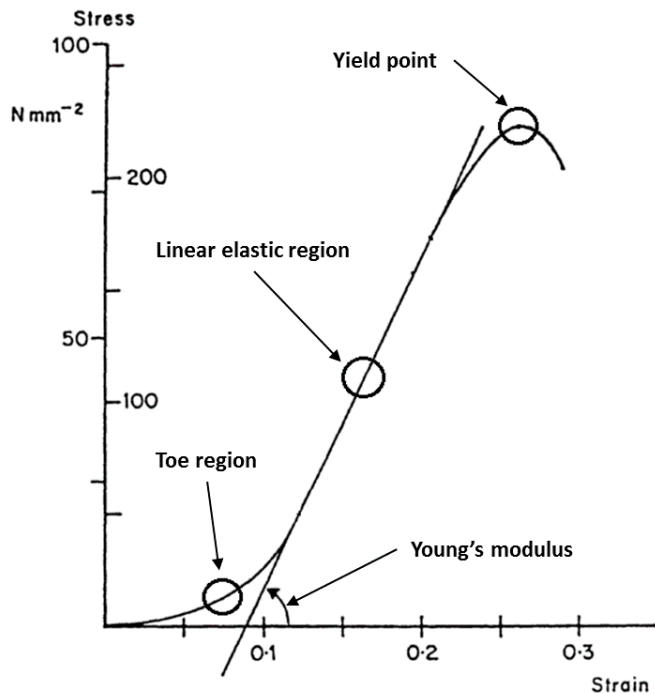


Figure 3.7: Tendon stress-strain curve. Image adapted from [26].

The stress-strain curve in Figure 3.7 illustrates the mechanical properties of a human tendon. The stress is described as the tensile force per cross-sectional unit area experienced by the tendon. This stress causes the tendon to elongate (deform). In the chart, the elongation is represented as the strain, which is the tendon deformation in relation to its original length. Along with the stress-strain curve, the force-elongation curve is also used to visualize the mechanical properties of tendons. These experiments are performed in a static state, i.e. the strain rate is the same throughout the whole experiment. Therefore, they do not provide any information about the viscoelastic properties of the tendon.

Viscoelastic materials exhibit both elastic and viscous characteristics. Viscosity describes a fluid's resistance to flow, the more viscous a fluid is, the more slowly it will flow and vice versa. The latter suggests a time-dependent behaviour. In the case of viscoelastic materials, this time-dependent behaviour is shown when subjecting the material to different rates of strain or deformation. For example, the stress-strain curve of the human tendon, illustrated in Figure 3.7, would have a greater slope in the elastic region if a greater strain rate is applied. The viscoelastic behaviour of the human tendon can be analysed with the following mechanical tests: stress relaxation, creep (deformation over time) and hysteresis [93].

3. BIOMECHANICS OF THE LOWER LIMB AS DESIGN GUIDELINES FOR ASSISTIVE DEVICES

During the stress relaxation experiment, the tendon is subjected to a constant deformation (length remains the same throughout the whole experiment). To avoid plastic deformations, i.e. incorrect measurements, the parameter of deformation for this experiment must not exceed the linear region of the material. The initial force/stress triggered as a response of the applied deformation will decrease over time (relax) until reaching equilibrium. From this experiment a chart of force against time is generated (Figure 3.8). In a similar way, in the creep experiment a constant force, avoiding plastic deformations, is applied to the material. The material will creep as time passes, in other words, the deformation caused by the applied force will increase over time until reaching equilibrium. A chart of deformation against time is generated (Figure 3.8). Finally, during the hysteresis experiment the tendon is subjected to cyclic tests where a load is applied up to a certain stress level and then released (unloading). The tendon behaviour shows two different paths, one for loading and one for unloading. Due to the time-dependent behaviour of viscoelastic materials, each cycle will generate different load-unload paths since the time interval for each cycle to be executed are intentionally defined to prevent the material of reaching equilibrium (Figure 3.9).

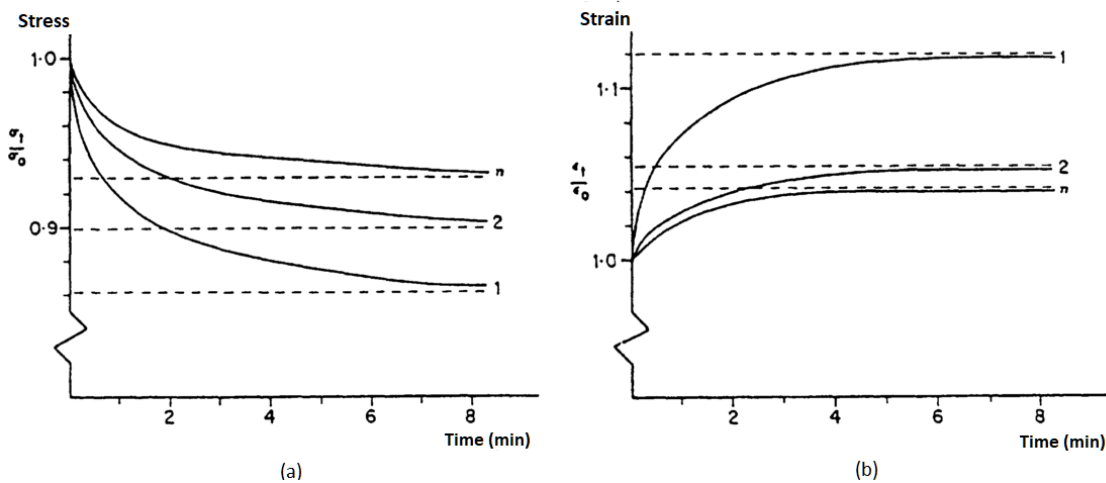


Figure 3.8: Tendon curves for the experiments of: (a) stress relaxation and (b) creep. The experiments were executed several times under the same conditions, the curve labelled n illustrates the tendon reaching a steady state where repeatability between experiments is achieved. Image reproduced from [26]

When performing mechanical experiments to find the tendon properties at failure, the obtained results are different between a preconditioned and an unconditioned tendon, as proved in [27]. This effect is illustrated in Figure 3.8 as well, for

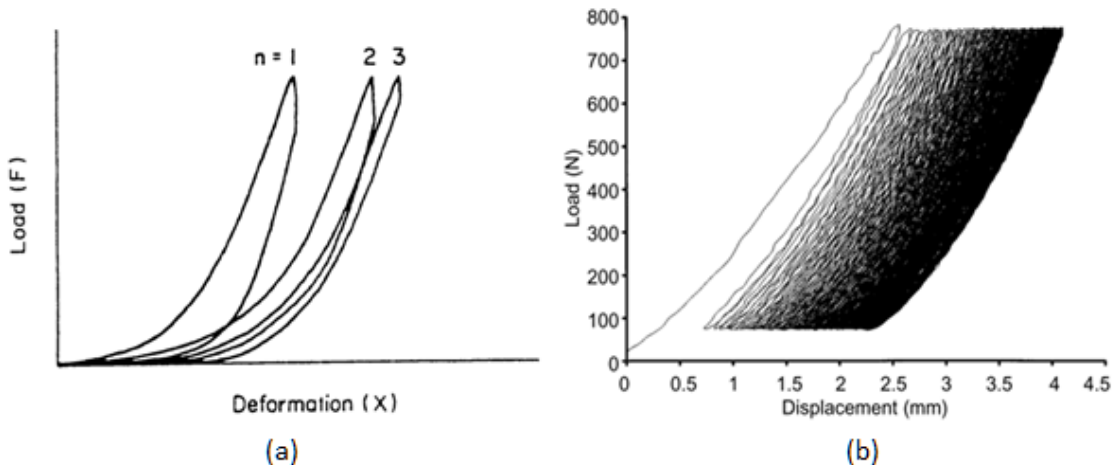


Figure 3.9: Hysteresis of the human tendon. (a) Deformation chart shows both loading and unloading paths for few cycles and (b) displacement chart shows 200 loading-unloading cycles. The preconditioned state of the tendon is reached for cycles above 50. Images taken from [26, 27] respectively.

both experiments, the tendon relaxation and creep are smaller for each new testing cycle until reaching an equilibrium state, i.e. the preconditioning state. The previous set of experiments is useful to characterize the non-linear viscoelastic properties of tendons and soft materials. Therefore, to perform the comparison analysis mentioned in Section 3.3, the soft materials of interest must be characterized using some of these mechanical tests. The study of the creep and hysteresis is out of the scope of this research. Instead, the tensile strength and stress relaxation are analysed. The selection criteria for the synthetic soft materials to be used is explained in the next section.

3.4 Soft Materials to Match the Properties of the Human Tendon

The selection of the soft material to be implemented was based on the literature about tendon reconstruction applications. A comprehensive review about the usage of synthetic materials in tendon reconstruction is made by Andullah in [94], where the most common materials used as artificial tendons and for tendon reconstruction are reported as: carbon, polyester, polytetrafluoroethylene, among others. The latter suggest that polymers are highly compatible with the human skeletal system and have similar mechanical properties as the human tendon. This assumption

3. BIOMECHANICS OF THE LOWER LIMB AS DESIGN GUIDELINES FOR ASSISTIVE DEVICES

is further verified in the study performed by Duenwald et al. in [95], which is about the viscoelastic relaxation and recovery of the human tendon. In this work, a high density polyethylene material was tested to find great similarities between this material and the mechanical properties of the human tendon. In fact, the viscoelastic properties of the human tendon during loading and unloading are similar to the ones found in polyethylene. However, high density polyethylene is not able to sustain high strains without suffering plastic deformations nor it has a very fast elastic response.

Among the current developments in soft orthoses, silicone rubber is a common choice, due to its high compliance, high elasticity and softness. Silicone rubber is usually implemented to create inflatable elements, but it is also known to have non-linear elastic properties, as reported in [96]. These findings suggest that the limitations of polymers, in terms of their elasticity, could be circumvented when combined with elastomers, such as rubber. A material with the latter characteristics, is known as a composite material. Many composite materials are created by injecting polymer particles, such as the previously mentioned polyethylene, into a rubber mixture. Thanks to the advances in manufacturing of composite materials, there is a wide variety of commercially available materials that fit with the requirements of this research. Due to the latter information, the selection of the soft materials to be studied in this work are from the family of composite materials, as follows: Polyethylene Rubber, Ethylene Polypropylene, Natural Rubber with Polyester, Natural Rubber, Silicone Rubber, Fluorocarbon Rubber, and Nitrile Rubber. All the materials were acquired from RS Components UK®, with the exception of the Natural Rubber, which was acquired from CoreZone Sports® in the form of resistance bands of different thickness. Finally, the characterization process and more details about the materials are provided in Chapter 4.

3.5 Modelling Techniques for Soft Materials

In Section 2.3, the lack of a reliable model to predict the mechanical behaviour of soft materials was identified as a gap in the body of knowledge. This limitation plays a crucial role in the process of investigating the potential benefits of mimicking the human skeletal muscle functionality, and so it is addressed in this section.

Most of the documented soft robotic applications use soft materials from the family of thermoplastic elastomers (TPE). These type of materials are known to have a non-linear stress response, low stiffness, high deformation lengths, and a time-

dependent and temperature-dependent response [31]. These mechanical properties are similar to the ones found in biological skin or muscle tissue, which is why soft materials are being implemented in soft robotic applications, despite of the many challenges. However, it is imperative to have a reliable modelling technique to fully take advantage of the latter mechanical properties.

At this point, it has been established the complexity of the mechanical behaviour of soft materials, such as TPE. In general terms, the stress response of these materials is non-linear and viscoelastic. The most commonly modelling technique used when dealing with viscoelastic materials is the development of a mathematical constitutive model. Many authors, choose the Linear Viscoelastic Models (LVM) as the starting point [97–100]. This has also been the case when modelling the mechanical behaviour of biological tissues [101]. The LVM are a set of mathematical models which use two basic components, a spring and a damper, in different configurations and quantities to describe the viscoelastic mechanical behaviour of materials [102]. Inside this family of mathematical models, there are a couple of them which are considered able to describe the viscoelastic behaviour of any material, as long as the required number of parameters of the model is met. This immediately imposes the restriction of having enough computational power to deal with the model complexity when high accuracy is required.

At this stage of the research, the implementation of soft materials in soft robotic applications for human assistance has gained more attention. Most of the efforts are focused on improving the traditional series-elastic actuator (SEA) by replacing its elastic element, commonly a metallic spring, with a viscoelastic material, such as rubber. SEA are from the family of cable-driven actuators and are commonly based on electric motors. The main feature of these actuators is that they have an elastic element between the actuator and the load. SEA have greatly impacted the field of robotics, specifically in legged robotics and powered orthoses, due to many benefits such as: greater shock tolerance, low output impedance, passive energy storage, and better force feedback accuracy [103–105]. Almost two decades after Pratt et al. documented the first SEA prototype, SEA are now considered a mature actuation technology, and as such, they have a well-defined trade-off, caused by the fixed stiffness provided by linear springs traditionally used. More often than not, variable stiffness is more suitable for legged robots and powered orthoses. The latter limitation have been addressed by developing variable stiffness actuators [106], using non-linear metallic springs [107], and very recently by using viscoelastic materials,

3. BIOMECHANICS OF THE LOWER LIMB AS DESIGN GUIDELINES FOR ASSISTIVE DEVICES

such as polymers and rubber [28–30]. However, these works, specifically the ones dealing with soft materials, are still facing the challenge of modelling the mechanical properties of this type of materials.

In [28], where the concept of a series-viscoelastic actuator (SVA) is first mentioned, the modelling of the soft material is based on the Burger Model, one of the most complete LVM, in combination with a controlling technique known as the state space observer. The accuracy of the system was found to be proportional to the complexity of the mathematical model used. The studied material in this work was a rigid-acrylic based photopolymer (FullCure720). The reported control system contained the viscoelastic model, the state space observer, and a cascaded force-velocity scheme, in other words, a very complex and well thought control system for a linear viscoelastic polymer. The developed SVA is illustrated in Figure 3.10.

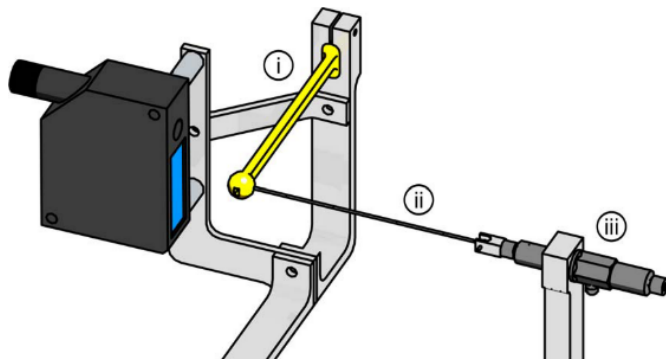


Figure 3.10: Series-viscoelastic actuator proposed by Parietti et al. The end-effector is rigidly mounted on the revolving lever (i), which also supports the laser sensor. A Nylon line (ii) connects the end-effector handle to the high-precision piezoelectric force sensor (iii), which is fixed to a rigid support [28].

Following this line of research, Rollinson et al. attempted to add viscoelasticity to a SEA, this time a soft material is used, natural rubber, instead of a rigid polymer [29]. The developed SEA has a rotary spring. Two different types of rubber, and a type of neoprene, were studied. In here, the stress response of the materials is considered linear and instead, the hysteresis of the material is modelled. Again, the modelling of the soft material is based on one of the LVM, the Standard Linear Solid (SLS) model, which is slightly less complex than the Burger model. Thanks to the proposed mechanical design for the rotary SEA, the reported stress response of the studied rubbers was surprisingly linear under a specific range of deformations. The authors concluded that more work is required to create better modelling techniques

for the hysteresis and non-linear behaviour of soft materials like elastomers. The developed rotary spring is illustrated in Figure 3.11.

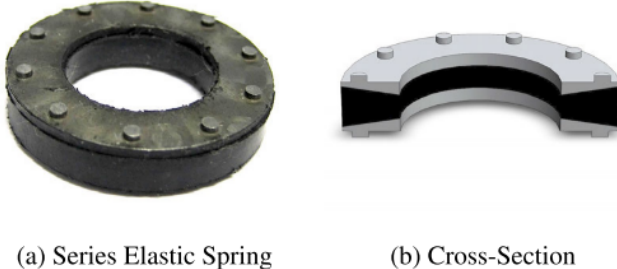


Figure 3.11: Developed soft rotary spring: a)photo and b)cross-section [29].

Following a more traditional approach, Schepelmann et al. incorporated viscoelasticity in cable-driven SEA by using a rubber material as the elastic element, instead of the traditional metallic spring [30]. In here, no LVMs are used, instead the non-linear stress response of the rubber is simplified by fitting a second order exponential curve to the stress-strain curve of the material. The main motivation of this work is to tackle the limitations of SEA with non-linear springs (NLS), where computer-aided manufactured (CAM) structures are used to define a known deflection trajectory of the spring, thus defining a torque trajectory. Essentially, CAM structures are able to relate the spring deformation with the generated torque, allowing the implementation of control systems. This work successfully validated the suitability of rubber to be incorporated as part of a SEA (Figure 3.12). However, under the limited range of testing parameters, the authors were not able to observe any velocity-dependency on the stress response of the rubber. In the conclusions, a state space observer is recommended to improve the accuracy of the reported forces transmitted by the the soft material, i.e. to allow the controller to compensate the hysteresis and non-linear stress response of the material.

In an attempt to relieve the controller for such load, the latter work was continued by Austin et al. in [33], this time the focus was on developing a modelling tool to better model the complex behaviour of rubber. In here, the complexity of modelling the non-linear and strain-dependent stress response of soft materials is addressed, for the first time, by upgrading the SLS model without greatly increasing its complexity. A piecewise linearization method is implemented, to transform the equilibrium spring in the SLS model into several springs in parallel which sequentially engages in proportion to the strain applied to the material. The developed mathematical

3. BIOMECHANICS OF THE LOWER LIMB AS DESIGN GUIDELINES FOR ASSISTIVE DEVICES

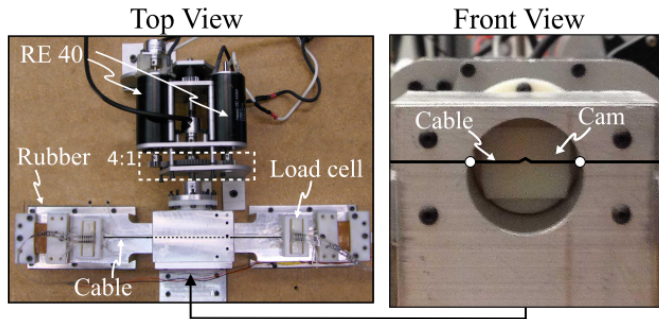


Figure 3.12: Benchtop setup for rubber characterization and observer testing. The load side of the rubber is fixed. Load cells in-line with the rubber give rubber force measurements for testing. The choice of electric motors and transmission is illustrated [30]

model is called the Standard Linear Solid model with Strain-Dependent Stiffness. (Std. Lin. SDS). Although, the SLS is not the most complete model among the LVM, the reported accuracy of the developed model is impressive. The control system implemented a state space observer, as well, which was able to correctly estimate the torque generated by the rubber spring. However, despite the large improvement in accuracy obtained by the developed Std. Lin. SDS, the hysteretic properties of the rubber lead to instability at higher frequencies, suggesting that there is still work to be done in this field.

3.6 Summary

In this chapter, the terminology on the biomechanics of the human lower limb is presented. Subsequently, the characterization of the kinetic and kinematic parameters of the hip, knee and ankle joints is performed by reviewing many clinical trials about gait analysis of the lower limb. The collected data had the potential to be used as design guidelines when developing robotic devices targeted for human assistance. Therefore, many visualization techniques were proposed and analysed in this context. The latter work resulted in a published conference paper (Section 3.2).

The main element of the human skeletal muscle system, the muscle-tendon component, was described in Section 3.3. In the literature, the works that implement the concept of mimicking the muscle skeletal system are focused on the contractile element of the muscle-tendon component, i.e. the muscle. Very little attention is paid to the series element, the tendon. Furthermore, it was found that the viscoelasticity

present in the human tendon, and biological tissues in general, is also present in certain polymers and composite materials. Therefore, the proposal of performing a comparison analysis between different off-the-shelf composite materials and the human tendon mechanical properties is presented. This comparison analysis will contribute to the aforementioned aim of the research. The first step to perform this comparison analysis is to characterize the mechanical properties of the selected materials, listed in Section 3.4. This is described in Chapter 4.

Recently, attempts of adding viscoelasticity to well-established actuation technologies have been done. Specifically, viscoelasticity has the potential to address many of the limitations found in series-elastic actuators. The available literature on the subject is scarce but very well documented. In general, the reviewed works face a common challenge, the modelling of the viscoelastic properties of the materials used to accurately estimate their reaction force or torque. Rubber is the most common choice in these applications. Almost all of the documented works are based on a model-driven approach, based on the Linear Viscoelastic Models, for the prediction of the material behaviour. However, the work performed by Austin et al. in [33], is the first attempt to upgrade the potential of the LVMs by applying a piecewise linearization method. The authors succeeded in developing a mathematical model, called the Standard Linear Solid model with Strain-Dependent Stiffness. (Std. Lin. SDS) which achieved higher accuracy than traditional models. However, even with the aid of controlling techniques such as the state space observer, the implemented control system is still unable to account for properties of the material, such as hysteresis and the velocity-dependency in their stress response. Nevertheless, the developed mathematical model has the potential to be upgraded further by using the same piecewise linearization method but on a more complex LVM. This idea is further explored in an attempt to develop a reliable modelling tool for the prediction of the mechanical properties of soft materials. This is presented in Chapter 5.

CHAPTER 4

Characterization of the Mechanical
Properties of Soft Materials

4.1 Introduction

In the previous chapter, the trend in soft robotic applications for human assistance of mimicking the human skeletal muscle system was identified. This trend is mainly focused on the contractile element (CE) of the muscle-tendon component. Recently, research has been done on implementing soft materials as the elastic element of series-elastic actuators (SEAs). This is motivated by the fact that viscoelasticity, found in biological tissue and many soft materials, may be able to overcome current limitations on SEAs. This is inline with the literature, which states that polymers, such as polyethylene, have similar mechanical properties as the human tendon. The literature available on the concept of series-viscoelastic actuators (SVAs) is very scarce and is currently facing the challenge of accurately estimating the force/torque transmitted by soft materials, such as rubber. One of the aims of this research is to develop a modelling tool able to address the latter. Therefore, this chapter covers the following points.

Firstly, a selection of different off-the-shelf soft materials is made from the family of composite materials, specifically thermoplastic elastomers (TPEs). The selection is based on the literature, which suggest that this type of materials have similar viscoelastic properties as the human tendon. The materials are as follows: Polyethylene Rubber (PR), Ethylene Polypropylene Rubber (EPR), Natural Rubber with Polyester (NatPolR), Natural Rubber (NatR), Silicone Rubber (SR), Fluorocarbon Rubber (FR), and Nitrile Rubber (NR). All the materials were acquired from RS Components UK®, with the exception of the Natural Rubber, which was acquired from CoreZone Sports® in the form of resistance bands of different thickness.

Secondly, the mechanical property of viscoelasticity of this type of materials is discussed. Thirdly, the characterization of the mechanical properties of these materials is presented. In here, the mechanical tests of tensile strength and stress relaxation are performed to extract both the elastic and viscoelastic properties of the materials. As previously mentioned, the study of the creep and hysteresis effect is out of the scope of this research. Finally, the collected data was processed in Matlab® prior to creating the visual representation of the studied properties.

4.2 Mechanical Properties of Soft Materials

The soft materials studied in this work belong to the family of thermoplastic elastomers or TPE. These materials are created by mixing a thermoplastic material,

4. CHARACTERIZATION OF THE MECHANICAL PROPERTIES OF SOFT MATERIALS

such as natural or synthetic rubber, with other materials, such as carbon and sulfur. This process is called vulcanization which creates cross-linked structures inside the material. Since elastomers are based on rubber, the terms elastomer and rubber are often used interchangeably. Elastomers are known to have nonlinear stress response, low stiffness and to achieve high deformation lengths. Some elastomers can fully recover their shape after stretched many times their length. They are also known to exhibit both elastic and viscoelastic properties. The latter means the stress response of elastomers is also time-dependent [31]. The main mechanical properties of elastomers are described in following paragraphs.

4.2.1 Elasticity

Elasticity, or elastic behaviour, refers to the ability of a material to be deformed up to a certain length and completely recover its shape and dimensions when the load deforming it is removed. Elasticity also refers to ability of a material to comply with the law of constant proportionality between the stress and the strain, described by Hooke's Law. However, elastomers are not purely elastic materials and tend to have a nonlinear stress-strain response, i.e. they do not obey Hooke's Law over the whole range of strains in the sense that the proportionality between the stress and the strain does not remain constant. This typical nonlinear behaviour in the stress-strain curve of elastomers is illustrated in Figure 4.1.

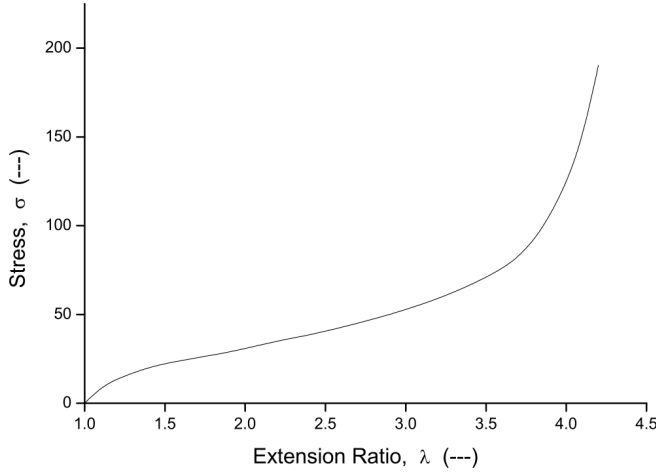


Figure 4.1: Typical stress-strain curve of elastomers. There are three main regions: the toe region ($1.0 < \lambda < 1.5$), the elastic region ($1.5 < \lambda < 3.5$), and the yield/failure region ($\lambda > 3.5$) [31].

The stress-strain curve of elastomers, illustrated in Figure 4.1), has three main

regions: the toe region ($1.0 < \lambda < 1.5$), the elastic region ($1.5 < \lambda < 3.5$), and the yield/failure region ($\lambda > 3.5$). In the toe region, the internal molecular chains of the material are misaligned, experiencing greater friction forces which greatly oppose to initial deformations. In contrast, when the molecular chains are aligned the friction forces decrease and the material deforms as a whole. The latter conditions dictates the beginning of the elastic region, in which the slope of the curve (stiffness) is slightly smaller than in the toe-region. The elastic region of many materials exhibit a proportional or linear relationship between the stress and the strain. This is not the case for elastomers, where most of them exhibit a nonlinear relationship. When the internal molecular chains have been elongated to its maximum length they demand higher forces to fail, this is observed as a peak in the load-elongation curve which also highlights the beginning of the yield/failure region [31].

Elastomers exhibit elastic behaviour over a certain range of deformations, i.e. the elastic region or elastic limit. Beyond this limit the material is likely to undergo plastic or permanent deformation, this means the material will not recover its original shape completely. In some cases, the elastic limit is not easily visible on the stress-strain curve of a material, and instead the proportional limit is used to approximate the location of the elastic limit. The proportional limit is defined as the point in the stress-strain curve where the nonlinear response (change in the curve's slope) is first observed. Another way to approximate the elastic limit of a material is based on using the yield strength, which is defined as the largest stress value on the curve, or the first point in which an increase in strain occurs without an increase in the stress [108]. These are some of the parameters that can be extracted from the tensile strength test and are useful to delimit the operating conditions of the materials. For this reason, particular care is put into accurately defining the elastic region, hence the safe operating conditions, of the studied soft materials. This is better described in Section 4.3.1.2.

4.2.2 Viscoelasticity

Viscoelasticity, is a property of some materials which are not purely elastic, do not fully obey Hooke's Law, nor purely viscous, do not fully obey Newton's Law, i.e. the stress is not proportional to the rate of change of the strain with time. In other words, the stress experienced by viscoelastic materials are dependent on both the amount and the speed of the strain applied to them. An example of a purely elastic material is a spring; whereas an example of a purely viscous material is a dashpot.

4. CHARACTERIZATION OF THE MECHANICAL PROPERTIES OF SOFT MATERIALS

The mechanical model of a viscoelastic material contains both elements, which can be arranged in different configurations. The set of mathematical models created out of these different configurations are known as the Linear Viscoelastic Models (LVMs). The time dependency or viscosity, of viscoelastic materials is appreciated in phenomena such as creep, stress relaxation, hysteresis, the Mullin's Effect and in the Van der Waals forces.

Stress relaxation and creep are both time-dependent phenomena observed in elastomers. On the one hand, stress relaxation refers to the decrease over time of the stress experimented by a material when subjected to a constant strain (or deformation). On the other hand, creep refers to the increment over time of the material strain when subjected to a constant stress (or load). The latter phenomena is observed in elastomers because they are composed of an internal network of molecular chains. Inside this network, entanglements form naturally. According to J. Bauman in [31], stress relaxation is mainly caused by the slipping of these entanglements ultimately causing a loosening of force applied by the network of molecular chains. Stress relaxation and creep occur in both constant and cyclic deformations. There are two mechanical tests designed to study these behaviours, from where the relaxation modulus and creep modulus of a material can be extracted [109].

Hysteresis in a material is defined as the mechanical energy dissipated as heat when the material is undergoing deformations. This phenomenon is observed in a loading-unloading cycle, where the stress trajectory of the material while loading (extension) is different than the trajectory during unloading (retraction), as illustrated in Figure 4.2. Hysteresis is mainly caused by internal friction of the molecular chain, also known as Van der Waals forces, in both elongation and contraction. Van der Waals forces are caused by the momentary bonding experienced between molecular chains that are close together. This constant making and breaking of bonds caused by deforming a material produces heat which ultimately becomes a mechanism to dissipate mechanical energy. This energy is represented as the enclosed area in Figure 4.2. Stress relaxation and creep play a role in the amount of hysteresis experienced by a material in each consecutive loading-unloading cycle. The effect of hysteresis alone can be isolated by subjecting the elastomer to a conditioning process (preconditioning) in which it undergoes several loading-unloading cycles until the stress response stops changing with every new cycle.

The Mullin's effect is another important phenomenon in the mechanical behaviour of elastomers. This effect refers to the breakage of tense molecular chains

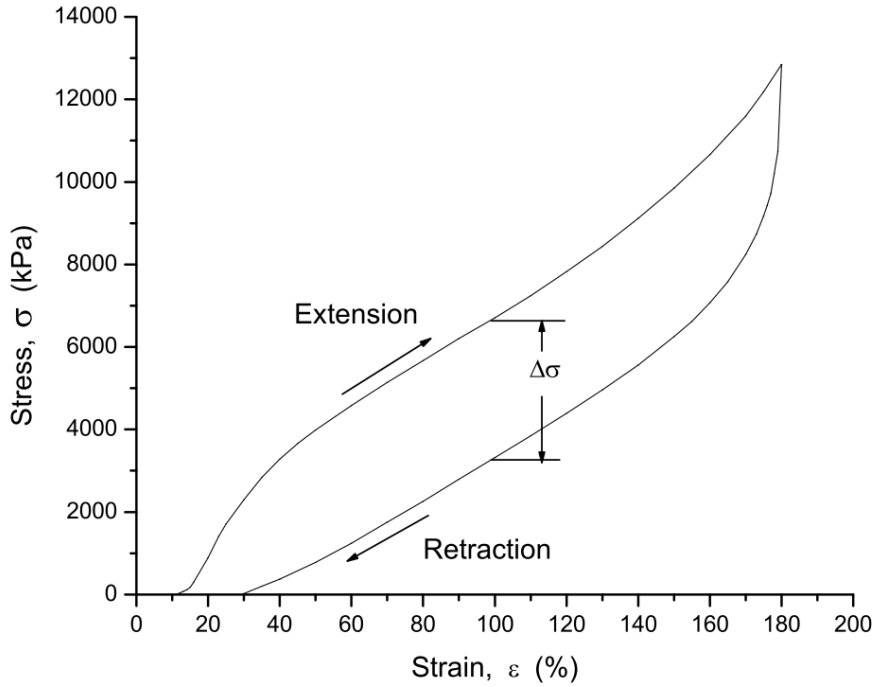


Figure 4.2: Hysteresis in stress-strain curve. [31].

resulted from the manufacturing process of the material. Therefore, the very first time the material is subjected to deformations it exhibits a larger stress response in comparison to consecutive deformations. The latter is also referred to as a weakening of the material. This effect is more dramatic than the stress relaxation but can be easily avoided when preconditioning the material. Having defined the expected mechanical properties of elastomers, the mechanical tests of tensile strength and stress relaxation are described in the following section.

4.3 Characterization Process

In this section, the mechanical tests of tensile strength and stress relaxation, performed as part of the characterization process, are described. The tests are performed in an Instron 3369 Dual Column Testing System equipped with a 50 kN load cell, at room temperature (25°C). The experimental data is expected to contain some noise due to the accuracy limitations of the available load cell. The algorithm implemented to filter this noise is described in ?? . As previously mentioned, the elastomers selected for this research are: Polyethylene Rubber (PR), Ethylene Polypropylene (EPR), Natural Rubber with Polyester (NatPolR), Natural Rubber (NatR), Silicone Rubber (SR), Fluorocarbon Rubber (FR), and Nitrile Rub-

4. CHARACTERIZATION OF THE MECHANICAL PROPERTIES OF SOFT MATERIALS

ber (NR). The Natural Rubber material is acquired from CoreZone Sports® and comes in the form of resistance bands of different thickness. The other materials are acquired from RS Components UK®, and come in the form of a rectangular sheet form. Laser cutting was used to extract individual specimens from each material sheet with the layout illustrated in Figure 4.3, as recommended in the Standard Test Method for Vulcanized Rubbers - Tension (ASTM D412) [32]. Finally, all the specimens were preconditioned prior to testing by applying a small deformation to them.

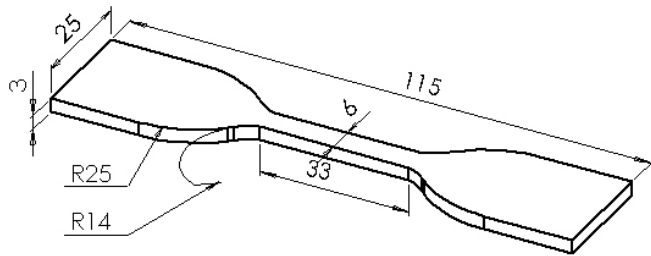


Figure 4.3: Specimen Type C Dumbbell Layout from the ASTM D412 [32]. In this example, the specimen thickness is 3mm, the width is 6mm, and the initial length, l_0 , is 33mm.

4.3.1 Tensile Strength Test

In a tensile strength test the material is loaded to failure at a certain deformation (strain) rate. The main purpose of this test is to extract the stress-strain curve of the material. From the stress-strain curve, the elastic properties of the material, such as stiffness, elastic modulus, ultimate strain, ultimate stress, elastic limit and yield strength, can be extracted.

The tensile strength test performed in this work is in accordance with the Standard Test Method for Vulcanized Rubbers - Tension (ASTM D412) [32]. Also, the Standard Test Method for Tensile Properties of Plastics (ASTM D638), was consulted on how to interpret the obtained stress-strain curves [110]. In here, it is recommended to elongate the material specimen until failure using a deformation rate of 500 mm/min, whenever possible. However, under certain circumstances where the previous deformation rate is not suitable, the test can be performed using the deformation rate of 250 mm/min. The latter was required for the silicon rubber, natural rubber and some resistance bands, where the gripper of the testing machine

was not able to hold the material during the entirety of the test. In addition to the previous two deformation rates, a third one of 50 mm/min is used whenever possible. In summary, most of the materials are tested using at least two out of the three deformation rates of 50, 250 and 500 mm/min. The decision of characterizing the mechanical behaviour of the materials under different strain rates is motivated by the known velocity-dependency of the stress-response of this type of materials. This will be useful during the modelling stage. The exact number of tests performed to each material is summarized in Table 4.1.

Table 4.1: Number of specimens used per type of test

Type of Rubber	Thickness mm	50	250	500
		mm/min	mm/min	mm/min
Ethylene Polypropylene	1.5	16	–	5
Fluorocarbon	1.5	8	8	5
Natural with Polyester	1.5	11	5	1
Nitrile	1.5	8	7	6
Silicone	1.5	15	7	–
Polyethylene	6	13	7	1
Natural (Resistance Bands)	0.33 – 1.49	1	33	11

The testing machine used for these experiments output the following parameters: reaction force, elongation, and time. In this work, the conventional parameters of stress, σ , and strain, ε , are used instead of the reaction force, F , and elongation, ΔL . The latter is calculated using the initial length $l_o = 33\text{mm}$, and cross-sectional area A_o , of the specimen, illustrated in Figure 4.3 and Table 4.1, respectively. Then it follows that $\sigma = F/A_o$, and $\varepsilon = \Delta L/l_o$.

4.3.1.1 Data Processing

The main objective of the data processing stage is to get rid of any noise added to the experimental data, normally due to sensor limitations, and also to filter out any undesired data. Removing noise from the data, i.e. filtering or smoothing, is avoided whenever possible because meaningful data can be lost in the process. Unfortunately, some of the collected datasets showed signs of high frequency noise which make it vary rapidly. A smoothing algorithm was applied to these datasets. In addition to noise, there are two sections of the collected stress-strain curve which

4. CHARACTERIZATION OF THE MECHANICAL PROPERTIES OF SOFT MATERIALS

are not desired. The first one is the section of the curve beyond the failure point of the material, when the stress value precipitates to zero. The working conditions of the soft material are desired to be limited to its elastic region, therefore, the final section of the stress-strain curve is not critical for the modelling of the materials behaviour. The second undesired section of the stress-strain curve is located at the very beginning. According to the literature, the very first portion of the stress-strain curve can be contaminated with phenomena such as: take-up of slack, and seating of the specimen. This effect was observed for most of the studied materials in here. The process of how to get rid of this phenomenon is called toe compensation (for a detailed description, refer to [110]). The mentioned sections are illustrated in Figure 4.4.

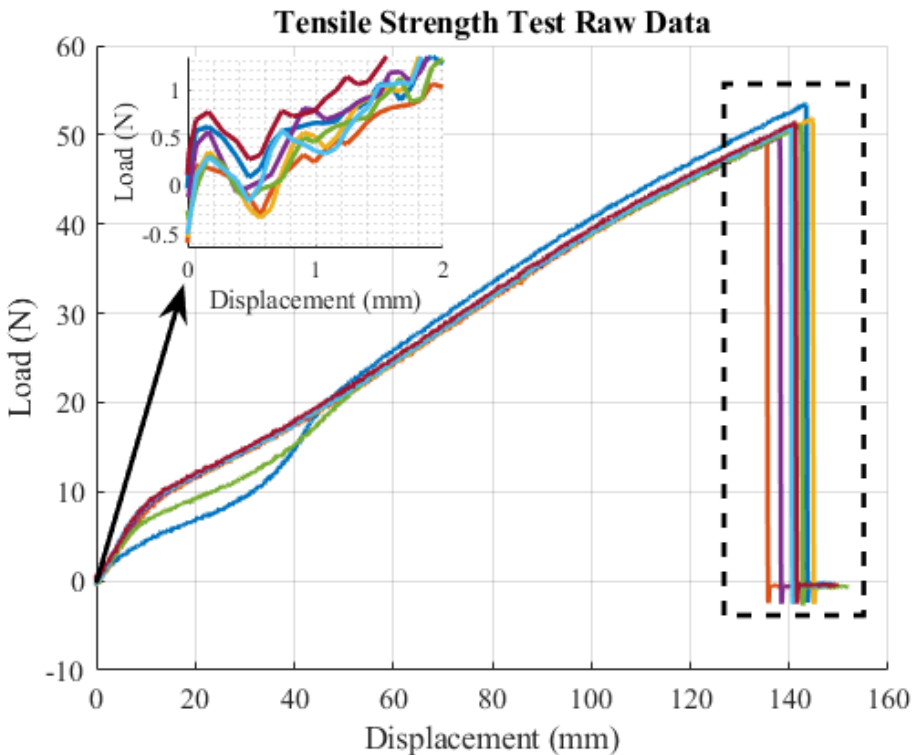


Figure 4.4: Undesired data on the tensile strength results. On the top left, the take-up slack phenomenon at the beginning of the experiment is observed. On the right, the different failure points of each specimen from the same material are highlighted.

The stress-strain curve from different specimens of the same material is expected to be slightly different, as illustrated in Figure 4.4. This variability is caused by many reasons such as the manufacturing process, temperature, and micro fissures inside the material due to handling. For this reason, and as recommended in [32, 110], the

engineering ultimate values of stress σ_{ue} and strain ε_{ue} are reported as the median value from all the tests involving one material and one strain rate. This variation has an impact on the unification of the data performed by averaging the values from all the tests. The latter will yield a single stress-strain curve from all the specimens involved in a test. This is required for the modelling process. In Figure 4.5 this impact is illustrated in the form of abrupt changes around the end section of the curve, caused by the different failing points of each specimen. The presence of this variation is not critical for the modelling stage because the material is unlikely to be elongated to such high lengths in a real wearable robotic application. However, the decision of discarding this section of the curve in favour of calculating the mean ultimate values of stress σ_u and strain ε_u , was made. This section of the curve was also not included when generating the final stress-strain curves of the materials.

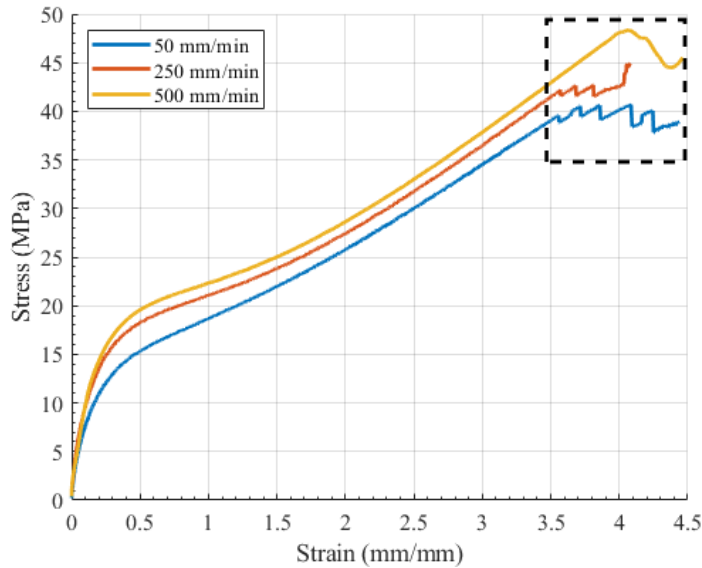


Figure 4.5: Abrupt changes observed at the last portion of the stress-strain curve, caused by the different failure points for each specimen. This phenomenon is observed after unifying the data from all individual specimens of a specific strain rate, into a single stress-strain curve.

The processing algorithm, developed in Matlab (R), was applied to the datasets that exhibit large amount of noise. These datasets were identified by looking at positive and negative peaks, specifically by looking at the mean absolute difference (MAD). Any dataset with peaks having a MAD greater than zero was considered noisy and subsequently filtered out. The filtering of the noise was done using the `smoothdata` function with the Savitsky-Golay algorithm. This function requires

4. CHARACTERIZATION OF THE MECHANICAL PROPERTIES OF SOFT MATERIALS

a window parameter to which the smoothing algorithm is applied, the larger the window, the greater the smoothing. However, a large window size also introduces a bias or offset to the extreme points of the data. This trade-off is described in [111]. Due to this, the chosen window size was based on the amount of data contained in one second in this way the window size depends on both the strain rate and the sampling frequency for each case.

The implemented data processing is summarized as follows:

1. Load raw data from tensile strength tests, i.e. elongation and reaction force (load);
2. Discard section of the stress-strain curve beyond the failure point;
3. Extract engineering ultimate load and displacement, latter converted to stress and strain.
4. Discard take-up slack phenomenon;
5. Unify processed data from all specimens into a single dataset by calculating the mean value;
6. Smooth datasets which have a peak-to-peak MAD greater than zero, in the initial portion of the curve;
7. Discard negative offset induced by processing and smoothing;
8. Calculate $\sigma = F/A_o$, and $\varepsilon = \Delta L/l_o$.

4.3.1.2 Elastic Properties of the Material

One of the main parameters to extract from the stress-strain curves of the materials is the elastic limit of each material. As previously mentioned in Section 4.2, this parameter dictates the maximum amount of deformation a material can sustain without losing the ability to fully recover its original shape. Commonly, the proportional limit is used to approximate the location of the elastic limit, and by extension, the elastic region. The proportional limit is the point in the curve where the proportionality between stress and strain becomes nonlinear. It can be safely assumed that the elastic region of the material is located below this point. However, most elastomers do not have a clear elastic region due to their nonlinear stress-strain curve, hence the proportional limit cannot be obtained. Under this circumstance, the elastic region of the material can be approximated using the yield strength of the material. The latter is defined as the first point in the curve where an increment in strain happens without an increment in the stress, in other words when the slope becomes zero or even negative [110]. The yield strength is inside the region

of plastic deformations of the material, hence this parameter by itself is not a safe way to approximate the elastic region.

A better alternative to approximate the elastic region is the offset yield strength. This parameter requires an offset strain value, and the elastic modulus E (slope of the curve) at a specific strain, to be calculated. In the literature, an offset strain of $\varepsilon_{offset} = 0.02$, or 2%, is recommended for plastics and elastomers [112]. This recommendation is mainly to allow comparisons between different laboratories data and does not indicate a goodness of fit when approximating the elastic region or the yield point of a material. In here, we chose a $\varepsilon_{offset} = 0.2$, or 20%, due to the large values of elongation achieved by most of the materials. The main recommendation to calculate E is to choose a strain range inside the initial part of the stress-strain curve in which a linear behaviour can be observed. The elastic modulus is then approximated using a function fitting method such as linear regression. Therefore, the optimal strain range for E was extracted from the obtained stress-strain curves of the materials illustrated in Figures 4.6 to 4.9.

In Figures 4.6 to 4.9, the stress-strain curve of all the materials studied under different strain rates are presented. The process to obtain the stress-strain curve of the Natural Rubber material was longer than for the other materials, due to the different available thicknesses. This material was acquired in the form of resistance bands, commonly used for rehabilitation. A total of two different batches were acquired. Each batch contained one band for each strength level, a total of six levels. The weakest band was the tiniest, whereas the strongest band was the thickest. The measured force response of one band from the same strength level varied from one batch to the other. The measured thicknesses were not the same among the two batches for a band of the same type. This is directly related to manufacturing practices and is reported in the literature [113]. For this reason, the individual thickness of each type of rubber band, from each batch was used to convert the raw data to the final stress-strain curve. With this, the impact from the latter differences is decreased and the material behaviour was better captured.

4. CHARACTERIZATION OF THE MECHANICAL PROPERTIES OF SOFT MATERIALS

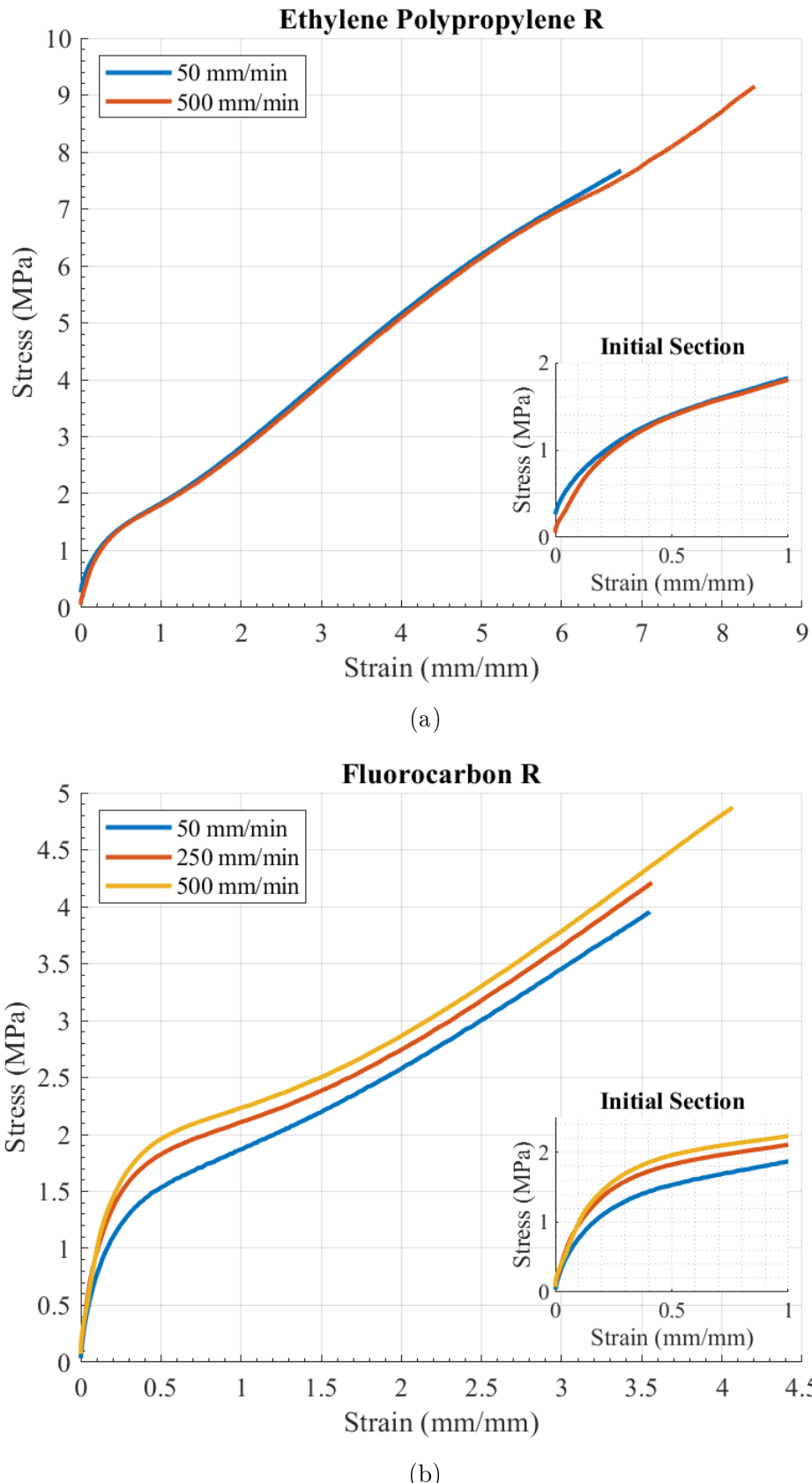


Figure 4.6: Stress-strain curves, during different strain rates, for the (a) EPR and (b) FR materials. On the bottom right, the initial section of the curve, where a linear behaviour was observed, is presented.

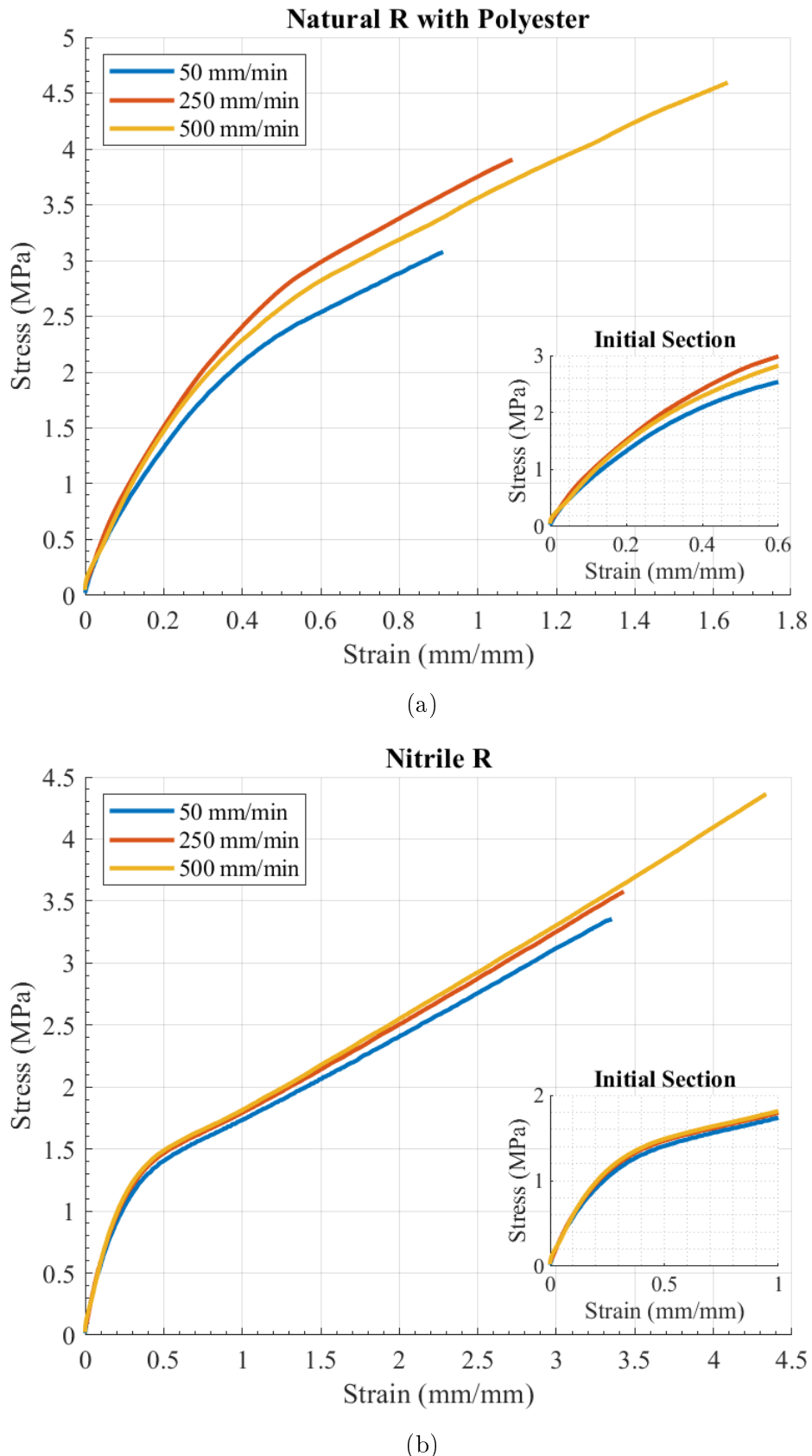


Figure 4.7: Stress-strain curves, during different strain rates, for the (a) NatPolR and (b) NR materials. On the bottom right, the initial section of the curve, where a linear behaviour was observed, is presented.

4. CHARACTERIZATION OF THE MECHANICAL PROPERTIES OF SOFT MATERIALS

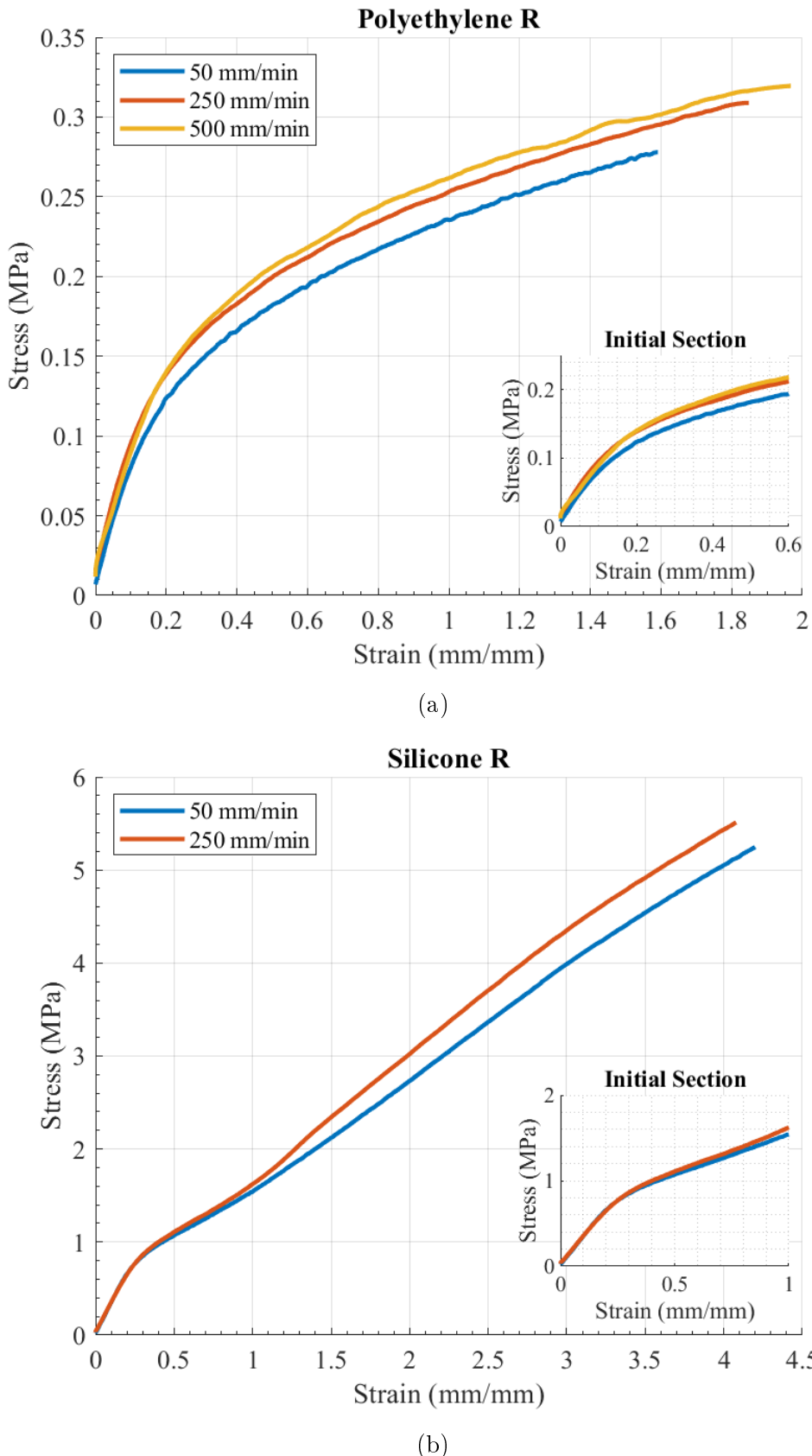


Figure 4.8: Stress-strain curves, during different strain rates, for the (a) PR and (b) SR materials. On the bottom right, the initial section of the curve, where a linear behaviour was observed, is presented.

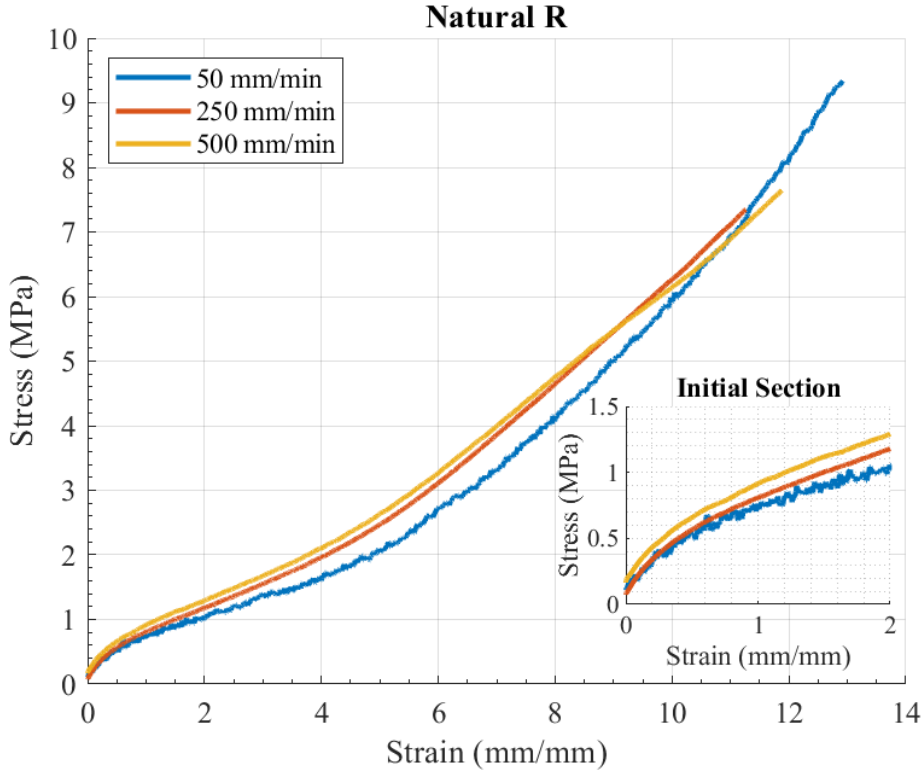


Figure 4.9: Stress-strain curve, during different strain rates, for the NatR. On the bottom right, the initial section of the curve, where a linear behaviour was observed, is presented.

In Figures 4.6 to 4.9, the velocity-dependency on the stress response of elastomers can be observed. In general, for larger strain rates, the materials exhibited a larger stress response. Moreover, a large difference in the ultimate values of the stress-strain curve of the Natural Rubber with Polyester material at 500 mm/min was observed in comparison to the other two curves (Figure 4.7a). This is a side effect from the unification step in the processing of the data, which is being amplified in here due to the small number of datasets involved in the 500 mm/min tensile strength test for this material (Table 4.1). Also, the Natural Rubber and Fluorocarbon material showed signs of crystallization, a phenomenon described in [31] which happens when the internal molecular chains of the material are completely extended and greatly oppose to further deformation, hence the increase in stiffness just before the failure point. Moreover, most of the materials have two regions in which the proportionality between the stress and strain appears to be constant. This is inline with the expected nonlinear behaviour from elastomers previously described. The slope of these regions, i.e. the stiffness, can be approximated by linear regression. A method such as the yield offset strength can be used to separate these regions into an initial and small elastic region, and a final and large elastic region. Therefore, the

4. CHARACTERIZATION OF THE MECHANICAL PROPERTIES OF SOFT MATERIALS

offset yield strength, σ_y and ε_y , is obtained and illustrated in Figures 4.10 to 4.16.

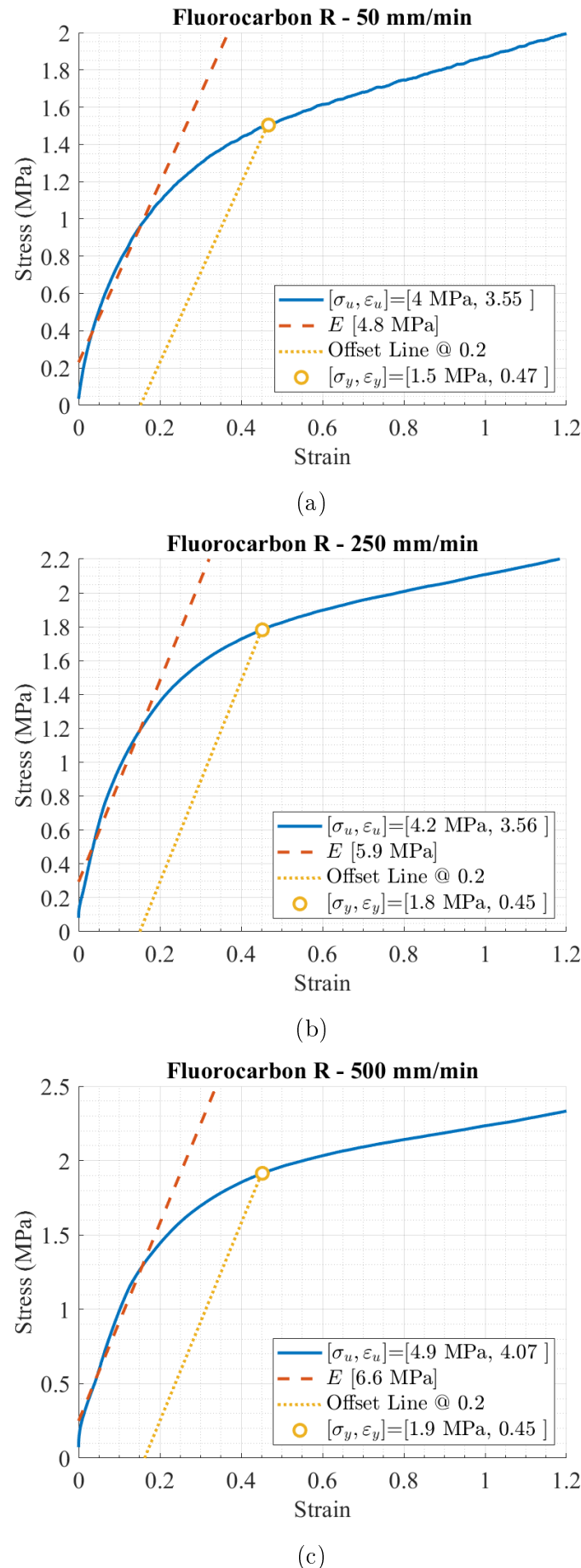
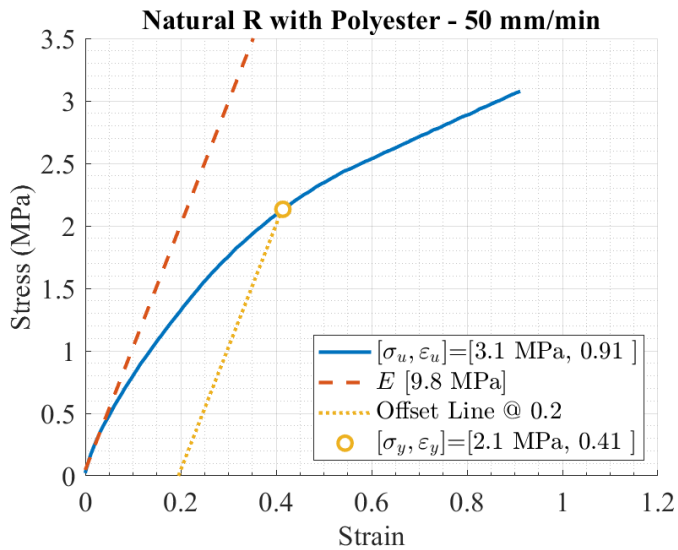
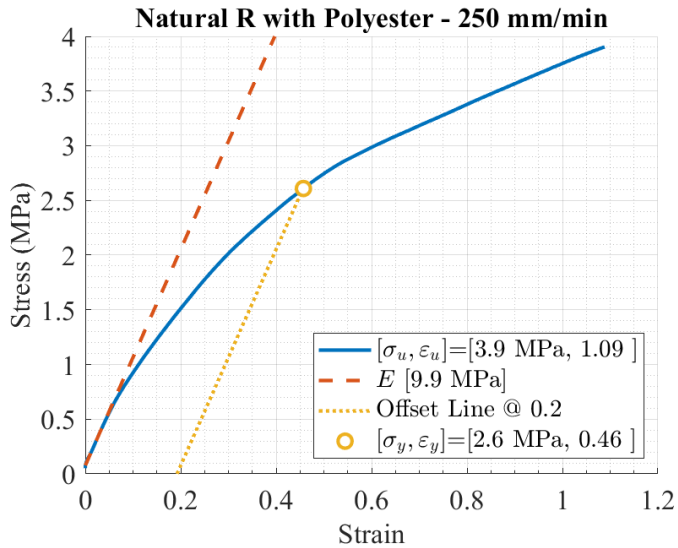


Figure 4.10: Offset Yield Strength for the FR material

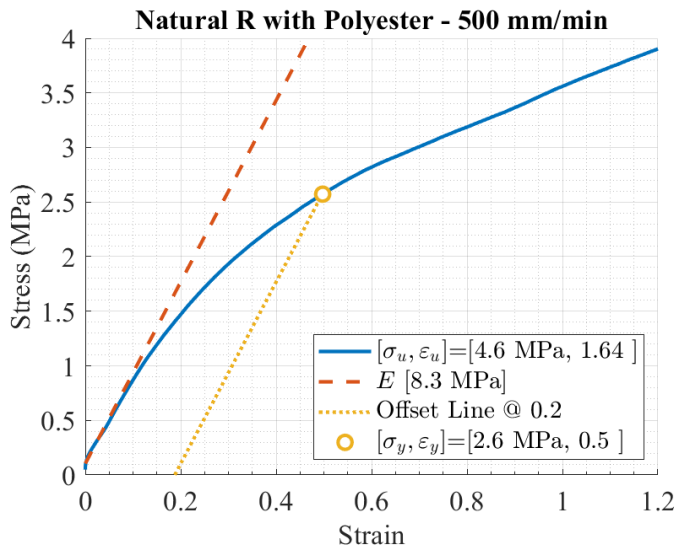
4. CHARACTERIZATION OF THE MECHANICAL PROPERTIES OF SOFT MATERIALS



(a)

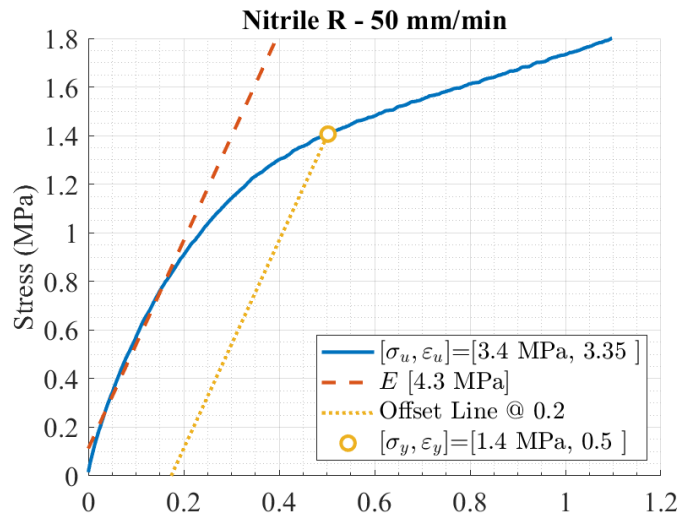


(b)

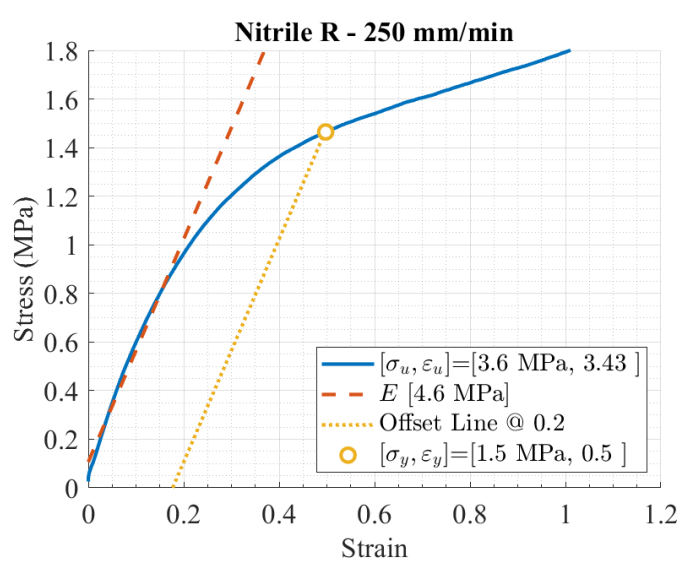


(c)

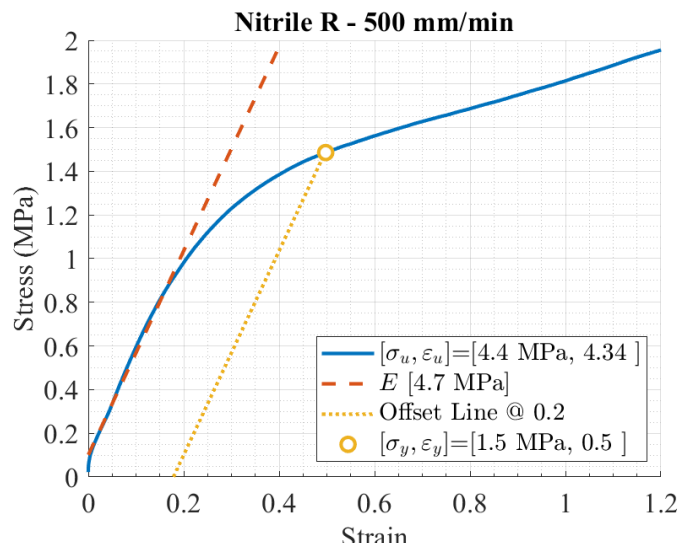
Figure 4.11: Offset Yield Strength for the NatPolR material



(a)



(b)



(c)

Figure 4.12: Offset Yield Strength for the NR material

4. CHARACTERIZATION OF THE MECHANICAL PROPERTIES OF SOFT MATERIALS

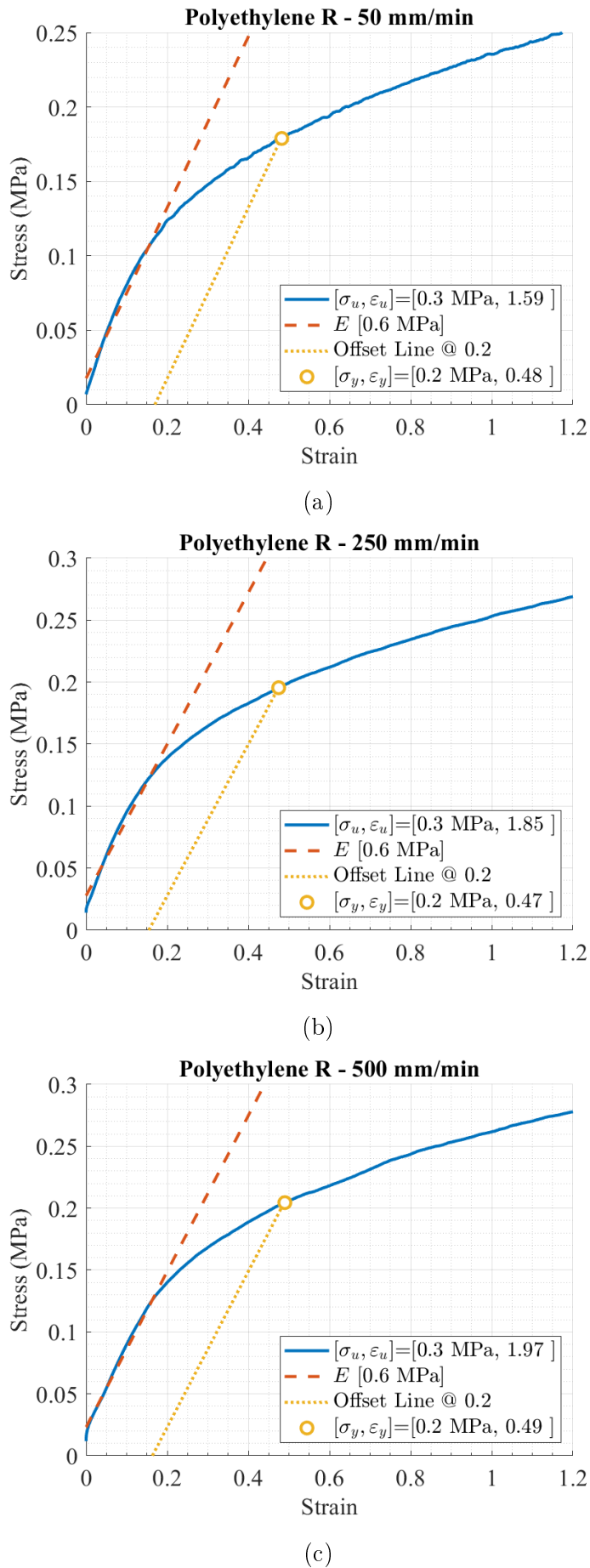
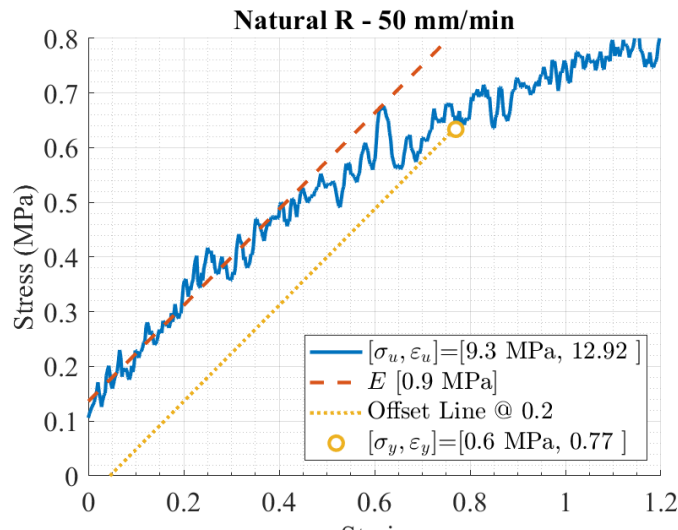
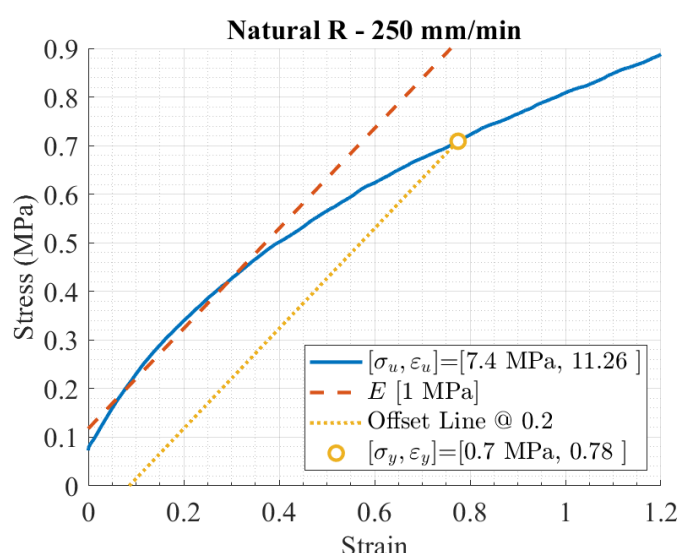


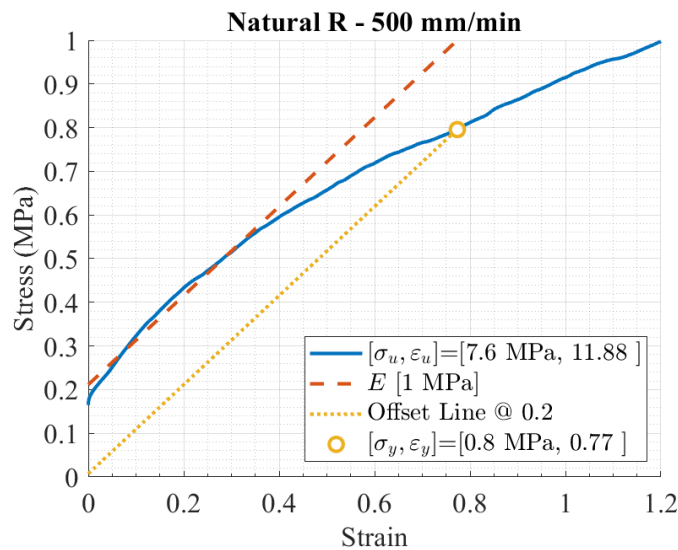
Figure 4.13: Offset Yield Strength for the PR material



(a)



(b)



(c)

Figure 4.14: Offset Yield Strength for the NatR material

4. CHARACTERIZATION OF THE MECHANICAL PROPERTIES OF SOFT MATERIALS

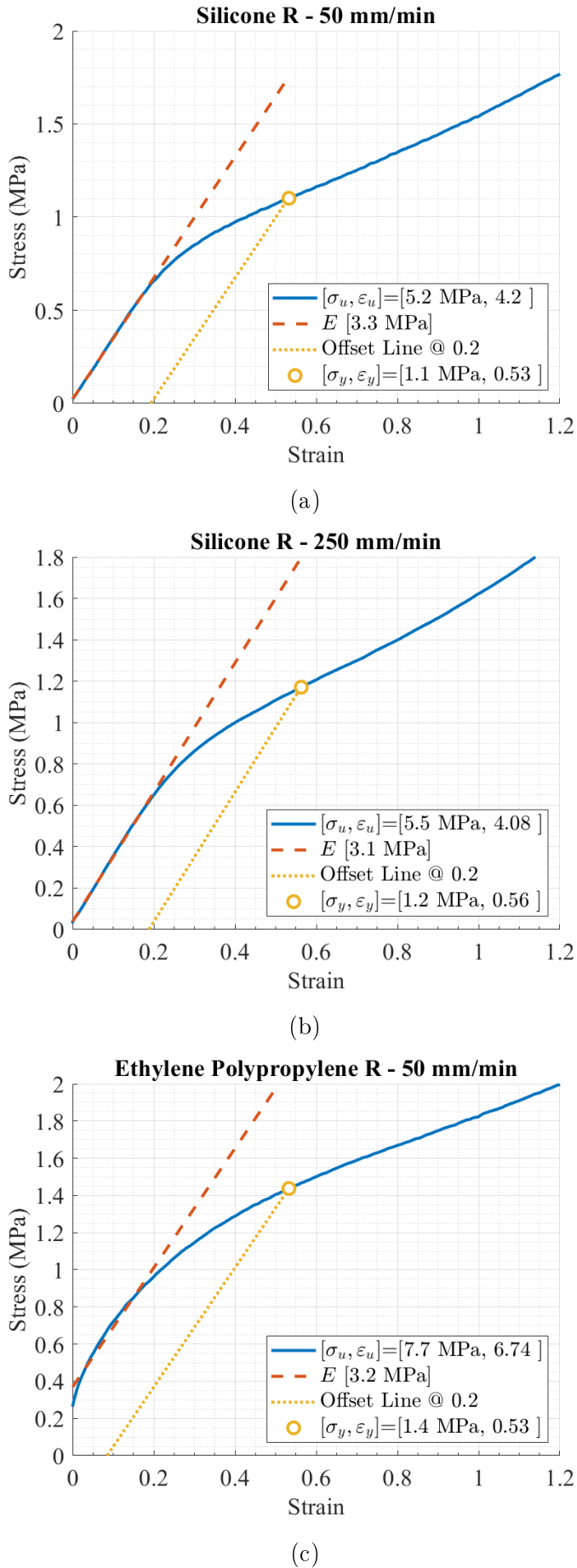


Figure 4.15: Offset Yield Strength for the SR and EPR (50mm/min) material.

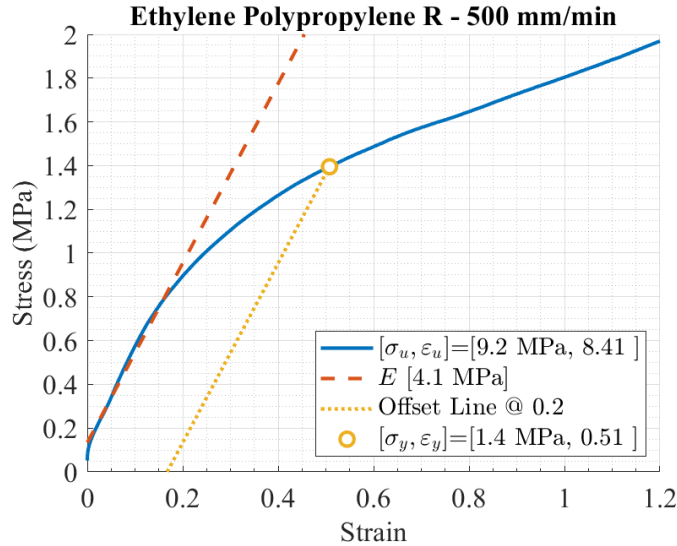


Figure 4.16: Offset Yield Strength for the EPR (500mm/min) material

In Figures 4.10 to 4.16, the elastic region is approximated by using the offset yield strength parameter, described previously. Also, the values for the ultimate strength, yield strength, and the elastic modulus at the elastic region, are provided. Any value below the offset yield strain can be assumed to be inside the elastic region of the material, hence the material will recover its original shape after undergoing any deformation inside this range of values. Having delimited the elastic region and its elastic modulus (now E_{small}), the slope of the second linear portion of the curve, i.e. the elastic modulus E_{large} , can be approximated. Finally, the elastic properties of the material are compiled in Table 4.2.

In Table 4.2, the σ_{ue} and ε_{ue} are reported as the median value from all the specimens of a specific test type. The yield values σ_y and ε_y were obtained using the offset yield strength method. The parameters E_{small} and E_{large} are the elastic modulus at the initial section, and middle section of the stress-strain curve. Also, E_{small} is the most useful parameter for assessing the performance of a material in a real robotic application, because it describes the stiffness of a material inside the elastic region, i.e. safe working conditions. In this regards the PR material had the smallest value, whereas the NatR had the highest.

4.3.2 Stress Relaxation Test

The stress relaxation test allows the extraction of the viscoelastic properties of the materials, i.e. the time-dependent properties. In this test, a predefined and constant elongation, also called initial strain ε_o is applied to the material specimen. The material is held in place for the whole duration of the test and the stress response is

4. CHARACTERIZATION OF THE MECHANICAL PROPERTIES OF SOFT MATERIALS

Table 4.2: Elastic properties of the selection of soft materials. The materialas are: Polyethylene Rubber (PR), Ethylene Polypropylene Rubber (EPR), Natural Rubber with Polyester (NatPolR), Natural Rubber (NatR), Silicone Rubber (SR), Fluorocarbon Rubber (FR), and Nitrile Rubber (NR).

Materials	Speed mm/min	σ_{ue} MPa	ε_{ue}	σ_u MPa	ε_u	σ_y MPa	ε_y	E_{small} MPa	E_{large} MPa
EPR	50	8.48	7.56	7.67	6.74	1.44	0.54	3.23	0.99
	500	9.59	8.84	9.16	8.41	1.39	0.51	4.16	1.1
FR	50	4.36	3.97	3.96	3.56	1.5	0.47	4.83	0.65
	250	4.41	3.93	4.22	3.57	1.78	0.45	5.95	0.58
	500	5.35	4.29	4.87	4.07	1.91	0.45	6.78	0.61
NatPolR	50	3.57	1.19	3.08	0.91	2.12	0.41	9.97	2.05
	250	4.06	1.19	3.91	1.09	2.51	0.43	10.74	2.28
	500	4.59	1.64	4.59	1.64	2.52	0.48	8.77	1.9
NR	50	3.55	3.57	3.36	3.36	1.41	0.5	4.29	0.64
	250	3.65	3.62	3.58	3.43	1.47	0.5	4.63	0.69
	500	4.62	4.61	4.37	4.34	1.48	0.5	4.72	0.72
PR	50	0.3	1.87	0.28	1.59	0.18	0.48	0.58	0.11
	250	0.33	1.97	0.31	1.83	0.19	0.45	0.66	0.1
	500	0.32	1.97	0.32	1.97	0.2	0.49	0.64	0.1
SR	50	6.03	5.77	5.26	4.22	1.1	0.53	3.26	1.08
	250	5.68	4.27	5.52	4.08	1.15	0.54	3.26	1.35
NatR	50	9.43	13.02	9.37	12.93	0.61	0.69	1.01	0.33
	250	15.88	12.11	7.38	11.27	0.69	0.74	1.11	0.41
	500	11.93	12.26	6.61	11.22	0.73	0.71	1.19	0.43

recorded. The material will relax over time, i.e. the stress response will decrease. Similarly as for the tensile strength test, different combinations of test duration and initial strain values were chosen for the tests. Also, a varying number of specimens were included in each test. Some of these combinations were based on similar characterization processes available in the literature in where the duration time was no longer than 200 minutes [113, 114]. Nonetheless, a second test is proposed with a shorter duration. The diverse parameters used in the tests are aimed to create a richer dataset. As a recommendation, the value for the applied ε_o must fall bey-

ond the elastic region of the material to avoid plastic deformation, i.e. irreparable damage. However, for highly elastic materials, such as elastomers, large values of ε_o are used in the literature. Also, the material must be elongated from zero strain to the value of ε_o as fast as possible. Therefore, the strain rate chosen for this test was 500 mm/min. With this in mind, the first test was performed using relatively large values of ε_o which were beyond the elastic region of the materials, identified in Section 4.3.1.2. For this case, the test duration was the longest, of 180 minutes. A second test was performed using ε_o values inside the elastic region of the materials and with a shorter duration of 15 minutes. The parameters for the performed tests are compiled in Table 4.3.

Table 4.3: Parameters and number of collected datasets for the stress relaxation tests.

Test	Parameters	EPR	FR	NatPolR	NR	PR	SR	NatR
1	ΔL_o (mm)	5	5	7	6	3	6	40
	ε_o	0.15	0.15	0.21	0.18	0.09	0.18	1.21
	Duration (minutes)	15	15	15	15	15	15	15
2	Datasets	5	5	5	5	5	5	2
	ΔL_o (mm)	20	10	6	5	4	15	-
	ε_o	0.61	0.3	0.18	0.15	0.12	0.45	-
	Duration (minutes)	180	180	180	180	180	180	180
	Datasets	1	1	1	1	1	1	-

Similar to the tensile strength tests, the collected data was processed prior to the extraction of the relevant parameters. The data of interest is the one found after the machine has reached the predefined ε_o value. In here, several smoothing algorithms such as, moving average, Gaussian-weighted moving average, and the Savitzky-Golay algorithm, were analyzed. During testing of these algorithms, a direct relationship between the decrease in the value of the initial stress σ_o , and the selected window size, was observed. The selected window size was based on the sampling frequency and the duration of the test. The Savitzky-Golay algorithm has the least impact on the initial stress σ_o in relation to the achieved smoothing, hence it performed better than the other two algorithms.

4. CHARACTERIZATION OF THE MECHANICAL PROPERTIES OF SOFT MATERIALS

4.3.2.1 Stress Relaxation Properties

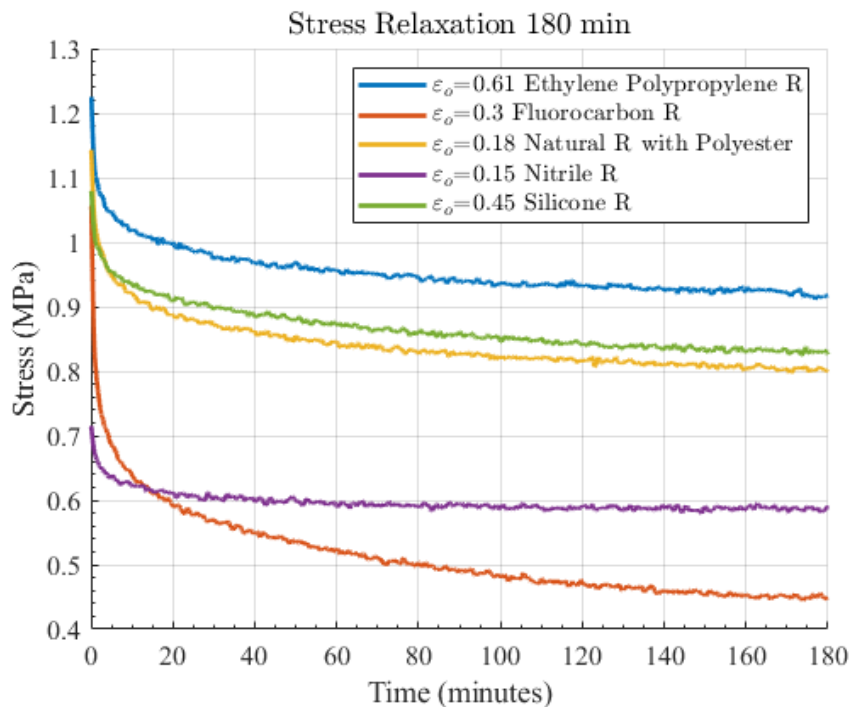
The stress relaxation test is useful for approximating the time relaxation constants of the materials. Commonly, viscoelastic materials have more than one relaxation constant. This is caused by the many number of internal molecular chains which relax at different rates. The stress relaxation curve of viscoelastic materials exhibit a decaying exponential stress relaxation curve. This known mathematical function, in combination with the LVMs, can be used to approximate the time relaxation constants of the material. The LVMs have the flexibility to get as complex as required by adding extra elements to the model. The latter means that the number of relaxation constants that can be extracted from the stress relaxation curve is directly proportional to the number of exponential functions contained in the LVM. This is described in detail in Chapter 5. The stress at the starting and ending points of the test, σ_o and σ_{end} , respectively, are the minimum required parameters to approximate one relaxation constant of the material using a LVM. Another parameter of interest is the achieved stress relaxation, which is defined as follows:

$$S.R. = 100 \left(\frac{\sigma_o - \sigma_{end}}{\sigma_o} \right) \quad (4.1)$$

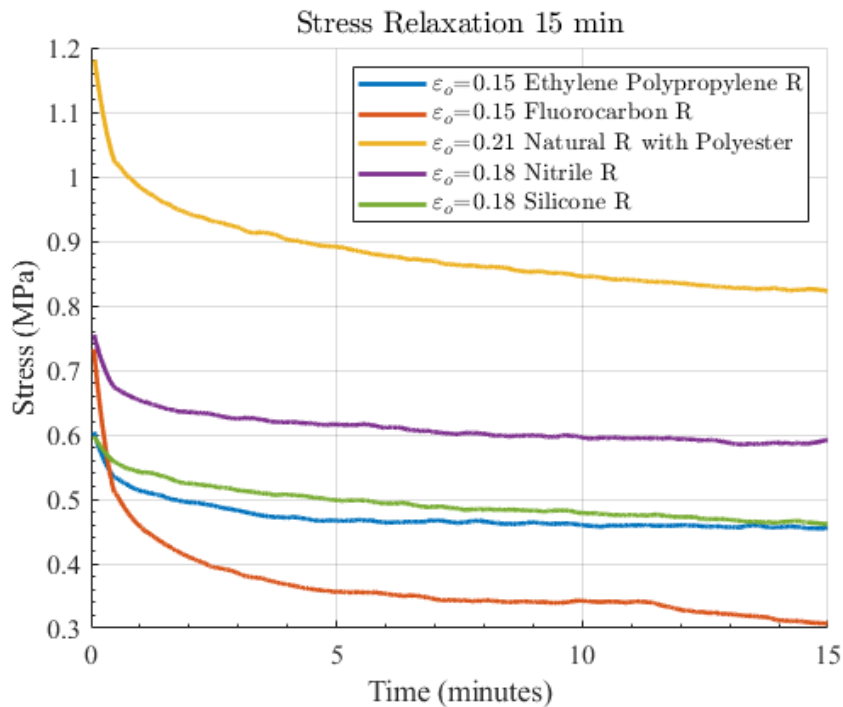
The parameters extracted from the stress relaxation test are compiled in Table 4.4. The obtained stress relaxation curves of all the materials are illustrated in Figures 4.17 and 4.18. The values of σ_o and σ_{end} are obtained by finding the median value of all tests included in each scenario, using the collected raw data. The values of the $S.R.$ are very similar in both tests, in terms of the duration of the test and the chosen value for ε_o . This means most of the $S.R.$ happens very early into the test, and that only one relaxation time constant is required to model the stress relaxation of these materials.

Table 4.4: Stress relaxation properties for the selection of soft materials.

Test	Properties	EPR	FR	NatPolR	NR	PR	SR	NatR
1	σ_o (MPa)	0.61	0.84	1.22	0.77	0.06	0.61	2.15
	σ_{end} (MPa)	0.42	0.27	0.80	0.55	0.02	0.43	1.82
	$S.R.(%)$	32	67	35	29	63	31	15
2	σ_o (MPa)	1.28	1.13	1.18	0.72	0.07	1.11	
	σ_{end} (MPa)	0.89	0.41	0.76	0.55	0.03	0.80	
	$S.R.(%)$	31	63	36	24	51	28	



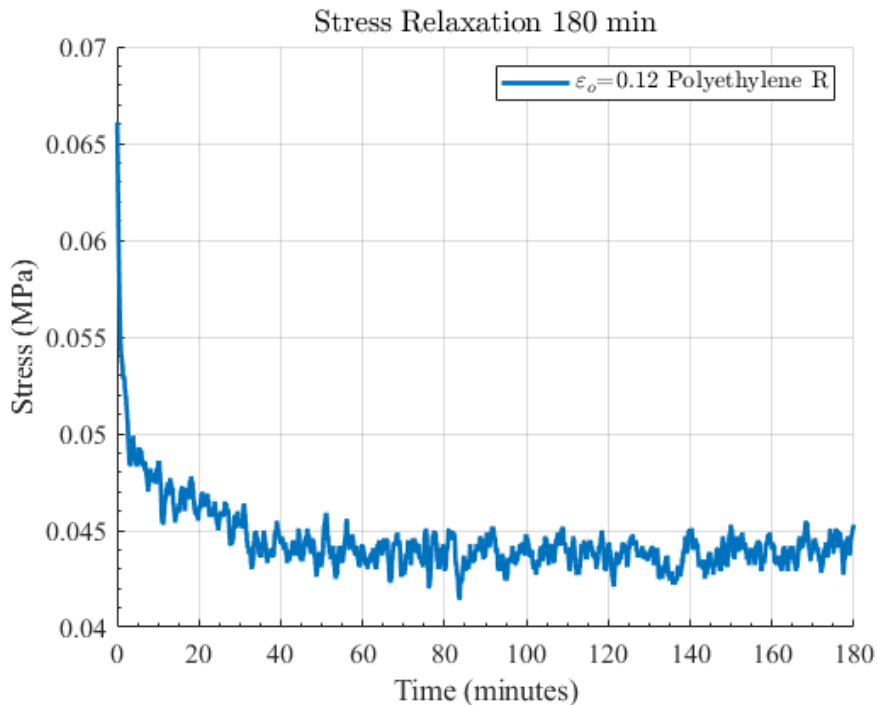
(a) Caption



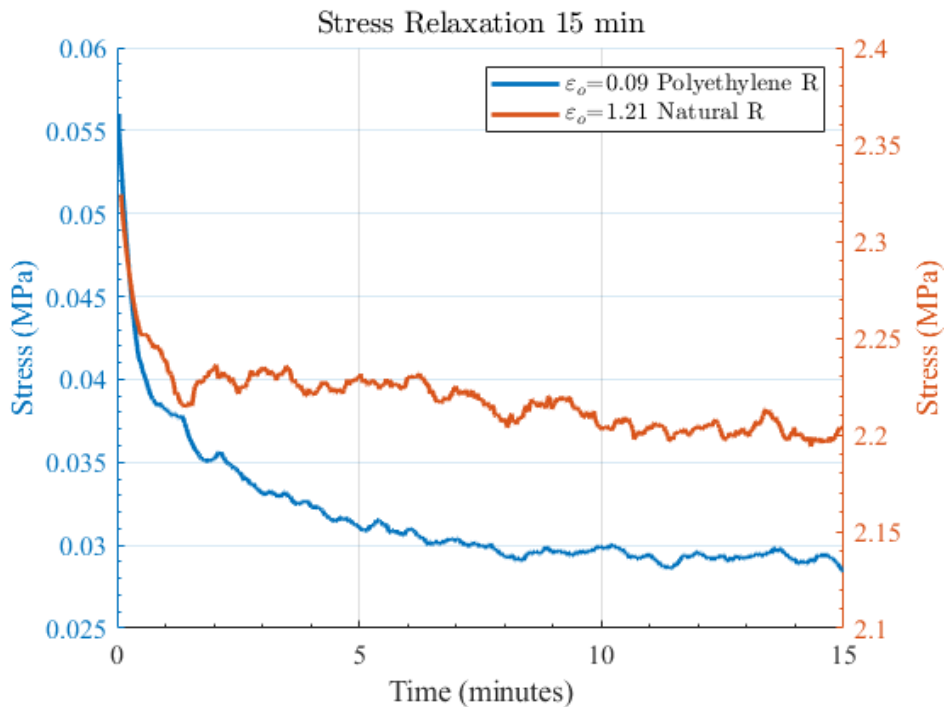
(b) Caption

Figure 4.17: Stress Relaxation curves for (a) 180 minutes and (b) 15 minutes, of the EPR, FR, NatPolR, NR and SR materials. Different values of ε_o were investigated.

4. CHARACTERIZATION OF THE MECHANICAL PROPERTIES OF SOFT MATERIALS



(a) Caption



(b) Caption

Figure 4.18: Stress Relaxation curves for (a) 180 minutes and (b) 15 minutes, of the PR, and NatR materials. Different values of ε_o were investigated.

4.4 Summary

In this chapter, the characterization process of the viscoelastic mechanical properties of a selection of seven different TPEs was presented. For this, the mechanical tests of tensile strength and stress relaxation was performed. In the tensile strength test, the materials were elongated until failure using up to three different strain, or elongation, rates. The latter will allow the modelling of the velocity-dependent stress response of the materials. The processing algorithm used to condition the collected data was also described in detail. The smoothing algorithm chosen for both mechanical tests was the Savitsky-Golay algorithm. In the case for the Natural Rubber material, where two batches were acquired, the thickness from one batch to the other varied significantly. Nevertheless, the mechanical behaviour of the material was captured accurately in the stress-strain curves. This suggests a linear proportionality between the thickness of the material and the increment on the response of the material. The elastic region of the materials was difficult to be identified directly due to their nonlinear stress-strain curve. Therefore, the elastic region was approximated using the offset yield strength parameter. This region is very important to delimit the working conditions of the soft materials in a real robotic application. Finally, the ultimate values of strain and stress, the elastic region location, the elastic modulus in two distinctive regions of the curve, and the offset yield strength parameters, were reported. The E_{small} is the most useful parameter for assessing the performance of a material in a real robotic application, because it describes the stiffness of a material inside the elastic region, i.e. safe working conditions, in contrast to the ultimate strength values. In this regard the PR material had the smallest value, whereas the NatR had the highest.

The performed stress relaxation tests can be divided into two sets. One with a low deformation, and low duration. The other, with large deformation, large duration. Regarding this, the achieved stress relaxation of the materials was very similar for both cases. Knowing the resemblance of the stress relaxation curve with an exponential decaying function, the latter finding could suggest that only one relaxation time constant is responsible for the majority of the *S.R.* achieved. This hypothesis will be explored in the modelling stage.

CHAPTER 5

Soft Materials Modelling: Linear
Viscoelastic Models

5. SOFT MATERIALS MODELLING: LINEAR VISCOELASTIC MODELS

5.1 Introduction

In this chapter, the performance of two model-driven tools for the prediction of the viscoelastic properties of seven soft materials is investigated. This chapter describes the development of a new model, the PL-SLS model, which is based on a very successful approach found in the literature, the Standard Linear Solid model with Strain-Dependent Stiffness model (Std. Lin. SDS) [33]. This model makes use of a piecewise linearization (PL) to improve the capabilities of one of the Linear Viscoelastic Models (LVMs), the Standard Linear Solid model (SLS). The capabilities of the Std. Lin. SDS model of accounting for velocity-dependent stress responses have not been assessed. The latter is investigated in this chapter. In the process, several optimizations are performed to the Std. Lin. SDS model which directly address its main limitations.

In addition to this, the PL method is applied to a more complex model from the family of LVMs, which is the Wiechert model. This model have the advantage of accounting for the velocity-dependent stress response of viscoelastic materials, with the trade-off of added complexity. Nevertheless, the PL method have the potential to reduce the latter complexity.

In contrast with the fitting process described in the literature [33], the stress relaxation test is used to extract the relevant parameters for the SLS and Wiechert model. Subsequently, the PL method is applied to both models, allowing them to account for strain-dependent stress responses. The performance of both models is assessed, initially, using the collected stress-strain curves of the following soft materials: ethylene polypropylene rubber (EPR [50]), fluorocarbon rubber (FR [51]), nitrile rubber (NR [52]), natural rubber with polyester (NatPolR [53]), polyethylene rubber (PR [54]), and silicone rubber (SR [55]). Subsequently, an extra soft material, natural rubber (NatR [56]), is added to the analysis.

The results highlight the incompatibility between the PL method and the Wiechert model. Nevertheless, the performance of the optimized Std. Lin. SDS model, i.e. the PL-SLS model is adequate. Similarly, the linearized version of the Wiechert model is called the PL-Wiechert model.

The relationship between the accuracy of the model and the required complexity is assessed. Furthermore, the capabilities of the PL-SLS to account for velocity-dependent stress responses is investigated. On the one hand, the PL-SLS is able to generalize well the stress response, under different strain rates, of some of the studied soft materials. On the other hand, the performance of the model is found to

be biased towards the materials that have more dominant elastic properties. Due to this, an alternative modelling tool is proposed to be investigated in the next chapter, this time, a data-driven modelling tool.

5.2 The Linear Viscoelastic Models

Thermoplastic elastomers have nonlinear and viscoelastic mechanical properties which cannot be easily described by mathematical models. The latter represents an important challenge for current soft robotic developments. However, the benefits of using soft materials are many: energy storing, passive compliance and safe human-robot interaction. This have motivated their implementation in robotic applications, as well as the development of robust modelling tools able to describe their viscoelastic properties [115].

The natural property of the human skeletal muscle system of storing and releasing energy, have motivated the inclusion of elasticity in robotic applications. Series-elastic actuators (SEAs) are the most commonly used technology. The addition of an elastic element between the actuator and the load greatly simplifies the controller design. The deformation of the elastic element can provide an indirect measurement of the applied force to the load, essentially transforming a force-control problem into a displacement-control problem [116].

Traditional SEAs use metallic springs, considered as purely elastic. However, the human skeletal muscle system exhibits viscoelastic behaviour. In the literature, attempts of adding viscoelasticity to SEAs have been done by using soft materials instead of metallic springs. In fact, viscoelasticity has the potential to address many of the limitations found in series-elastic actuators, such as: low torque resolution and low bandwidth [30, 117, 118].

The mechanical behavior of a rigid element (metallic spring) can be accurately described by known mathematical models. This is not the case for soft materials which have nonlinear and viscoelastic properties. The benefits of adding viscoelasticity to SEAs can only be fully exploited by developing a reliable modelling tool. Substantial research has been done on this. However, The most accurate models are mathematically complex and computationally expensive [97, 99, 100]. Nonetheless, even these complex models cannot account for all the different factors which modify the materials properties, such as the manufacturing process and internal weakening of the material after being loaded for the first time [113]. The latter highlights the

5. SOFT MATERIALS MODELLING: LINEAR VISCOELASTIC MODELS

difficulty of developing mathematical models which account for both microscopic and macroscopic aspects of the materials. This has motivated researchers to implement alternative methods for characterizing a material, such as Finite Element Analysis (FEA).

In robotics applications, where the controller can compensate the lack of accuracy in describing the controlled plant, a simple and fairly accurate model is preferred over a very accurate and highly complex one. For this reason, a known set of mathematical models, the Linear Viscoelastic Models (LVMs) are commonly used for the prediction of viscoelasticity in soft materials. In contrast to the mechanical model for Hooke's Law, which is based on a single spring, the LVMs are based on two fundamental mechanical components, a spring and a dashpot, which can be arranged in different configurations and quantities. This is illustrated in Figure 5.1, where the parameters k and η represent the spring stiffness and the dashpot viscous constant, respectively.

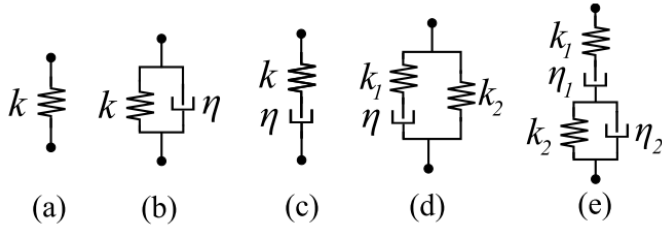


Figure 5.1: Hooke's Law and linear viscoelastic models: (a) Hooke's Law (b) Kelvin-Voigt, (c) Maxwell, (d) Standard Linear Solid, and (e) Burger. The parameters k and η represent the spring stiffness and the dashpot viscous constant, respectively [33].

In line with the mentioned approach of relying on the controller to compensate the limitations of simple models, the work performed by Austin et al. modifies the viscoelastic Standard Linear Solid (SLS) model by implementing a piecewise linearization (PL) [33]. The authors chose this model instead of the more complete, hence more complex, Burger model to keep the modelling process as simple as possible. The implementation of the PL method allowed the SLS model to account for the nonlinear properties of the material stress response in proportion to the applied strain. Due to this, the developed model is called the Standard Linear Solid model with Strain-Dependent Stiffness (Std. Lin. SDS). Unfortunately, the developed model was still unable to account for the material hysteresis, and, due to hardware limitations, the velocity-dependent stiffness effects were not validated. Nonetheless,

experimental tests validated the changes on the material stiffness depending on the velocity of the applied deformation.

The PL method have proven to be a successful way to improve the prediction ability of traditional LVMs. Although it still has some limitations. The latter is addressed in this chapter by implementing the PL method in a more complex member of the LVMs, the Wiechert model. This is described in detail in Section 5.3.

5.3 The piecewise linearization method on the Wiechert model

The SLS model is frequently used when modelling viscoelastic materials, mainly due to its fairly simple mathematical model and its ability to account for creep and stress relaxation of the material (time-dependent properties). The SLS model can be viewed as a Maxwell model (also known as Maxwell branch) with an extra spring connected in parallel. The simplicity of the SLS model is also its main limitation. Viscoelastic materials are known to have more than one relaxation time, i.e. more than one Maxwell branch. In the linear viscoelastic models, the relaxation time depends on the viscous elements, i.e. dashpots. The Wiechert model, which is essentially a SLS model with j Maxwell branches, is able to account for j relaxation times and is illustrated in Figure 5.2. The time-dependent behavior of any viscoelastic material can be fully described by this model, given enough numbers of elements. However, the complexity of the model increases in proportion to the number of extra branches. Mathematically, each extra branch increases the derivative order of the model since more equations are required to account for the extra variables [98, 102].

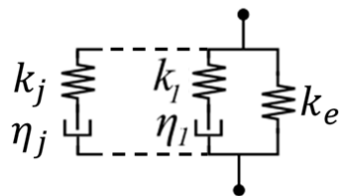


Figure 5.2: Wiechert Model. The components k_1 , η_1 , and the equilibrium spring k_e , together represents the SLS model. The components k_j , and η_j represents the Maxwell Branch. The Wiechert model can contain as many branches as required, this is symbolised by the subscript j .

5. SOFT MATERIALS MODELLING: LINEAR VISCOELASTIC MODELS

As previously described in Section 4.2, in addition to time-dependent and history-dependent properties, elastomers also have a nonlinear stress response. This can be partially described by the LVMs. The relaxation time constant of the dashpots in these models describes the nonlinear and time-dependent stress response of the material. Nonetheless, LVMs are not able to account for the strain-dependent response of materials. The latter can be addressed by the PL method as described in [33].

The spring in parallel with the other elements, in both the SLS model and the Wiechert model, is known as the equilibrium spring, and its stiffness k_e , is assumed constant. In reality, the stiffness k_e of most elastomers is strain-dependent. Early attempts of modelling a strain-dependent stress response in viscoelastic materials are described by Schepelmann et al. in [30], where the stress-strain curve of a nonlinear rubber spring is approximated with an exponential model. In subsequent works, Austin et al. describe a piecewise linear regression fitted to the stress-strain curve of a material, in combination with the SLS model [33].

The slope of the stress-strain curve represents the material's Young Modulus which is proportional to the material stiffness. During a tensile strength test the material is deformed at a constant rate, i.e. $\dot{\varepsilon}$ is constant. The stress response of a viscous element is proportional to the strain rate $\dot{\varepsilon}$. Therefore, it can be safely assume that the observed nonlinear stress response on the stress-strain curve is solely caused by changes in the equilibrium spring stiffness k_e .

Using the PL method, the nonlinear behavior of the equilibrium spring is approximated by considering it as several springs in parallel which “engage” in sequence as the material strain increases. This is modeled by a summation of Heaviside functions centered in the desired strain in which each of the mentioned springs “engage” and contributes with the total stress response of the material. In other words, the stress-strain curve of the material is segmented in several sections which relates a single stiffness to a range of strains. This is illustrated in Figure 5.3.

5.4 Model fitting

The mathematical expression for the SLS model and the Wiechert model can be simplified when considering a constant strain input (stress relaxation test). This simplification allows these models to be fitted into the stress relaxation curve and to approximate the parameters of interest, k and η [102]. The mathematical expression for the Wiechert model under a constant strain input is given by:

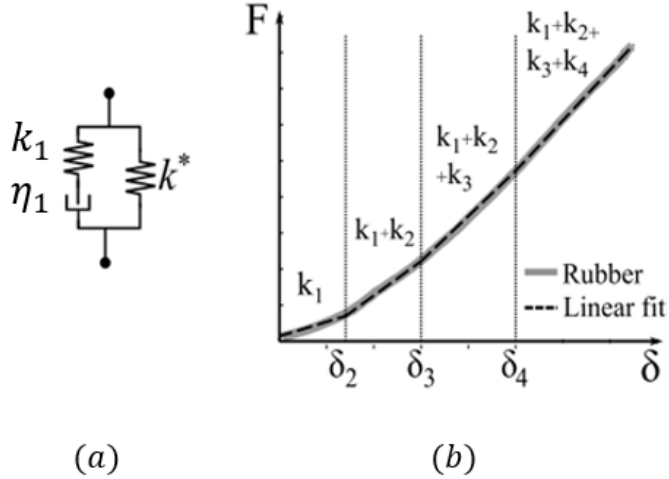


Figure 5.3: (a) Standard Linearized Solid model with Strain-Dependent Stiffness. (b) Piecewise linearization method applied to the slope of the material load-displacement curve. This is analogous to many parallel springs which contribute to the material response depending on the material strain [33]

$$\sigma(t) = \left(k_e + \sum_j k_j e^{-t/\tau_j} \right) \varepsilon_o \quad (5.1)$$

where σ is the stress at a given time, k_e is the equilibrium spring stiffness and ε_o is the initial strain. For the summation, $\tau_j = \eta_j/k_j$ is the relaxation time constant, k_j and η_j are the spring stiffness and viscous constant of the elements in the j^{th} Maxwell branch, respectively. For the specific case when $j = 1$, the resulting equation describes the SLS model under a constant strain input, which is as follows:

$$eq11)\sigma(t) = (k_e + k_1 e^{-t/\tau}) \varepsilon_o \quad (5.2)$$

In equation ??, the three main parameters of the SLS model. i.e. the equilibrium spring stiffness k_e , the dashpot viscous constant $\eta = \tau k_1$, and the spring stiffness in the Maxwell branch k_1 , can be obtained from the stress relaxation curve by analyzing three significant points: $t = 0$, $t = \tau$, and $t = \infty$, as illustrated in Figure 5.4. Due to the decaying exponential nature of this curve, the time constant τ can be related to the point in time t where the stress has decayed to approximately 36.8% of its initial value σ_o . The longer the duration of the test, the better the approximation of k_e .

The process to extract the parameters of the Wiechert model is more complicated

5. SOFT MATERIALS MODELLING: LINEAR VISCOELASTIC MODELS

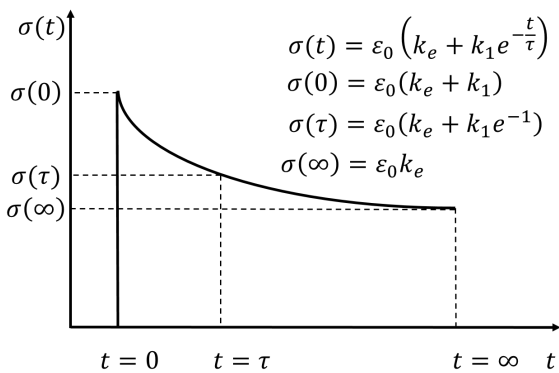


Figure 5.4: SLS model fitted to a typical stress relaxation curve of a viscoelastic material. The parameters k_e , k_1 and η can be obtained by analyzing three points in the curve: $t = 0$, $t = \tau$, and $t = \infty$. The variable τ is the time constant of the exponential decaying curve.

due to its extra Maxwell branches, i.e. there are more than three points in time to be analyzed. These points can be selected using a collocation technique [102, 119]. In the reviewed literature, the points of interest are linearly scattered throughout the whole duration of the stress relaxation curve. Nevertheless, the decaying exponential term in Equation (5.1) is better approximated by selecting the points of interest using a logarithmic scale. This is possible with the MATLAB function `logspace` which spreads evenly the desired number of points between the allowable decades. This is better described with the following example. A Wiechert model with six branches, $j = 6$, is to be fitted into a stress relaxation curve with four decades of duration ($t = 10^4$ seconds). In total it would be required seven points in time, one for each branch and one for $t = 0$. These points are spread as evenly as possible, using the total duration of the test, by the function `logspace`. The point $t = 0$ is required for a correction described in the following paragraph.

Similar to the process illustrated in Figure 5.4, each point in time represents a time constant τ_j for which there is a known stress σ_j from the experimental data. This can be rearranged into an equation system of j equations with k_j as the unknown variable as described in [119].

Prior to this step, k_e can be obtained using the equation for $\sigma(\infty) = \varepsilon_0 k_e$, as illustrated in Figure 5.4. Subsequently, the Wiechert model in Equation (5.1) can be completely described by solving the mentioned system of equations. Finally, after obtaining all the k_j , the value of k_1 is corrected, as described in [102], by analyzing the point in time $t = 0$.

The previous process allows the Wiechert model equation to be fitted into the stress relaxation curve for a defined number of branches j . However, to obtain the optimal number of branches for each material, an iterative algorithm to find the smallest root mean square error (RMSE) between the Wiechert model response and the experimental data after testing different number of branches in the range of $j = [1, 10]$ is implemented. The obtained optimal number of branches for each material varied between the range $j = [8, 10]$. A higher number of branches has a meaningless improvement on the RMSE. Furthermore, beyond the number of branches $j = 20$ the Wiechert model response shows an oscillatory behavior, hence a higher RMSE. Having obtained the parameters of interest for the SLS and the Wiechert model, their stress response under a constant strain is compared against the experimental data in Figure 5.5.

Figure 5.5 highlights the better accuracy delivered by the extra Maxwell branches in the Wiechert model in comparison to the simpler SLS model. As previously mentioned, Equation (5.1) is a simplification helpful to approximate the parameters of both models but it is only applicable when the strain input is constant. The mathematical expression for the Wiechert model which describes the stress response under an unknown strain input, also called the constitutive equation can be found in [102], in its Laplace. As previously mentioned, the Wichert model is an extension of the SLS model. Hence, when making $j = 1$, the constitutive equation of the SLS model can be obtained, i.e. for an unkown strain input, and is presented as follows:

$$\dot{\sigma} + \frac{\sigma}{\tau_1} = (k_e + k_1)\dot{\varepsilon} + \frac{k_e\varepsilon}{\tau_1} \quad (5.3)$$

where ε , $\dot{\varepsilon}$, and $\dot{\sigma}$ are the strain, the strain rate and the stress rate, respectively (for the detailed procedure refer to [102]). Notice that the previous procedure will yield into a higher derivative order equation when applied to the Wiechert model due to its extra branches. A higher number of branches will increase the model accuracy at the cost of increasing its mathematical complexity. The constitutive equation of a Wiechert model with j branches would result in a j order differential equation similar to Equation (5.3). The aim of this chapter is to apply the PL method to the Wiechert model and evaluate its performance. Therefore, dealing with differential equations is out of the scope. Nonetheless, the Wiechert model can be evaluated by transforming it into a finite-differences equation, as explained in [102], yielding the following equation:

5. SOFT MATERIALS MODELLING: LINEAR VISCOELASTIC MODELS

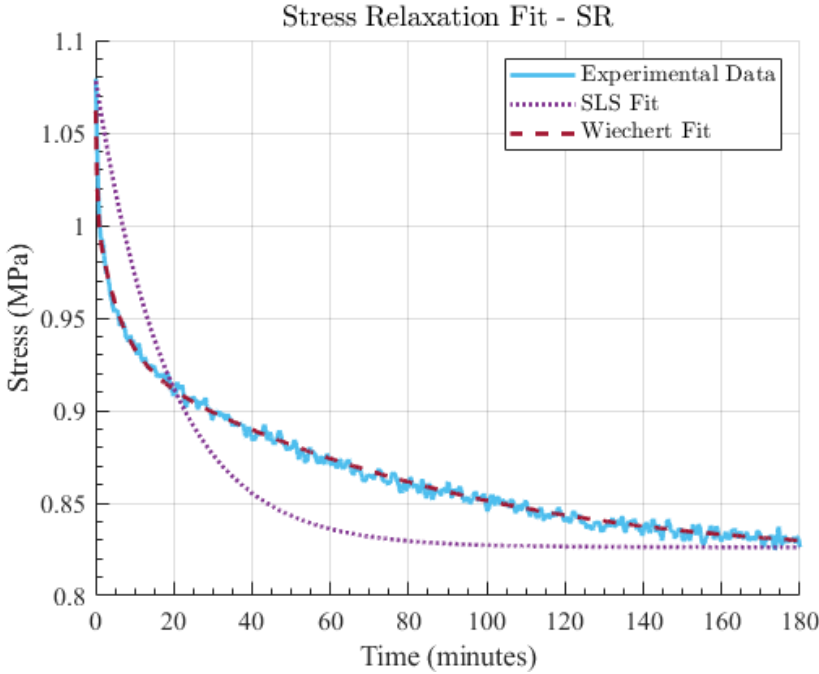


Figure 5.5: Obtained fit from the Standard Linear Solid (SLS) and Wiechert model on the stress relaxation curve of the Silicone Rubber material. The obtained optimal number of branches of the Wiechert model fit is $j = 8$.

$$\sigma^t = k_e \varepsilon^t + \sum_j \frac{k_j (\varepsilon^t - \varepsilon^{t-1}) + \sigma_j^{t-1}}{\left(1 + \frac{\Delta t}{\tau_j}\right)} \quad (5.4)$$

where the superscript $t - 1$ and t refers to values before and after a small time step Δt have passed. Once again, making $j = 1$ on Equation (5.4) yields the finite difference version of the SLS model. The response of the two viscoelastic models of interest will be compared against the experimental data from the tensile strength test.

The next step of the fitting process is focused on the tensile strength test. In this test, the strain rate is constant, hence the resulting stress for both models (Figure 5.1) is dependent on both the equilibrium spring and the Maxwell branches. At this stage of the model fitting process, the parameters of the Maxwell branches in both models are known and their stress response can be calculated. The stress response of the equilibrium spring, k_e , can be isolated by subtracting the stress response of the Maxwell branches to the stress measured in the tensile strength test.

After isolating the stress response of k_e , the final step in the fitting process is to implement the PL to both models and compare their response against the

experimental data. Firstly, the stress-strain curve from the tensile strength test is divided into n segments. As previously explained, k_e is considered as a group of parallel springs which “engage” as the strain increases. This means, each subsequent stiffness is a combination of the ones found in previous segments of the stress-strain curve (Figure 5.3). Lastly, a linear regression is applied on the stress-strain curve for the desired n strain segments to find the slope of the curve. This slope represents the stiffness of the equilibrium spring in each segment. By combining the n obtained stiffness, the stress response of the strain-dependent stiffness k_i^* is defined as follows:

$$\sigma^* = \sum_i^n k_i^* H_{\varepsilon-\varepsilon_i}(\varepsilon - \varepsilon_i) \quad (5.5)$$

where n is the desired number of strain intervals to fit, ε_i represents the strain value at which the i^{th} spring starts contributing to the stress response, the $H_{\varepsilon-\varepsilon_i}$ is the Heaviside or unitary step function centered at ε_i , i.e. the function output goes from 0 to 1 when $\varepsilon - \varepsilon_i = 0$. By substituting Equation (5.5) into Equation (5.3), the Standard Linear Solid model with Strain-Dependent Stiffness is obtained [33].

The LVMs describe a nonlinear relationship between the applied strain and the resulting stress in a material. However, they only account for a linear stress response of the equilibrium spring. In reality, the relocation of internal molecular chains causes viscoelastic materials to exhibit a nonlinear and strain-dependent stress response. This can be solved by implementing a PL into Equation (5.4). The equilibrium spring stiffness k_e is replaced by the strain-dependent stiffness k_i^* , yielding the linearized Wiechert model (PL-Wiechert) in Equation (5.6). Subsequently, the Std. Lin. SDS model, found in [33], is transformed into a finite difference equation, yielding the PL-SLS model described in Equation (5.7).

$$\sigma^t = \sigma^* + \sum_j \frac{k_j(\varepsilon^t - \varepsilon^{t-1}) + \sigma_j^{t-1}}{\left(1 + \frac{\Delta t}{\tau_j}\right)} \quad (5.6)$$

$$\sigma^t = \frac{1}{\left(1 + \frac{\Delta t}{\tau}\right)} \left[\frac{\Delta t}{\tau} \sigma^* + (\sigma^* + k_1)(\varepsilon^t - \varepsilon^{t-1}) + \sigma^{t-1} \right] \quad (5.7)$$

In this chapter, the linearized SLS model (Equation (5.7)) is labeled as the piecewise linearized SLS (PL-SLS) model, differentiating it from the Std. Lin. SDS model documented in [33] due to the different fitting process performed, e.g. removing the stress response of Maxwell branches. The experimental data from the stress relaxation test was used to obtain the parameters in the Maxwell branches of both

5. SOFT MATERIALS MODELLING: LINEAR VISCOELASTIC MODELS

models. Lastly, the required number of branches was different per material, ranging from $j = 8$ to $j = 10$.

5.5 Findings

The following section contains a total of three subsections. Due to the sequence in which this work is performed, Section 5.5.1 and Section 5.5.2 include six out of the seven soft materials included in this work. The material missing from these analyses is the Natural Rubber. Nonetheless, Section 5.5.3 include all the seven studied soft materials. Section 5.5.1 is focused on analyzing the trade-off between the number of strain segments fitted to the stress-strain curve, i.e. complexity, and the achieved accuracy, when being applied to the PL-SLS model and the PL-Wiechert model. Section 5.5.2 is focused on analyzing the accuracy of the PL-SLS model and the PL-Wiechert model in terms on the achieved normalized mean square error. Lastly, Section 5.5.3 is focused on analyzing the capabilities of the PL-SLS model to account for the velocity dependency of the materials stress response. The latter is also directly proportional to the generalization capabilities of the models.

The stress-strain curves from the materials studied in this section are from the tensile strength test with 500 mm/min strain rate. With the exception of the Silicon Rubber material, for which the stress-strain curve for a strain rate of 50 mm/min was used, as mentioned in Chapter 4. The complete list of the different tensile strength tests performed per material can be found in Table 4.1.

5.5.1 Analysis of the optimal number of strain segments

The amount of strain segments and their proper collocation have an impact on the PL method accuracy. In the work presented by Austin et al. there is no explanation about the criteria used to select the strain segments, only an illustration is provided [33]. In this work, the variation of the slope in the stress-strain curve was used as the selection criteria. An optimization algorithm, which automatically collocates a new strain segment when the slope has varied outside a defined tolerance boundary, was developed. The tolerance criteria is based on how much the slope of the stress-strain curve has changed. The extraction of the slope value is done by numerical differentiation of the stress and strain values. The algorithm then takes the first calculated value of the slope as reference to compare it against the rest of the slopes. Whenever the variation between the reference slope and the current slope is beyond

the percentage established by the tolerance, a new strain segment is created. In this way, the tolerance criteria is closely related to the PL method, in the sense that only when the slope of the curve, i.e. the stiffness, has changed enough, then it is justified to apply the PL method to a new section of the stress-strain curve. This also means, that a stricter tolerance criteria will yield in higher number of strain segments.

Furthermore, the proposed tolerance criteria allows the characterization of the relationship between the number of strain segments and the desired tolerance, which provides insights to the relationship between the complexity of the model and its accuracy. This relationship was found to be exponential. In other words, beyond a certain number of strain segments, small improvements in the model accuracy requires a very large number of strain segments. This highlights a design trade-off between good accuracy and high computational complexity. In this analysis, the normalized RMSE (NRMSE) is used as the parameter for measuring the goodness of fit, which also allows to compare the model performance among all available materials [120]. The RMSE is described in Equation (5.8).

$$\text{NRMSE} = \sqrt{\frac{\langle (\sigma^{pred} - \sigma^{exp})^2 \rangle}{\langle \sigma^{exp2} \rangle}} \quad (5.8)$$

where the $\langle \dots \rangle$ represents the arithmetic mean, σ^{pred} and σ^{exp} represent the predicted and experimental values of the stress response of the material.

The PL-SLS model benefits the most from the PL method. It delivers a good accuracy even for small number of strain segments (Figure 5.6). In contrast, the accuracy of the PL-Wiechert does not improve when using higher numbers of strain segments. Moreover, in the cases for the SR and EPR materials, the accuracy gets worse as the number of strain segments increases (Figure 5.6a and Figure 5.6b). These charts are useful to select a proper value for the slope variation tolerance, taking into account the previously mentioned trade-off. It can be appreciated that the optimal tolerance certainly depends on the intended application and on the soft material of choice.

5. SOFT MATERIALS MODELLING: LINEAR VISCOELASTIC MODELS

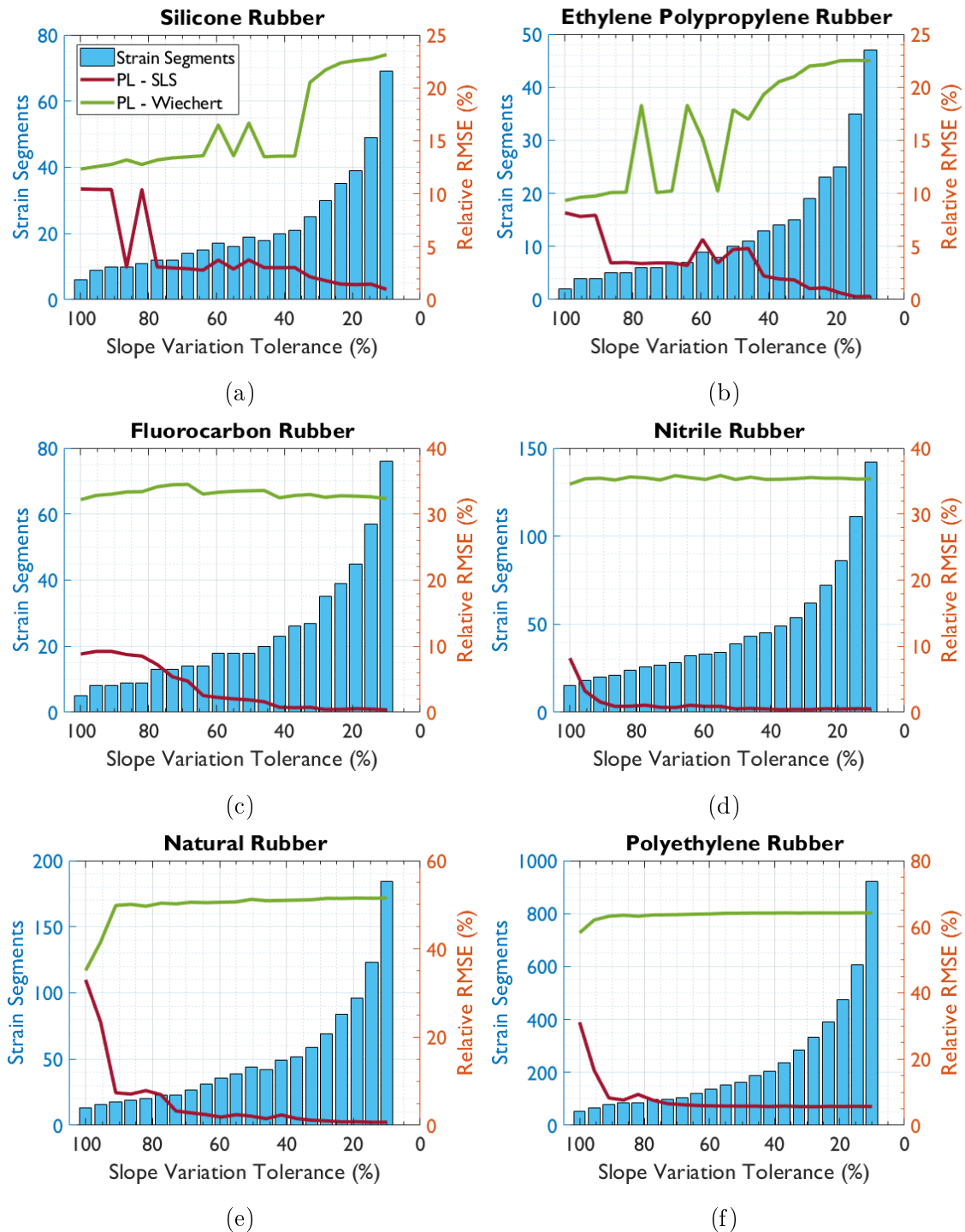


Figure 5.6: Relationship of the desired tolerance between the number of strain segments (blue bars), and the achievable NRMSE of the PL-SLS (solid red) and the PL-Wiechert (solid green) models, for all the soft materials (a-f) [34]

5.5.2 Analysis of model fit accuracy

In the analysis presented in this section, a tolerance value of 20%, for the implementation of the PL in both developed models, the PL-SLS and the Pl-Wiechert, is chosen. This allows the effect of the number of strain segments in the stress response of both models to be analyzed. The obtained fit of both models is compared against the experimental data in Figure 5.7. In general, the stress response of the PL-SLS model outperforms the response of the PL-Wiechert model (Figure 5.7). The PL-SLS model is able to accurately describe the stress-response of all the soft materials. Furthermore, it is able to achieve low values of NRMSE (less than 5%) in four of the six rubber-based materials tested (Figures 5.6b to 5.6e). The slightly higher NRMSE for the SR (Figure 5.6a) and PR (Figure 5.6f) materials might be caused by different factors, being one of them, the simplicity of the SLS model in which the PL-SLS model is based on. As previously mentioned, the SLS model only accounts for a single time relaxation constant. Another possible cause of the slightly higher error in these materials is due to the embedded noise on the processed data due to the limitations on the load cell used in the mechanical tests. Also, it could be possible that even with the precautions taken, the initial deformation applied to the PR material during the stress relaxation test caused it to suffer plastic deformations, hence the extracted data could be erroneous. Another factor, which in theory should affect more the PL-Wiechert model, could be the time collocation method. The poor selection of the points in time to analyze can affect the accuracy of the parameters extracted. The logarithmic collocation approach used here yielded a large number of branches required to describe the material. This can cause the model response to oscillate. Keeping the fitted number of branches to a minimum optimized value can impact the removal of the stress response from the Maxwell branches. This optimization is dependent on the number of branches obtained from the time collocation method. Having more branches allows a better isolation of the stress response on the equilibrium spring. The inverse also applies for a smaller number of branches. This represents a clear trade-off which on the optimal selection on the number of branches to be fitted to the stress relaxation curve.

In the case of the PL-Wiechert model, the very low obtained accuracy might be caused by an essential difference between Equation (5.6) and Equation (5.7). In the latter equation, the strain-dependent stiffness k_i^* interacts with the strain and the strain rate whereas in the former, k_i^* only interacts with the strain. This lack of interaction of k_i^* in the PL-Wiechert allows the abrupt step changes caused by the

5. SOFT MATERIALS MODELLING: LINEAR VISCOELASTIC MODELS

Heaviside function to disrupt the model stress response (Figures 5.7a, 5.7b and 5.7f).

The main limitation of the PL-SLS model is the inability to account the stress offset from the Maxwell branches. This was solved using the parameters obtained from the Wiechert model with j branches, ultimately improving the stress response of the PL-SLS model. The PL-Wiechert model response can be improved by using its constitutive differential equation, similar to Equation (5.3). Even in its simplest form, i.e. $j = 2$, the resulting second order differential equation might outperform the PL-SLS model due to the fact that the strain dependent stiffness k_i^* will interact with different terms of the equation, providing that the process of transforming it into a finite-difference equation does not add extra complications.

Summarizing, in this section the design and development of two mathematical models for the prediction of the viscoelastic behaviour of soft materials is presented. On the one hand, the PL-SLS model, an optimized version of the documented Std. Lin. SLS model, is developed. On the other hand, the PL method was applied to the Wiechert model, a more complex LVMs. The results highlight the incompatibility of the PL method with a complex model such as the Wiechert model. However, the accuracy obtained by the developed PL-SLS is very promising. Hence, the PL-SLS model is used for further analyses.

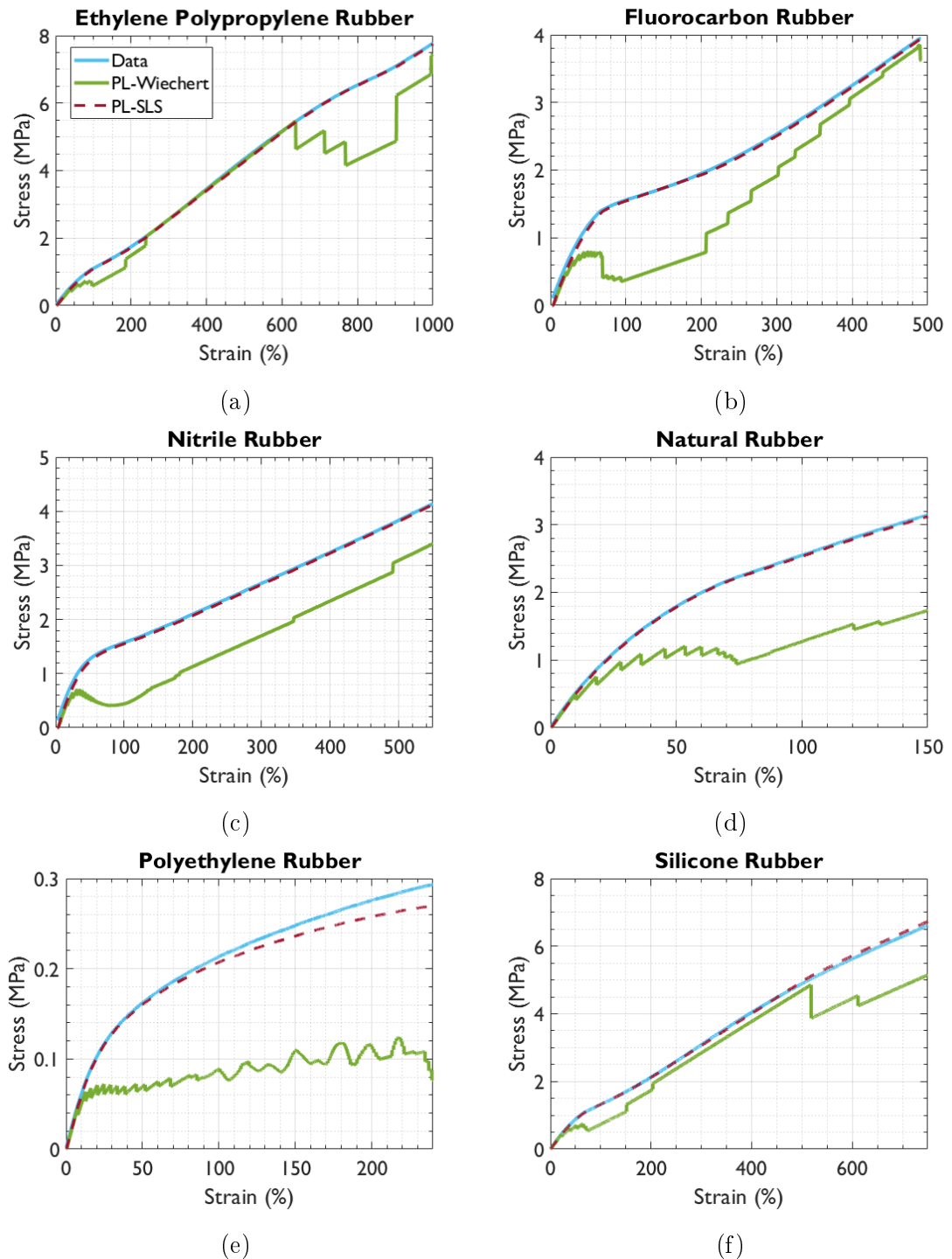


Figure 5.7: Comparison between the experimental data from the Tensile Strength test and the stress response of the PL-SLS (dashed red) and the PL-Wiechert (solid green) models for all the soft materials (a-f). The number of strain segments required to meet the slope variation tolerance of 20% for each material are EPR=20, FR=37, NatPolR=88, NR=73, PR=455 and SR=33 [34]

5. SOFT MATERIALS MODELLING: LINEAR VISCOELASTIC MODELS

5.5.3 Analysis on the velocity-dependent stress response

The PL-SLS model developed in here is based on the Std. Lin. SDS model, developed by Austin et al. [33]. In their work, they were not able to test the ability of the developed model to account for the velocity-dependent stiffness on the studied material, due to hardware limitations. In this section, the latter is investigated by using the tensile strength data of seven soft materials under different strain rates. A total of three different strain rates were used in the tensile strength tests. Refer to Table 4.1, for the complete list of available datasets per material.

In the previous section, the capabilities of the PL-SLS model to predict the stress-response of the materials under a single strain rate were demonstrated. In the following analysis, the strain-dependent stiffness of the equilibrium spring k^* has a major role. This parameter is to be extracted from one of the stress-strain curves of the materials when being deformed at a specific strain rate. The extracted k^* is then used to predict the stress response of the soft material when a different strain rate is applied to it, remembering that there are up to three available strain rates per material.

Looking back to the mechanical representation of the PL-SLS model in Figure 5.3, it can be seen that the only time-dependent component is the dashpot located in the Maxwell branch. The relaxation time constant of this component was approximated using the stress relaxation test. Therefore, at this point, all the parameters from the PL-SLS model are known, i.e. all the parameters of the material are known.

The PL-SLS model accuracy is exponentially proportional to the number of strain segments used. Previously, the NRMSE was used as the parameter for measuring the performance of the model. Nonetheless, having a very small error does not necessarily reflect a good fit, and can in fact cause the fitted model to only perform well for a specific set of data, or in this case, a specific strain rate. Therefore, there must be an adequate number of strain segments which describes the strain-dependent stiffness of the materials under different scenarios, i.e. strain rates. The latter is investigated in this section.

The analysis performed in here is described as follows. The same stress-strain curves used in the previous section are used in here. That is, the strain rate of 500 mm/min is used for all the materials, with the exception of the SR material, in which the stress-strain curve of a 50 mm/min strain rate is used. Subsequently, the PL-SLS model is fitted into these curves to extract the strain-dependent stiffness

of the spring k^* . The latter is done for different tolerance values, ranging from 100 to 10, in steps of 10. Therefore, the fitting process is performed 10 times, i.e. 10 different k^* are extracted. Then, the extracted k^* are used to predict the stress-strain curve of the materials for all the other available strain rates (Table 4.1). The NRMSE between the prediction of the PL-SLS model and the experimental data is calculated. Finally, the results are illustrated in Figures 5.8 and 5.9.

In Figures 5.8 and 5.9 the performance of the PL-SLS to account for the velocity-dependent stress response of the materials is assessed. In general, there is not an immediate relationship between the tolerance values and the achieved NRMSE. In some cases, using a lower tolerance value, hence fitting more strain segments to the stress-strain curve of the material, does improve the achieved NRMSE (Figures 5.8a, 5.8d, 5.8e and 5.9a). Moreover, the accuracy of the PL-SLS model decreases as the strain rate used for prediction is farther away from the strain rate used for extracting the strain-dependent stiffness k^* . This is very evident for the materials in which the stress-strain curve with the strain rate of 500 mm/min was used for the fitting process. In these cases, the PL-SLS model performs the worst for the stress-strain curve with the 50 mm/min strain rate (Figures 5.8a to 5.8e and 5.9b). This is not as evident for the SR material, in which the stress-strain curve with strain rate of 50 mm/min was used. However, the NRMSE does increase as the strain rate increases (Figure 5.8f). Furthermore, the performance of the PL-SLS model for the stress-strain curve with a 50 mm/min strain rate of the NatR material was found to be very poor (Figure 5.9b). This could be caused by the low amount of data available for this specific strain rate. Therefore, this is considered as an isolated scenario.

In general, the PL-SLS model showed decent generalization capabilities for the NatPolR, SR and NatR materials, in which the highest NRMSE obtained is below 20% (Figures 5.8d, 5.8f and 5.9a). Nonetheless, the PL-SLS model performed poorly for the remaining materials, as observed in Figures 5.8a to 5.8c and 5.8e, in which the highest NRMSE achieved is close to 100%.

5. SOFT MATERIALS MODELLING: LINEAR VISCOELASTIC MODELS

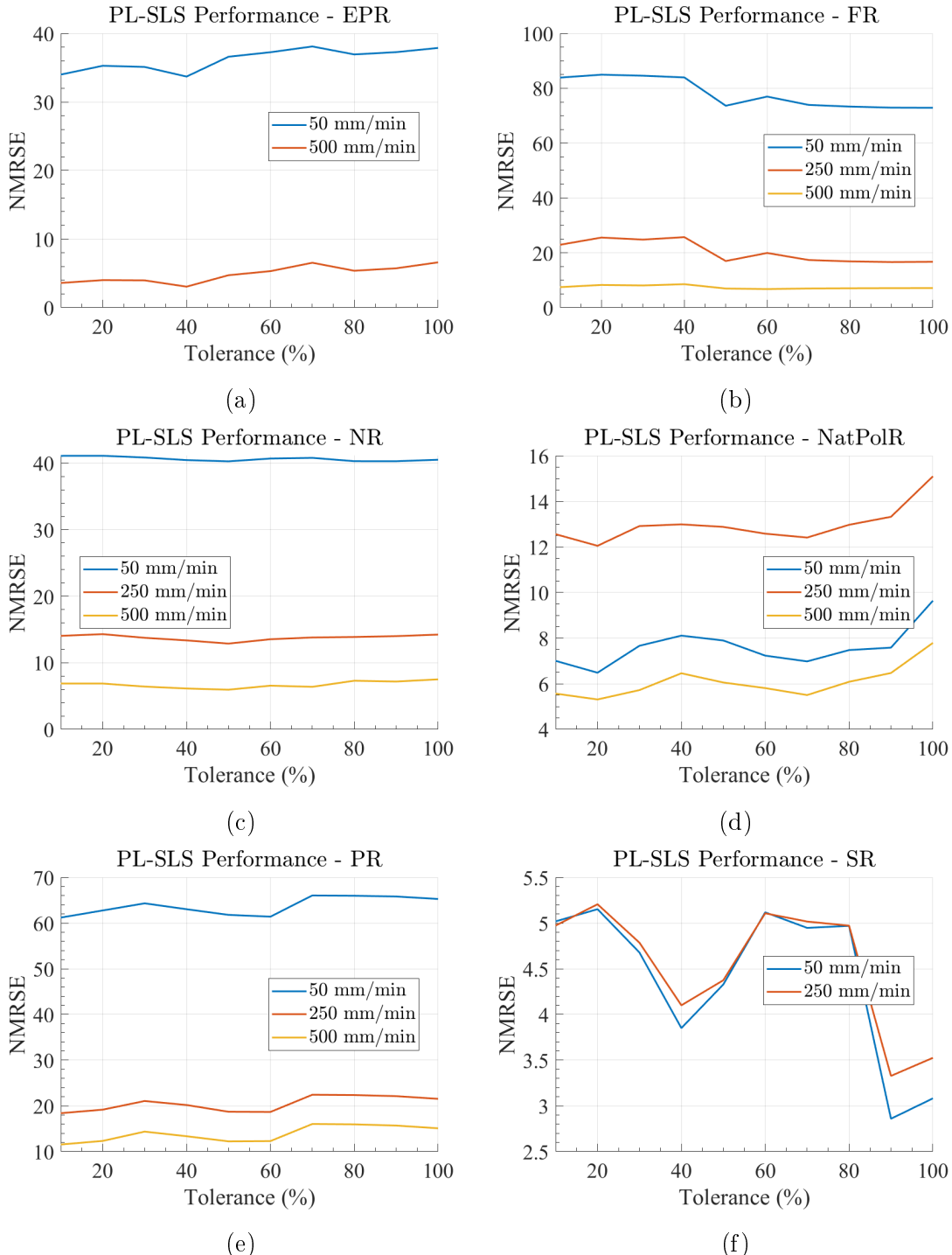


Figure 5.8: Generalization capabilities of the PL-SLS model for the (a) EPR, (b) FR, (c) NR, (d) NatPolR, (e) PR and (f) SR materials. The strain dependent stiffness k^* is extracted from the stress-strain curve of the studied materials using a range of 10 different tolerance values. Subsequently, the obtained k^* is used to predict the stress-strain curves of the strain rates that were not used in the extraction of k^* .

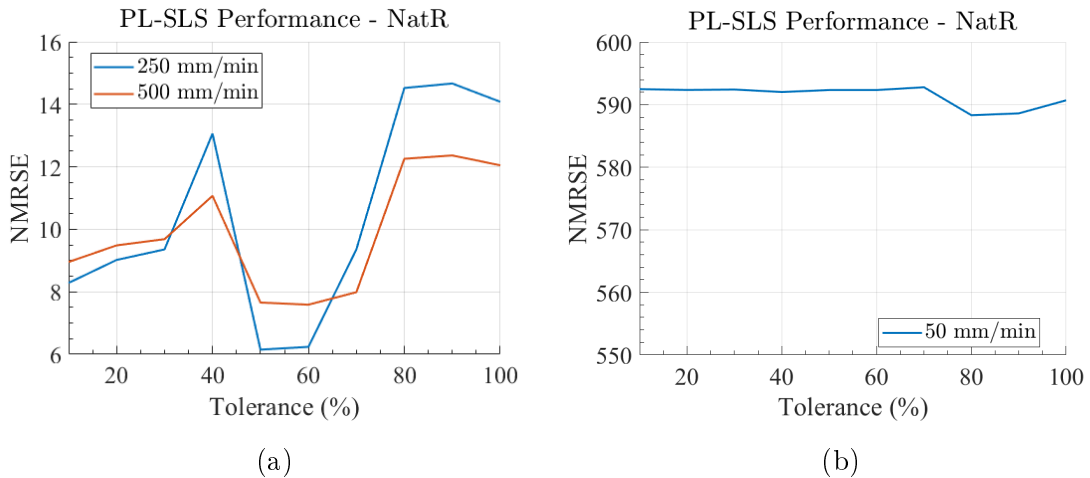


Figure 5.9: Generalization capabilities of the PL-SLS model for the NatR material. The chart was divided into two due to the large difference in the achieved NRMSE for the strain rate of (a) 250 mm/min and (b) 50 mm/min. The strain dependent stiffness k^* is fitted to the stress-strain curve of the materials for a 500 mm/min strain rate, using a range of 10 different tolerance values. Subsequently, the obtained k^* is used to predict the stress-strain curve of the mentioned materials for other strain rates.

An example for the case in which the PL-SLS performed the worst and the best, are illustrated in Figures 5.10a and 5.10b, respectively. Due to the high tolerance used for the worst case example, six out of the seven of the strain segments fitted were located in the strain range of $0 < \varepsilon < 0.3$, preventing the PL-SLS model from describing a large part of the curve.

As previously mentioned, the capability of the PL-SLS model to account for time-dependent, or velocity-dependent, stress responses is because of the single viscous element in the SLS model (Figure 5.3). Therefore, the performance of the PL-SLS model could be limited by the fact of only accounting for one time relaxation constant. In other words, the PL-SLS model is able to perform well for viscoelastic soft materials that are more on the elastic side than for those which have very strong viscous properties. The latter was one of the main motivations to analyze the Wiechert model as a potential alternative. However, this turned out to be unsatisfactory. The fact that the PL-SLS model performs well for soft materials with more dominant elastic properties means that the capabilities of accounting for velocity-dependent stress responses are poor.

5. SOFT MATERIALS MODELLING: LINEAR VISCOELASTIC MODELS

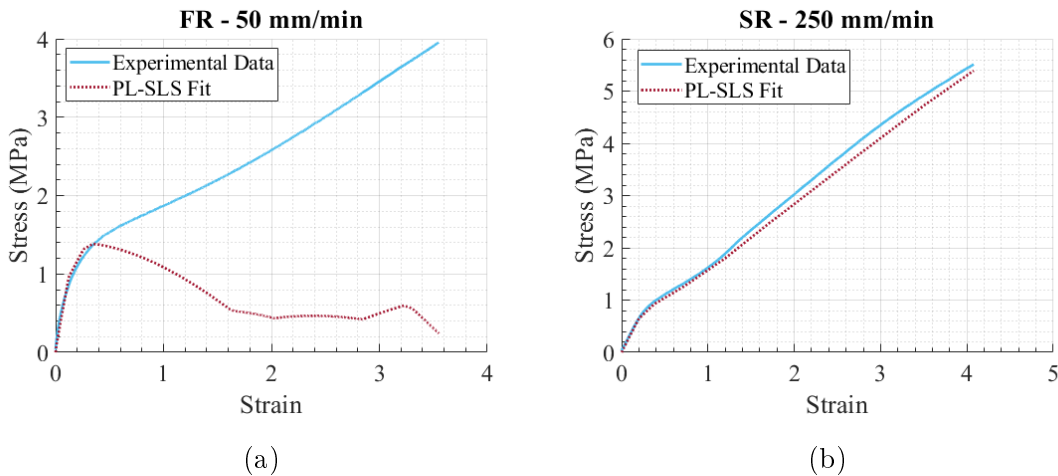


Figure 5.10: PL-SLS model prediction of a strain rate different to the one used in the fitting process. (a) Worst prediction performance case, for the FR material stress-strain curve with mm/min strain rate. (b) Best prediction performance case, for the SR material stress-strain curve with mm/min strain rate. The chosen tolerances values for (a) and (b), were 50% and 10%, respectively.

In conclusion, an in depth analysis of the elastic and viscous properties of the studied soft materials is not required to understand the main limitation of the PL-SLS model, which is not having more viscous components to account for more time relaxation constants. Nevertheless, the performed analysis highlighted the great potential of the PL-SLS model to describe the nonlinear and strain-dependent stress response of all the studied soft materials. Furthermore, the findings of the latter analysis indicate that there is little room left for making further optimizations to the developed model. Therefore, an alternative data-driven approach is investigated in the following sections of this research.

5.6 Summary

The experimental data obtained from the stress relaxation tests of six soft materials is used to describe the parameters of two mathematical models, the SLS and the Wiechert model. Both models were fit into the stress relaxation curve to extract their parameters. The fitting process for the SLS model is straight forward and the simplicity of the model yielded in a large RMSE. In contrast, the Wiechert model was fitted using a time collocation technique which yielded in a system of equations required to be solved to obtain all the model parameters. In addition to this,

an optimization algorithm is implemented to obtain the right amount of Maxwell branches required to minimize the RMSE. The optimal number of branches varies from one material to the other in the range of $j = [8, 10]$. The stress response of the optimal number of Maxwell branches is subtracted from the tensile strength test data. This step allows the piecewise linearization to better approximate the strain-dependent stiffness of the equilibrium spring. Due to the lack of explicit information regarding the PL method implementation [33], an algorithm to locate the strain segments for the PL method using the variation of the slope of the stress-strain curve as the selection criteria, is developed. The relationship between the previous tolerance with the achievable NRMSE and the number of strain segments is obtained (Figure 5.6). These set of charts have the potential to be used as design guidelines when using the reported soft materials in robotic applications, since they highlight the trade-off between the achievable accuracy and the computational cost. The process of implementing the PL method into the linear viscoelastic models yielded the PL-Wiechert and PL-SLS models. These models are presented in the form of finite difference equations to evaluate their stress response. The results demonstrates the great accuracy of the PL-SLS model in describing the stress-strain curve of six soft materials, in comparison to the PL-wiechert model. The PL-method turned out to be incompatible with the Wiechert model. The latter is due to an essential difference between Equation (5.6) and Equation (5.7). In the latter equation, k_i^* interacts with the strain and the strain rate whereas in the former, k_i^* only interacts with the strain. This lack of interaction allows the abrupt step changes caused by the Heaviside function to disturb the PL-Wiechert model response. The analysis performed up to this point included six out of the seven soft materials. The material missing is the Natural Rubber.

The developed PL-SLS model, an optimized version of the Std. Lin. SDS model, was identified as the best candidate for the prediction of the nonlinear and strain-dependent stress response of the studied soft materials. In addition to this, the capabilities of the PL-SLS model to account for velocity-dependent stress responses was assessed. This analysis was not available in the reviewed literature. The analysis, which included all of the seven soft materials, yielded very interesting findings. On the one hand, the PL-SLS model is able to generalize well the stress-stain curves of the NatPolR, SR, and NatR materials, for up to three different strain rates. On the other hand, the PL-SLS model performed very poorly for the remaining materials. The poor performance of the PL-SLS model is directly related to the fact

5. SOFT MATERIALS MODELLING: LINEAR VISCOELASTIC MODELS

that the model only accounts for one time relaxation constant. In other words, the PL-SLS model is able to generalize well the stress response under different strain rate of viscoelastic soft materials with more dominant elastic properties. Therefore, the model capabilities to account for velocity-dependent (time-dependent) stress responses is poor. Lastly, due to the latter findings, an alternative modelling tool is investigated in the following chapter.

CHAPTER 6

Soft Materials Modelling: Artificial Neural Networks

6. SOFT MATERIALS MODELLING: ARTIFICIAL NEURAL NETWORKS

6.1 Introduction

In the previous chapter, the development of a mathematical model for the prediction of viscoelastic behaviour in soft materials is described. The PL-SLS model is able to successfully model the nonlinear stress response of seven soft materials. Nevertheless, the model is not able to account for the velocity-dependency response of the soft materials. The latter is critical to predict the time-dependent properties of commonly used soft materials in soft robotic applications. Therefore, an alternative approach is investigated.

The field of machine learning provides reliable data-driven modelling tools, such as artificial neural networks (ANNs). ANNs have been successful in extracting complex mechanical parameters of soft materials, and are now being used to model the stress-strain curve of many materials. Nonetheless, back in 2016 the literature on the latter subject was very scarce. It is until 2019, that a surge in research dealing with the implementation of different architectures of ANNs, in combination with Dynamic Mechanical Analysis (DMA), is being performed as an attempt to model the viscoelastic properties of soft materials. Nonetheless, there is still plenty of research to be done, such as implementing ANNs for the real-time prediction of the viscoelastic properties of soft materials. In this context, real-time prediction refers of deploying the trained ANN model into a control system, essentially replacing the mathematical model commonly used to estimate the stress-strain curve of elastic elements used in series-elastic actuators. This gap in the body of knowledge is addressed in this research.

In this work, a feedforward ANN model is developed. The Bayesian Regularization algorithm is used during the training process. The selection of inputs and outputs to be included to the network is optimized by observing the generalization capabilities of different combinations. The total number of neurons in the hidden layer is also optimized to minimize the risk of a common phenomenon known as over-fitting. The optimal number of neurons varies from one soft material to the other, but in any case exceeds 10 neurons.

Finally, the generalization error of the developed ANN is compared against the previously developed PL-SLS model. In general, the developed ANN outperforms the PL-SLS model in both achievable error and generalization capabilities. Hence, the ANN is considered successful in accounting for the velocity-dependent stress response of the materials. Nonetheless, the PL-SLS performs better than the ANN model for one single material, the SR material. This is correlated with the fact that

the SR material is very elastic, hence its stress response is not dependent on the strain rate. This could play a role in the performance of the ANN which has the strain rate as input, ultimately confusing the ANN rather than contributing to the learning process.

6.2 Artificial Neural Networks

Artificial Neural Networks (ANNs) are computational systems inspired in the structure and functionality of the biological nervous system. Neurons, a specific type of cell, are the basic components in the brain. They form connections with a vast number of other neurons, allowing us to remember, think, and apply previous knowledge to our present actions. The basic functionality of a neuron is to receive information in its inputs from many sources, to combine this information, to apply a nonlinear operation, and to output the end result. Moreover, neurons are capable of specializing for a specific task by amplifying or reducing the impact of their individual inputs. Neurons are also capable of reorganizing themselves in complex interconnected clusters in a three-dimensional space, called biological neural networks, where the information flows from one group of neurons to the other.

Similarly, Artificial Neural Networks are composed of many basic components, known as artificial neurons, working in parallel. The clustering found in biological neural networks, can be replicated in ANNs by creating layers, containing many neurons, which can be interconnected between each other in different ways. The simplest structure of an ANN is composed of three layers: an input layer, a hidden layer, and an output layer. As the name suggest, the input and output layers interface the ANN with the outside world. The main learning process happens in the hidden layer. The way in which the interconnections between these three layers are formed, are mainly dependent on the application. The strength of each interconnection depends on a weighting factor, enabling the artificial neuron to amplify or reduce the contribution of a specific input. The fine tuning of these weights, performed in a process called training, allows ANNs to specialize in a particular task, i.e. allow them to learn. The latter highlights the capability of ANNs to simulate two key functionalities of the human brain, which are: acquiring knowledge from the environment through a learning process, and storing this knowledge in the form of inter-neuron connection strengths, i.e. synaptic weights. The capability of learning from experience, i.e. experimental data, make ANNs particularly useful when deal-

6. SOFT MATERIALS MODELLING: ARTIFICIAL NEURAL NETWORKS

ing with complex scientific and engineering problems where an adequate analytical description is not available, or is too complex [121, 122].

Artificial Neural Networks can have as many layers as required, simulating the clustering phenomenon found in biological neural networks. These type of multi-layered ANNs can be categorized depending on how the information flows inside it. For example, an ANN in which the information flows in one direction, from the input layer up to the output layer, is called Feedforward Neural Network (FFNN). This type of ANN, illustrated in Figure 6.1a is one of the most commonly used for function approximation, pattern recognition and classification [121].

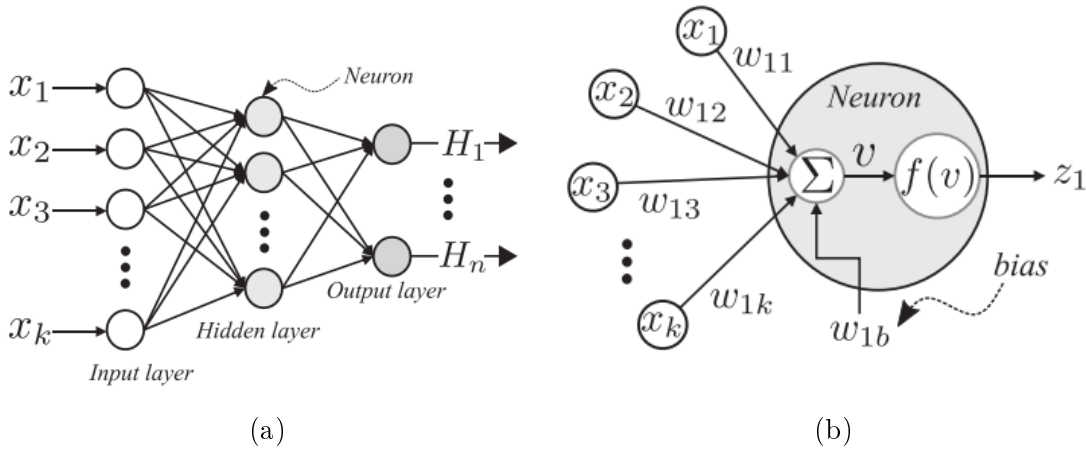


Figure 6.1: (a) Feedforward artificial neural network (b) Internal structure of an artificial neuron [35]

The variables illustrated in Figure 6.1a are as follows. The inputs of the ANN are represented by the variable \mathbf{x} , in the form of:

$$\mathbf{x} = [x_1, x_2, x_3, \dots, x_k] \quad (6.1)$$

where k represents the total number of inputs. Similarly, the outputs of the ANN are represented by the variable \mathbf{H} in the form of:

$$\mathbf{H} = [H_1, H_2, H_3, \dots, H_n] \quad (6.2)$$

where n represents the total number of outputs. Furthermore, the output of the neuron illustrated in Figure 6.1b, combines the individual weighted values of the input vector x with a bias value. Then, a nonlinear function is applied to the result of this sum. This is described as follows:

$$z_1 = f \left(\sum_{i=1}^k (x_i w_{i,j}) + w_{1,bias} \right) \quad (6.3)$$

where $w_{1,1}$ to $w_{1,k}$ represents the weights of one neuron which interacts with all the inputs. The first subscript in $w_{i,j}$ indicates to which neuron this weight is interacting, whereas the second subscript indicates the input that this weight is related to.

In order for the ANN to learn, they must be trained first. In FFNN the most common approach for training is based on the backpropagation algorithm. The training process of ANN commonly involves dividing the available data into a training and a test subset. The former subset is used for training of the ANN, whereas, the latter is used for testing the prediction capabilities of the ANN after being trained. During training, the ANN is presented with known values of the output, called targets, which are related to a specific combination of inputs. In each training session the ANN will adapt slightly until its output is close to the target value. The backpropagation algorithm is based on minimizing the sum of square errors (SSE) between the target and predicted values, by modifying the weights and biases of the ANN [121]. This algorithm is so powerful in minimizing the error that it could cause the ANN to memorize the training dataset instead of generalizing it. This means that the ANN will not be able to provide accurate predictions when new data is presented to it. This issue is called over-fitting.

According to the literature, FFNN are capable of representing any functional relationship between a set of inputs and outputs, as long as the ANN has enough number of neurons in its hidden layers. However, having too many neurons increases the risk of over-fitting. As previously mentioned, over-fitting will prevent the ANN to generalize well. Therefore, when designing an ANN, it is better to use the minimum amount of resources which are able to provide a good fit. There are two main methods for preventing over-fitting from happening, i.e. improving generalization, during the training process: early stopping and regularization. On the one hand, in the early stopping method, a third subset of data is involved, called the validation subset. In general terms, when the error during the validation process increases during certain number of consecutive training sessions, then over-fitting is detected and the training process is stopped. On the other hand, in a regularization method the performance function used during training, commonly the SSE of the ANN prediction, is modified. For example, in the Bayesian Regularization method, the performance function has an additional condition, which is to minimize the SSE of the weights and biases of the ANN. This puts a check on the correction power

6. SOFT MATERIALS MODELLING: ARTIFICIAL NEURAL NETWORKS

of the backpropagation algorithm, which allows the weights and biases to be fine-tuned rather than have large variations. There are many variables involved in the process of designing and optimizing an ANN for a specific application. Therefore, the relevant works on implementation of ANN for the modelling of soft materials are presented as follows

6.3 ANN for Modelling of Soft Materials

Artificial Neural Networks have been implemented in a wide number of applications, such as: forecasting, control, power systems, robotics, signal processing, manufacturing, pattern recognition and optimization [123]. At the time of writing this document, the available literature about the implementation of ANNs for the modelling of the complex behaviour of soft materials, specifically elastomers, was scarce. Recently there has been an increase in the number of published papers focusing on modelling soft materials using ANNs which highlights the relevance of this field of research.

One of the earliest works in this field is documented in [124] by Zhang et al.. In here, a FFNN is developed to model the dynamic mechanical properties of short fibre reinforced materials. The trained ANN was able to provide prediction values for the storage modulus and damping of the material for temperature values not used during the training process. Many properties of the material are provided as input to the network. The developed ANN had 25 neurons in its single hidden layer with a tan-sigmoidal transfer function, whereas the output layer had a linear transfer function. The Bayesian Regularization algorithm was used for training. The prediction capabilities of the ANN were assessed using the percentage of correct predictions, in which a prediction with an R^2 value greater than 0.9 is considered correct. The ANN was tested 50 times with a randomized test set each time. Moreover, the authors found a proportional relationship between the complexity of the parameters to model, and the amount of data required for training to achieve a good accuracy.

The review paper of Zhang et al. about the implementation of ANNs in polymer composite applications, found that the available literature on the subject was scarce at that time [121]. Moreover, the documented applications ranged from modelling of the fatigue life of the material, to prediction of tribological and dynamic mechanical properties of composite materials [124, 125]. This review paper provided very insightful evidence of the potential of ANNs for applications such as: design of new

composite materials, optimization of the manufacturing process, and modelling the relationship between different manufacturing parameters. From the reviewed works, the authors were able to find a well defined sequence of actions which describes the process of implementing ANNs for the prediction of the mechanical properties of composite materials:

1. **Data collection:** the first step in designing an ANN is to collect enough data from experimentation. On top of this, processing of the collected data, mainly to filter out noise, might be required.
2. **ANN design and training:** the second step is to design the ANNs depending on the application at hand. This involves deciding on the best parameters to use, in terms of: number of neurons, number of hidden layers, training algorithm and neuron's activation function. Also, this step involves the training of the proposed ANN.
3. **Test of the trained network:** this step is about assessing the prediction and generalization capabilities of the trained ANN. The former is commonly assessed by looking at the difference between predicted and experimental values, as a general rule, the lower the error, the better the prediction. The generalization of the network is assessed by statistical methods such as p-fold cross-validation and the coefficient of determination.
4. **Use of the trained network:** the last step is to use the trained network to simulate new data or for prediction.

The latter process highlights the large number of configurations available when tackling a modelling problem. Due to this, some works in the literature opt for a “trial and error” approach when investigating the potential of ANN for a specific application. Nonetheless, many works do perform optimizations in more than one of the ANN hyper-parameters. For example, motivated by the limitations of traditional viscoelastic models, the viscoelastic behaviour of polymer composites is investigated by Al-Haik et al. in [126]. In here an ANN is developed to predict the stress relaxation characteristics of a polymer composite. The amount of data used in here is rather large, having 900 datasets covering different conditions of the stress relaxation process. The training algorithm used is the scaled conjugate gradient. In addition to this, the optimal brain surgeon algorithm is used to optimize the topology of the network. The latter algorithm assesses the contribution of each neuron to the

6. SOFT MATERIALS MODELLING: ARTIFICIAL NEURAL NETWORKS

final results, by removing neurons one by one. This process is also known as pruning. The developed ANN had two hidden layers with 45 and 39 neurons, respectively; and was successful in modelling the stress relaxation characteristics of the material for ranges in which viscoelastic models were unsuccessful.

Initial works on this field of research were solely focused on one specific material. However, as the research matured, more materials were studied in a single work. This is the case for the work from Trebar et al. where a total of 12 different composite materials, natural rubber among them, were studied [122]. This work is more oriented towards assessing the generalization capabilities of ANN for this specific selection of materials, having the previous knowledge of ANN being successful for the modelling of viscoelastic materials. Therefore, more attention is given to the validation of the ANN prediction. This is done by using three different statistical parameters: (i) the root mean square error (RMSE), (ii) the normalized to the standard deviation, (iii) the mean absolute percentage difference (MAPE), and (iv) the percentage of correctly classified samples. In this case, the Levenberg-Marquardt algorithm, an early stopping method, was used to prevent over-fitting. The dataset was divided into training (80%) and testing (20%) subsets. The training subset was further subdivided, allocating 80% of the data for the actual training and 20% for the validation process required for the early stopping algorithm. Different number of neurons in the hidden layer were tested, ranging from three neurons to three times the number of inputs. The latter ratio has also been mentioned in [121], where three to four neurons per input node are found to be the optimal ratio. Although this is more a suggestion rather than a rule. Trebar et al. assessed the impact of using raw and preprocessed data for the training process. The preprocessed data consisted of the statistical parameters of the mechanical properties used as input, such as the standard deviation and mean values. The authors found that the developed ANN was in agreement with the experimental data of studied mechanical parameters of hardness and tensile properties.

Current implementations of ANN in this field are focused more on using the ANN as an alternative to current mathematical models for the prediction of the stress relaxation and stress-strain curves of the materials. For example, in [127], the prediction capabilities of an ANN are compared against one of the LVMs, the Generalized Maxwell model, also known as the SLS model. A rather simple ANN was developed here, having only one input, the time, and one output, the stress. The back-propagation with declining rate algorithm was used for training. The

performance of the ANN was assessed by the total sum of squared errors (TSSE) and by commonly used statistical parameters, such as the RMSE and R^2 coefficient. The optimal number of neurons was found by trial and error, keeping the learning rate, momentum and total number of epochs constant. In this case, the logarithmic sigmoid function was chosen due to the compatibility with the stress relaxation behaviour. The main difference between the latter function and the tan-sigmoid function is that the former have an output range of $[0, 1]$, whereas the latter range is $[-1, 1]$. In another work, the SLS model is again compared to an ANN [128]. In this case, many hyper-parameters, such as the number of neurons, number of hidden layers, and activation function in the hidden layers, are optimized by trial and error. Particular attention is put to the activation function of choice, which are tan-sigmoid (tansig) and logarithmic sigmoid (logsig). All combinations of using the latter function for a single and double layer network were assessed. The combination of using logsig and tansig in a double layered network was found to be the most optimal. The assessment of the performance of the ANN is based on the training time, overall training error and maximum error. The ideal network would have these parameters at its minimum values. This approach of minimizing the number of resources of the ANN was previously mentioned as a way to avoid over-fitting. Lastly, both mentioned works are good examples of the potential of ANN of replacing traditional mathematical model for the prediction of the stress relaxation of soft materials.

In line with the aim of this work of implementing ANN for the prediction of the complex stress-strain curve of some materials, the relevant works available in the literature are as follows. The literature on ANN for the modelling of the stress-strain curve of soft materials is very scarce and fairly recent, in comparison to the literature available for metals [129–131]. Nonetheless, one of the earliest attempts of modelling the stress-strain curve of non-metal materials is documented in [132]. In this work, polymer composite materials are studied. The ANN developed in here follows the same trend of using FFNN. However, the number of neurons and hidden layers are larger than in previous applications. In this work, up to three hidden layers and up to 45 neurons, are investigated. The aim of this work was to analyse the effect of polymer blending ratio in the stress-strain curve of these materials. Current mathematical models were only effective, for the previously mentioned task, inside the elastic range of the material. The developed ANN was able to overcome this limitation. Moreover, a logsig activation function was used,

6. SOFT MATERIALS MODELLING: ARTIFICIAL NEURAL NETWORKS

together with a backpropagation training algorithm. No information is given on the reasoning behind the selection of neurons and hidden layer, therefore a trial and error approach must have been adopted.

More recent works specifically investigated the performance of ANN for the modelling of soft materials such as elastomers and thermoplastic elastomers (TPEs). An example of this is documented in [133]. The aim of this work is to model the temperature dependency on the dynamic mechanical properties of TPEs. Therefore, the materials are characterized using a Dynamic Mechanical Analysis (DMA), which describes the stress response of the material on a range of frequencies or strain rates. Nonetheless, the study is focused on a single frequency of 1 Hz. This particular work is closely related to the research presented in this thesis. Therefore, the methodology implemented by the authors is of interest. The work focuses on thermoplastic polyurethanes (TPUs). Again, the FFNN architecture is chosen for the developed ANN. The temperature history is presented as input to the network, whereas the storage modulus, damping factor, and loss modulus are the desired parameters to predict. Three individual ANN were developed, one for each parameter. The latter parameters describes the viscoelastic properties of materials. In terms of the activation functions, the commonly used configuration of having a tangent-sigmoid function in the hidden layer and a linear function (purelin) in the output layer is chosen. The Levenberg-Marquardt back-propagation minimization algorithm was implemented. No particular measurements, besides the already provided by the training algorithm, were implemented to ensure good generalization capabilities of the network. Among the three developed ANN, no more than 15 neurons were used.

Kopa et al. continued the latter research in a recently published paper [134], this time focusing on predicting the uni-axial tensile response of vulcanized rubber. Again, a FFNN is developed. The inputs were the engineering strain and the carbon black content in the rubber blend. The output was the engineering uni-axial stress. The optimal number of neurons was found by trial and error, being six the optimal number of neurons. Similarly to previous applications, the tansig-purelin combination of transfer function was chosen. The Levenberg-Marquardt algorithm was also used. The main contribution of this work is the validation approach implemented, which is based on knowing the relationship between the material stress-strain ultimate values, and the carbon black content of the material. A quadratic regression was able to describe the latter with adequate accuracy. This is a simpler approach in comparison to fit the whole stress-strain curve of a material with a LVM. In

summary, the ANN was presented with unknown values of carbon content, obtained from the regression model. The validation was successful since the ANN was able to, not only agree with the ultimate strain-stress values corresponding to that carbon black content, but to also describe the whole stress-strain curve.

Lastly, the most recent work on this research field was performed by Rodriguez et al. in [35]. Many thermoplastic elastomers are studied in this work. Their stress/strain curves are extracted from an available dataset, hence no mechanical characterization is performed. The developed ANN is aimed to model the stress-strain curve of many thermoplastic elastomers under different values of temperature. In comparison to previous works, several optimizations are performed in this one. For example, the training process of the ANN consist of two steps. Initially, the Simulated Annealing (SA) algorithm is used to explore initial solutions for the weights of the network prior to applying the greedy gradient-based Levenberg-Marquardt (GGLM) algorithm. The main objective of the SA algorithm is to prevent the weights, tuned by the GGLM algorithm, to fall into a local minimum. The latter is a well-known side effect of Levenberg-Marquardt-based algorithms. Furthermore, the ANN developed in here is a FFNN with 10 neurons in its single hidden layer. The process of finding the optimal number of neurons involved the training and test of many ANNs with different number of neurons ranging from 1 to 20 neurons. The decision of using 10 neurons is based on the small improvement of the achieved prediction error when further increasing the number of neurons. No explicit mention of the activation function used in either of the ANN layers is given. The authors opted to use the Neural Lab software to developed the ANN, instead of the commonly used Neural Network Toolbox from Matlab®. The temperature and strain values were used as inputs, and the stress response as output. This work implements similar methods as the one found in the literature for data division, measurement of performance, and validation of the ANN prediction capabilities. Nonetheless, the validation process implemented is extensive because five different hyper-elastic models, and a Probabilistic Neural Network are used for comparison. The validation process was mainly focused on the prediction error rather than the generalization capabilities of the developed ANN. The latter was assessed using the Normalized Absolute Difference (NMAD) and the R^2 coefficient. An extra validation step was performed which consisted of retraining the ANN using the data from another material from the same type. In this case, the prediction error was slightly higher but still adequate, considering that no further optimizations were performed in this test.

6. SOFT MATERIALS MODELLING: ARTIFICIAL NEURAL NETWORKS

Summarizing, the implementation of ANN for the modelling and prediction of soft materials, such as composite materials, is still in its early stages. The available literature is very limited for the specific application of modelling the stress-strain curve of soft materials. Available works are focused on the effect of the temperature. Moreover, works focusing on the effect of the strain rate, hence the velocity-dependency, of the stress response of the soft materials are currently not available in the literature. The latter is addressed in this thesis. Nonetheless, the potential of ANN for this application has been proven in the documented works. Despite the many differences in the selection of hyper-parameters for the developed ANN, the architecture of choice has been the same, feedforward neural networks. Moreover, a very comprehensive review can be found in [135] which includes information about the commonly used validation methods, measurement of performance, sample size, and the type of statistical model implemented, in engineering applications. More detailed information on the specific statistical methods for the validation of the developed ANN, such as the p-fold cross-validation method can be found in [136, 137]

6.4 Methodology: Artificial Neural Network Design

As previously discussed in Chapter 3, modelling the strain-dependent stress response of soft materials is critical for the implementation of reliable control systems in soft robotic applications. This has been attempted in many ways, one of those is the developed PL-SLS model described in Chapter 5. The obtained results highlight the main limitation of this model, which is accounting for the velocity-dependency of the stress response. Therefore, an alternative modelling approach is proposed, a data-driven one based on artificial neural networks.

In line with the work available in the literature, a feed-forward back-propagation neural network is developed in here. Nonetheless, the optimization of many of the hyper-parameters of the ANN is performed to increase its generalization capabilities. These hyper-parameters include: the number of neurons in the hidden layer, and the selection of inputs. The remainder hyper-parameters used in here are based on successful implementations from the literature. The latter is summarized in Table 6.1.

In this work, the training function `trainbr` is used to train the ANNs, which is based on the Bayesian Regularization (BR) algorithm. This is one of the two most commonly implemented methods to avoid overfitting in ANNs. The BR algorithm

6.4 Methodology: Artificial Neural Network Design

Table 6.1: Summary of proposed and optimized hyper-parameters.

Proposed Hyper-parameters	
Topology	Feedforward Neural Network
No. of Hidden Layers	1
Hidden Layer Activation Function	Hyperbolic Tangent Sigmoid (tansig)
Output Layer Activation Function	Linear (purelin)
Training Algorithm	Bayesian Regularization (BR)
Training Function	Mean Squared Error (MSE)
Output	Stress (σ)
Dataset Size	All available data
Dataset Division Function	Random Division
Dataset Division Proportions	80% Training/ 20% Testing
Error Measure	Normalized Root Mean Squared Error (NRMSE)
Validation Method	Multiple Training Sessions (5)
Optimized Hyper-parameters	
Number of Neurons	1 - 20
Inputs	1 - 3

is more computational demanding than the Levenberg-Marquardt algorithm, which is commonly implemented as an early stopping training method. Nevertheless, the BR algorithm performs better for function approximation applications, and when the dataset is small [138]. These characteristics are inline with the dataset used in this research.

The analyses presented in the following sections summarizes the large exploration process, initially based on a trial and error approach, performed as part of assessing the capabilities of ANNs for the prediction of the viscoelastic properties of the soft materials included in this research. These tests provided with enough evidence on the capabilities of ANNs for the mentioned application. Lastly, the optimization processes performed to some of the ANN hyper-parameters are described in detail in the following sections.

6. SOFT MATERIALS MODELLING: ARTIFICIAL NEURAL NETWORKS

6.4.1 Analysis: Impact of the selection of inputs/outputs

The first hyper-parameter to optimize is the selection of inputs. For this application, in which the modelling of the velocity-dependent stress response of the material is desired, the decision to include both the strain and the strain rate as inputs of the ANN models, seems reasonable. However, in the scenario where the developed ANN is deployed as part of a control system in a real application, having a derivative term might add unnecessary complexity to the system. An alternative to circumvent the limitations of having the strain rate as input to the ANN models, is to use the current and past values of the strain as inputs, i.e. the strain history, allowing the network to learn the time dependency of the stress response without having to differentiate any input. The latter configuration describes a very basic form of a Recurrent Neural Network.

In this work, both described scenarios are analysed. On the one hand, the proposed ANN architectures which have derivative terms in its inputs is considered rate-dependent. On the other hand, the ANN architecture which has current and past values of their inputs, instead of a derivative term, is considered rate-independent. The proposed combination of inputs used to create the ANN models studied in this section, are described in Table 6.2.

Table 6.2: Proposed ANN architectures. The architectures FFRI1, FFRI2 and FFRI3 are rate-independent, whereas the architecture FFRD4 is rate-dependent.

	FFRI1	FFRI2	FFRI3	FFRD4
Inputs	ε_t	ε_t	ε_t	ε_t
		ε_{t-1}	ε_{t-1}	$\dot{\varepsilon}_t$
			ε_{t-2}	
Output	σ_t	σ_t	σ_t	σ_t

As previously mentioned, the inputs and outputs listed in Table 6.2 must be presented to the ANN in the form described in Equations (6.1) and (6.3), yielding:

$$\mathbf{X} = \begin{bmatrix} \varepsilon_{t_1} & \varepsilon_{t_2} & \varepsilon_{t_3} & \dots & \varepsilon_{t_n} \\ \varepsilon_{t-1_1} & \varepsilon_{t-1_2} & \varepsilon_{t-1_3} & \dots & \varepsilon_{t-1_n} \end{bmatrix} \quad (6.4)$$

$$\mathbf{H} = \begin{bmatrix} \sigma_{t_1}^{pred} & \sigma_{t_2}^{pred} & \sigma_{t_3}^{pred} & \dots & \sigma_{t_n}^{pred} \end{bmatrix} \quad (6.5)$$

$$\mathbf{T} = \begin{bmatrix} \sigma_{t_1}^{exp} & \sigma_{t_2}^{exp} & \sigma_{t_3}^{exp} & \dots & \sigma_{t_n}^{exp} \end{bmatrix} \quad (6.6)$$

where \mathbf{X} , \mathbf{H} , and \mathbf{T} are the inputs, outputs, and targets matrices. The variables σ^{exp} and σ^{pred} represent the experimental and predicted values of the stress response of the material for a given strain, respectively. The subscript n refers to the total number of samples in each matrix. The assessment of the best combination of input parameters is based on 10-fold cross-validation approach which includes the execution of several training sessions. During each training session, up to 10 sessions, the training dataset is randomized prior to be presented to the ANN. Due to the 90-10 proportion used to create the training and test subset, the latter means that the ANN will learn from a different 90% of the data and at the same time, it will be tested with a different 10% of the data, at random. Also, the initial weights of the ANN are randomized in each training session. By default, the measurement of performance used during training is the mean square error (MSE). However, the normalized root mean square error (NRMSE), between the ANN prediction and the experimental data, is extracted from each training session and used for validation (Equation (5.8)) [120]. Finally, generalization error is defined as the mean NRMSE value from all the training sessions. The architecture with the lowest generalization error is considered as the best candidate.

Due to the findings from Chapter 5, where the performance of the developed PL-SLS model could be correlated to soft materials having more dominant elastic properties, the decision to optimize the selection of inputs presented to the ANN on the remainder of the studied soft materials is made. In other words, it is not safe to assume a “one fits all” approach due to the differences between the materials properties.

Table 6.3: Proposed parameters for the selection of best inputs

Fixed Hyper-parameters	
Number of Neurons	20
Data Set Size	10% of available data
Data Division	90% for training, 10% for testing
Error Measure	NRMSE and Generalization Error
Validation Method	10-fold Cross Validation

In Table 6.3, the hyper-parameters chosen for this optimization are described. This is intended to isolate the impact of the different inputs presented to the ANN. Similarly, the impact of the amount of data used during training is isolated by using

6. SOFT MATERIALS MODELLING: ARTIFICIAL NEURAL NETWORKS

only 10% of all the complete dataset previously described in Table 4.1. Subsequently, the data is divided into training and testing subsets, containing 90% and 10% of the data, respectively. The size of the testing set is based on the number of training session to perform, which is 10. The matlab function `cvppartition` is used to obtain 10 nonstratified subsets of data which guarantees a unique subset of data is used for each training session. The testing subset is used to validate the generalization capabilities of the ANN when unknown data is presented to it. Similarly, a relatively large number of neurons is used in this optimization to avoid limiting the performance of the ANN. Finally, the results are illustrated in Figures 6.2 and 6.3.

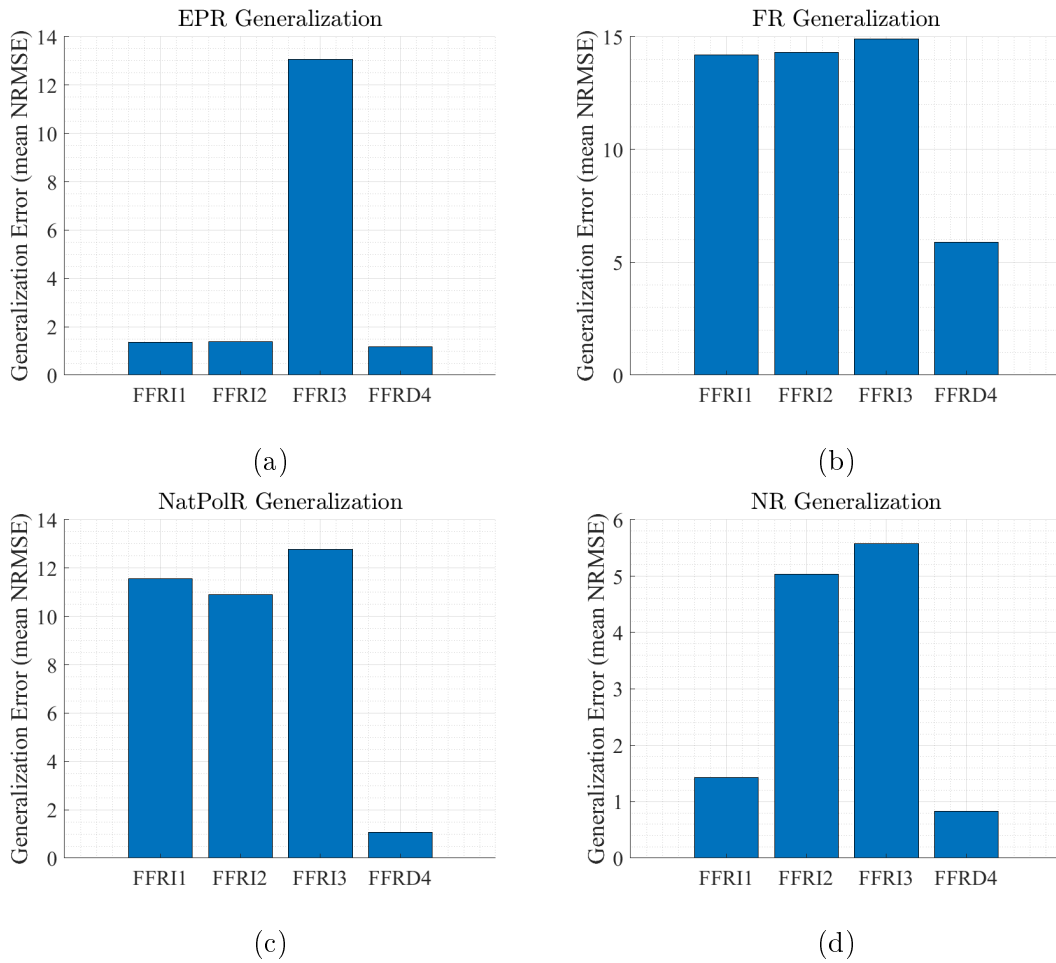


Figure 6.2: Generalization error, based on a 10-fold cross-validation, for the (a) EPR, (b) FR, (c) NatPolR, (d) NR, (e) PR, and (f) SR materials. The best input combination is the one with the smallest generalization error, which in most cases is the FFRD4 configuration.

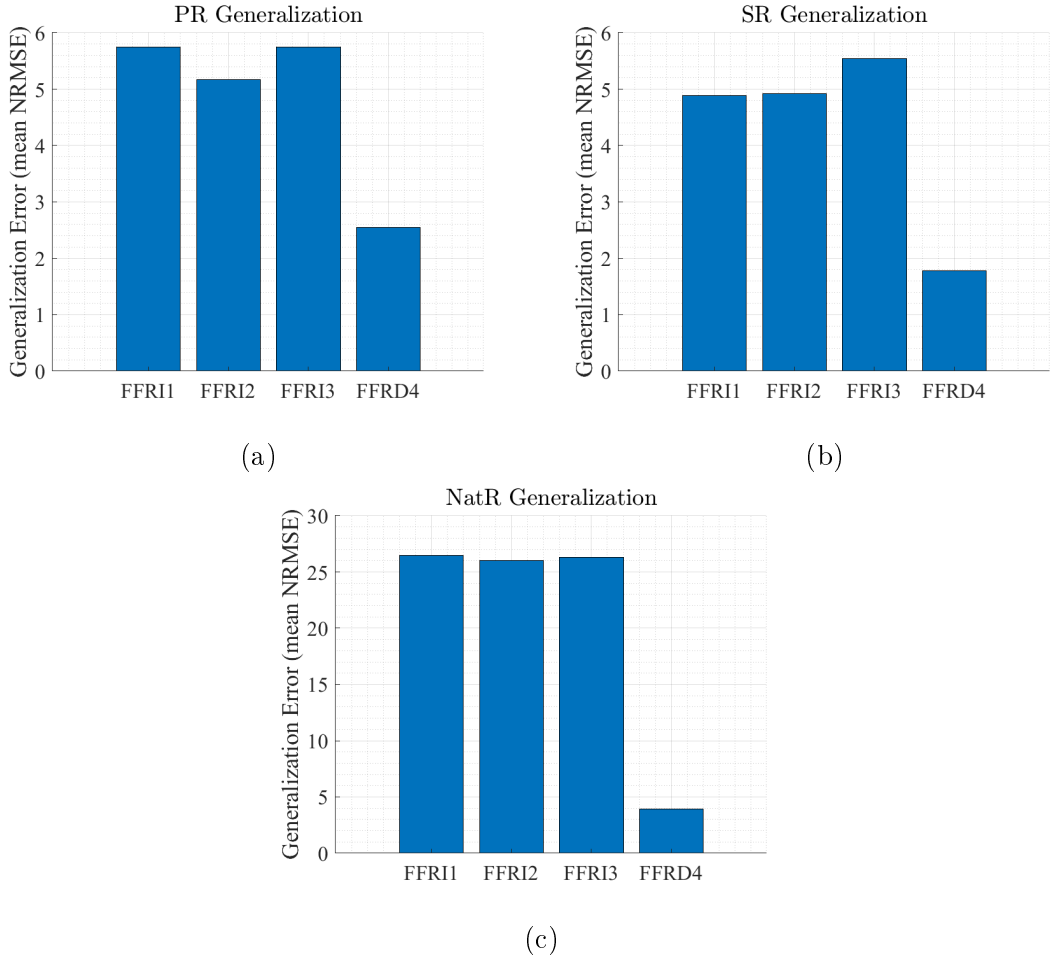


Figure 6.3: Generalization error, based on a 10-fold cross-validation, for the (a) PR, (b) NR, and (c) NatR materials. The best input combination is the one with the smallest generalization error, which in most cases is the FFRD4 configuration.

In Figures 6.2 and 6.3, the FFRD4 architecture is identified as the one with the best generalization capabilities, i.e. smallest generalization error. In some cases, such as the EPR and NR materials, the achieved error of the FFRI1 and FFRD4 architectures are very similar. Nonetheless, due to the consistency on the achieved error, the FFRD4 architecture is selected as the best candidate.

Another important observation is the relationship between the achieved error and the complexity of the rate-independent architectures. In other words, presenting the ANN models with more inputs, in the form of past values of the strain, does not always yield in a performance increase. This is the case for the FR, NR, and SR materials. These results could be related to a weak velocity-dependency of the previously mentioned materials. Presenting the ANN model with additional inputs, aimed to account for velocity dependencies in the materials stress response, can

6. SOFT MATERIALS MODELLING: ARTIFICIAL NEURAL NETWORKS

harm the learning process rather than aid it.

As part of this analysis, the concept of having past values of the material stress response as input to the ANN model was also investigated. The achieved generalization error of this architecture was at least one order of magnitude lower than the other four architectures. Nonetheless, this concept was later dropped due to its incompatibility with a real robotic application. In other words, having the stress response of the material as input to the ANN model would translate into adding a load cell to the application. This cancels out one of the main benefits behind series-elastic actuators, which is transforming the force control problem into a position control problem. In other words, using a modelling tool to predict the stress response of the material based on the measured deformation of the material. Finally, the optimization performed in here showed that rate-dependent architectures, such as the FFRD4 architecture, are more suitable for accounting the velocity-dependency of the stress-strain curve of soft materials.

6.4.2 Analysis: Optimal number of neurons

In the literature, the recommendation of having two to three neurons for each input of the ANN is mentioned. This recommendation seems to be in accordance to the number of neurons used in the documented implementations [35, 131, 134]. Nonetheless this is not true for all implementations [132, 133]. Moreover, the number of neurons must be kept at its minimum to avoid the ANN to over-fit the training dataset. Therefore, it is desirable to search for the optimal number of neurons which allows the developed ANN models to achieve a desired accuracy. In here, the latter search is performed, initially, for a range of 1 to 10 neurons. Although, this range was further expanded to up to 20 neurons because the desired performance was not met for most of the materials. The coefficient of determination, R^2 value, is used to assess the performance of the ANNs, in combination with the multiple training session of randomized datasets method. An adequate performance must has a value of $R^2 > 99\%$. Moreover, the multiple training method performed consists of training each developed ANN, in the range from 1 to 20 neurons, five times. In each session, the whole dataset is randomized and divided into training and test subsets. The main objective of this optimization process is to limit the resources of the developed ANN, i.e. to avoid over-fitting, by finding the training session with the minimum number of neurons that has a value of $R^2 > 99\%$. A similar process to this, but using the percentage of correct prediction, is documented in [124]

In this optimization, the complete dataset available for each material is subdivided to allocate 80% of the data for training and 20% for testing. As previously mentioned, no validation subset is required when using the Bayesian Regularization algorithm. Moreover, the list of hyper-parameters used in this case are compiled in Table 6.4.

Table 6.4: Proposed hyper-parameters for the number of neurons optimization

Fixed Hyper-parameters	
Architecture	FFRD4 (see Table 6.2)
Number of Neurons	1 to 20
Data Set Size	100% of available data
Data Division	80% for training, 20% for testing
Error Measure	R^2 value
Validation Method	5-fold Cross Validation

The results of this optimization are illustrated in Figures 6.4 to 6.6. In there, the achieved generalization errors, based on the mean NRMSE value from the executed tests, and the R^2 values, are presented. Regarding the generalization error, the benefits of having more than ten neurons are negligible, and even detrimental in some cases. This is observed in Figures 6.4e, 6.5c and 6.6a.

The R^2 value, or coefficient of determination, indicates the fraction of the data variation which is explained by the ANN model. Traditionally, a R^2 value closer to 1 indicates a very good model fit. However, in the field of ANNs, a very high R^2 value could actually indicate over-fit in the developed ANN. In general, most of the achieved R^2 values are below the desired threshold of $R^2 > 99\%$. Only the ANN models for the EPR and NR materials are able to meet the latter threshold. Furthermore, the lowest R^2 value is reported for the NatR material. The PL-SLS model also performed poorly for this specific material. Nonetheless, the information presented in Figures 6.4 to 6.6 is useful for the selection of the most optimal number of neurons.

The ANN models with the optimal number of neurons must have the right combination of good accuracy (small NRMSE), low number of neurons, and high R^2 values. The first parameter to consider is the R^2 value. For the cases in which the threshold of this value is achieved, i.e. $R^2 > 0.99$, the optimal candidate is the one with the lowest number of neurons. For the cases in which the threshold is not

6. SOFT MATERIALS MODELLING: ARTIFICIAL NEURAL NETWORKS

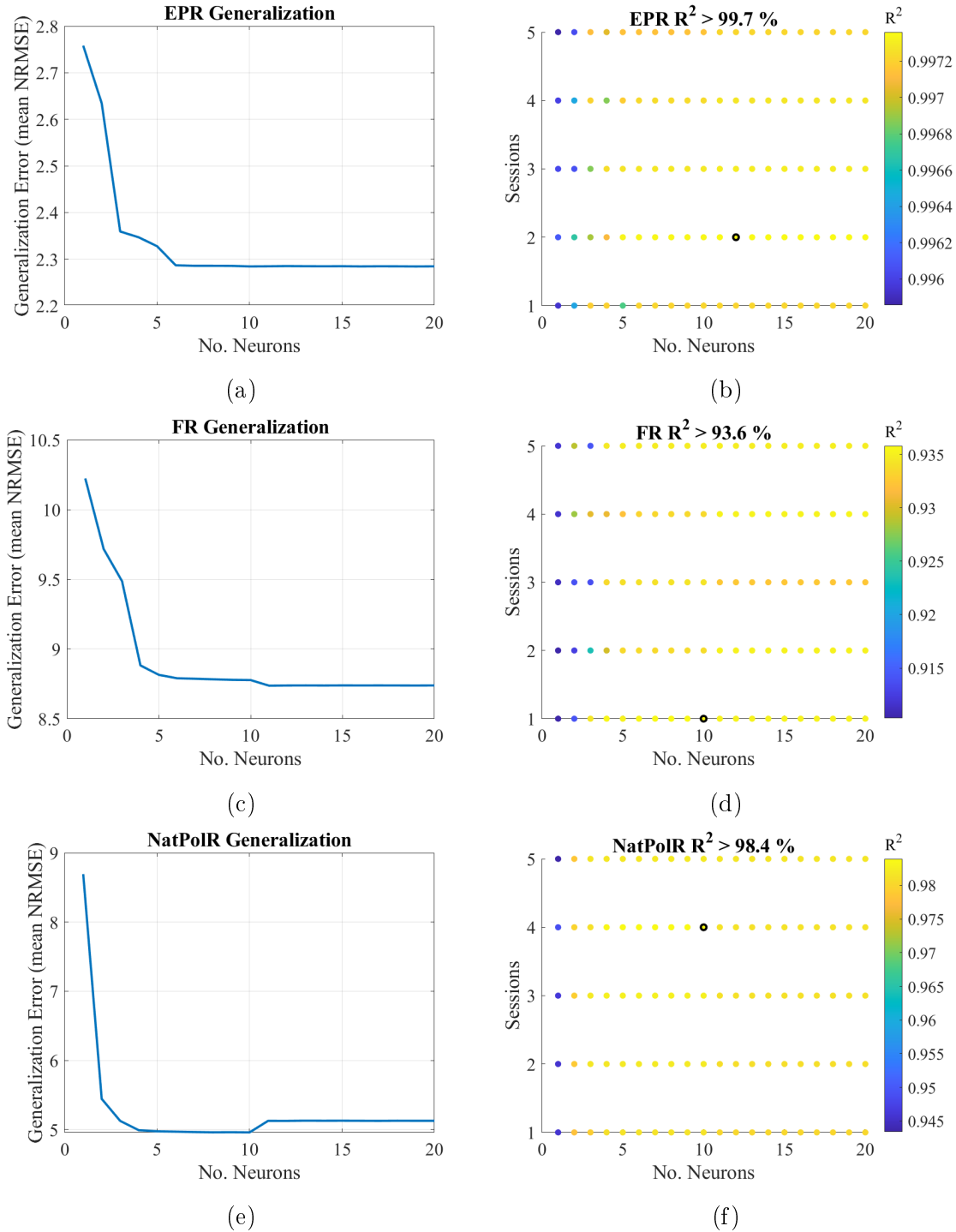


Figure 6.4: Impact of the number of neurons on the Generalization error (a), (c), (e), and the R^2 value (b), (d), (f), for the EPR, FR, and NatPolR materials. A total of five training sessions were executed per number of neurons. The best R^2 value is circled.

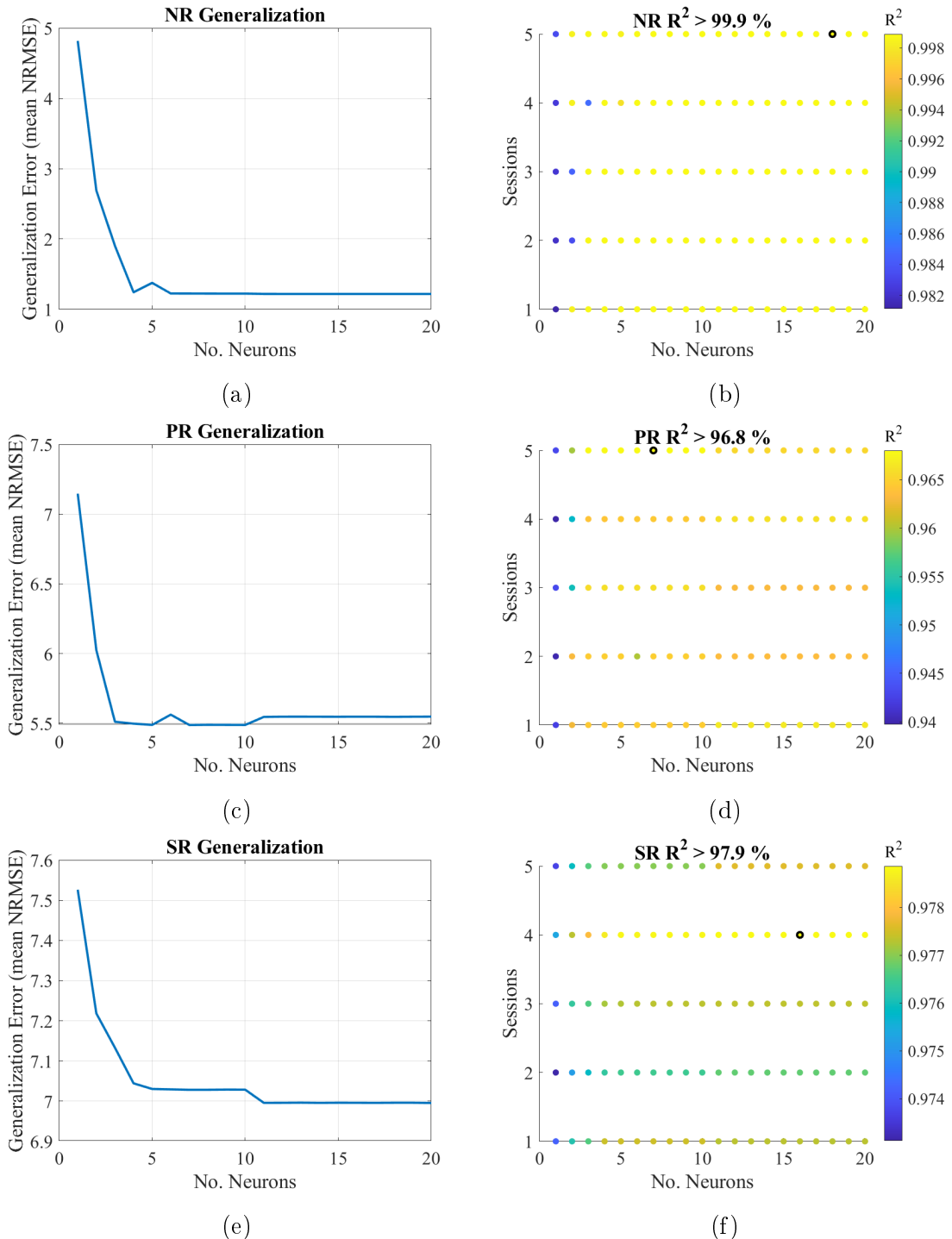


Figure 6.5: Impact of the number of neurons on the Generalization error (a), (c), (e), and the R^2 value (b), (d), (f), for the NR, PR, and SR materials. A total of five training sessions were executed per number of neurons. The best R^2 value is circled.

6. SOFT MATERIALS MODELLING: ARTIFICIAL NEURAL NETWORKS

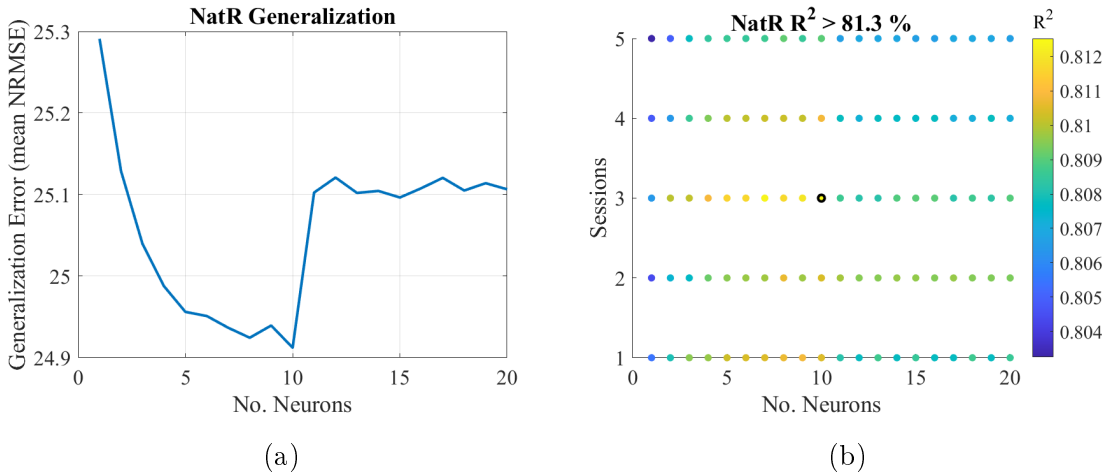


Figure 6.6: Impact of the number of neurons on the Generalization error (a) and the R^2 value (b), for the NatR material. A total of five training sessions were executed per number of neurons. The best R^2 value is circled.

achieved, a closer look is given to the NRMSE to detect if an increase in the number of neurons translate in an improvement of the NRMSE. Following these conditions, the optimal number of neurons per soft material are extracted and presented in Table 6.5. In here, the PL-SLS model is also compared against the developed ANN model.

Table 6.5: Best ANN candidate compared against the PL-SLS model. The generalization error is based on the mean NRMSE value. In the case of the PL-SLS the latter is based on the mean NRMSE value from the available strain rates in Figures 5.8 and 5.9

	EPR	FR	NatPolR	NR	PR	SR	NatR
ANN model							
Generalization Error (%)	2.3	8.8	4.9	1.2	5.5	7	24.9
No. of Neurons	6	10	10	6	7	6	10
R^2 @ No. of Neurons	99.7	93.4	98.2	99.8	96.5	97.7	81
PL-SLS model							
Generalization Error (%)	18.4	32.1	7.9	19.7	30.4	3	202
Tolerance Criteria	40	90	20	50	10	90	50
Strain Segments	12	6	9	12	12	3	8

From Table 6.5 it can be observed that the ANN models have much better

generalization capabilities in comparison to the PL-SLS model. However, the generalization error from both models is calculated slightly different. In the ANN model, the generalization error is the mean NRMSE value from all the training sessions performed. Whereas, in the PL-SLS, the generalization error is the mean NRMSE value among the other predicted strain rates, as illustrated in Figures 5.8 and 5.9. Nonetheless, the generalization error is very useful to indicate the performance of both models when accounting for the velocity-dependency of the stress response, i.e. different strain rates.

Interestingly enough, the PL-SLS model actually performs better than the ANN model for the SR material. This is the only soft material, in which the tensile strength tests had to be performed using the 250 mm/min strain rate, instead of the recommended 500 mm/min strain rate. The latter aided the PL-SLS model to achieve the same NRMSE for both the strain rates available for this material (250 mm/min and 50 mm/min). In addition to this, the PL-SLS model performed better for the soft materials which exhibited a more dominant elastic behaviour, i.e. materials with less-dominant viscous properties. Based on this, it can be concluded that the velocity dependency in the stress response of the SR material is not observed over these ranges of deformation or it is negligible. This also explains the low performance of the ANN model which relies on the strain and the strain rate to predict the stress response of a soft material with properties closer to the elastic range than to the viscoelastic range.

The combination of inputs used for the developed ANN, of strain and strain rate, could be playing a role in the slightly worse performance of the ANN model in comparison to the PL-SLS model. In other words, it could be possible that the ANN is not able to find a relationship between the strain rate and the stress response of the material, and hence that input is proven detrimental to the achieved accuracy rather than improving it.

Nonetheless, the developed ANN models have proven to be adequate for modelling the velocity-dependency of the stress response of viscoelastic materials, due to the small NRMSE achieved. The next step is to validate the performance of both models in a real robotic application, which is described in the following chapter.

6. SOFT MATERIALS MODELLING: ARTIFICIAL NEURAL NETWORKS

6.5 Summary

In this chapter, a data-driven modelling approach is proposed and developed as an alternative to traditional model-driven approaches which can be very computationally costly. Artificial neural networks has been successfully implemented in many applications, but the literature available on the prediction of the viscoelastic properties of soft materials is still scarce.

In line with the literature, a feedforward artificial neural network is developed to model the viscoelastic properties of seven soft materials. The developed ANN models are aimed to be used in real robotics applications, specifically to predict the mechanical behaviour of the viscoelastic element found in a recent actuation technology, the series-viscoelastic actuator.

The process of developing the ANN models involved the optimization of the number of neurons in the hidden layer and the most appropriate selection of inputs and outputs, to account for the viscoelastic properties of the studied soft materials. The optimal number of neurons varied from one material to the other but it does not exceed 10 neurons. The inputs of the ANN models were defined to be the strain and the strain rate of the materials. As the output, the ANN models were aimed to predict the stress response. In order to avoid over-fitting, the Bayesian Regularization algorithm was used instead of a traditional early stopping method based on the Levenberg-Marquardt algorithm.

The generalization capabilities of the ANN models was assessed using a multiple training approach in which the network was presented with slightly different data from a randomized test set. The mean normalized root mean square error from the latter training sessions is known as the generalization error. In general the ANN models performed better than the previously developed PL-SLS model in Chapter 5. The only isolated case for which the PL-SLS model performs better than the ANN models is for the prediction of the SR material stress response. The latter could be attributed to the fact that the SR material stress response is not affected by the velocity, i.e. strain rate. Hence, having the strain rate as input to the ANN models could be detrimental to the performance of the network. Nonetheless, the question still remains on whether these different modelling approaches could be implemented as part of a control system for the prediction, in real time, of the stress response of a viscoelastic material. This is investigated in the following chapter.

CHAPTER 7

Modelling a bio-inspired series-viscoelastic actuator

7. MODELLING A BIO-INSPIRED SERIES-VISCOELASTIC ACTUATOR

7.1 Introduction

In the previous chapters, the development of two modelling tools for the prediction of the viscoelastic behaviour of soft materials is described. The assessment of their prediction capabilities favoured the ANN models as the more accurate modelling tool in terms of accounting for the velocity-dependent stress response of the soft materials. Despite the latter, the performance of the developed ANN models is still required to be validated in a real-time simulation environment. This is in line with the motivation of this research of addressing the current limitations of traditional modelling tools when being deployed as part of a control system, i.e. as part of a real robotic application. These limitations are high complexity and large computational power requirements.

In this chapter, the performance of the ANN model in a real-time simulation environment is assessed. The latter is done by including the ANN models in a series-viscoelastic actuator model. The ANN model is aimed to predict the stress response of the viscoelastic element included in the actuator. A control system is built on top of the latter model, and the torque-displacement requirements of the human knee joint is used to investigate the performance of the soft-viscoelastic actuator. This study is performed in Simulink.

(ADAPT after including the control system) Results highlight an unexpected limitation of the developed ANN model which is not able to perform well under a variable strain rate input. This can be circumvented by keeping the strain rate input constant. However, this is a limitation which must be addressed for the ANN model to be reliable in real robotics applications.

(ADAPT after including the control system) In summary, the design process presented in here consists of: the selection of the best soft material to match the human tendon properties; the selection of the electric motor and gearbox combination suitable to deliver 50% assistance, based on the knee torque requirements during walking activities; the evaluation of the ANN model in real time under different strain input signals; the experimental protocol proposed, based on mimicking the human muscle skeletal system functionality, and the 3D design of a clamping device aimed to hold several pieces of soft materials in a bundle-form.

7.2 Matching the Human Tendon Properties

In line with the aim of implementing the human skeletal muscle system functionality in soft robotic applications, i.e. a bio-inspired soft actuator, this section presents a comparison analysis between the mechanical properties of the seven studied soft materials, and the human tendons and ligaments involved in the motion of the knee joint. The latter is motivated due to the large contribution of this joint on the activities of daily living (Chapter 3). Due to the limited availability of clinical studies focusing on the tensile strength and stress relaxation properties of the tendons and ligaments involved in the human knee joint, a selection of three separate clinical studies is made. The first study is solely focused on the tensile strength properties of the patellar tendon [38], the second one is focused on the stress relaxation properties of the quadriceps tendon [27], and the third study is focused on the tensile strength properties of both the patellar tendon and the quadriceps ligaments [39]. The aim of this comparison analysis is to identify which of the studied soft materials is able to match the human tendon mechanical properties. Due to this, the viscoelastic properties of the human patellar tendon and the quadriceps ligaments are compiled in Table 7.1, alongside the mechanical properties of the studied soft materials for direct comparison.

Table 7.1: Viscoelastic properties of the patellar tendon and the quadriceps ligament ([27, 38, 39]), compared against the viscoelastic properties of the studied soft materials (Tables 4.2 and 4.4).

	Human Tendon	EPR	FR	NatPolR	NR	PR	SR	NatR
Tensile Strength								
σ_{ue} (MPa)	33.6	8.48	4.36	3.57	3.55	0.3	6.03	9.43
ε_{ue}	0.14	7.56	3.97	1.19	3.57	1.87	5.77	13.02
E_{small} (MPa)	303.9	3.23	4.83	9.97	4.29	0.58	3.26	1.01
Stress Relaxation								
$S.R$ (%)	41	32	67	35	29	63	31	15

In Table 7.1, it can be appreciated that there is a large difference between the elastic properties of the quadriceps tendon and the studied soft materials, specifically for the elastic modulus, E_{small} . Nonetheless, the achieved stress relaxation is very

7. MODELLING A BIO-INSPIRED SERIES-VISCOELASTIC ACTUATOR

similar to the one found in the soft materials. Therefore, they share similar viscous (time-dependent) properties. This is a positive finding, because the elastic properties, of stress and strain, are structural parameters which depends on the dimensions of the material, as explained in Section 4.3. The stress is inversely proportional to the cross-sectional area of the material. Moreover, the stress has a nonlinear relationship with the material strain. Hence, a material with larger cross-sectional area will require a larger force to achieve the same deformation. With this in mind, a new questioning arises regarding the cross-sectional area increment required for the soft materials to match the properties of the human tendon.

The latter questions must be answered considering the end application of the soft materials. As previously mentioned, these are intended to be used as part of a series-viscoelastic actuator. Having this in mind, the way in which the soft materials match the human tendon properties by an increase in their cross-sectional area can be better visualized. The implementation of a bundle of many strips of a soft material is proposed. The dimensions of each strip must be in line with the dimensions in which the material is available from the manufacturer. As previously mentioned, they all come in a rectangular shape. The thickness among all the studies soft materials vary from one to the other. Moreover, it is useful to think in the end application of the soft actuator itself, which is human assistance. According to the literature, a robotic wearable device for rehabilitation applications must deliver an assistance of 60% of the peak torque required [139]. Due to this, an objective assistance percentage of 50% is proposed in here as design guidelines for the selection of the motor-gearbox combination. In addition to this, the safe working conditions of the studied soft materials, i.e. the elastic region, are considered. The elastic region of each studied soft material, approximated using the offset-yield strength, is compiled in Section 4.3. Lastly, all this information is considered in the matching factor calculation, in which the elastic modulus E_{small} of the human tendon is desired to be matched by the soft materials. The latter is compiled in Table 7.2.

In Table 7.2 the matching factors obtained are from a two fold process. First, the cross-sectional area of each soft material is matched with the cross-sectional area of the human tendon. Second, the elastic modulus of the human tendon is matched, considering the previous increase in the cross-sectional area of the materials. As previously mentioned, the materials thickness is defined by the manufacturer, therefore fixed. Nonetheless, many samples (strips) can be extracted from the material rectangular sheet using laser cutting. The width of these strips can be modified to increase

Table 7.2: Matching factors required for the soft materials to achieve the human tendon E_{small} value. The width proposed for the material strips is 66 mm. (REVIEW THIS)

	EPR	FR	NatPolR	NR	PR	SR	NatR
Matching factors							
A_o	7	7	7	7	2	7	12
E_{small}	77	52	25	58	375	76	248
E_{small} @ 50%	39	26	12	29	188	38	124
Material Dimensions							
Old A_o (mm^2)	9	9	9	9	36	9	5.22
New A_o (mm^2)	4852	3245	1572	3653	27020	4807	15517
New A_o @ 50% (mm^2)	2426	1622	786	1827	13510	2404	7758
Strip Width (mm)	66	66	66	66	66	66	66
No. of strips	49	33	16	37	68	49	270
No. of strips @ 50%	25	16	8	18	34	24	135

the cross-sectional area of the material. Hence, a width of 66 mm is proposed for the latter calculations. The latter was decided taking into consideration the application in which the bundle of strips will be implemented. That is, bio-inspired actuator. Moreover, this actuator is aimed to be used to assist the knee joint. This in fact puts a limit to the width of the bundle of strips, and that is the dimensions of the human shank. Taking this into consideration, and the relationships between the required number of strips and the strips width. The previously mentioned value of 66mm was adequate. In practice, it is possible for all the materials to match the human tendon elastic modulus as long as enough strips are used. The exact number is stated in Table 7.2. Finally, by analyzing the obtained matching factor in combination with the stress relaxation properties of the human tendon, the soft material with the closest properties is identified to be the NatPolR material.

7.3 ANN Model Validation in Real-time

In this validation, the PL-SLS model is not included because its formulation makes use of past values of the stress response. This contradicts the benefits of implementing a SEA in the first place, which is to use the deformation of the elastic element

7. MODELLING A BIO-INSPIRED SERIES-VISCOELASTIC ACTUATOR

as an indirect way to measure the stress response. Nonetheless, the accuracy of the PL-SLS model when modelling the strain-dependent stiffness of the soft materials has been validation in Chapter 5. Also, the previous version of the PL-SLS model was validated through experimentation in [33]. Therefore, only the ANN model is validated in here.

The developed ANN model, takes two inputs, the strain and strain rate, and outputs the stress response of the material, in MPa. Therefore, particular care must be taken with regard to the conversion to avoid undesired results. As previously mentioned the stress is defined as $\sigma = F/A_o$, whereas the strain is defined as $\varepsilon = \Delta L/l_o$. The value of $l_o = 33\text{mm}$ applies to all studies soft materials, whereas the value of A_o varies from one material to the other. The units from the stress output (MPa) and A_o (mm^2) are compatible and can be used as they are in the conversion. In addition to this, the stress response of the ANN model must be multiplied by the number of strips to be used. As a first step, the ANN model is tested using a Step input, and Sinusoidal input signals to verify its functionality. The block diagram of this setup is illustrated in Figure 7.1.

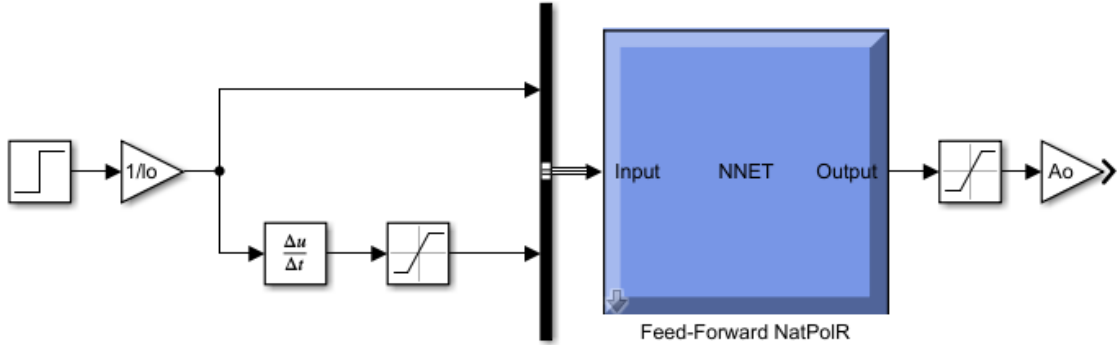


Figure 7.1: Simulink implementation of the ANN model. The ANN model takes the strain and strain rate as inputs, and delivers the stress response of the material in MPa as output. The gain blocks ensure that the units are consistent.

The stress response of the ANN model for a Step input is in accordance to the values reported in Figure 4.11. The ANN model outputs negative stress values when a zero strain and zero strain rate are given as inputs. The latter could be a consequence of not providing enough data to the ANN during training for the zero input scenario. Nonetheless, a negative stress output is not realistic since the soft material will only have reaction forces under uni-axial extension. Therefore, a saturation block is used to prevent the latter. Similarly, the strain rate input is

saturated to avoid presenting the ANN model with large values and negative values, and also to keep the strain range variation inside the ranges of values used during training, from 50 mm/min to 500 mm/min.

The stress response of the ANN model showed an unstable behaviour for a sine wave input signal. In this case, the ANN model performance was affected by both the frequency and the amplitude of the signal, as illustrated in Figures 7.2a to 7.2c. This could be related to the fact that the strain rate in this scenario is changing over time, whereas the strain rate used for training was fixed between three different values. This however, does not indicate that the ANN model is not able to generalize well with other constant strain rates, as the one present in a tensile strength test. Nonetheless, this shows an unexpected limitation of the developed ANN model when being implemented as part of a control system. In contrast, the stress response of the ANN model was stable when using a constant strain rate as illustrated in Figure 7.2d.

The latter test provided useful information about the behaviour of the ANN model under different input signals in real-time. An important limitation was found, which is the erratic prediction of the ANN model when the strain rate varies over time. The lack of a bigger and richer training dataset could be the cause of this. The relevance of understanding the role of the strain rate on the stress response of soft materials is highlighted in the literature recently. In the work performed by Xu et al. last year, development of an ANN model able to predict the elastic modulus of soft materials under different strain rates is described [140]. The studied material was a graphene reinforced composite, and was characterized using a dynamic mechanical analysis over a range of frequencies and temperatures. These ranges of values are the input of the ANN model which in fact, does not directly predict the stress response of the material, and instead, predicts the storage modulus of the material which is a parameter related to the viscoelasticity of materials. Using this parameter in combination with known mathematical equations, the stress response of the material can be extracted, as described in their work. The fact that ongoing research is being done on ANN model for the prediction of the velocity-dependent stress response of the materials highlights the relevance and feasibility of the research presented in here.

7. MODELLING A BIO-INSPIRED SERIES-VISCOELASTIC ACTUATOR

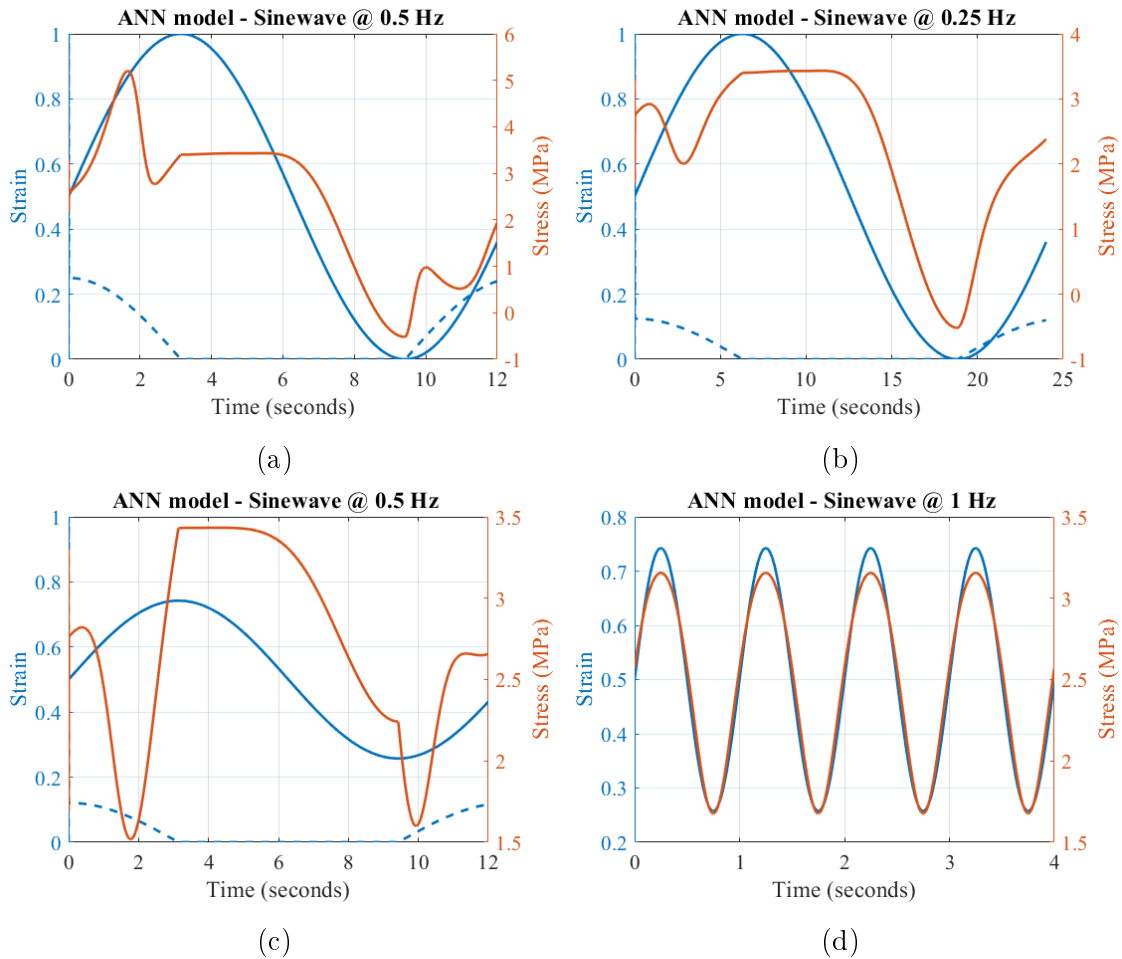


Figure 7.2: ANN model stress response to a sine wave strain input. The solid and dotted blue line are the strain and strain rate, respectively. The ANN model response is affected by both the frequency (a), (b), and the amplitude (c) of the input signal. Also, the ANN model is only stable when the strain rate presented to it is constant, as in (d)

7.4 Preliminary Design Concept of a Series-viscoelastic Actuator

Series and parallel elastic actuators have been implemented in human assistance applications to achieve a muscle-like performance and increase the assistance capability of the robotic wearable devices. Traditionally, the mechanical element used to provide elasticity in actuators is a metallic spring. However, the idea of replacing the metallic spring with a soft material, such as rubber, is being researched now. The works performed by D. Rollinson has proved this idea to be beneficial for

series elastic actuators (SEA) by developing a rotational spring based on natural rubber [29, 141]. In fact, the latter research gave birth to HEBI Robotics and to the first SEA implementing a soft material as the elastic element [142]. In addition to this, other SEA concepts implementing rubber [33], dielectric elastomer [143] and polyurethane [117] are being researched.

The benefits of series and parallel elasticity have been demonstrated in many works both with rigid and soft materials as the elastic element. However, there is only one actuator concept documented in the literature which implements both series and parallel elasticity in the same actuator, creating a series-parallel elastic actuator (SPEA) [144]. This actuator implements rigid springs and is based on the variable recruitment process observed in human muscles, which means that depending on the required torque and displacement, more springs will be engaged.

As previously mentioned, an objective assistance of 50% of the required peak torque is proposed. Moreover, the research is focused on the human knee joint due to its major role in the activities of daily living. In line with this, the required peak torque and angular speed range for the knee joint during normal walking was found to be 29 Nm and ± 50 rpm respectively [139, 145]. Therefore, the peak torque aimed to be delivered to achieve a 50% assistance is 18 Nm. The previous parameters will be used as guidelines when selecting the electric motor/gearbox combination to be used in the simulation. In addition to this, the working range of the soft materials is also important. The latter is indicated by the elastic region of the material, which was approximated using the offset yield strength in Section 4.3. In summary, the parameters aimed to be used in a future experimental validation are presented in Table 7.3.

As part of the preliminary design of the series-viscoelastic actuator, and in line with using a bundle of soft materials to match the human tendon mechanical properties, a clamping device was designed in SolidWorks® (Figure 7.3). The width of the clamp was in line with the end application, which is an assistive wearable device for the human knee joint. The idea behind this design is to stack several pieces of the same material on top of each other and then clamp them together to create a bundle of soft materials. This design is similar to the one used in the literature when dealing with rubber materials and cable-driven actuators [33].

The clamp mechanism of Figure 7.3 was designed to be detachable. This is achieved by having a T-shape element which can be glued to a bundle of materials strips. Each soft material strip must also be glued to each other to allow for even

7. MODELLING A BIO-INSPIRED SERIES-VISCOELASTIC ACTUATOR

Table 7.3: Simulation parameters

Soft Material	Natural Rubber with Polyester (NatPolR)
Working Range	Up to 0.5 strain (16.5 mm)
Strip Width	20 mm
Strip length	33 mm
A_o	9 mm ²
No. of strips	8
Torque reference	Knee joint motion capture data
Position reference	Knee joint motion capture data
Electric motor	Maxon RE53-323891 [146]
Nominal Voltage	24 V
L_a	0.191 mH
R_a	0.583 Ω
K_a	29.2 mNm/A
K_b	0.029 V/(rad/s)
J_m	79.2 g/cm ²
Gearbox	Maxon GP 42 C-203124 [147]
n	1/81

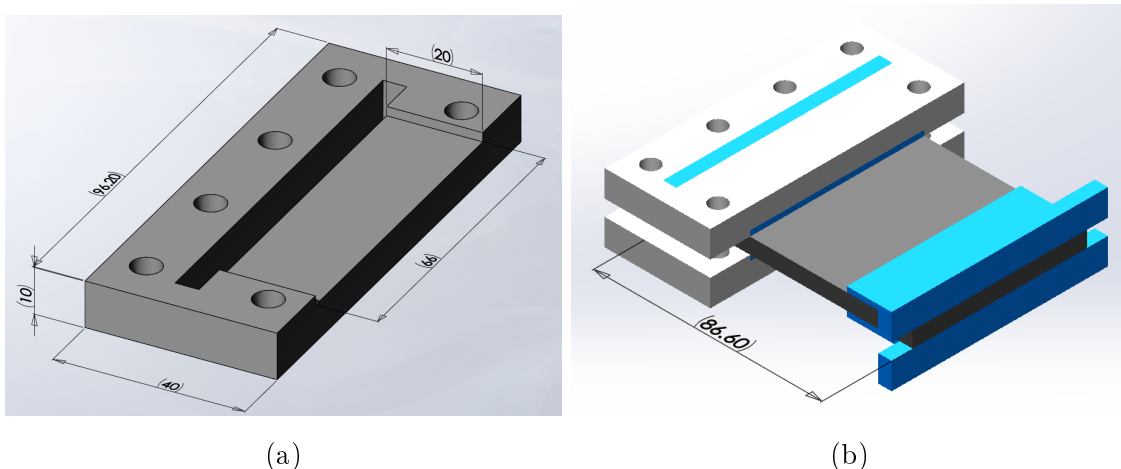


Figure 7.3: CAD Design of the detachable clamping device (a) Bottom part, (b) Final assembly, the soft material is coloured in black, and the T-shape attachment in blue. Units are in millimeters.

deformation of the whole bundle. The T-shape attachment, which resembles a “plug and play” device, fits inside the clamp base (Figure 7.3a) and also in the clamp top element. This allows the quick testing of different bundles of soft materials. Once in place, the clamp mechanism can be secured with bolts going through the holes added to the clamp base and top parts. This is illustrated in Figure 7.3b. As previously mentioned, this design was inspired in the one used in [33], with the addition of designing it as detachable clamping mechanism to allow the test of different soft materials bundles, when being used as part of a test bench. This clamping mechanism was not manufactured.

Finally, an experimental protocol was designed and documented as well (Appendix B). The tests proposed in there aim to investigate the concept of variable recruitment in soft cable-driven actuators, i.e. series-viscoelastic actuators. In addition to this, the concept of co-contraction is also aimed to be investigated.

7.5 Summary

In this chapter, the preliminary design concept of a series-viscoelastic actuator was presented. As the very first step in the design process and in line with the aim of mimicking the human muscle skeletal system, the comparison of the human tendon mechanical properties against the soft materials was made. In addition to this, the validation of the ANN model performance under real-time conditions was investigated. The results were unexpected due to the erratic stress response prediction of the ANN model. The latter is directly related with the fact that only up to three different strain rates were included in the training set. Moreover, the stress response of the ANN model is also affected by the selection of frequency and amplitude of the strain input. Nonetheless, the ANN model was able to follow a sine wave strain input when having a constant strain rate in its input. The latter limitation must be addressed in future works to develop a robust ANN model.

Finally, the work related to the design process of the series-viscoelastic actuator was presented, which included: the selection of actuator technologies, selection of the best soft material to match the human tendon properties, design of a clamping device to hold a bundle of stacked soft material pieces, and the designed experimental protocol which can be found in the Appendix B.

CHAPTER 8

Summary, Conclusions, and Future Work

8. SUMMARY, CONCLUSIONS, AND FUTURE WORK

8.1 Summary

The aim of this research, is to investigate the concept of implementing viscoelasticity, a property found in the human skeletal muscle system, in soft robotics applications for the assistance of the human lower limb. Narrowing this a little further, special focus is put into the human knee joint and the concept of a series-viscoelastic actuator. In addition to this, this research aims to address current limitations on the modelling soft materials, specially their viscoelastic mechanical properties such as the strain rate dependency of the stress response. The latter is systematically investigate by investigating traditional modelling tools and by developing a data-driven modelling tool based on artificial neural networks (ANNs). The motivation behind investigating different modelling approaches is to address the known limitations of traditional modelling tools, based on mathematical models, when being deployed as part of a control system. These limitations are high complexity and large computational power requirements. Due to the latter, the performance of the developed ANN model is assessed in a real-time simulation environment using Simulink. The control system proposed for the simulation is based on the model of a bio-inspired series-viscoelastic actuator (SVA). The main difference between a SVA and traditional series-elastic actuators is in the type of elastic element implemented. In here, the aim is to implement a bundle of strings made of a specific soft material. Lastly, this last chapter of the thesis provides a summary of the actions taken towards completing the aims and objectives presented in Chapter 1, as follows:

Survey the literature to identify: the terminology related to the biomechanics of the human lower limb, and the current soft robotic developments for the field of human assistance.

The tendency of mimicking the human muscle skeletal system functionality when developing soft robotic applications for human assistance, was presented in Chapter 2. Furthermore, the most matured soft actuation technologies commonly used were identified as: pneumatic/hydraulic artificial muscles, and cable-driven actuators. The benefits and limitations of these technologies were described. In the field of soft sensing applications, the literature is mainly focused on elastomers with embedded micro-conductive channels. The lack of literature describing the modelling of the soft materials used for these applications was detected as a research opportunity. Lastly, the implementation of soft actuation technologies as a way to imitate the functionality of the muscle-tendon component is mainly focused on the

contractile element rather than the elastic element. From here, the idea of researching the potential of using soft material to replicate the human tendon functionality was proposed and addressed in the next chapter.

Investigate the biomechanics of the human lower limb during activities of daily living.

In Chapter 3, the terminology on the biomechanics of the human lower limb during activities of daily living was presented. Special attention is given to the mechanical model commonly used in soft robotic applications, the Hill's model, when mimicking the functionality of the human skeletal muscle system. Moreover, the characterization of the kinematic and kinetic parameters of the hip, knee, and ankle joints was performed. The potential of using the compiled data was identified and a conference paper was produced. The latter paper presents several visualization techniques which can be useful for the design phase of any soft robotic application for human assistance of the lower limb. The complete collected dataset is presented, visually, in Appendix A. Polymer materials were identified as potential candidates to be used as part of a bio-inspired actuator due to the similarities of these materials with the mechanical properties of the human tendon, and due to the medical application in which it has been used, e.g. tendon reconstruction. Lastly, viscoelasticity, a property of most soft materials, is now being researched as an alternative to improve mature actuation technologies, such as series-elastic actuators. The concept of a series-viscoelastic actuator is very recent and further validates the feasibility of this research.

Characterize the viscoelasticity of suitable soft materials.

The characterization process of seven soft materials from the family of composite materials is presented in Chapter 4. The studied rubber-based materials are as follows: Polyethylene Rubber (PR), Ethylene Polypropylene Rubber (EPR), Natural Rubber with Polyester (NatPolR), Natural Rubber (NatR), Silicone Rubber (SR), Fluorocarbon Rubber (FR), and Nitrile Rubber (NR). The concept of elasticity and viscoelasticity were described in here. The mechanical tests of tensile strength and stress relaxation were performed. The processing of the collected data was described in detail. Moreover, particular attention was paid to find the elastic region of the studied materials since these regions dictates the safest working conditions for each material. This information is latter used for the design of a bio-inspired soft actuator.

8. SUMMARY, CONCLUSIONS, AND FUTURE WORK

Identify the soft materials with the most similar mechanical properties to the human tendon.

The motivation behind characterizing many composite materials is to identify the material with the most similar viscoelastic properties as the human tendon. This is another step towards implementing viscoelasticity in soft robotic applications for human assistance. The process to identify the best candidate was presented in Chapter 7, as part of the design process of a bio-inspired actuator. In this comparison, the human tendons involved in the motion of the knee joint were investigated. These are the patellar and quadriceps tendons. The results showed a large difference between the elastic properties of the materials and properties of the human tendon. Nonetheless, their viscoelastic behaviour was found to have similarities. Due to this, the calculation of a matching factor was performed. The idea is to combine several pieces of a material into a bundle to increase the effective cross-sectional area of the material, hence its elastic properties. Lastly, the soft material with the most similar properties as the human tendon, in terms of the achievable stiffness, is identified by looking at the obtained matching factors. This material is the Natural Rubber with Polyester material (NatPolR).

Address the limitations of the modelling tools currently being used for the prediction of the viscoelastic behaviour of soft materials, by optimizing a current modelling tool or by developing a new modelling tool.

In Chapter 5 the current modelling approach for the prediction of stress response of soft materials is presented. In general, modelling approaches are based on the Linear viscoelastic Models (LVMs), which are able to describe any viscoelastic materials using a combination of two basic components: a spring and a dashpot. Nonetheless, the accuracy of these models is tightly linked to a high complexity and large computational power requirements. One of the recent methods described to circumvent the latter limitation was found in the literature as the Standard Linear Solid with Strain-Dependent Stiffness model (Std. Lin. SSD). This model is able to account for the nonlinear stress response of viscoelastic materials by implementing a piecewise linearization on the equilibrium spring stiffness k_e , from the Standard Linear Solid model (SLS). Nonetheless, the model has not been validated when predicting the velocity-dependent properties of viscoelastic materials. Therefore, a case study is performed on this model, aimed to address its limitations. The latter is done by linearizing the Wiechert model, a more complex model from the family of

LVMs, using the piecewise linearization technique. The hypothesis behind this is that a more complex model might be able to account for velocity-dependencies of the viscoelastic materials. During this process, the Std. Lin. SSD was optimized in many aspects that a differentiation is made between the version found in the literature and the one developed in here, which is called the PL-SLS model. One of the main contributions of the latter was proposing a tolerance criteria which related the complexity of the model with its accuracy. The developed PL-Wiechert model was incompatible with the PL technique and only the PL-SLS model is further analysed. The work done in here was substantial enough to produce a second conference paper. Lastly, the generalization of the PL-SLS model was found to be poor in most cases, i.e. the model was not able to accurately account for velocity-dependencies. Hence, an alternative modelling approach was investigated in a subsequent part of the research.

Assess the modelling tool prediction accuracy in a real-time environment

Prior to assess the model performance in a real-time environment, a different modelling approach was investigated and is presented in Chapter 6. A data-driven approach was proposed, based on feedforward artificial neural network. The literature available on the implementation of artificial neural networks for the prediction of the stress response of viscoelastic materials is very scarce. Nonetheless, this research area is rapidly growing due to the proven potential of ANN to approximate complex functions. The data from the same seven materials was adapted and used for the training of the artificial neural networks (ANN). The developed ANN model was aimed to address the limitations of the PL-SLS model, which is not accounting for velocity-dependencies. The ANN model achieved better accuracy and better generalization capabilities, than the PL-SLS model. The latter was assessed by statistical parameters such as the root mean square error and coefficient of determination. At first glance, this suggested that the ANN model was able to account for velocity-dependencies. Nonetheless, the real-time validation performed in Simulink showed a completely different result. This was presented in Chapter 7. In summary, the ANN model was unstable due to the varying strain rate used for testing. For a constant strain rate, as the one used when validating the accuracy, the ANN model performed as expected. The PL-SLS model was not validated in here because its formulation requires past values of the stress response which are only obtainable by experimentation.

8. SUMMARY, CONCLUSIONS, AND FUTURE WORK

Design a bio-inspired soft actuation for human-assistance applications

The design of a series-viscoelastic actuator is presented in Chapter 7. due to time restrictions, the information presented in here is focused on the concept design. The proposed actuator is aimed to assist the knee joint, hence the torque knee requirements of the joint during walking activities were used as guidelines for the selection of the electric motor and gearbox combination. Moreover, and in line with the aim of mimicking the human skeletal muscle functionality, a experimental protocol is designed to investigate concepts like co-contraction and variable recruitment, two phenomena found in human muscles. Lastly, the design of a clamping device to be used in the experimentation was designed. The clamping mechanism was designed to be detachable and allow the testing of many materials without modifying the experimental setup.

8.2 Conclusions

In conclusion, this research presented two novel modelling approaches, one model-driven and the other data-driven, for the prediction of the viscoelastic properties of soft materials. Specifically, the developed modelling tool were aimed to account for the nonlinear, velocity-dependent, and strain-dependent stress response of soft materials. In the model-driven approach, two mathematical models were developed and assessed: the PL-Wiechert model and the PL-SLS model. The former one was incompatible with the picewise linearization method proposed in the literature. In contrast, the PL-SLS model showed adequate accuracy, in terms of the normalized mean square error (NRMSE). The smallest achieved NRME value was close to 5%. The generalization capabilities of the PL-SLS model showed varied results which suggested that the PL-SLS model performance is biased towards soft materials with dominant elastic properties, i.e. small velocity-dependencies. The latter is reflected in the generalization errors reported in Table 6.5. This limitation motivated the investigation of an alternative modelling tool which was based on a feedforward artificial neural network. In this case, the selection of input parameters, and the number of neurons in the hidden layer, were optimized. From there it followed that the topology code-named FFRD4 had the best generalization error and was hence chosen as the best candidate. Nonetheless, the FFRD4 topology made use of the strain and strain rate as its inputs. This initially, allowed the ANN model

to achieve better accuracy, in comparison to the PL-SLS model (Table 6.5), but then it was found detrimental for the performance of the ANN model in real-time. The latter is directly related to the limited number of strain rates used for training, but also to the varying strain rate used during the test. The real-time analysis was performed in Simulink, in here the test ANN model also delivered a negative offset when the values of its input were both zero. All these findings suggest that having the strain rate as input to the network require a more comprehensive dataset to allow the ANN model to learn the relationship between the stress and the strain-rate. Alternatively, another topology could be used, which is not rate-dependent, for real-time predictions. In this case, stability during real-time prediction would be favour over achieving an excellent prediction accuracy.

The investigation performed on the concept of mimicking the human skeletal system by implementing viscoelastic materials yielded three important conclusions. Firstly, research is being done on series-elastic actuators to convert them into series-viscoelastic actuators, due to the proven benefits of adding viscoelasticity to robotic applications for human assistance. The latter highlights the feasibility of the research presented in here. Secondly, the matching factor analysis performed in Chapter 7 identified the best soft materials to match the viscoelastic properties of the human tendon, which can be used as design guidelines. Thirdly, a growing interest of mimicking the functionality of the human muscles such as co-contraction and variable recruitment are already being applied to robotic applications. However, this has the potential to be applied to soft robotic applications. Due to this, a experimental protocol was designed to investigate the latter but unfortunately it was not possible to execute in time.

Finally, this research has further proven the potential of ANN model for the prediction of the viscoelastic properties of soft materials. Nonetheless, this is another step taken towards developing a reliable and easy to deploy modelling tool, which will ultimately translate into the optimization and development of new soft robotic applications.

8.3 Future Work

The findings of this research have allowed the identification of the following issues still needed to be addressed:

- Dynamic mechanical analysis can be used to characterize the soft materials

8. SUMMARY, CONCLUSIONS, AND FUTURE WORK

under a wide range of frequencies to create a more comprehensive dataset to train ANN models.

- Further investigation on the concept of series and parallel elasticity in combination with soft materials.
- Validation of the ANN model when being deployed as part of a control system must be investigated.
- Further characterization of the viscoelasticity of soft materials could be done by extracting their hysteresis, creep and cyclic behaviour.
- Different input combinations for the ANN model could be explored, mainly the ones which do not have the strain rate of the material as input.
- Alternative types of ANNs could be investigated, such as Radial Basis Neural Networks and Recurrent Artificial Neural Networks.
- Further investigation on the implementation of the concepts of co-contraction and variable recruitment could be performed for soft robotics applications.
- Further investigation on the field of the human skeletal system functionality, such as muscle redundancy, which is a compatible approach for cable-driven actuators.

Appendices

APPENDIX A

Characterization of the Human Body Lower Limb

A. CHARACTERIZATION OF THE HUMAN BODY LOWER LIMB

A.1 Stacked Clustered Bar Charts

This appendix presents the compiled data from the reviewed gait analysis studies in the form of charts, as the ones presented in Section 3.2, for the hip, knee and ankle joints. The parameters of torque, angle and power, were extracted.

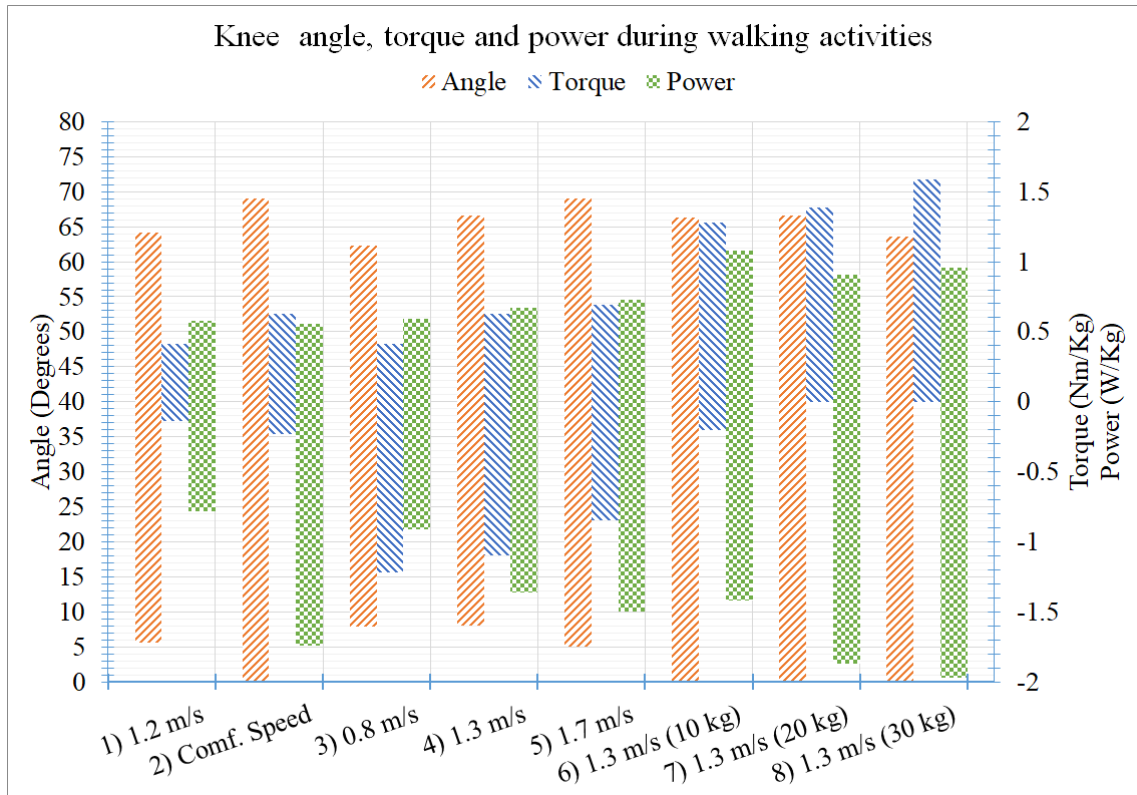


Figure A.1: Knee joint characteristics for walking over ground activities. The weight next to the name of some activities dictates the load carried by the subjects during the experiment [16]. Data collected from: (1) [17], (2) [18], (3-8) [19].

A.1 Stacked Clustered Bar Charts

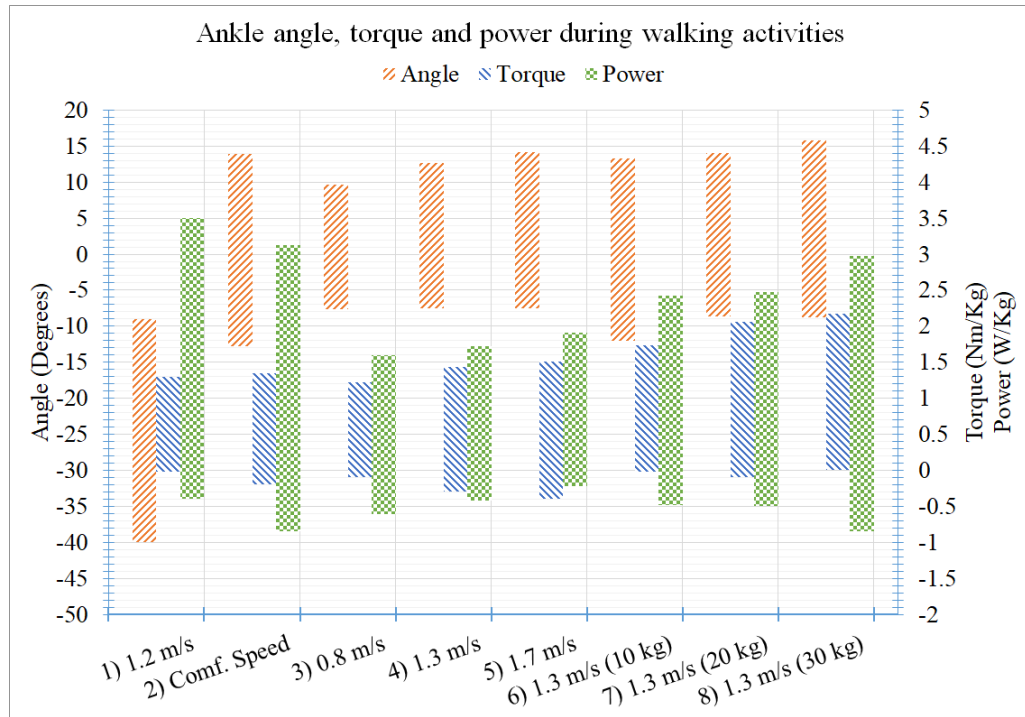


Figure A.2: Ankle joint characteristics for walking over ground activities. The weight next to the name of some activities dictates the load carried by the subjects during the experiment [16]. Data collected from: (1) [17], (2) [18], (3-8) [19].

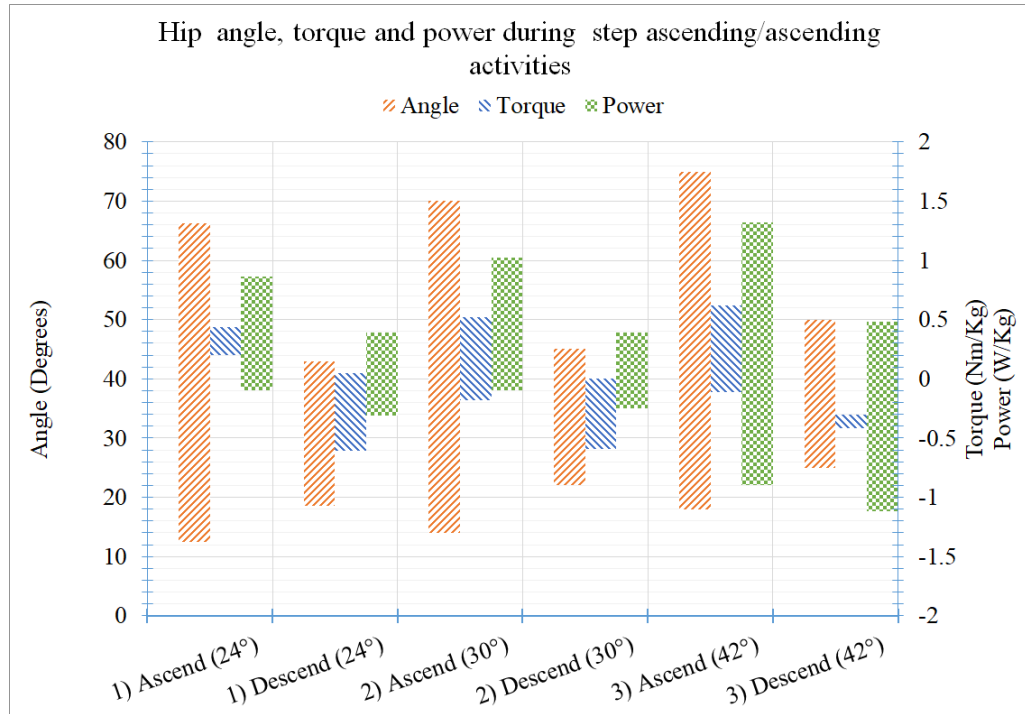


Figure A.3: Hip joint characteristics for step ascending/descending experiments [16]. Data collected from: (1) [20], (2) [21], (3) [36].

A. CHARACTERIZATION OF THE HUMAN BODY LOWER LIMB

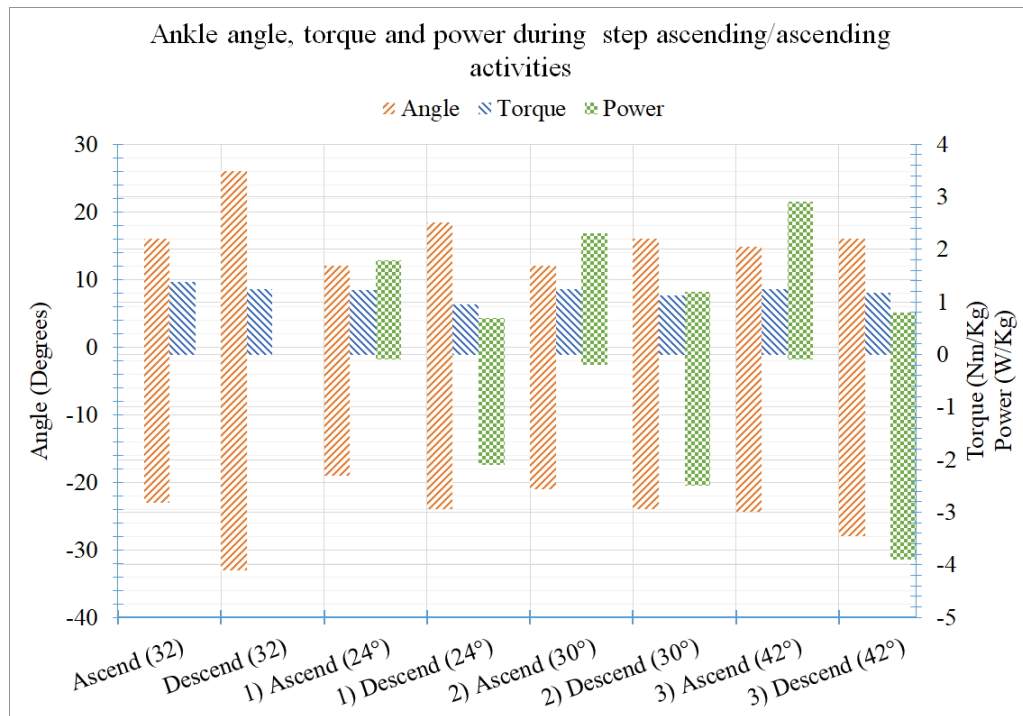


Figure A.4: Ankle joint characteristics for step ascending/descending experiments [16]. Data collected from: (1) [20], (2) [21], (3) [36].

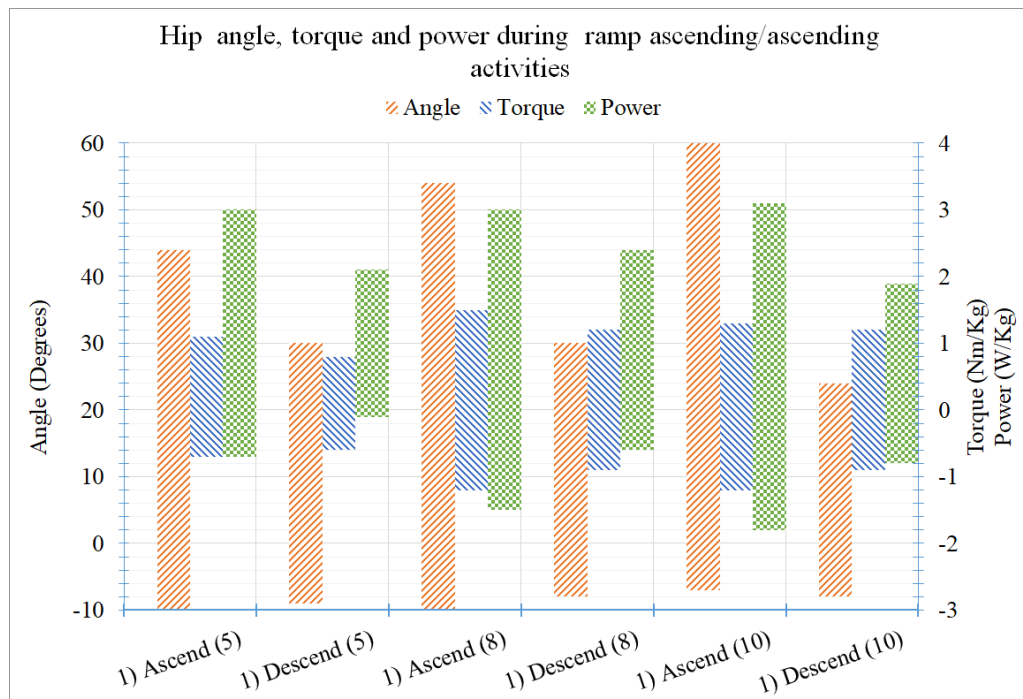


Figure A.5: Hip joint characteristics for ramp ascending/descending experiments [16]. Inclination in brackets. Data collected from [22]

A.1 Stacked Clustered Bar Charts

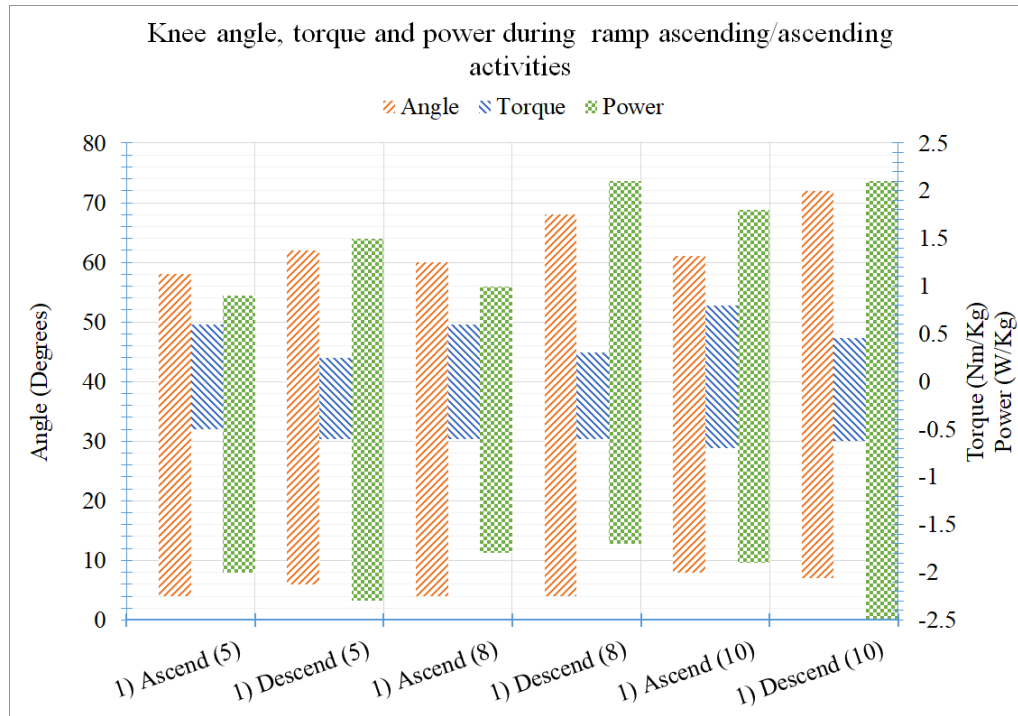


Figure A.6: Knee joint characteristics for ramp ascending/descending experiments [16]. Inclination in brackets. Data collected from [22].

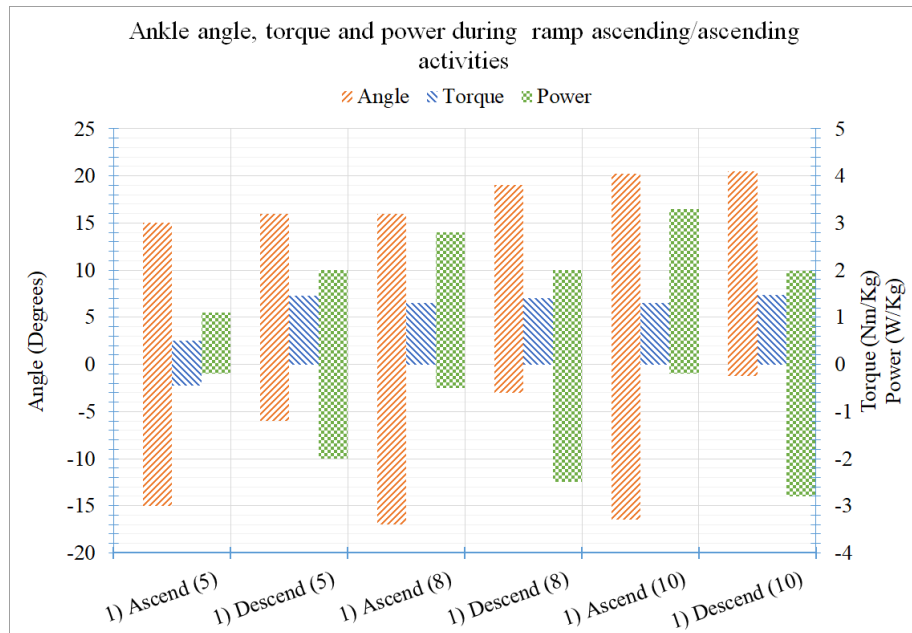


Figure A.7: Ankle joint characteristics for ramp ascending/descending experiments [16]. Inclination in brackets. Data collected from [22].

A. CHARACTERIZATION OF THE HUMAN BODY LOWER LIMB

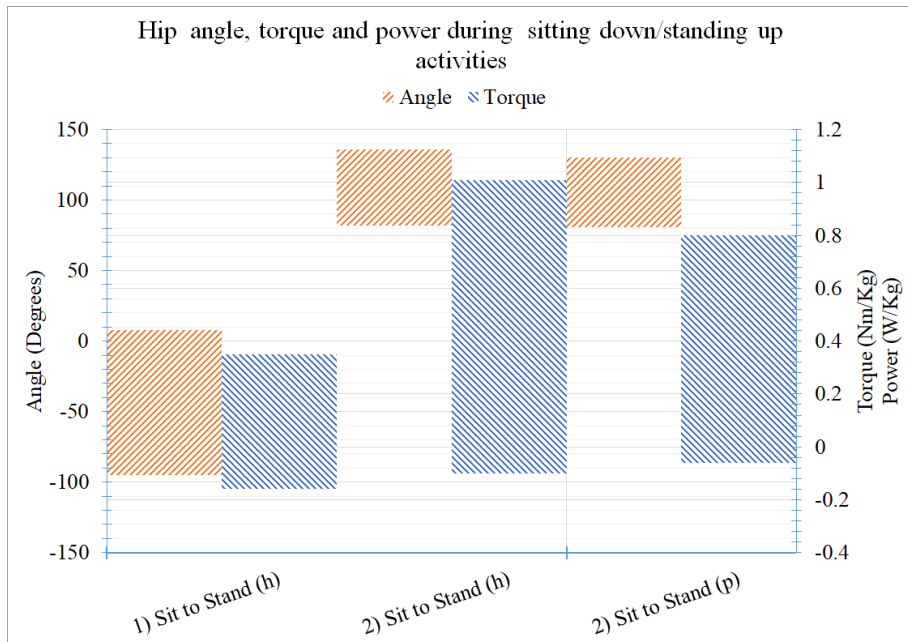


Figure A.8: Hip joint characteristics for sit to stand/stand to sit experiments [16]. In brackets (h) healthy subjects, and (p) subjects with Parkinson's. Data collected from: (1) [23], (2) [24].

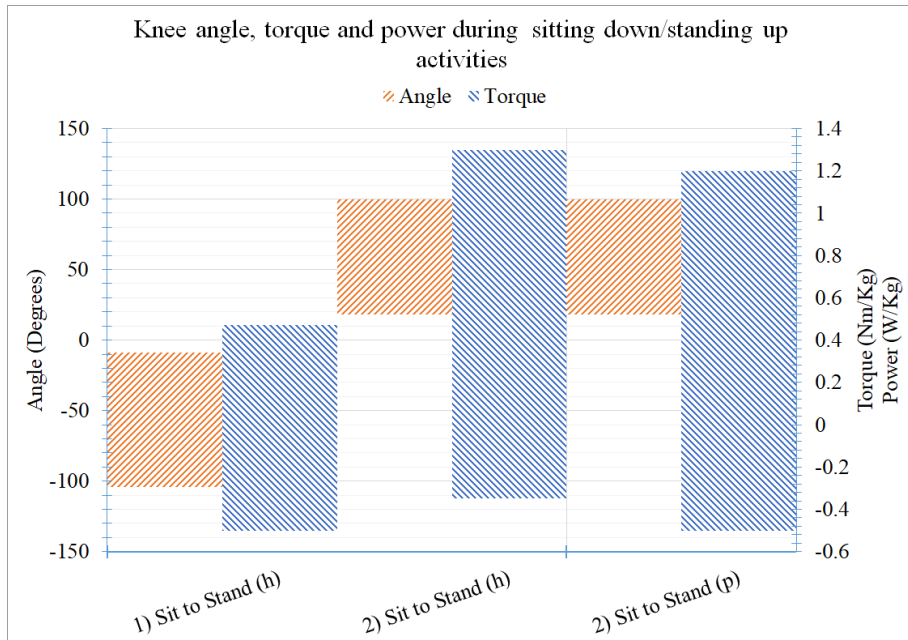


Figure A.9: Knee joint characteristics for sit to stand/stand to sit experiments [16]. In brackets (h) healthy subjects, and (p) subjects with Parkinson's. Data collected from: (1) [23], (2) [24].

A.1 Stacked Clustered Bar Charts

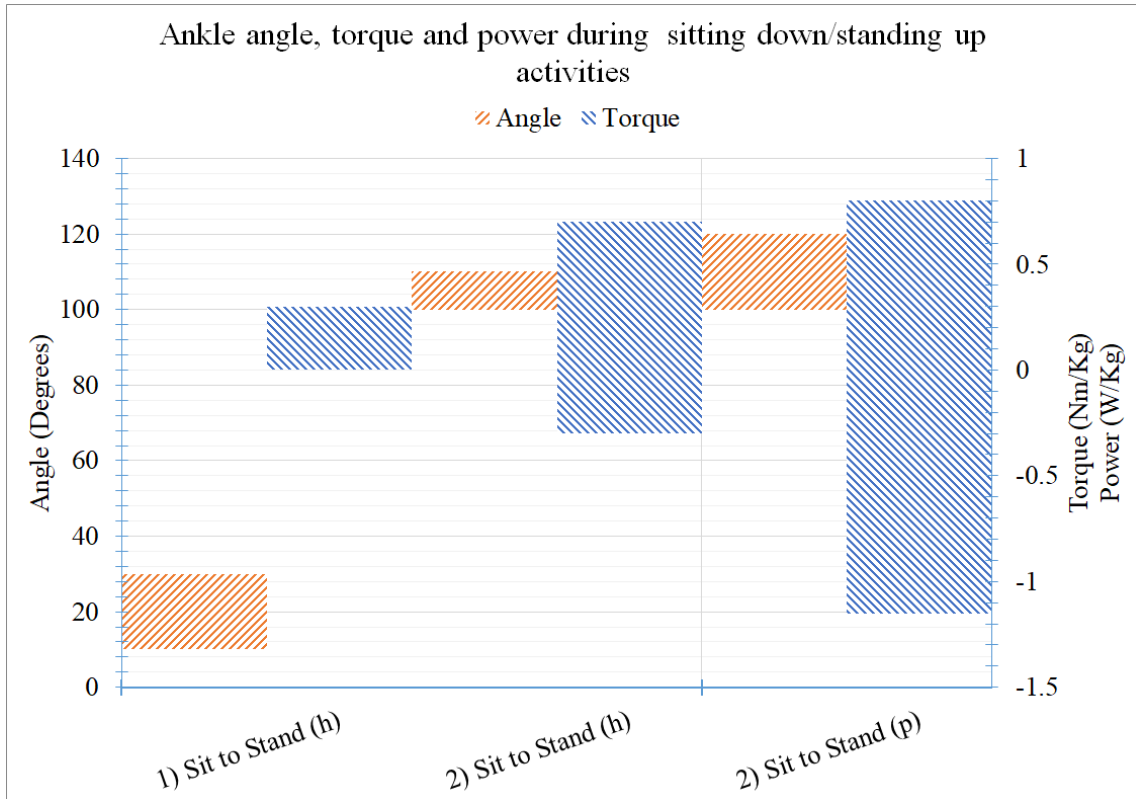


Figure A.10: Ankle joint characteristics for sit to stand/stand to sit experiments [16]. In brackets (h) healthy subjects, and (p) subjects with Parkinson's. Data collected from: (1) [23], (2) [24].

APPENDIX B

Designed Experimental Protocol to
Investigate the Concepts of Variable
Recruitment and Co-contraction in
Series-viscoelastic Actuators

B. DESIGNED EXPERIMENTAL PROTOCOL TO INVESTIGATE THE CONCEPTS OF VARIABLE RECRUITMENT AND CO-CONTRACTION IN SERIES-VISCOELASTIC ACTUATORS

B.1 Aims and Objectives

B.1.1 Aim:

Characterize the performance of a motor-based tendon driven actuator, intended to assist the knee joint, when series/parallel elasticity is added to it.

B.1.2 Objectives:

- Evaluate the performance of the actuator without series/parallel elasticity (rigid) when displacing a hanging load with a sinusoidal trajectory.
- Evaluate the performance of the rigid actuator implementing the concept of variable recruitment when displacing a hanging load with a sinusoidal trajectory.
- Evaluate the performance of the actuator with series/parallel elasticity (SPEA) when displacing a hanging load with a sinusoidal trajectory.
- Evaluate the performance of the SPEA implementing the concept of variable recruitment when displacing a hanging load with a sinusoidal trajectory.

B.2 Methodology

An assistive device must provide around 50% of the peak torque of the assisted joint. The required peak torque and angular speed range for the knee joint during normal walking is 29 Nm and ± 50 rpm respectively [139, 145]. Therefore, the required peak torque to be delivered is 18 Nm. The previous parameters will be used as guidelines when selecting the electric motor/gearbox combination to be used in the experiments. The experiments to be performed are inspired in the human muscle functionality. In this context, there is a very common configuration based on the human muscles that function in pairs, such as the biceps/triceps pair, also called agonistic/antagonistic configuration. The basic functionality of these muscles is as follows: when the biceps contracts, the triceps relaxes to allow motion in one direction. Similarly, when the triceps contracts, the biceps relax. In real activities, the muscles cooperate with each other to displace a load, this principle is called co-contraction.

B.3 Experiment 1

There are several implementations of the agnostic/antagonistic configuration. In this experimental protocol we are focusing on the simplest one involving co-contraction, i.e. collaboration of the actuators when displacing a load. The first experimental setup (Figure B.1) consists of two actuators (tendon-driven electric motors) controlling a single joint via pulling forces in both directions. This configuration allows the maximum applied torque to be the sum of both motors peak torque. Two main aspects are to be observed in this experiment:

- Synchronous co-contraction via sinusoidal wave input
- Stiffness variation via activation of both motors with opposite direction of rotation and different torque amplitudes

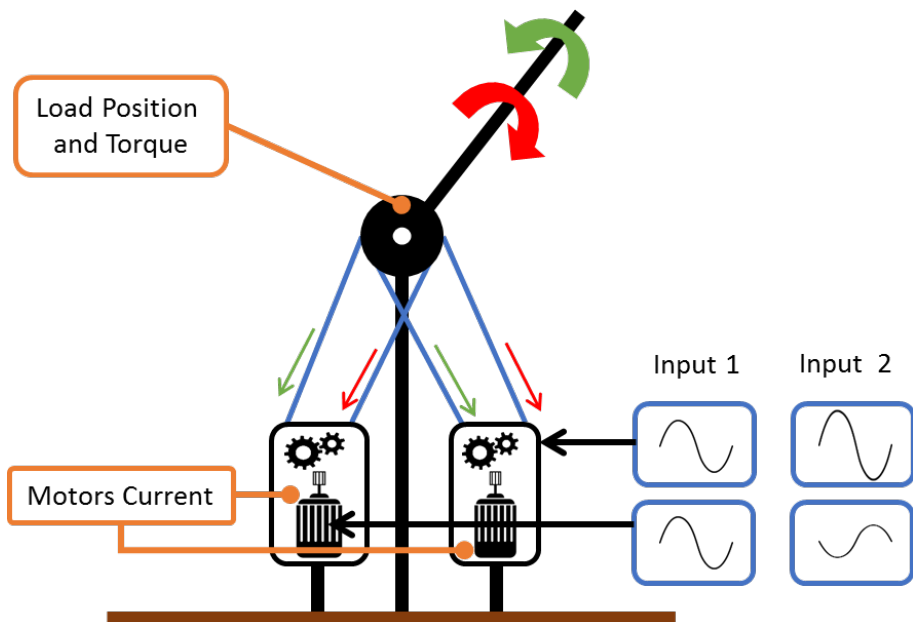


Figure B.1: Experimental setup 1. Two electric motors work together to create the co-contraction effect in the joint. The required instrumentation is highlighted in yellow. Two different inputs are provided, and the actuator's performance observed.

B.4 Experiment 2

The second experiment intended to evaluate the process in which the human muscles recruit several fibres sequentially depending on the desired load. This process is

B. DESIGNED EXPERIMENTAL PROTOCOL TO INVESTIGATE THE CONCEPTS OF VARIABLE RECRUITMENT AND CO-CONTRACTION IN SERIES-VISCOELASTIC ACTUATORS

called variable recruitment and has been already implemented in a SPEA with metallic springs as the elastic element [144]. In this experiment, the flexion and extension motion of the rigid link is performed by groups of several motors instead of a single one. Therefore, the required peak torque T_p to be delivered is divided among all the participating motors, as described in Table B.1. At the beginning of this section it was mentioned that the total peak torque T_p delivered by the motors must be 50% of the knee joint peak torque during normal walking, i.e. 18 Nm. The latter means, that for a group composed of two motors, each of them must deliver 50% of T_p . The latter is better described in Table B.1.

Participating motor	Desired Peak Torque	Torque per motor
2	$T_p = 18 \text{ Nm}$	9 Nm
4	$T_p = 18 \text{ Nm}$	4.5 Nm
6	$T_p = 18 \text{ Nm}$	3 Nm
8	$T_p = 18 \text{ Nm}$	1.5 Nm

Table B.1: Torque requirements for each individual motor in relation to the number of participating motors in the task. The actuator's peak torque $T_p = 18 \text{ Nm}$ is based on the 50% of the knee joint peak torque (29 Nm).

For this experiment, it is necessary for the actuators to be back-drivable and to function in their most efficient region (torque-speed). Initially, the first pair of motors in the activation sequence will attempt to displace the load by applying a torque. When the required torque is higher than the maximum allowable torque of the active motor, a second motor in the activation sequence will aid the load displacement. Therefore, the number of active motors in the sequence is entirely dependent on the required torque. The variable recruitment approach allows the motors to operate in a smaller range of speeds, which if carefully selected, ensure the motors to operate in their most efficient region. This is not the case when implementing a single motor which has to comply with a broad range of torques and speed. Therefore, great energy savings potential can be obtained from the variable recruitment approach. The experimental setup is illustrated in Figure B.2. It is important to mention that when a motor is in OFF state it must be back-drivable.

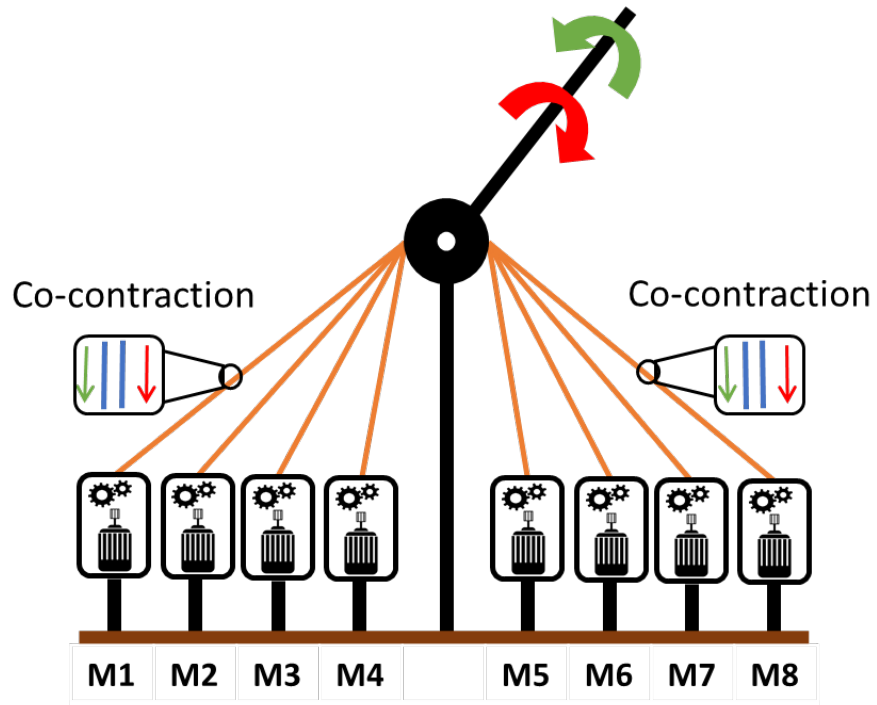


Figure B.2: Experimental setup 2. Several motors activate in pairs to create co-contraction of the rotating joint. For the sake of clarity in the illustration, the two Bowden cables of each motor are grouped into a single orange cable.

B.5 Experiment 3

This experimental setup is the same as in experiment 1 with the only variation of including an elastic element in series with the rotating link (Figure B.3), creating a SPEA. The elastic element is composed of several fibres from the mentioned soft materials. Depending of the stiffness of each soft material, the number of fibres in the elastic element will change taking as reference the recommended optimal stiffness for knee assistance applications.

B.6 Experiment 4

Similarly to experiment 2, the variable recruitment approach will be tested using the soft materials. In this case, it is expected a more complex behaviour caused by the deformation of the viscoelastic element and its time dependent properties. The latter will also affect the frequency bandwidth in which the motor is able to transmit the desired torque to the load. The same combinations of motors as in experiment 2 will be used (Table B.1). The experimental setup is illustrated in Figure B.4.

B. DESIGNED EXPERIMENTAL PROTOCOL TO INVESTIGATE THE CONCEPTS OF VARIABLE RECRUITMENT AND CO-CONTRACTION IN SERIES-VISCOELASTIC ACTUATORS

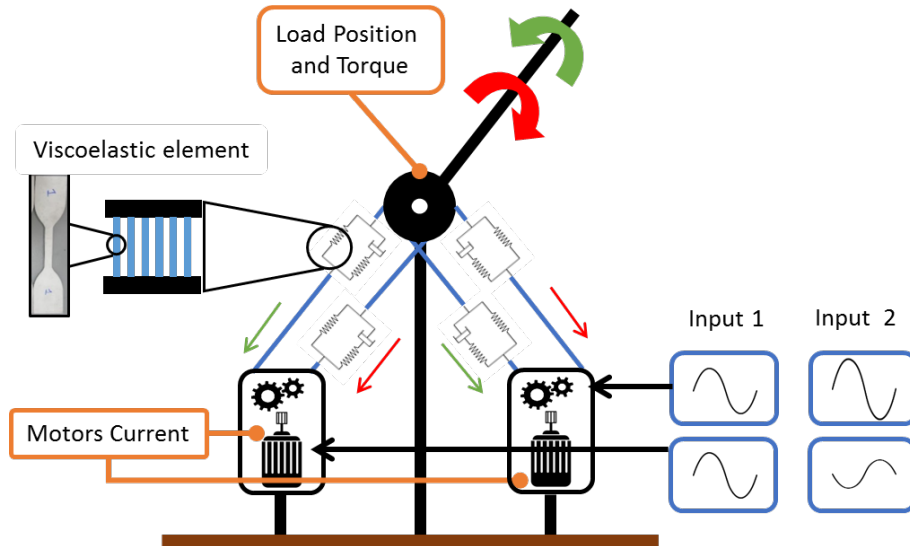


Figure B.3: Experimental setup 3. Same as in experiment 1 with the only variation of including a viscoelastic element in series with the rotating link.

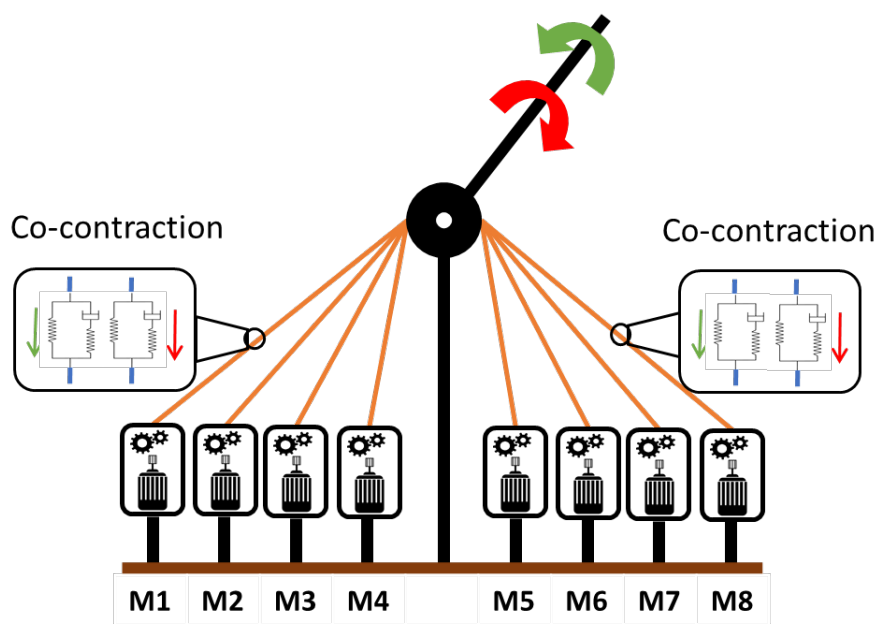


Figure B.4: Experimental setup 4. Same as in experiment 2 with the only variation of including a viscoelastic element in series with the rotating link.

REFERENCES

- [1] Yong-Lae Park, Bor-rong Chen, Diana Young, Leia Stirling, Robert J Wood, Eugene Goldfield, and Radhika Nagpal. Bio-inspired active soft orthotic device for ankle foot pathologies. In *2011 IEEE/RSJ International Conference on Intelligent Robots and Systems*, pages 4488–4495. IEEE, 2011.
- [2] Yong Lae Park, Bor Rong Chen, Carmel Majidi, Robert J. Wood, Radhika Nagpal, and Eugene Goldfield. Active modular elastomer sleeve for soft wearable assistance robots. In *IEEE Int. Conf. Intell. Robot. Syst.*, pages 1595–1602, 2012.
- [3] Michael Wehner, Brendan Quinlivan, Patrick M Aubin, Ernesto Martinez-Villalpando, Michael Baumann, Leia Stirling, Kenneth Holt, Robert Wood, and Conor Walsh. A lightweight soft exosuit for gait assistance. In *2013 IEEE International Conference on Robotics and Automation*, pages 3362–3369. IEEE, 2013.
- [4] Yong-Lae Park, Jobim Santos, Kevin G. Galloway, Eugene C. Goldfield, and Robert J. Wood. A soft wearable robotic device for active knee motions using flat pneumatic artificial muscles. In *2014 IEEE Int. Conf. Robot. Autom.*, pages 4805–4810, 2014.
- [5] Saivimal Sridar, Corey J. Majeika, Phillip Schaffer, Matthew Bowers, Seiichiro Ueda, Andrew J. Barth, Jon L. Sorrells, Jon T. Wu, Thane R. Hunt, and Marko Popovic. Hydro Muscle -a novel soft fluidic actuator. *2016 IEEE Int. Conf. Robot. Autom.*, pages 4014–4021, 2016.
- [6] Alan T Asbeck, Robert J Dyer, Arnar F Larusson, and Conor J Walsh. Biologically-inspired soft exosuit. In *2013 IEEE 13th International Conference on Rehabilitation Robotics (ICORR)*, pages 1–8. IEEE, 2013.

REFERENCES

- [7] Volker Bartenbach, Kai Schmidt, Matthias Naef, Dario Wyss, and Robert Riener. Concept of a Soft Exosuit for the Support of Leg Function in Rehabilitation. In *IEEE Int. Conf. Rehabil. Robot.*, pages 125–130, 2015.
- [8] Inc Images Scientific Instrument. Nitinol / Flexinol® Actuator Wire, 2016.
URL <http://www.imagesco.com/articles/nitinol/04.html>.
- [9] Jianjun Zhang, Yuehong Yin, and Jianying Zhu. Sigmoid-based hysteresis modeling and high-speed tracking control of SMA-artificial muscle. *Sensors Actuators, A Phys.*, 201:264–273, 2013.
- [10] A. Villoslada, A. Flores, D. Copaci, D. Blanco, and L. Moreno. High-displacement flexible Shape Memory Alloy actuator for soft wearable robots. *Rob. Auton. Syst.*, 73:91–101, 2015.
- [11] Kazuto Takashima, Jonathan Rossiter, and Toshiharu Mukai. McKibben artificial muscle using shape-memory polymer. *Sensors Actuators, A Phys.*, 164 (1-2):116–124, 2010.
- [12] Yiğit Mengüç, Yong-Lae Park, Ernesto Martinez-Villalpando, Patrick Aubin, Miriam Zisook, Leia Stirling, Robert J Wood, and Conor J Walsh. Soft wearable motion sensing suit for lower limb biomechanics measurements. In *2013 IEEE International Conference on Robotics and Automation*, pages 5309–5316. IEEE, 2013.
- [13] Jean Baptiste Chossat, Yong Lae Park, Robert J. Wood, and Vincent Duchaine. A soft strain sensor based on ionic and metal liquids. *IEEE Sens. J.*, 13 (9):3405–3414, 2013.
- [14] Wyatt Felt, Khai Yi Chin, and C. David Remy. Contraction Sensing with Smart Braid McKibben Muscles. In *IEEE/ASME Trans. Mechatronics*, volume 4435, pages 1–1, 2015.
- [15] PhysicalSolutions. Understanding Planes and Axes. <https://www.physical-solutions.co.uk/wp-content/uploads/2015/05/Understanding-Planes-and-Axes-of-Movement.pdf>, 2016. [Online; accessed 10-Sep-2016].
- [16] Rodrigo D Solis-Ortega, Abbas A Dehghani-Sanij, and Uriel Martinez-Hernandez. Characterization of kinetic and kinematic parameters for wearable

- robotics. In *Annual Conference Towards Autonomous Robotic Systems*, pages 548–556. Springer, 2017.
- [17] Gabriele Bovi, Marco Rabuffetti, Paolo Mazzoleni, and Maurizio Ferrarin. A multiple-task gait analysis approach: kinematic, kinetic and emg reference data for healthy young and adult subjects. *Gait & posture*, 33(1):6–13, 2011.
 - [18] Song Joo Lee and Joseph Hidler. Biomechanics of overground vs. treadmill walking in healthy individuals. *Journal of applied physiology*, 104(3):747–755, 2008.
 - [19] YaLi Han and XingSong Wang. The biomechanical study of lower limb during human walking. *Science China Technological Sciences*, 54(4):983–991, 2011.
 - [20] Anastasia Protopapadaki, Wendy I Drechsler, Mary C Cramp, Fiona J Coutts, and Oona M Scott. Hip, knee, ankle kinematics and kinetics during stair ascent and descent in healthy young individuals. *Clinical biomechanics*, 22(2):203–210, 2007.
 - [21] Robert Riener, Marco Rabuffetti, and Carlo Frigo. Stair ascent and descent at different inclinations. *Gait & posture*, 15(1):32–44, 2002.
 - [22] Andrew Stuart McIntosh, Karen T Beatty, Leanne N Dwan, and Deborah R Vickers. Gait dynamics on an inclined walkway. *Journal of biomechanics*, 39(13):2491–2502, 2006.
 - [23] ME Roebroeck, CAM Doorenbosch, J Harlaar, R Jacobs, and GJ Lankhorst. Biomechanics and muscular activity during sit-to-stand transfer. *Clinical Biomechanics*, 9(4):235–244, 1994.
 - [24] Margaret KY Mak, Oron Levin, Joseph Mizrahi, and Christina WY Hui-Chan. Joint torques during sit-to-stand in healthy subjects and people with parkinsonâ€™s disease. *Clinical Biomechanics*, 18(3):197–206, 2003.
 - [25] Archibald Vivian Hill. The heat of shortening and the dynamic constants of muscle. *Proceedings of the Royal Society of London. Series B-Biological Sciences*, 126(843):136–195, 1938.
 - [26] Walter Maurel, Yin Wu, Nadia Magnenat Thalmann, and Daniel Thalmann. *Biomechanical models for soft tissue simulation*. Springer, 1998.

REFERENCES

- [27] L Schatzmann, P Brunner, and HU Stäubli. Effect of cyclic preconditioning on the tensile properties of human quadriceps tendons and patellar ligaments. *Knee Surgery, Sports Traumatology, Arthroscopy*, 6(1):S56–S61, 1998.
- [28] Federico Parietti, Gabriel Baud-Bovy, Elia Gatti, Robert Riener, Lino Guzzella, and Heike Vallery. Series viscoelastic actuators can match human force perception. *IEEE/ASME Transactions on Mechatronics*, 16(5):853–860, 2011.
- [29] David Rollinson, Steven Ford, Ben Brown, and Howie Choset. Design and modeling of a series elastic element for snake robots. In *ASME 2013 Dynamic Systems and Control Conference*. American Society of Mechanical Engineers, 2013.
- [30] Alexander Schepelmann, Kathryn A Geberth, and Hartmut Geyer. Compact nonlinear springs with user defined torque-deflection profiles for series elastic actuators. In *2014 IEEE International Conference on Robotics and Automation (ICRA)*, pages 3411–3416. IEEE, 2014.
- [31] Judson T Bauman. *Fatigue, Stress, and Strain of Rubber Components*. Hanser Publications, 2008.
- [32] ASTM D412-06ae2. Standard Test Methods for Vulcanized Rubber and Thermoplastic Elastomers - Tension. Technical report, ASTM International, West Conshohocken, PA, 2006.
- [33] Jessica Austin, Alexander Schepelmann, and Hartmut Geyer. Control and evaluation of series elastic actuators with nonlinear rubber springs. In *2015 IEEE/RSJ International Conference on Intelligent Robots and Systems (IROS)*, pages 6563–6568. IEEE, 2015.
- [34] Rodrigo D Solis-Ortega, Abbas A Dehghani-Sanij, and Uriel Martinez-Hernandez. The assessment of viscoelastic models for nonlinear soft materials. In *2018 7th IEEE International Conference on Biomedical Robotics and Biomechatronics (Biorob)*, pages 1274–1279. IEEE, 2018.
- [35] Alejandro E Rodríguez-Sánchez, Elías Ledesma-Orozco, Sergio Ledesma, and Agustín Vidal-Lesso. Application of artificial neural networks to map the mechanical response of a thermoplastic elastomer. *Materials Research Express*, 2019.

- [36] Samantha M Reid, Scott K Lynn, Reilly P Musselman, and Patrick A Costigan. Knee biomechanics of alternate stair ambulation patterns. *Medicine and science in sports and exercise*, 39(11):2005, 2007.
- [37] Guido Belforte, Gabriella Eula, Alexandre Ivanov, and Silvia Sirolli. Soft Pneumatic Actuators for Rehabilitation. *Actuators*, 3(2):84–105, 2014.
- [38] Greg A Johnson, Dawn M Tramaglini, Rebecca E Levine, Kazunori Ohno, Nam-Yong Choi, and Savio L-Y. Woo. Tensile and viscoelastic properties of human patellar tendon. *Journal of orthopaedic research*, 12(6):796–803, 1994.
- [39] Hans U Stäubli, Lukas Schatzmann, Peter Brunner, Liliana Rincón, and Lutz-P Nolte. Mechanical tensile properties of the quadriceps tendon and patellar ligament in young adults. *The American journal of sports medicine*, 27(1):27–34, 1999.
- [40] C Laschi. Soft robotics: from scientific challenges to technological applications. In *Micro-and Nanotechnology Sensors, Systems, and Applications VIII*, volume 9836, page 983626. International Society for Optics and Photonics, 2016.
- [41] Sangbae Kim, Cecilia Laschi, and Barry Trimmer. Soft robotics: a bioinspired evolution in robotics. *Trends in biotechnology*, 31(5):287–294, 2013.
- [42] Daniela Rus and Michael T Tolley. Design, fabrication and control of soft robots. *Nature*, 521(7553):467, 2015.
- [43] Roberto Filippini, Soumen Sen, and Antonio Bicchi. Toward soft robots you can depend on. *IEEE Robotics & Automation Magazine*, 15(3):31–41, 2008.
- [44] Deepak Trivedi, Christopher D Rahn, William M Kier, and Ian D Walker. Soft robotics: Biological inspiration, state of the art, and future research. *Applied bionics and biomechanics*, 5(3):99–117, 2008.
- [45] Fumiya Iida and Cecilia Laschi. Soft robotics: challenges and perspectives. *Procedia Computer Science*, 7:99–102, 2011.
- [46] Alan T Asbeck, Stefano MM De Rossi, Ignacio Galiana, Ye Ding, and Conor J Walsh. Stronger, smarter, softer: next-generation wearable robots. *IEEE Robotics & Automation Magazine*, 21(4):22–33, 2014.

REFERENCES

- [47] Yong-Lae Park, Bor-rong Chen, Néstor O Pérez-Arcibia, Diana Young, Leia Stirling, Robert J Wood, Eugene C Goldfield, and Radhika Nagpal. Design and control of a bio-inspired soft wearable robotic device for ankle-foot rehabilitation. *Bioinspiration & biomimetics*, 9(1):016007, 2014.
- [48] P. J. Colombo, M. E. Crawley, B. S. East, and A. R. Hill. Aging and the Brain. https://www.who.int/ageing/publications/global_health.pdf, 2012. [Online; accessed 28-Aug-2019].
- [49] Amelia Hill. Nearly one in seven Britons could live alone by 2039, study shows. <https://www.theguardian.com/society/2019/apr/04/nearly-one-in-seven-britons-could-live-alone-2039-study-shows>, 2019. [Online; accessed 28-Aug-2019].
- [50] RS Components Ltd. Black epdm rubber sheet. <https://uk.rs-online.com/web/p/ethylene-polypropylene-epdm-sheets/8405523/>, 2019. [Online; accessed 28-Aug-2019].
- [51] RS Components Ltd. Black fluorocarbon rubber sheet. <https://uk.rs-online.com/web/p/fluorocarbon-rubber-sheets/5062974/>, 2019. [Online; accessed 28-Aug-2019].
- [52] RS Components Ltd. White nitrile rubber sheet. <https://uk.rs-online.com/web/p/nitrile-rubber-nbr-sheets/5063242/>, 2019. [Online; accessed 28-Aug-2019].
- [53] RS Components Ltd. Black natural rubber sheet. <https://uk.rs-online.com/web/p/natural-rubber-sheets/5063078/>, 2019. [Online; accessed 28-Aug-2019].
- [54] RS Components Ltd. Black polyethylene foam. <https://uk.rs-online.com/web/p/polyethylene-rubber-sheets/7336690/>, 2019. [Online; accessed 28-Aug-2019].
- [55] RS Components Ltd. White silicone rubber sheet. <https://uk.rs-online.com/web/p/silicone-rubber-sheets/5063264/>, 2019. [Online; accessed 28-Aug-2019].
- [56] COREZONE Sports. Resistance loop bands. <https://www.corezonesports.co.uk/collections/resistance-bands/products/resistance-loop-bands-6-pack>, 2019. [Online; accessed 28-Aug-2019].

- [57] Tomoyuki Noda, Tatsuya Teramae, Barkan Ugurlu, and Jun Morimoto. Development of an upper limb exoskeleton powered via pneumatic electric hybrid actuators with bowden cable. In *IEEE Int. Conf. Intell. Robot. Syst.*, pages 3573–3578, 2014.
- [58] Juan Manuel Florez, Benjamin Shih, Yixin Bai, and Jamie K. Paik. Soft pneumatic actuators for legged locomotion. In *2014 IEEE Int. Conf. Robot. Biomimetics, IEEE ROBIO 2014*, pages 27–34, 2014.
- [59] John Morrow, Hee-sup Shin, Jacob Torrey, Riley Larkins, Steven Dang, Calder Phillips-grafflin, Yong-lae Park, and Dmitry Berenson. Improving Soft Pneumatic Actuator Fingers through Integration of Soft Sensors , Position and Force Control , and Rigid Fingernails, 2015.
- [60] Harshal Arun Sonar and Jamie Paik. Soft Pneumatic Actuator Skin with Piezoelectric Sensors for Vibrotactile Feedback. *Front. Robot. AI*, 2(January):1–11, 2016.
- [61] Chansu Suh, Jordi Condal Margarit, Yun Seong Song, and Jamie Paik. Soft Pneumatic Actuator skin with embedded sensors. In *IEEE Int. Conf. Intell. Robot. Syst.*, pages 2783–2788, 2014.
- [62] Ellen T. Roche, Robert Wohlfarth, Johannes T B Overvelde, Nikolay V. Vasiliyev, Frank A. Pigula, David J. Mooney, Katia Bertoldi, and Conor J. Walsh. A bioinspired soft actuated material. *Adv. Mater.*, 26(8):1200–1206, 2014.
- [63] M Hamedi, P Salimi, A Aliabadi, and M Vismeh. Toward intelligent ankle foot orthosis for foot-drop, a review of technologies and possibilities. In *Biomed. Eng. (ICoBE), 2015 2nd Int. Conf.*, pages 1–6, 2015.
- [64] Fan-Zhe Low, Hong Han Tan, Jeong Hoon Lim, and Chen-Hua Yeow. Development of a Soft Pneumatic Sock for Robot-Assisted Ankle Exercise. *J. Med. Device.*, 10(1):014503, 2016.
- [65] Elliot W Hawkes, David L Christensen, and Allison M Okamura. Design and implementation of a 300% strain soft artificial muscle. In *2016 IEEE International Conference on Robotics and Automation (ICRA)*, pages 4022–4029. IEEE, 2016.

REFERENCES

- [66] Ye Ding, Ignacio Galiana, Alan Asbeck, Brendan Quinlivan, Stefano Marco, and Maria De Rossi. Multi-joint Actuation Platform for Lower Extremity Soft Exosuits. In *IEEE Int. Conf. Robot. Autom.*, pages 1327–1334, 2014.
- [67] Ye Ding, Ignacio Galiana, Alan Asbeck, Stefano De Rossi, Jaehyun Bae, Thiago Santos, Vanessa Araujo, Sangjun Lee, Kenneth Holt, and Conor Walsh. Biomechanical and Physiological Evaluation of Multi-joint Assistance with Soft Exosuits. In *IEEE Trans. Neural Syst. Rehabil. Eng.*, volume 0, pages 1–1, 2016.
- [68] Vishalini Bundhoo. *Design and evaluation of a shape memory alloy-based tendon-driven actuation system for biomimetic artificial fingers*. PhD thesis, University of Victoria, 2009.
- [69] Vishalini Bundhoo, Edmund Haslam, Benjamin Birch, and Edward J. Park. A shape memory alloy-based tendon-driven actuation system for biomimetic artificial fingers, part I: design and evaluation. *Robotica*, 27(01):131, 2009.
- [70] Ehsan Tarkesh, Mohammad H Elahinia, and Mohamed Samir Hefzy. Developing an active ankle foot orthosis based on shape memory alloy actuators. In *ASME 2007 Summer Bioengineering Conference*, pages 769–770. American Society of Mechanical Engineers Digital Collection, 2007.
- [71] Leia Stirling, Chih Han Yu, Jason Miller, Elliot Hawkes, Robert Wood, Eugene Goldfield, and Radhika Nagpal. Applicability of shape memory alloy wire for an active, soft orthotic. *J. Mater. Eng. Perform.*, 20(4-5):658–662, 2011.
- [72] S. Pittaccio, S. Viscuso, M. Rossini, L. Magoni, S. Pirovano, E. Villa, S. Bessegini, and F. Molteni. SHADE: A shape-memory-activated device promoting ankle dorsiflexion. *J. Mater. Eng. Perform.*, 18(5-6):824–830, 2009.
- [73] Thomas P Chenal, Jennifer C Case, Jamie Paik, and Rebecca K Kramer. Variable Stiffness Fabrics with Embedded Shape Memory Materials for Wearable Applications. In *2013 IEEE/RSJ Int. Conf. Intell. Robot. Syst.*, pages 2827–2831, 2014.
- [74] Simone Pittaccio and Stefano Viscuso. Shape memory actuators for medical rehabilitation and neuroscience. *Smart Actuation and Sensing Systems-Recent Advances and Future Challenges*, 4:83–120, 2012.

- [75] William Coral, Claudio Rossi, Julian Colorado, Daniel Lemus, and Antonio Barrientos. Sma-based muscle-like actuation in biologically inspired robots: a state of the art review. *Smart Actuation and Sensing Systems-Recent Advances and Future Challenges*, pages 53–82, 2012.
- [76] Yiğit Mengüç, Yong-Lae Park, Hao Pei, Daniel Vogt, Patrick M Aubin, Ethan Winchell, Lowell Fluke, Leia Stirling, Robert J Wood, and Conor J Walsh. Wearable soft sensing suit for human gait measurement. *The International Journal of Robotics Research*, 33(14):1748–1764, 2014.
- [77] N.C. C. Goulbourne, S. Son, and J.W. W. Fox. Self-sensing McKibben actuators using dielectric elastomer sensors. *Proc. SPIE*, 6524:652414–652414–12, 2007.
- [78] Yong Lae Park and Robert J. Wood. Smart pneumatic artificial muscle actuator with embedded microfluidic sensing. *IEEE SENSORS 2013 - Proc.*, pages 1–4, 2013.
- [79] Wyatt Felt and C David Remy. Smart braid: Air muscles that measure force and displacement. In *2014 IEEE/RSJ International Conference on Intelligent Robots and Systems*, pages 2821–2826. IEEE, 2014.
- [80] MingKun Chang. Adaptive Self-Tuning Fuzzy Controller for a Soft Rehabilitation Machine Actuated by Pneumatic Artificial Muscles. *Open J. Appl. Sci.*, 5(5):199–211, 2015.
- [81] Erik H. Skorina, Ming Luo, Selim Ozel, Fuchen Chen, Weijia Tao, and Cagdas D. Onal. Feedforward augmented sliding mode motion control of antagonistic soft pneumatic actuators. *Proc. - IEEE Int. Conf. Robot. Autom.*, 2015-June(June):2544–2549, 2015.
- [82] Joshua Bishop-Moser and Sridhar Kota. Design and Modeling of Generalized Fiber-Reinforced Pneumatic Soft Actuators. In *IEEE Trans. Robot.*, volume 31, pages 536–545, 2015.
- [83] A. Hošovský, J. Piteček, K. Žídek, M. Tóthová, J. Sárosi, and L. Cveticanin. Dynamic characterization and simulation of two-link soft robot arm with pneumatic muscles. *Mech. Mach. Theory*, 103:98–116, 2016.

REFERENCES

- [84] Fausto A Panizzolo, Ignacio Galiana, Alan T Asbeck, Christopher Siviy, Kai Schmidt, Kenneth G Holt, and Conor J Walsh. A biologically-inspired multi-joint soft exosuit that can reduce the energy cost of loaded walking. *Journal of neuroengineering and rehabilitation*, 13(1):43, 2016.
- [85] Sai-Kit Wu, Garrett Waycaster, and Xiangrong Shen. Electromyography-based control of active above-knee prostheses. *Control Engineering Practice*, 19(8):875–882, 2011.
- [86] Han Yali and Wang Xingsong. Biomechanics study of human lower limb walking: Implication for design of power-assisted robot. In *2010 IEEE/RSJ International Conference on Intelligent Robots and Systems*, pages 3398–3403. IEEE, 2010.
- [87] Jason K Moore, Sandra K Hnat, and Antonie J van den Bogert. An elaborate data set on human gait and the effect of mechanical perturbations. *PeerJ*, 3: e918, 2015.
- [88] PJ Rowe, CM Myles, C Walker, and R Nutton. Knee joint kinematics in gait and other functional activities measured using flexible electrogoniometry: how much knee motion is sufficient for normal daily life? *Gait & posture*, 12(2): 143–155, 2000.
- [89] Jianjun Zhang and Yuehong Yin. Sma-based bionic integration design of self-sensor–actuator-structure for artificial skeletal muscle. *Sensors and Actuators A: Physical*, 181:94–102, 2012.
- [90] Felix E Zajac. Muscle and tendon: properties, models, scaling, and application to biomechanics and motor control. *Critical reviews in biomedical engineering*, 17(4):359–411, 1989.
- [91] David G Lloyd and Thor F Besier. An emg-driven musculoskeletal model to estimate muscle forces and knee joint moments in vivo. *Journal of biomechanics*, 36(6):765–776, 2003.
- [92] Massimo Sartori, David G Lloyd, Monica Reggiani, and Enrico Pagello. A stiff tendon neuromusculoskeletal model of the knee. In *2009 IEEE Workshop on Advanced Robotics and its Social Impacts*, pages 132–138. IEEE, 2009.

- [93] Margareta Nordin and Victor Hirsch Frankel. *Basic biomechanics of the musculoskeletal system*. Lippincott Williams & Wilkins, 2001.
- [94] Shalimar Abdullah. Usage of synthetic tendons in tendon reconstruction. In *BMC proceedings*, volume 9, page A68. BioMed Central, 2015.
- [95] Sarah E Duenwald, Ray Vanderby, and Roderic S Lakes. Viscoelastic relaxation and recovery of tendon. *Annals of biomedical engineering*, 37(6):1131–1140, 2009.
- [96] David Roylance. Mechanical properties of materials. *Massachusetts Institute of Technology*, pages 51–78, 2008.
- [97] Qinwu Xu and Bjorn Engquist. A mathematical and physical model improves accuracy in simulating solid material relaxation modulus and viscoelastic responses. *arXiv preprint arXiv:1412.5225*, 2014.
- [98] Annalisa Tirella, Giorgio Mattei, and ARTI Ahluwalia. Strain rate viscoelastic analysis of soft and highly hydrated biomaterials. *Journal of Biomedical Materials Research Part A*, 102(10):3352–3360, 2014.
- [99] Tongqing Lu, Jikun Wang, Ruisen Yang, and TJ Wang. A constitutive model for soft materials incorporating viscoelasticity and mullins effect. *Journal of Applied Mechanics*, 84(2):021010, 2017.
- [100] Ana Paula Delowski Ciniello, Carlos Alberto Bavastri, and Jucélio Tomás Pereira. Identifying mechanical properties of viscoelastic materials in time domain using the fractional zener model. *Latin American Journal of Solids and Structures*, 14(1):131–152, 2017.
- [101] R Sanjeevi. A viscoelastic model for the mechanical properties of biological materials. *Journal of biomechanics*, 15(2):107–109, 1982.
- [102] David Roylance. Engineering viscoelasticity. *Department of Materials Science and Engineering–Massachusetts Institute of Technology, Cambridge MA*, 2139:1–37, 2001.
- [103] Gill A Pratt and Matthew M Williamson. Series elastic actuators. In *Proceedings 1995 IEEE/RSJ International Conference on Intelligent Robots and Systems. Human Robot Interaction and Cooperative Robots*, volume 1, pages 399–406. IEEE, 1995.

REFERENCES

- [104] Jerry E Pratt and Benjamin T Krupp. Series elastic actuators for legged robots. In *Unmanned Ground Vehicle Technology Vi*, volume 5422, pages 135–144. International Society for Optics and Photonics, 2004.
- [105] Samuel K Au and Hugh M Herr. Powered ankle-foot prosthesis. *IEEE Robotics & Automation Magazine*, 15(3):52–59, 2008.
- [106] Stefan S Groothuis, G Rusticelli, A Zucchelli, Stefano Stramigioli, and Raf-faella Carloni. The vsaut-ii: A novel rotational variable stiffness actuator. In *2012 IEEE International Conference on Robotics and Automation*, pages 3355–3360. IEEE, 2012.
- [107] Shane A Migliore, Edgar A Brown, and Stephen P DeWeerth. Novel nonlinear elastic actuators for passively controlling robotic joint compliance. *Journal of Mechanical Design*, 129(4):406–412, 2007.
- [108] Robert O Ebewele. *Polymer science and technology*, chapter Mechanical Properties of Polymers I. CRC press, 2000.
- [109] Horton H. Ryffel H. McCauley C. Oberg E., Jones F. *Machinery’s Handbook (30th Edition)*, chapter Properties of Plastics. Industrial Press, 2016.
- [110] ASTM D638-14. Standard Test Method for Tensile Properties of Plastics. Technical report, ASTM International, West Conshohocken, PA, 2014.
- [111] Mohammad Sadeghi and Fereidoon Behnia. Optimum window length of savitzky-golay filters with arbitrary order. *arXiv preprint arXiv:1808.10489*, 2018.
- [112] Instron. Yield strength. <https://www.instron.co.uk/en-gb/our-company/library/glossary/y/yield-strength>, 2019. [Online; accessed 28-Aug-2019].
- [113] Jennifer C Case, Edward L White, and Rebecca K Kramer. Soft material characterization for robotic applications. *Soft Robotics*, 2(2):80–87, 2015.
- [114] Mats Delin, Rodney W Rychwalski, Michael J Kubát, and Josef Kubát. Volume changes during stress relaxation in polyethylene. *Rheologica acta*, 34(2):182–195, 1995.
- [115] Chiwon Lee, Myungjoon Kim, Yoon Jae Kim, Nhayoung Hong, Seungwan Ryu, H Jin Kim, and Sungwan Kim. Soft robot review. *International Journal of Control, Automation and Systems*, 15(1):3–15, 2017.

- [116] Priyanshu Agarwal and Ashish D Deshpande. Series elastic actuators for small-scale robotic applications. *Journal of Mechanisms and Robotics*, 9(3):031016, 2017.
- [117] Leandro Tomé Martins, Christopher A Arend Tatsch, Eduardo Henrique Ma-cieli, Reinhard Gerndt, and Rodrigo da Silva Guerra. A polyurethane-based compliant element for upgrading conventional servos into series elastic actuators. *IFAC-PapersOnLine*, 48(19):112–117, 2015.
- [118] Nevio Luigi Tagliamonte, Dino Accoto, and Eugenio Guglielmelli. Rendering viscoelasticity with series elastic actuators using cascade control. In *2014 IEEE International Conference on Robotics and Automation (ICRA)*, pages 2424–2429. IEEE, 2014.
- [119] C Machiraju, A-V Phan, AW Pearsall, and S Madanagopal. Viscoelastic studies of human subscapularis tendon: Relaxation test and a wiechert model. *Computer methods and programs in biomedicine*, 83(1):29–33, 2006.
- [120] Jorgen S Bergstrom. *Mechanics of solid polymers: theory and computational modeling*, chapter 9, pages 437–446. William Andrew, 2015.
- [121] Z Zhang and K Friedrich. Artificial neural networks applied to polymer composites: a review. *Composites Science and technology*, 63(14):2029–2044, 2003.
- [122] Mira Trebar, Zoran Susteric, and Uros Lotric. Predicting mechanical properties of elastomers with neural networks. *Polymer*, 48(18):5340–5347, 2007.
- [123] Shahzad Maqsood Khan, Samander Ali Malik, Nafisa Gull, Sidra Saleemi, Atif Islam, and Muhammad Taqi Zahid Butt. Fabrication and modelling of the macro-mechanical properties of cross-ply laminated fibre-reinforced polymer composites using artificial neural network. *Advanced Composite Materials*, pages 1–15, 2019.
- [124] Z Zhang, P Klein, and K Friedrich. Dynamic mechanical properties of ptfe based short carbon fibre reinforced composites: experiment and artificial neural network prediction. *Composites Science and Technology*, 62(7-8):1001–1009, 2002.
- [125] Z Zhang, K Friedrich, and K Velten. Prediction on tribological properties of short fibre composites using artificial neural networks. *Wear*, 252(7-8):668–675, 2002.

REFERENCES

- [126] MS Al-Haik, MY Hussaini, and H Garmestani. Prediction of nonlinear viscoelastic behavior of polymeric composites using an artificial neural network. *International journal of plasticity*, 22(7):1367–1392, 2006.
- [127] Mohammad Hossien Saeidirad, Abbas Rohani, and Saeed Zarifneshat. Predictions of viscoelastic behavior of pomegranate using artificial neural network and maxwell model. *Computers and Electronics in Agriculture*, 98:1–7, 2013.
- [128] Yubin Gao, Haibin Li, Guangmei Wei, and Yun He. Viscoelastic analysis of a sleeve based on the bp neural network. *Journal of Mechanical Science and Technology*, 29(11):4621–4629, 2015.
- [129] Necat Altinkok and Rasit Koker. Use of artificial neural network for prediction of physical properties and tensile strengths in particle reinforced alüminum matrix composites. *Journal of materials science*, 40(7):1767–1770, 2005.
- [130] Srinivasu Gangi Setti and RN Rao. Artificial neural network approach for prediction of stress-strain curve of near β titanium alloy. *Rare Metals*, 33(3):249–257, 2014.
- [131] Ivan Jeník, Petr Kubík, František Šebek, Jiri Hulka, and Jindrich Petruska. Sequential simulation and neural network in the stress-strain curve identification over the large strains using tensile test. *Archive of Applied Mechanics*, 87(6):1077–1093, 2017.
- [132] Basem F Yousef, Abdel-Hamid I Mourad, and Ali Hilal-Alnaqbi. Prediction of the mechanical properties of pe/pp blends using artificial neural networks. *Procedia Engineering*, 10:2713–2718, 2011.
- [133] Ivan Kopáč, Marta Harničárová, Jan Valíček, and Milena Kušnerová. Modeling the temperature dependence of dynamic mechanical properties and viscoelastic behavior of thermoplastic polyurethane using artificial neural network. *Polymers*, 9(10):519, 2017.
- [134] Ivan Kopáč, Ivan Labaj, Marta Harničárová, Jan Valíček, and Dušan Hrubý. Prediction of the tensile response of carbon black filled rubber blends by artificial neural network. *Polymers*, 10(6):644, 2018.
- [135] Mukta Paliwal and Usha A Kumar. Neural networks and statistical techniques: A review of applications. *Expert systems with applications*, 36(1):2–17, 2009.

- [136] G Gary Wang and S Shan. Review of metamodeling techniques in support of engineering design optimization. *Journal of Mechanical Design*, 129(4):370–380, 2007.
- [137] Timo Koskela et al. *Neural network methods in analysing and modelling time varying processes*. Helsinki University of Technology, 2003.
- [138] MathWorks®. Improve Shallow Neural Network Generalization and Avoid Overfitting. <https://uk.mathworks.com/help/deeplearning/ug/improve-neural-network-generalization-and-avoid-overfitting.html>, 2019. [Online; accessed 28-Aug-2019].
- [139] Wilian M dos Santos and Adriano AG Siqueira. Impedance control of a rotary series elastic actuator for knee rehabilitation. *IFAC Proceedings Volumes*, 47(3):4801–4806, 2014.
- [140] Xianbo Xu and Nikhil Gupta. Artificial neural network approach to predict the elastic modulus from dynamic mechanical analysis results. *Advanced Theory and Simulations*, 2(4):1800131, 2019.
- [141] David Rollinson, Yigit Bilgen, Ben Brown, Florian Enner, Steven Ford, Curtis Layton, Justine Rembisz, Mike Schwerin, Andrew Willig, Pras Velagapudi, et al. Design and architecture of a series elastic snake robot. In *2014 IEEE/RSJ International Conference on Intelligent Robots and Systems*, pages 4630–4636. IEEE, 2014.
- [142] HEBI Robotics. <https://www.hebirobotics.com/>, 2019. [Online; accessed 28-Aug-2019].
- [143] Edgar Bolivar, David Allen, Gregory Ellson, Jorge Cossio, Walter Voit, and Robert Gregg. Towards a series elastic actuator with electrically modulated stiffness for powered ankle-foot orthoses. In *2016 IEEE International Conference on Automation Science and Engineering (CASE)*, pages 1086–1093. IEEE, 2016.
- [144] Glenn Mathijssen, Dirk Lefeber, and Bram Vanderborght. Variable recruitment of parallel elastic elements: Series-parallel elastic actuators (spea) with dephased mutilated gears. *IEEE/ASME Transactions on Mechatronics*, 20(2):594–602, 2014.

REFERENCES

- [145] David A Winter. *Biomechanics and motor control of human movement*. John Wiley & Sons, 2009.
- [146] Maxon. Maxon RE motor. https://www.maxongroup.com/medias/sys_master/root/8833415839774/19-EN-130.pdf, 2019. [Online; accessed 28-Aug-2019].
- [147] Maxon. Maxon Planetary Gearhead. https://www.maxongroup.com/medias/sys_master/8831071158302.pdf, 2019. [Online; accessed 28-Aug-2019].